University of Alberta

Structure and Kinematic Development of the northwest Skeena Fold Belt, northwestern British Columbia

by

Walter Adrian Loogman

A thesis submitted to the Faculty of Graduate Studies and Research
in partial fulfillment of the requirements for the degree of

Master of Science

Department of Earth and Atmospheric Sciences

Edmonton, Alberta
Fall, 2008

Library and Archives Canada

Published Heritage Branch

395 Wellington Street
Ottawa ON K1A 0N4
Canada

Bibliothèque et Archives Canada

Direction du Patrimoine de l'édition

395, rue Wellington
Ottawa ON K1A 0N4
Canada

Your file Votre référence
ISBN: 978-0-494-47298-9
Our file Notre référence
ISBN: 978-0-494-47298-9

NOTICE:
The author has granted a non-exclusive license allowing Library and Archives Canada to reproduce, publish, archive, preserve, conserve, communicate to the public by telecommunication or on the Internet, loan, distribute and sell theses worldwide, for commercial or non-commercial purposes, in microform, paper, electronic and/or any other formats.

The author retains copyright ownership and moral rights in this thesis. Neither the thesis nor substantial extracts from it may be printed or otherwise reproduced without the author's permission.

AVIS:
L'auteur a accordé une licence non exclusive permettant à la Bibliothèque et Archives Canada de reproduire, publier, archiver, sauvegarder, conserver, transmettre au public par télécommunication ou par l'Internet, prêter, distribuer et vendre des thèses partout dans le monde, à des fins commerciales ou autres, sur support microforme, papier, électronique et/ou autres formats.

L'auteur conserve la propriété du droit d'auteur et des droits moraux qui protège cette thèse. Ni la thèse ni des extraits substantiels de celle-ci ne doivent être imprimés ou autrement reproduits sans son autorisation.

In compliance with the Canadian Privacy Act some supporting forms may have been removed from this thesis.

While these forms may be included in the document page count, their removal does not represent any loss of content from the thesis.

Conformément à la loi canadienne sur la protection de la vie privée, quelques formulaires secondaires ont été enlevés de cette thèse.

Bien que ces formulaires aient inclus dans la pagination, il n'y aura aucun contenu manquant.

Canada

Abstract

The Skeena Fold Belt in northwest British Columbia encompasses the Jurassic-Cretaceous Bowser Basin. Structural mapping indicates that northeast-trending folds, dominant in the west, formed first; these were overprinted by northwest-trending folds, recognized. *En echelon* vein arrays and brittle faults associated with F2 folds indicate relatively brittle conditions. A local brittle D3 deformation, represented by predominantly strike-slip conjugate faults resulted from north-south shortening. Cleavage is most strongly developed along the west of the fold belt and resulted from pressure solution. Strain shadows represent new mineral growth during deformation. Preliminary whole rock argon geochronology from the western basin margin yields partial plateau ages between 128 and 146 Ma, interpreted as the ages of cleavage development. Deformation probably began in earliest Cretaceous time, coeval with late sedimentation in the Bowser Basin. Structural relationships are consistent with hypothesized sinistral transpression along the paleo-Pacific margin followed by convergence and late strike-slip deformation.

Acknowledgements

There are many people deserving of thanks for their assistance with this thesis during its preparation.

First of all I would like to thank my supervisor, Dr. John Waldron, whose support and enthusiasm for this project and all aspects of geology continues to be an inspiration. His diverse knowledge and willingness to teach and ponder new findings greatly benefited this project.

The remote fieldwork conducted in this study could not have been accomplished without the help of my field assistants: Heidi Tomes, Cordell Bloomberg, and Jeff Samson. Their presence kept me safe, light-hearted and on track through many minor triumphs, mishaps, bear encounters and bizarre weather.

Fellow graduate student and Bowser Basin colleague Jean-François Gagnon was invaluable for collaboration, sharing logistical responsibilities and his knowledge of the stratigraphic aspects of the Bowser Basin. He and Kenny Wallace were excellent office-mates when we returned from the field.

Financial support for logistical operations of this project was provided by grants from GeoscienceBC, in part delivered through the Geological Survey of Canada. Lab analyses were supported by an NSERC Discovery grant to Dr. John Waldron. The department of Earth and Atmospheric Sciences at the University of Alberta provided TA and RA funding during completion of the thesis.

The Spatsizi Plateau Wilderness Park, Eskay Creek gold mine and Sabina Silver were all gracious in allowing us to visit their areas and conduct research. In particular I would like to thank Ted Mahoney of Barrick Gold and Tony Baressi of Sabina Silver for helping to arrange access. The excellent people of Stewart, BC and Hyder, Alaska also made for enjoyable and productive logistical planning days, and some excellent Alaskan King Crab.

I owe thanks to many members of the Geological Survey of Canada for conducting the previous work necessary to inspire this project. In particular I am grateful to Carol Evenchick, Margot McMechan, Dave Ritcey and Jamel Joseph for collaboration, discussion and technical support. Thanks to Thomas Ullrich for performing Ar-Ar analyses at the University of British Columbia Argon Geochronology Laboratory.

I would also like to thank Sergei Matveev for assisting with microprobe analyses and many other members of the staff at the department of Earth and Atmospheric Sciences whose work behind the scenes allow projects like mine to come to fruition.

My many friends at the University of Alberta were instrumental in providing expertise outside my working knowledge, discussion, and support away from home.

Lastly, I would like to thank my family for their many years of continued support during my education.

Table of Contents

Chapter 1: Introduction 1

1.1 Regional Stratigraphic Units 2

1.1.1 Stikine Assemblage 2

1.1.2 Stuhini Group 6

1.1.3 Hazelton Group 6

1.1.4 Bowser Lake Group 9

1.1.4-1 Ritchie-Alger assemblage 10

1.1.4-2 Todagin assemblage 10

1.1.4-3 Skelhorne assemblage 10

1.1.4-4 Eaglenest assemblage 11

1.1.5 Maitland Volcanics 11

1.2 Regional Structural Relationships 12

1.2.1 Generalized structural geometry 12

1.2.2 Regional geology beyond fold belt margins 13

1.2.3 Timing constraints on deformation 15

1.2.4 Hypotheses for development 17

1.3 Mapping Methodology 22

Chapter 2: Folds and related structures 23

2.1 Background 23

2.1.1 Fold Terminology 23

2.2 Field Observations 23

2.2.1 Maitland plateau 23

2.2.2 Mount Will 26

2.2.3 Cartmel Lake 32

2.2.4 Sweeny Creek 37

2.2.5 Oweegee Dome 43

2.2.6 Iskut ridge 47
2.2.7 Eskay Creek 54
2.2.8 Teigen Lake 57
2.2.9 Nelson Creek 60
2.3 Discussion of Folds and Related Structures 66
Chapter 3: Veins and Brittle Structures 70
3.1 Background 70
3.1.1 Fault terminology and methodology 70
3.1.2 *En echelon* vein terminology 74
3.2 Field Observations 77
3.2.1 Maitland plateau 77
3.2.2 Mount Will 77
3.2.3 Cartmel Lake 82
3.2.4 Sweeny Creek 82
3.2.5 Oweegee Dome 89
3.2.6 Iskut ridge 91
3.2.7 Eskay Creek 95
3.2.8 Teigen Lake 96
3.2.9 Nelson Creek 98
3.3 Discussion of Veins and Brittle Structures 100
Chapter 4: Microstructural Analysis and Geochronology 103
4.1 Introduction 103
4.2 Cleavage – Field relationships 104
4.3 Microscopic observations 105
4.3.1 Spaced Cleavage 105
4.3.2 Slaty Cleavage 106
4.3.3 Metamorphic Minerals 108

4.3.4 Strain Indicators 110
4.4 Ar-Ar Geochronology 114
4.4.1 Cleaved Samples 114
4.4.2 Mafic Post-Kinematic Dike 118
4.5 Discussion of Microstructures and Geochronology 122
Chapter 5: Discussion 125
5.1 Introduction 125
5.2 Pre-D1 Structures (Early Jurassic or older) 125
5.3 D1 Structures (Late Jurassic to Early Cretaceous) 126
5.4 D2 Structures (Early to Late Cretaceous) 128
5.5 D3 Structures (Paleogene?) 130
5.6 Tectonic Synthesis 131
5.6.1 Models developed within the Skeena Fold Belt 131
5.6.2 Baja BC Hypothesis 136
5.6.3 Terrane Rotation 138
5.6.4 Summary 141
5.7 Conclusions 143
References 144
Appendix A - Supplement to Ar-Ar Geochronology 152

List of Tables

Table 4.1: Summary of lithologic and cleavage properties of samples collected for purpose of cleavage description.....106

Table 4.2: Table of properties of strain shadows measured and calculated finite elongations (*e*).....116

List of Figures

Figure 1.1: Simplified geological map of the Bowser Basin. 3

Figure 1.2: Summary of stratigraphic units discussed in text. 4

Figure 1.3: Major tectonic elements in the vicinity of the Skeena Fold Belt. 5

Figure 1.4: Simplified map of the northwest fold belt with study area locations. 7

Figure 1.5: Diagram illustrating previous model of development for fold belt 21

Figure 2.1: Structural map of the Maitland plateau area. 25

Figure 2.2: Equal-area projections of data from Maitland plateau. 25

Figure 2.3: Structural map of the Mount Will area. 27

Figure 2.4: Natural scale cross-section of the Mount Will area. 28

Figure 2.5: View of the Mount Will Thrust and associated gouge. 30

Figure 2.6: Equal-area projections of data from Mount Will area. 31

Figure 2.7: Panorama of asymmetric anticline in the Mount Will area. 31

Figure 2.8: Syncline in the Mount Will area cut by multiple faults. 32

Figure 2.9: Structural map of the Cartmel Lake area. 34

Figure 2.10: Metre-scale outcrop in Cartmel Lake displaying fold interference. 35

Figure 2.11: Panorama towards the southeast of km-scale NW-trending anticline. 36

Figure 2.12: Equal-area projections of data from Cartmel Lake area. 36

Figure 2.13: Schematic diagram of faulted outcrop in the Cartmel Lake area. 37

Figure 2.14: Panorama of NE-trending anticline and detachment in Cartmel Lake. 37

Figure 2.15: Structural map of the Sweeny Creek area. 39

Figure 2.16: View towards ESE of folded strata in the Sweeny Creek area. 40

Figure 2.17: Equal-area projections of poles to bedding collected along fold traces in the southeast Sweeny Creek area. 41

Figure 2.18: Equal-area projections of data from Sweeny Creek area. 41

Figure 2.19: Equal-area projections separating structure data from the northwest of Sweeny Creek and data from the southeast of Sweeny Creek. 42

Figure 2.20: Geological maps of the Oweegee Dome area. 44

Figure 2.21: Equal-area projections of data from Oweegee Dome. 46

Figure 2.22: View to NW of shale with three strong fabrics developed. 47

Figure 2.23: Exposures of folds in the southern Oweegee Dome area. 48

Figure 2.24: View to SSW of F1 anticline at Iskut Ridge. 49

Figure 2.25: View to north of F1 syncline in Iskut Ridge area. 49

Figure 2.26: Structural map of the Iskut ridge area. 50
Figure 2.27: F2 folds in the Iskut ridge area. 51
Figure 2.28: Outcrop-scale fold interference in the Iskut ridge area. 52
Figure 2.29: Equal-area projections of structure data from Iskut ridge. 53
Figure 2.30: Schematic W-E natural scale cross-section of the Iskut ridge area. 54
Figure 2.31: Structural map of the Eskay Creek area. 55
Figure 2.32: Succession of tight folds in the Eskay Creek area. 56
Figure 2.33: Equal-area projections of data from Eskay Creek area. 56
Figure 2.34: Strained ammonite in the Eskay Creek area. 57
Figure 2.35: Distorted S1 cleavage in the Eskay Creek area. 58
Figure 2.36: Structural map of the Teigen Lake area. 59
Figure 2.37: View to east of anticline-syncline pair in the Teigen Lake area. 60
Figure 2.38: Equal-area projections of data from Teigen Lake area. 60
Figure 2.39: Elongate lapilli tuffs in the Nelson Creek area. 62
Figure 2.40: Structural map of Nelson Creek area. 63
Figure 2.41: Complexly deformed sediments in the Nelson Creek area. 64
Figure 2.42: Equal-area projections of data from Nelson Creek area. 65
Figure 2.43: Schematic cross-sections of ridges in the Nelson Creek area. 65
Figure 2.44: Schematic diagram illustrating possible relationship between structures in the Nelson Creek area and a basement wedge. 69
Figure 3.1: Schematic block diagram of hypothetical fault illustrating fault terminology. 72
Figure 3.2: Equal-area projection illustrating method of P-T Dihedra 73
Figure 3.3: Schematic diagram of circular region cut by multiple faults to illustrate summation used in developing Linked Bingham Analysis. 74
Figure 3.4: Schematic idealized *en echelon* veins. 75
Figure 3.5: Joints in the Maitland plateau area 78
Figure 3.6: FaultKinWin plot of steep faults from Mount Will area. 79
Figure 3.7: View of *en echelon* veins in the Mount Will area near fold 80
Figure 3.8: Plot of steep faults from Cartmel Lake area constructed using FaultKinWin 83
Figure 3.9: Horse with convoluted internal structure bounded by lateral faults. 84
Figure 3.10: Fault surface in Sweeny Creek area. 85

Figure 3.11: Veins from a glacially polished outcrop in Sweeny Creek area. 86
Figure 3.12: Model of *en echelon* vein development in the Sweeny Creek area. 88
Figure 3.13: View towards SSE of horst in the Oweegee Dome area. 90
Figure 3.14: Gossanous weathering near faults in the Oweegee Dome area. 91
Figure 3.15: Sigmoidal asymmetric *en echelon* veins in the Iskut River area. 92
Figure 3.16: Arrays of *en echelon* veins from the Iskut River area. 94
Figure 3.17: Minor fault with synthetic Riedel shears in the Eskay Creek area. 95
Figure 3.18: Successive parallel fault planes with slickenline lineations. 96
Figure 3.19: Outcrop of NE-trending fold from the Eskay Creek area. 97
Figure 3.20: Veins in the lower Hazelton Group of the Nelson Creek area. 99
Figure 4.1: Images of spaced cleavage and amorphous residue lining cleavage. 107
Figure 4.2: CP electron microprobe images of anastamosing cleavage. 108
Figure 4.3: Thin section photomicrographs of conglomerate grain dissolution. 109
Figure 4.4: Thin section photomicrograph of cleavage-parallel pressure solution. ... 109
Figure 4.5: Thin section photomicrograph of conglomerate stylolitic dissolution. ... 110
Figure 4.6: Thin section photomicrograph of cleavage in the Eskay Creek area. 111
Figure 4.7: Images of strain shadows developed in rocks of the Eskay Creek area... 113
Figure 4.8: Thin section photomicrographs of strain shadows developed around elongate grains. 114
Figure 4.9: Strain analysis using strain shadows from the Eskay Creek area. 115
Figure 4.10: First-run Ar-Ar Age versus 39Ar % plots. 120
Figure 4.11: Inverse isochron 36Ar/40Ar vs. 39Ar/40Ar plots 121
Figure 4.12: Mafic dike in the Eskay Creek area dated using Ar-Ar dating 122
Figure 5.1: Limits of D1 structures described by this study. 129
Figure 5.2: Schematic SW-NE cross-section through the Skeena Fold Belt. 131
Figure 5.3: Model of development of the Skeena Fold Belt relative to structures in the Coast Belt. 137
Figure 5.4: Schematic diagram illustrating hypothesized northward translation and clockwise rotation of the Intermontane belt 139
Figure 5.5: Diagram of hypothesized Cordilleran orocline development. 140

Chapter 1: Introduction

This thesis aims to disentangle the structural relationships and development of the Mesozoic Skeena Fold Belt, located in northwestern British Columbia. Its central location and size in the northern Canadian Cordillera make understanding the Skeena Fold Belt critical to developing an integrated and cohesive history for adjacent parts of the Cordillera. Understanding the structural relationships which form the fold belt has potential benefits for aiding petroleum and mineral exploration within and adjacent to the vast sedimentary basin underlying the fold belt.

The primary method of this study is structural and stratigraphic mapping, conducted in the field. The main objective was to ascertain the relative timing relationships, overprinting, and styles of fold sets within each field area with enough detail to develop a regional picture of the deformation in the northwest Skeena Fold Belt. Brittle structures, such as faults, veins, and joints are less readily recognized but prove of great value in determining the deformation history and mechanisms. Folds and associated structures are described in Chapter 2, while veins and brittle structures follow in Chapter 3. Samples processed into thin sections for analysis of cleavage, strain shadows and metamorphic minerals are described in Chapter 4. To provide absolute timing constraints on deformation, cleaved siltstones were radiometrically dated using whole-rock Ar-Ar geochronology. A mafic dike that crosscuts a fold was also dated. This geochronology work is also included in Chapter 4.

This study integrates detailed mapping completed in several locations throughout the northwestern fold belt with lab-based structural analysis and geochronology to develop a more complete understanding of the origins of the Skeena Fold Belt. Folds that trend to the northwest were found to overprint northeast-trending folds. A newly identified late-stage brittle deformation has also been recognized. Thin section petrography indicates cleavage consistently forms through pressure solution processes and is more closely spaced than apparent from outcrop. New mineral growth is

identified in strain shadows that can be used as a kinematic indicator and targeted for Ar-Ar geochronology. These findings greatly improve constraints on the timing of fold development.

1.1 Regional Stratigraphic Units

The Skeena Fold Belt is located in northwestern British Columbia in the northern Intermontane physiographic belt of the Canadian Cordillera (Monger et al., 1972) (figure 1.1). The Skeena Fold Belt as defined by Evenchick (1991a) incorporates deformed Jurassic and Cretaceous marine and non-marine clastic rocks of the Bowser Lake and Sustut Groups (figure 1.2), deposited within the Bowser and Sustut Basins (figure 1.3), respectively (Eisbacher 1974b; Tipper and Richards, 1976; Evenchick and Thorkelson, 2005). The Stikine assemblage, Stuhini Group, and Hazelton Group of Devonian to Middle Jurassic age (Monger, 1977) underlie the Bowser Lake Group and are also considered to be part of the fold belt where they include contractional structures developed after the onset of deposition of the Bowser Lake Group in the Middle Jurassic (Evenchick 1991a).

1.1.1 Stikine Assemblage

The Stikine assemblage ranges in age from Early Devonian to Late Permian (Monger, 1977). It represents the oldest known rocks in the vicinity of the Skeena Fold Belt, interpreted by some authors (Logan et al., 1992; Anderson, 1993) to represent the basement in the region (figure 1.2). However, Thorkelson et al. (1995) proposed the existence of a basement older than the Stikine assemblage shown by Precambrian zircon inheritance in the Hazelton Group. Devonian units include highly deformed metavolcanic tuff, limestone, schist, argillite, mafic and felsic flows, and epiclastic rocks (Logan and Koyanagi, 1989; Logan et al. 1992, 2000). Carboniferous units are less deformed and primarily include reefal limestone and chert, and thin volcaniclastic rocks, hyaloclastite, tuff, and pillow basalt (Anderson, 1989; Logan et al., 1992, 2000). Permian

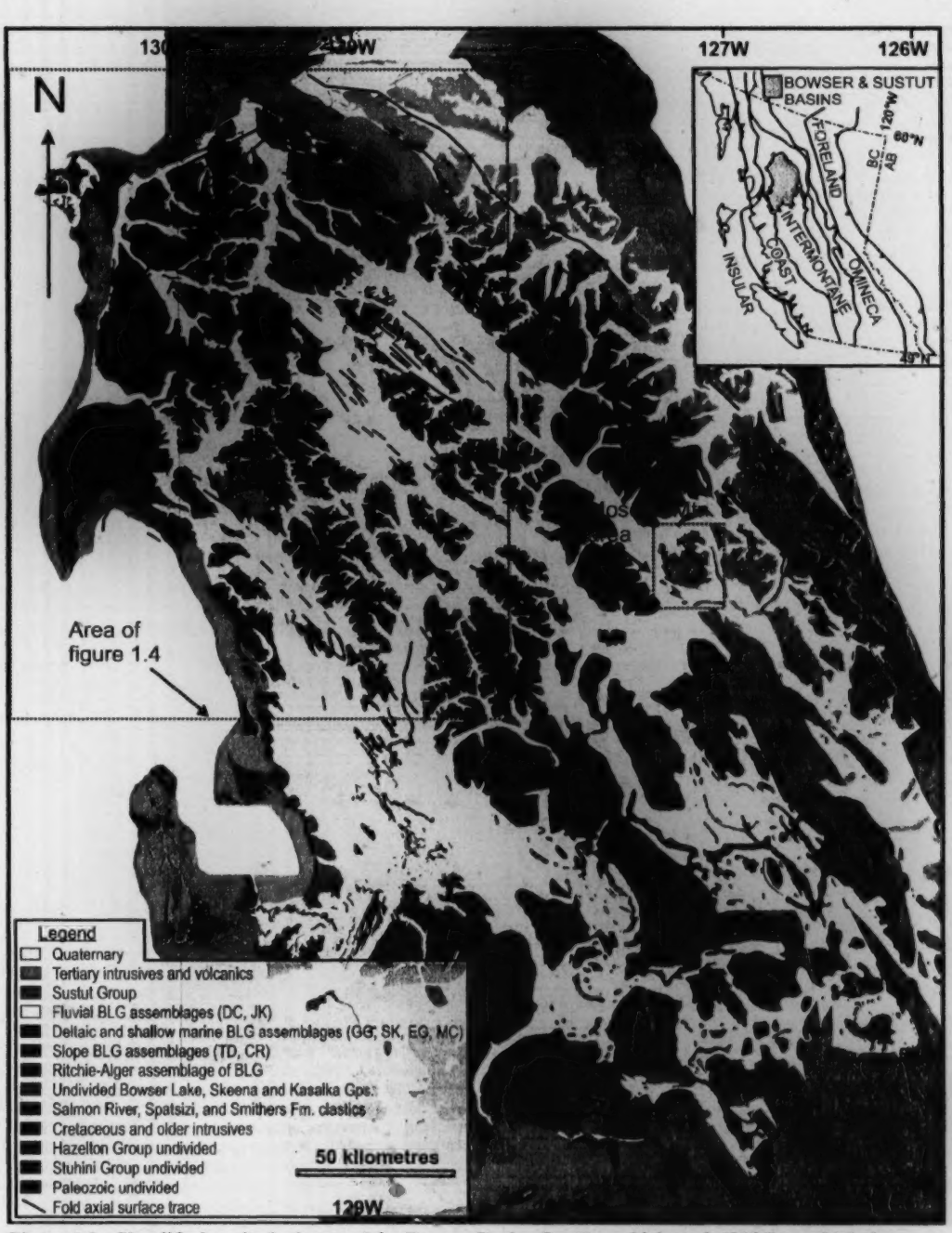

Figure 1.1: Simplified geological map of the Bowser Basin after Evenchick et al. (2006) to which the reader is referred. Stratigraphic units have been grouped for clarity based on similar ages and depositional settings. Ages and relations of most units are shown in figure 1.2 and discussed in text. Abbreviations: BLG-Bowser Lake Group, DC-Devil's Claw, JK-Jenkin's Creek, GG-Groundhog-Gunanoot, SK-Skelhorne, EG-Eaglenest, MC-Muskaboo Creek, TD-Todagin, CR-Cranberry River. Stratigraphy and fold trends from Evenchick et al. (2006). Inset: Location of basin within major physiomorphic belts of the Canadian Cordillera, from Wheeler et al. (1991) and Evenchick et al. (2002).

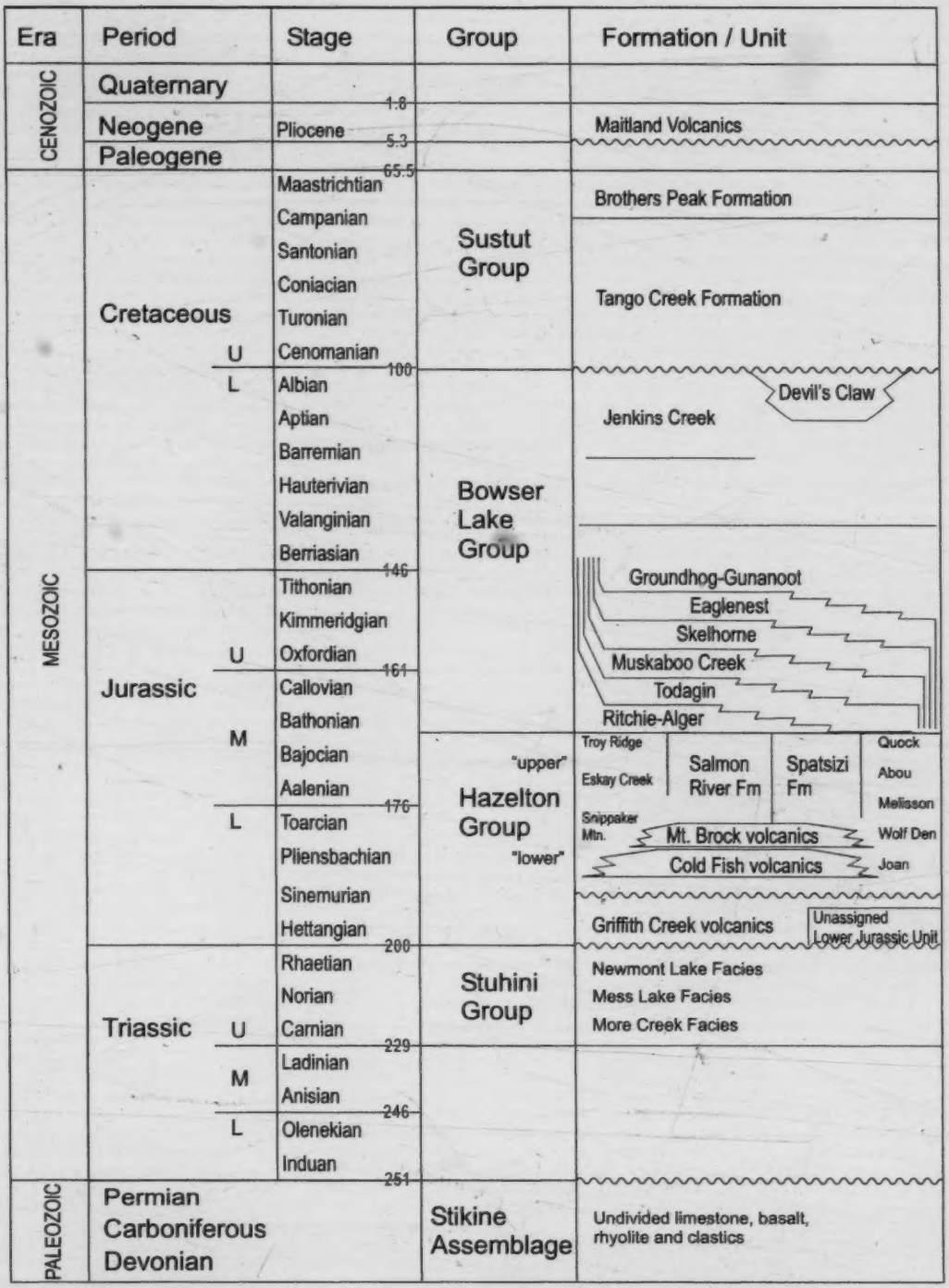

Figure 1.2: Summary of stratigraphic units in the Skeena Fold Belt. Stages not shown for all periods. Dotted lines indicate inferred contact relationships. Modified from Evenchick and Thorkelson (2005), additions from Logan et al. (2000) and Anderson (1993). Time scale from Gradstein et al. (2004).

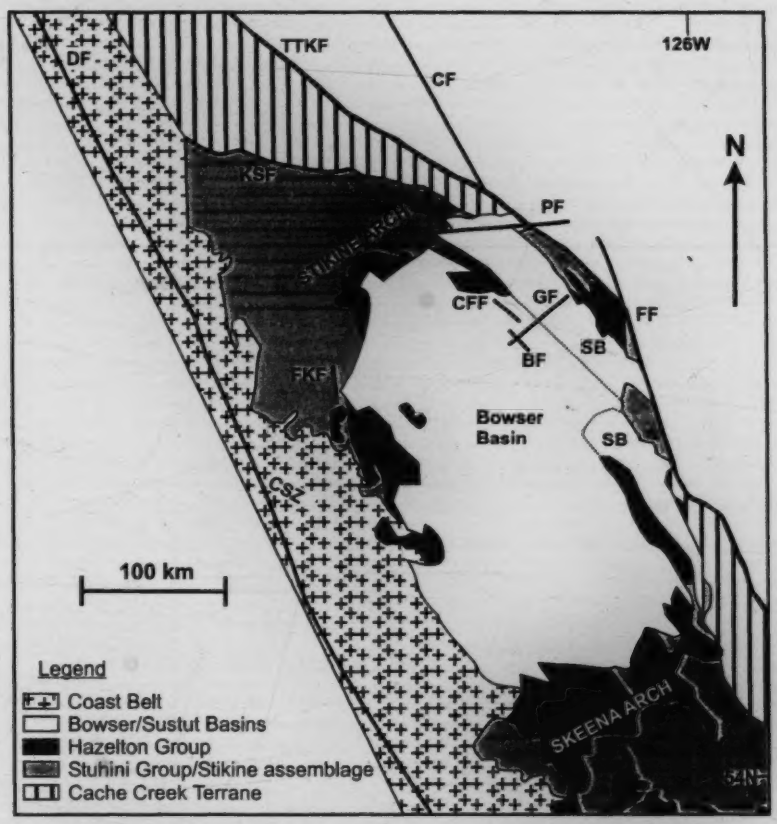

Figure 1.3: Major tectonic elements and faults in the vicinity of the Skeena Fold Belt. Faults approximately located. Abbreviations: SB-Sustut Basin, DF-Denali Fault, KSF-King Salmon Fault, TTKF-Teslin-Thibert-Kutcho Fault, CF-Cassiar Fault, PF-Pitman Fault, GF-Griffith Fault, FF-Finlay Fault, CFF-Cold Fish Fault, BF-Buckinghorse Fault, FKF-Forrest Kerr Fault, CSZ-Coast Shear Zone. Compiled from Marsden and Thorkelson (1992), Logan et al. (2000), Evenchick and Thorkelson (2005) and Gabrielse et al. (2006).

units are dominated by thick regionally extensive limestone successions that have been noted by many authors (Anderson, 1989; Logan and Koyagani, 1989; Brown and Greig, 1990; Gunning, 1990; Brown et al., 1992; Logan et al., 1992; Evenchick and Thorkelson, 2005) and lesser chert, cobble conglomerate, siltstone, sandstone, and felsic flows (Logan et al., 2000). The only exposure of Stikine assemblage in the areas studied occurs in the centre of Oweegee Dome (Greig and Evenchick, 1993) (figure 1.4). Metamorphism in the Stikine assemblage reaches greenschist facies (Read et al., 1991) with an early stage

of metamorphism occurring during Devonian deformation (Logan et al., 2000).

1.1.2 Stuhini Group

The Stuhini Group comprises Upper to Middle Triassic volcanic and sedimentary rocks exposed to the north and west of the current Bowser Basin. It unconformably overlies limestone of the Stikine assemblage (Brown et al., 1992; Logan et al., 2000). Volcanic rocks include basalt, felsic sills, dacite, andesite, and tuff, while sedimentary rocks include ribbon chert, limestone, volcaniclastic sandstone, pebble conglomerate, siltstone and shale (Read and Psutka, 1990; Logan et al., 1992, 2000; Greig and Evenchick, 1993; Evenchick and Thorkelson, 2005). Volcanic rocks are more common in the west, and pass into mainly sedimentary rocks in the east (Anderson and Thorkelson, 1990). The Stuhini Group is interpreted to represent a Triassic arc accumulated in a submarine environment (Logan et al., 2000).

1.1.3 Hazelton Group

The Hazelton Group is a diverse Early to Middle Jurassic assemblage of volcanic and sedimentary rocks (Marsden and Thorkelson, 1992). The Hazelton Group lies unconformably above the Stuhini Group. According to Marsden and Thorkelson (1992) the Hazelton Group was deposited on the flanks of an incipient rift; volcanism was the product of two volcanic arcs generated by convergent subduction zones beneath the Stikine terrane.

The Hazelton Group is for the purposes of this study informally divided into the lower and upper Hazelton Group on the basis of age and lithology. Volcanic and associated sedimentary rocks of Early Jurassic age are referred to as lower Hazelton Group, while primarily fine-grained sedimentary rocks of late Early to early Middle Jurassic age are referred to as upper Hazelton Group.

Major subdivisions of the lower Hazelton Group in the regions of study are the Griffith Creek, Cold Fish and Mount Brock volcanics (figure 1.2). The Griffith Creek

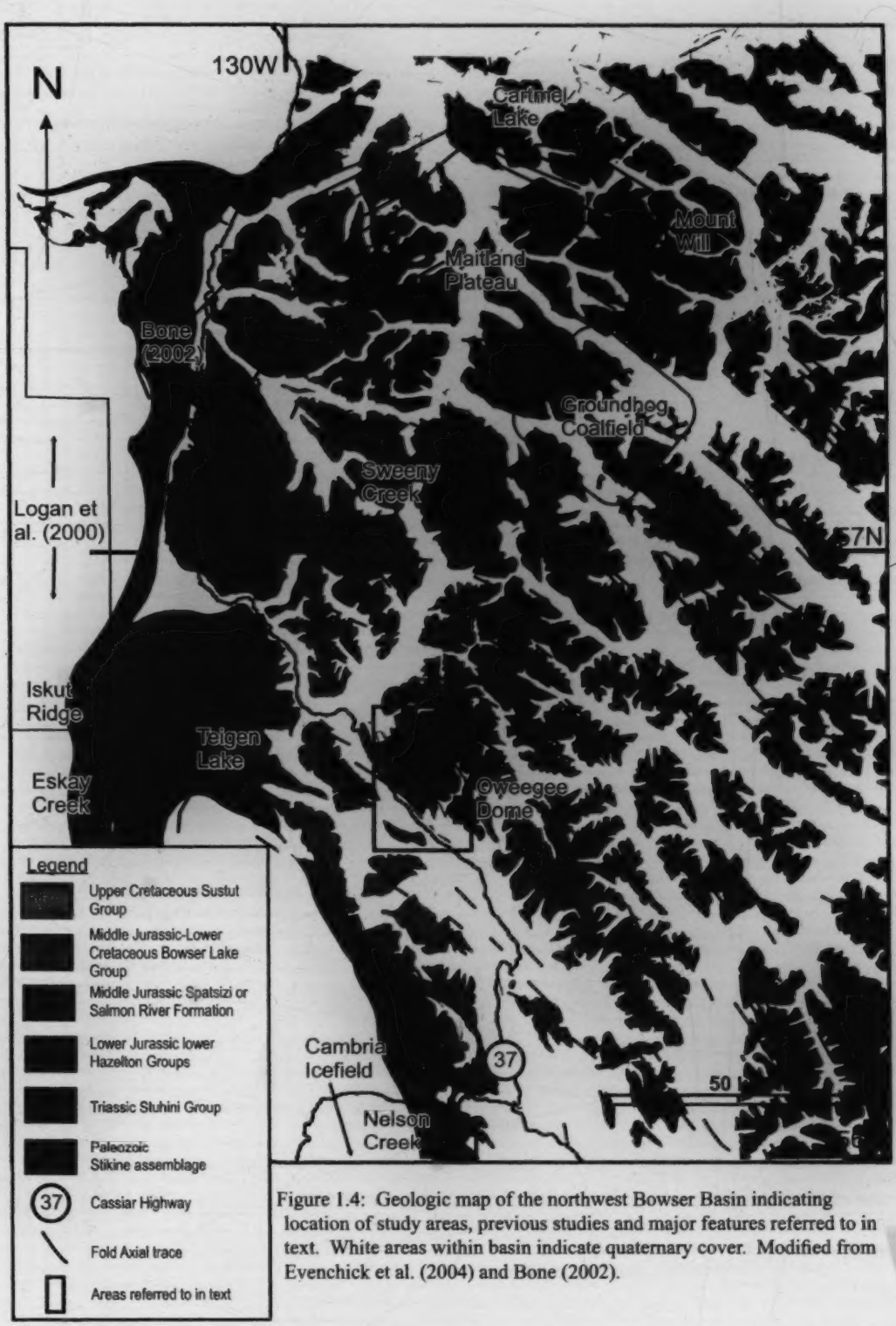

Figure 1.4: Geologic map of the northwest Bowser Basin indicating location of study areas, previous studies and major features referred to in text. White areas within basin indicate quaternary cover. Modified from Evenchick et al. (2004) and Bone (2002).

volcanics are primarily mafic and intermediate flows, subaerially formed tuffs and ignimbrite. The Cold Fish Volcanics include bimodal basalt and rhyolite flows, tuff and ignimibrite with a minor proportion of sedimentary rocks (Evenchick and Thorkelson, 2005). The Mount Brock volcanics are primarily mafic to felsic flows with thin limestone interbeds and represent the last major period of volcanic activity during Hazelton Group time (Marsden and Thorkelson, 1992; Evenchick and Thorkelson, 2005). The Mount Brock volcanics are here considered as transitional between the lower and upper Hazelton Group, as in some localities the Mount Brock volcanics overlie rocks assigned to the upper Hazelton Group Spatsizi Formation (Evenchick and Thorkelson, 2005). Other rock types in the lower Hazelton Group include volcaniclastic and clastic conglomerate, sandstone and shale (Anderson, 1993; Evenchick and Thorkelson, 2005).

The nomenclature in the upper Hazelton Group varies according to position in the vicinity of the basin. In the Spatsizi area (northeast Bowser Basin), the volcanic and sedimentary rocks assigned to the lower Hazelton Group are overlain by the Spatsizi Formation (Evenchick and Thorkelson, 2005), whereas along the western margins of the basin and around Oweegee Dome this stratigraphic position is occupied by the Salmon River Formation (Marsden and Thorkelson, 1992) (figure 1.2). The Spatsizi Formation has been divided into several members: the Quock, Abou, Melisson, Wolf Den, and Joan members (Thomson et al., 1986; Evenchick and Thorkelson; 2005). The latter four are generally fine-grained clastic rocks, but range from shale to conglomerate; these units are not common outside of their type area and were not identified in the areas of this study. The Quock member comprises thinly interbedded siliceous siltstone, shale, and tuffaceous shale, and has a much more widespread distribution.

The major units of the Salmon River Formation are a lowermost sedimentary unit of shale and siltstone with lesser sills and flows, a medial unit of pillowed basalt and breccia in the west, and an uppermost unit composed of thinly interbedded siliceous siltstone and tuffaceous shale (Troy Ridge Facies, figure 1.2) that grades into the Bowser

Lake Group (Anderson and Thorkelson, 1990; Anderson, 1993; Logan et al., 2000). The Troy Ridge Facies is equivalent to the Quock member of the Spatsizi Formation (Anderson and Thorkelson, 1990). A lateral equivalent of the Troy Ridge Facies of pebble and boulder conglomerate is documented to the east around Oweegee Dome (Greig and Evenchick, 1993).

1.1.4 Bowser Lake Group

The Bowser Lake Group consists of clastic rocks ranging from shale to conglomerate now known to have been deposited from the Middle Jurassic through most of the Early Cretaceous (Evenchick and Thorkelson, 2005). Minor metamorphism in the Bowser Lake Group does not reach greenschist facies (Read et al., 1991). Vitrinite reflectance (Ro_{max}) values differ by author and range from 5.8% to <2.0% (Bustin and Moffat, 1989) in the Groundhog Coalfield (figure 1.4) to basin-scale variation from >2.5% to <0.5% (Evenchick et al., 2002). Deposition occurred in the Bowser Basin (Tipper and Richards, 1976), which is bounded by the Stikine Arch, Cache Creek terrane and Sustut Basin, Skeena Arch, and Coast Belt to the north, east, south, and west respectively (figure 1.3). Clasts are most commonly chert; paleocurrent studies suggest southwest-directed transport (Eisbacher, 1974a; Green, 1992; Evenchick and Thorkelson, 2005). This has been interpreted to indicate provenance from the Cache Creek terrane (Green, 1992; Evenchick and Thorkelson, 2005), a likely source of abundant chert (Monger, 1977). This helps distinguish the Bowser Lake Group from the Hazelton and Sustut Groups. Other clast types include felsic volcanic lithic fragments, granitoid lithics, quartz and detrital glauconite, and local abundances of chlorite-rich rock fragments (Evenchick and Thorkelson, 2005). The basin has been interpreted to have developed due to flexural subsidence resulting from the obduction of the Cache Creek terrane to the northeast (Ricketts et al., 1992). Alternatively, the basin has been hypothesized to have formed due to extension in a pre-existing backarc basin, subsiding due to thermally

driven subsidence (Marsden and Thorkelson, 1992; Anderson, 1993).

The Bowser Lake Group has been subdivided into a number of informal assemblages based on lithology and interpreted facies due to the lack of distinctive basin-wide markers and the diachronous boundaries between the various strata that make formalized stratigraphy less feasible and useful (Evenchick et al., 2001; Evenchick and Thorkelson, 2005). General descriptions of these assemblages follow.

1.1.4-1 Ritchie-Alger assemblage

The Ritchie-Alger assemblage is a thick (up to 1800 m) succession of sandstone, siltstone, shale, and lesser conglomerate (Evenchick and Thorkelson, 2005). Most commonly these rocks are deposited as sheets, from centimetres to tens of metres thick. Lateral pinch-outs are relatively rare. Many beds are massive; those sedimentary structures that are present include planar and ripple cross-laminations, flute and groove casts, graded bedding, synsedimentary dikes and slump folds. These features have led to the interpretation that the Ritchie-Alger assemblage formed due to accumulation of turbiditites and debrites in a submarine fan complex (Evenchick et al., 2001; Evenchick and Thorkelson, 2005).

1.1.4-2 Todagin assemblage

The Todagin assemblage (Evenchick et al., 2001) is a relatively fine-grained unit formed mostly of thinly interbedded siltstone and shale. Sandstone and channelized conglomerate are also present. Sedimentary structures such as parallel and cross-lamination, loading structures, and graded bedding are common. This unit has been interpreted to have formed in a slope environment, with sandstones and conglomerates occupying submarine channels (Evenchick et al., 2001; Evenchick and Thorkelson, 2005).

1.1.4-3 Skelhorne assemblage

The Skelhorne assemblage (Evenchick et al., 2001) comprises thin to thickly

bedded siltstone, shale and conglomerate commonly arranged in coarsening-upward cycles capped by chert-pebble conglomerate. Wood fragments and sedimentary structures such as wave ripples exposed on bedding surfaces, parallel and cross-lamination, flaser lamination, and bioturbation expressed as *Skolithos* and *Diplocraterion* are found in this highly variable unit (Evenchick and Thorkelson, 2005). Wood fragments, bivalves, and trace fossils identified as *Scolicia* (pers. comm. M.Gingras, 2005) in the areas studied are found in local concentrations in medium-grained, rusty-weathering sandstone. Distinctive thin to medium orange sandstone beds with a calcareous matrix are interpreted to have resulted from a process of calcareous cementation. The Skelhorne assemblage is interpreted to have formed in a moderate-energy deltaic environment (Evenchick et al., 2001; Evenchick and Thorkelson, 2005).

1.1.4-4 Eaglenest assemblage

The Eaglenest assemblage (Evenchick et al., 2001) is found primarily in the northern Bowser Basin and consists of clast-supported pebble conglomerate and sandstone with small amounts of siltstone and coaly beds. Conglomerate is dominant and in some locations represents over 80% of stratal thickness. Strata are arranged in coarsening-upward cycles and have large cross beds sometimes with large foresets. These features have led to the interpretation that the Eaglenest assemblage formed in a high-energy deltaic environment (Evenchick et al., 2001; Evenchick and Thorkelson, 2005).

1.1.5 Maitland Volcanics

The Maitland volcanics are a Pliocene unit of volcanic flows and feeder pipes in the north-central Bowser Basin. They are composed of aphyric and feldspar-phyric basalt with lesser trachyte (Evenchick and Thorkelson, 2005). The Maitland volcanics are

relatively flat-lying and unconformably overlie folded rocks of the Bowser Lake Group.

1.2 Regional Structural Relationships

1.2.1 Generalized structural geometry

The dominant structures in the Skeena fold belt are gently-plunging folds that have axial traces trending NW-SE (figure 1.1) (Evenchick, 1991a; Evenchick and Thorkelson, 2005). This type of structure dominates the eastern two-thirds of the fold belt and is in subparallel alignment to the major structural grain in the Canadian Cordillera (Wheeler and McFeely, 1991). The western third of the fold belt is composed of several domains of folds, most of them trending to the NE-SW (Evenchick, 1991a, 2001; Evenchick and Thorkelson, 2005). Locally these two fold sets overprint each other (Evenchick, 2001; Bone, 2002), occasionally showing clear type I interference patterns (Ramsay, 1967). Thrust faults have been shown to be associated with folding (Evenchick, 1991a, b; Evenchick and Thorkelson, 2005), though there are markedly fewer identified thrust faults than folds. Strike-slip faults are expressed sporadically in the fold belt as are brittle veins. Steep normal faults with hundreds of metres of dip-slip movement result in block-like map patterns that have been documented in the northeastern fold belt (Evenchick, 1987; Evenchick et al. 2004). Diagrams and cross-sections illustrating the structure of the fold belt are presented by Evenchick and Thorkelson (2005), and in Chapter 5.

The tightness of folds within the fold belt is variable (Evenchick, 1991a), with most being open or close, and fewer gentle or tight folds (classification of Fleuty, 1964). The wavelength of folds varies from outcrop scale to kilometre scale. Vergence is predominantly to the northeast. Hinterland (SW) vergent thrust faults have been identified in a triangle zone in the Sustut Basin (Evenchick, 1991a). Several prominent thrust faults have been identified in a number of areas around the fold belt that suggest thrust faults are a major mechanism to accommodate shortening and are intimately

involved in deformation (Eisbacher, 1974b; Moffat and Bustin, 1993; Evenchick 1991a, b; Evenchick and Thorkelson, 2005). The fold belt has been interpreted to have developed as a classical fold and thrust belt similar to that of the Rocky Mountains (Moffat, 1985; Evenchick, 1991a). In general the number of documented thrusts appears to be insufficient to account for the degree of folding in the fold belt. This has been attributed to the presence of blind thrusts, or to a lack of correlatable horizons suitable for recognizing bedding cutoffs in the large thicknesses of similar strata in the fold belt (Evenchick, 1991a).

1.2.2 Regional geology beyond fold belt margins

The Skeena Fold Belt is bounded to the east by the Cache Creek terrane (figure 1.3) a narrow strip along the eastern edge of the Intermontane Belt, consisting of chert, argillite, carbonate, and ultramafics. The Cache Creek Group is considered to have formed in an ocean basin east of the Stikine terrane (Monger, 1977). Obduction of Cache Creek Group rocks onto the Stikine terrane during the early Middle Jurassic is interpreted as marking the closure of the Cache Creek basin (Monger, 1977; Ricketts et al., 1992). The influx of chert-rich clasts into the Bowser Basin sourced from Cache Creek indicates subaerial exposure of the latter during the Bajocian. Currently rocks of the Stikine terrane (Takwahoni Formation) north of the Bowser Basin are in thrust-faulted contact with the Cache Creek Complex along the King Salmon Fault (Gabrielse, 1998) (figure 1.3).

The Skeena and Stikine Arches are elongate NE-trending topographic highs forming the southern and northern margins of the Bowser Basin, respectively. The origins of these features are uncertain. They are likely to have been uplifted in the Early and Middle Jurassic and remained emergent throughout deposition of the Hazelton Group (Marsden and Thorkelson, 1992). Lower Jurassic plutonic rocks on both arches indicate that igneous activity was broadly coeval with uplift and that the two processes may be related. Some uplift of the Stikine Arch may have occurred by the Late Triassic as

indicated by conglomerate deposits north of, and derived from, the Stikine Arch (Marsden and Thorkelson, 1992). As the arches represent the boundaries of the Bowser Basin this suggests they remained emergent as the basin subsided. This is further supported in the south where stratigraphy above the Bowser Lake Group (Skeena Group) lies directly on volcanic rocks of the Hazelton Group (Tipper and Richards, 1976). Proposed origins of these features include buoyant uplift related to tectonic underplating that may have accompanied subduction, or convergence of Stikine terrane with neighbouring terranes (Marsden and Thorkelson, 1992).

The Bowser Basin is bounded to the west by the Coast Belt. At these latitudes the Coast Belt comprises a diverse array of intrusive, volcanic, and metamorphic rocks, including the Cretaceous to Tertiary Coast Plutonic Complex (Rusmore and Woodsworth, 1991). The Coast Belt also hosts the Coast Belt Thrust System, a middle to Late Cretaceous west-vergent thrust system (Rubin et al., 1990; Journeay and Friedman, 1993) and the Coast Shear Zone (Klepeis et al., 1998; McClelland and Mattinson, 2000). The rocks which host the plutonic rocks are poorly understood. A combination of several allochthonous terranes unique to the Coast Belt, portions of the Alexander and Stikine terranes, and fragments of pericratonic assemblages that may have formed proximal to the continental margin and were subsequently displaced have all been hypothesized to underlie and surround the plutonic rocks (Monger et al., 1982; Crawford et al., 1987; Rubin and Saleeby, 1991; Wheeler et al., 1991; Currie and Parrish, 1993; Journeay, 1993; Gareau and Woodsworth, 2000; Saleeby, 2000; Rusmore et al., 2000; Colpron et al., 2006; Israel et al., 2006).

The Coast Belt has been interpreted to contain the roots of the Skeena Fold Belt in the form of east-propagating detachment faults that have since been obliterated by widespread Cretaceous and Tertiary intrusion (Evenchick, 1991b). Convergence in the Coast Belt is depicted as the main engine behind development of the Skeena Fold Belt, and has been proposed to have propagated eastward to link the Skeena Fold Belt with

deformation in the Foreland Belt (Evenchick, 1991c).

1.2.3 Timing constraints on deformation

Multiple deformations have been recognized that occurred prior to development of the Skeena Fold Belt. Logan et al. (2000) examined strata including and beyond the northwest Bowser Basin (Forrest Kerr-Mess Creek Areas, figure 1.4) and identified multiple pre-Skeena Fold Belt phases of deformation they termed D1-D3. A Late Devonian contractional event (D1) visible in Stikine assemblage strata resulted in penetrative foliation and variably-oriented rootless isoclinal folding. A pre-Late Triassic deformation (D2) resulted in a penetrative foliation and NW-trending isoclinal folds. An early Jurassic contraction event (D3) resulted in E-plunging upright folds best recognized within Stuhini Group, below an Early Jurassic unconformity; uplift due to contraction likely resulted in this unconformity. The earliest Jurassic age of deformation is supported by folding of the Hettangian Griffith Creek volcanics prior to deposition of the Cold Fish Volcanics in the Pleinsbachian (Thorkelson et al., 1995). These deformations (D1-D3) may have influenced development of the Skeena Fold Belt by producing basement anisotropy.

The Sustut Basin provides the strongest framework for establishing timing constraints on development of the Skeena Fold Belt. The Sustut Basin has been interpreted to be a foreland basin formed in response to uplift during development of the Skeena Fold Belt (Evenchick, 1991a). The Sustut Group is a middle to Late Cretaceous clastic non-marine unit deposited in the Sustut Basin (figure 1.3) that has been subdivided into the Tango Creek and Brothers Peak Formations (Eisbacher, 1974b). A change in provenance in the Tango Creek formation from northeast sourcing in the lower parts of the formation to southwest sourcing in the upper Tango Creek Formation has been interpreted to result from a change in provenance to the Bowser Lake Group (Eisbacher, 1974b), a response to the developing Skeena Fold Belt. Eisbacher (1974b), conducting work near the Sustut Basin, noted deformed Hazelton Group volcanics unconformably

overlain by shales of the Bowser Lake Group. These shales were dated to be late Middle Jurassic (Callovian), and interpreted to indicate pre-Callovian deformation of the Hazelton Group. Eisbacher (1974b) also observed that much of the Sustut Group lies with angular unconformity upon the Bowser Lake Group or Hazelton Group and concluded that some deformation of Bowser Lake Group rocks must have preceded deposition of the Cretaceous (Barremian or Albian to Campanian; Evenchick and Thorkelson, 2005) Tango Creek Formation. This is confirmed by overlap of some thrust faults by the Tango Creek Formation indicating that deformation must have been taking place prior to the Late Cretaceous (Cenomanian or Albian, Evenchick and Thorkelson, 2005). The Sustut Basin also provides some constraint on the longevity of deformation, as the youngest rocks of the Late Cretaceous (early Maastrichtian) Brothers Peak Formation are folded (Evenchick and Thorkelson, 2005). This indicates deformation in this area was still active into the latest Cretaceous or early Tertiary.

Logan et al. (2000) working mostly west of the Bowser Basin (figure 1.4) recognized a Late Jurassic to Tertiary contraction event they termed D4A and D4B that is correlative with the Skeena Fold Belt. Open, upright chevron folds developed disharmonically. Associated cleavages strike N to NE and W to NW and produce pencil lineations. Logan et al. (2000) infer NNE-trending D4A folds predate NW-trending D4B folds. D4A folds are speculated to have formed in the Late Jurassic to Early Cretaceous and D4B folds in the Late Cretaceous to Tertiary. Late Tertiary E-W extensional faults and N-trending strike-slip fault systems are suggested to be related to dextral transpression.

Timing constraints provided by cross-cutting igneous bodies are limited in the Skeena Fold Belt. Greig et al. (1995) dated dikes and plutons in the west-central Bowser Basin (Cambria Icefield area, figure 1.4) that are post-kinematic with respect to folding of Oxfordian rocks. These dikes yielded an Eocene (51-48 Ma) age, thus bracketing deformation between the Late Jurassic and Eocene (Greig et al., 1995). Post-kinematic

intrusions in the southwest corner of the basin (Kinskuch Lake area) yield U-Pb ages suggesting emplacement at 53.7 Ma (Greig and Gehrels, 1995). A consistent pre-Eocene age limit of deformation is thus shown along the western basin margin. Haggart et al. (2006) dated an intrusion in the southern Bowser Basin that is post-kinematic with respect to NNW- to NNE-trending folds and interpreted a Campanian (83.2 Ma) crystallization age; some deformation in this area of the southern Bowser Basin therefore occurred prior to 83.2 Ma.

1.2.4 Hypotheses for development

Following mapping in the Groundhog Coalfield (figure 1.4), Moffat (1985) concluded the presence of two and possibly three periods of deformation. An initial D1 deformation produced an S1 cleavage interpreted to have formed early in the development of tight NW-trending F1 folds that dominate the structure in the region. A second F2 set of gentle NE-trending folds is nearly orthogonal to D1 structures and is most commonly expressed in the form of a change in plunge of F1 folds. Evidence for timing is given primarily from thrusts, interpreted to relate to F2 folds, which crosscut F1 folds (Moffat, 1985). A possible D3 deformation was interpreted from a D2 curviplanar fault surface and spread in S2 cleavage on stereographic projections; the fault and cleavage orientations both appear gently folded about a NW-SE axis.

Moffat (1985) interpreted the driving mechanisms of deformation within a framework of terrane accretion and displacement in the Canadian Cordillera. Mostly dextral transcurrent faults throughout the Cordillera were interpreted, based on palinspastic restoration, to have initially resulted from a NE-SW directed maximum compressive stress regime (Gabrielse, 1985). Moffat (1985; Moffat and Bustin, 1993) interpreted that this stress regime could have produced NW-trending F1 folds in the Groundhog Coalfield. Later contemporaneous movement occurred along two converging dextral fault systems near the Bowser Basin (the Kutcho Fault to the east and Denali Fault to the west, figure 1.3). The convergent geometry of these faults is hypothesized

to have restricted transport of the Stikine terrane northwards relative to the rest of North America. Restriction was interpreted to have been contemporaneous with thrusting along the King Salmon Fault (Moffat, 1985). This restriction resulted in a switch of maximum paleostress orientation from NE-SW to NW-SE and resulted in F2 NE-trending folds (Moffat, 1985). A transfer of displacement from the Kutcho fault system to eastward faults subparallel to the Denali Fault coupled with a possible slight change in relative plate motion ended the restriction of the Stikine terrane (Moffat, 1985). This restored maximum paleostress orientations to a NE-SW orientation that may have generated minor D3 structures.

Evenchick (1991a) defined and outlined the geology of the Skeena Fold Belt. Construction of balanced cross-sections along the northeast margin across NW-trending folds of the fold belt yielded average shortening estimates of 44%, inferred to be applicable to the Bowser Lake Group and the underlying volcanic rocks. NE-vergent detachment folding, culminating at a triangle zone along the NE-margin of the fold belt, was interpreted to be driven by detachments underlying the fold belt and rooted to the west. NE-verging structures in the Hazelton Group and overlying Bowser Lake Group along the western basin margin that are contemporaneous with the Skeena Fold Belt (Evenchick, 1991b) indicate that any major detachments driving deformation must be rooted to the west in the Coast Belt. These have since been masked by intrusion and metamorphism. Deformation was interpreted to be related to either terrane accretion or subduction-related shortening (Evenchick, 1991a).

NE-trending folds in the Skeena Fold Belt were examined in three widely separated regions of the western Skeena Fold Belt by Evenchick (2001). Geometries in two of these regions did not reveal clear timing relationships but interference of folds intersecting at near-orthogonal angles was interpreted to exclude the possibility of a gradual change in fold trends during a single deformation. A region in the SW fold belt exhibits N-striking cleavage transecting NE-trending folds. This was interpreted to

represent a transition from NW-SE contraction to E-W contraction. The NW-trending folds have been interpreted by Evenchick (1991a) to result from folding driven by a sub-Bowser detachment. Evenchick (2001) evaluated 4 possible origins for NE-trending fold sets existing close to NW-trending fold sets.

1) Lateral shortening variations can produce gradual variations in fold trend during a single deformation. This was discounted as an origin for NE-trending folds due to fold interference, implying more than one generation of folding, and the requirement to produce abrupt and often orthogonal variations in fold trend.
2) Rotation of several supracrustal blocks about a vertical axis has the potential to cause variations in previously existing surface structures if rotation is not equal in all areas. NE-trending folds could be developed on blocks that have rotated separately from areas with NW-trending folds. Strike-slip faults are expected to develop on the perimeter of such blocks to accommodate rotation. However, large faults capable of facilitating rotation have not been documented in the fold belt. Consistent SSW-directed paleocurrent indicators identified throughout the basin also indicate that significant block rotation has not taken place.
3) Basement anisotropy in the form of basement highs or pre-existing faults can cause variation in the orientations of overlying structures developed during deformation. Basement structure control on structure orientation was not considered a likely origin for NE-trending folds. The high degree of shortening (up to 50%) that accompanied NE-trending folding was considered to be unlikely to develop simply due to basement structure during NE-SW shortening. Structures oblique to the overall grain of the fold belt developed adjacent to a basement promontory would also be expected to have symmetry from W to E (i.e. be present on both sides of the high), which is not seen in the fold belt. Wrench faulting along east or north-striking basement faults is acknowledged as a possible origin of NE-trending folds but candidate structures are not known. The lack of

known basement units that could have been reactivated, and the lack of known pre-existing faults to the west of the fold belt or in the Stikine assemblage leave no candidate basement structures to result in NE-trending folds.

4) Sinistral transpression along NNW striking, right-stepping strike-slip faults (figure 1.5), hypothesized to exist on the western basin margin, was interpreted as the most likely cause of NE-trending folds by Evenchick (2001). Sinistral convergence along a NNW-trending plate margin would result in a partitioning of strain between postulated NW-trending strike-slip faults and NE-trending folds (Evenchick, 2001). The likelihood of sinistral plate convergence is supported by plate reconstructions indicating sinistral convergence of the Farallon Plate in the Late Jurassic and Early Cretaceous (Engebretson et al. 1985). NW-trending folds are interpreted to post-date this period of sinistral convergence, resulting from a switch in the Late Cretaceous to dextral convergence. Deformation following this change in convergence angle was driven by a thickening orogenic wedge (Evenchick, 2001) with critical taper (Davis et al., 1983). Late Cretaceous dextral transpression is documented to the west within the Coast Belt (e.g. Andronicos et al., 1999), and in many other areas of the Cordillera (e.g. Gabrielse, 1985; Price and Carmichael, 1986; Gabrielse et al. 2006).

Bone (2002) mapped three areas east of the Cassiar Highway in the northwestern fold belt (figure 1.4). In these areas NE-, N-, and NW-trending folds were identified. In one area a clear type I basin interference structure first identified by Evenchick (2001) was interpreted to result from local polyphase deformation producing a NE- and a NW-trending syncline. Transection of NE-trending folds by NW-striking cleavage in one area was given as evidence for a fold history beginning with NE-trending folds followed by N- and NW-trending folds (Bone, 2002). Another study area showed clockwise transection of N-trending folds by NE-striking cleavage. The apparent differences in temporal sequence from these two areas were attributed to small-scale partitioning of the

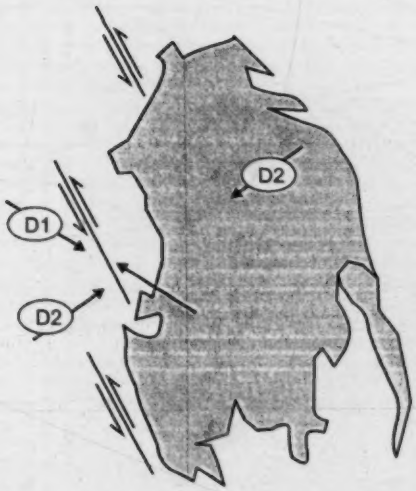

Figure 1.5: Schematic outline of the Bowser Basin illustrating sequential development of fold belt following the hypothesis of Evenchick (2001). D1 and D2 refer to sequence predicted by Evenchick (2001). Arrows indicate relative convergence during labelled deformation, solid lines represent hypothetical sinistral faults. For location of basin see figure 1.1.

fold belt into structural domains. The regional deformation history was then concluded to have initiated with NE-trending folds, followed by N- and NW-trending folds, compatible with that of Evenchick (2001), but with localised domains of opposite timing (Bone, 2002).

McMechan (2007) examined the Mosque Mountain area in the southeastern Skeena Fold Belt and documented NE- and NW-trending folds and fault sets; the presence of NE-trending folds is anomalous to this part of the fold belt (figure 1.1). Timing relationships between the two sets of structures were not consistent throughout the area. The oldest structures are interpreted to have formed prior to deposition of the Late Cretaceous Sustut Group. These structures formed a NW-trending basement uplift that terminates in the Mosque Mountain area. Late Cretaceous deformation then resulted in alternate formation of NW- and NE-trending structures. NW-trending structures formed at a high angle to regional stresses, consistent with other folds in this region, whereas NE-trending structures formed due to deflection of detachments around the now reactivated pre-Sustut basement uplift (McMechan, 2007). This is considered an explanation for a local domain of NE- and NW-trending structures and is not necessarily applicable to the western Skeena Fold Belt.

This study aims to resolve discrepancies between these hypotheses for

development of the fold belt and improve understanding of conditions of deformation and the timing relationships, both absolute and relative, between sets of structures.

1.3 Mapping Methodology

The principle method of research for this study has been field-based geological mapping conducted at a scale of 1:25000 in selected areas (figure 1.4). Mapping was conducted by visiting individual outcrops and identifying features with an emphasis on those relevant to interpreting the structural geology of the area. Two summer field seasons of mapping were completed. All areas were accessed from helicopter-supported camps of 2-5 persons, with the exception of the Eskay Creek area and outcrops along highway 37 (figure 1.4), which have road access. Exposure accessible from each camp was mapped in detail for 4-6 days. Study areas were chosen such as to meet a combination of the following requirements:

-high amount and quality of exposed rocks, as determined from airphotos, and general accessibility and suitability for a camp;

-geologic mapping by previous workers, especially Evenchick et al. (2004), that indicated proximity to mappable folds or major thrust faults;

-likelihood of overprinted folds, as indicated by intersecting fold trends on published geologic maps;

-attempting to place camps within a variety of structural domains throughout the northwestern fold belt and in areas underlain by a variety of stratigraphic units.

Nine areas were mapped for this study. These areas will be referred to as Maitland plateau, Mount Will, Cartmel Lake, Sweeny Creek, Oweegee Dome, Iskut ridge, Eskay Creek, Teigen Lake, and Nelson Creek (figure 1.4). These are informal names based on local geographic features that should not be considered accurate geographical locations. Maps are georeferenced using the NAD 83 Universal Transverse Mercator (UTM) grid for zone 9.

Chapter 2: Folds and related structures

2.1 Background

All the areas listed in the previous chapter contain folds. Structures were mapped in order to determine relative timing relationships. Structural data, including bedding, cleavage, bedding-cleavage intersection lineations, fold axial planes and hinges were recorded to aid in interpreting the kinematics of fold development. Where relevant, differences in style between NW- and NE-trending folds were also described.

2.1.1 Fold Terminology

The descriptions of folds that follow conform to the following classifications. Description of fold tightness, plunge of fold hinges and dip of axial planes follows the systems of Fleuty (1964). Where exposure permits, fold shape and layer geometries are classified using the methods of Ramsay (1967). In the areas were sufficient structural data have been collected, these have been plotted onto equal-area lower hemisphere projections using the program Spheristat for Windows 2.2 produced by Pangea Scientific. Data with girdle distributions are plotted with the location of the girdle and the location of the π-axis, represented by eigenvector 1 (e1 on diagrams). Girdle location is determined by moment-of-magnitude calculations performed by Spheristat. Structures referred to as having a widely scattered distribution do not have a clearly defined girdle or cluster.

2.2 Field Observations

2.2.1 Maitland plateau

The Maitland plateau area (figure 1.4) is a local topographic high selected to investigate previously published intersecting NE- and WNW-trending folds (Evenchick and Green, 2004c). Undeformed Pliocene Maitland volcanics, consisting here primarily of mafic volcanic flows, postdate formation of the fold belt and lie unconformably on

folded rocks of the Skelhorne assemblage. The Skelhorne assemblage here comprises siltstone, fine to medium grained sandstone, and moderately well sorted chert-pebble conglomerate, that form distinct coarsening-upwards sequences.

Two principal orientations of fold sets are present at Maitland plateau, while faults are rare (figure 2.1). Fold tightness ranges from open to gentle, and folds have rounded or kinked shapes. Class 1C, II and III fold types are most common. The first set of folds trend N- to NE and are subhorizontal to gently plunging. Axial planes are upright with the exception of one syncline steeply inclined to the west. The axial traces of these folds cannot generally be traced for more than a kilometre. WNW-trending folds are gentle and rounded. These folds are gently plunging and upright. The axial traces of W-trending folds can be followed across the map area suggesting that they have not been significantly deflected by any later folding. Cleavage is only sporadically developed in this area, present as locally developed spaced cleavage in siltstones or conglomerate. Cleavage is typically ~N-S or E-W striking, suggesting affinity to respective folds of similar trend. Veins are rare; those found are composed of quartz and commonly form parallel to bedding. Fibres in one sample of a bedding-parallel vein collected near the projected axial trace of a syncline are oriented nearly perpendicular to bedding, suggesting they formed during a period of extension. They may have served to accommodate extension at the crest of the fold.

Equal-area projections of poles to bedding show a widely scattered girdle distribution with a subhorizontal π-axis trending ESE (figure 2.2). The minimal cleavage data collected are widely scattered. Bedding-cleavage intersection lineations predominantly plunge SE. The spread in the girdle distribution of bedding may indicate two phases of folding; an initial phase formed a girdle distribution, the second imposes a girdle at a high angle to the first, resulting in a diffuse girdle. The ESE trend of the π-axis likely results from WNW-trending folds. This is consistent with the relatively

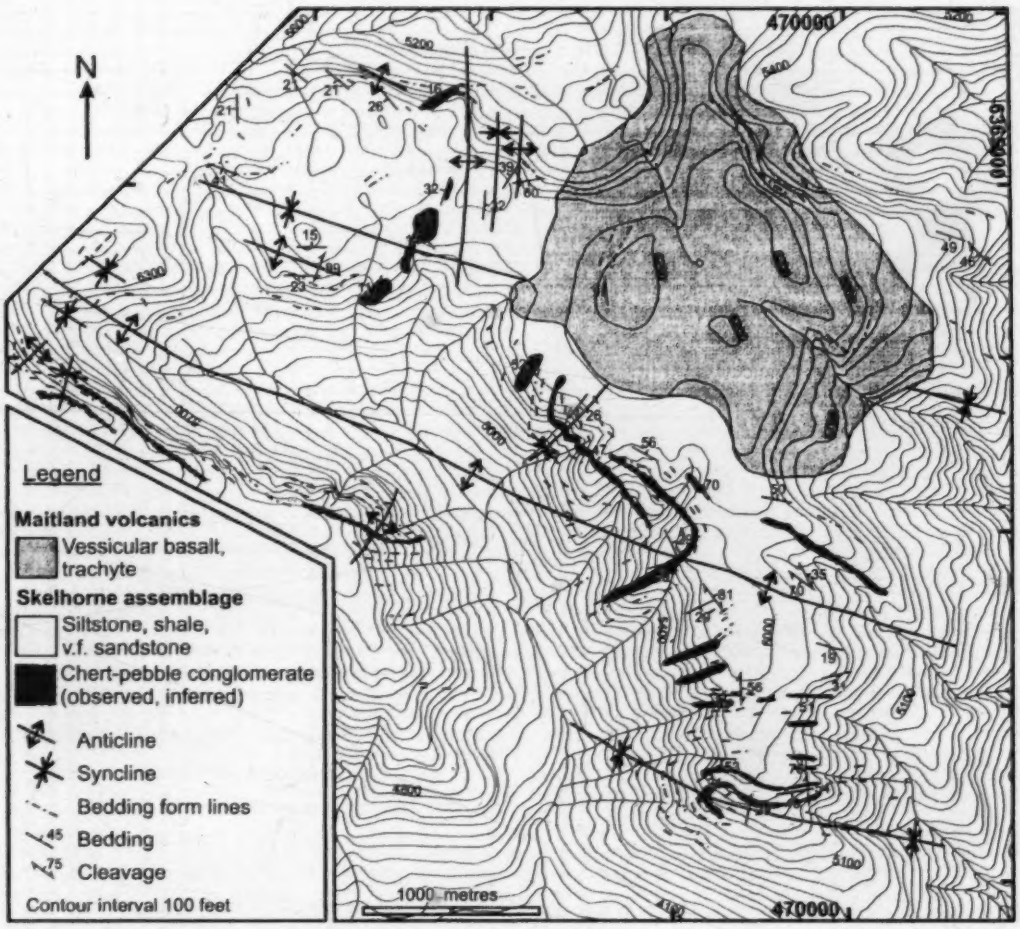

Figure 2.1: Structural map of the Maitland plateau area. Conglomerates with solid outlines are those observed in outcrop, those with dashed outlines are inferred.

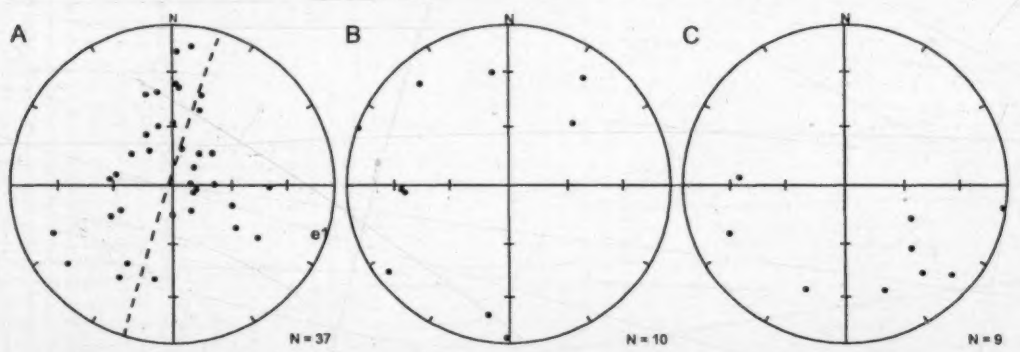

Figure 2.2: Equal-area lower hemisphere projections of structure data from Maitland plateau. A: poles to bedding. e1= eigenvector 1. Dashed line represents girdle distribution; B: poles to cleavage; C: bedding-cleavage intersection lineations.

undeformed nature of WNW-trending folds, suggesting they formed later as F2 folds.

2.2.2 Mount Will

The Mount Will area (figure 1.4) was selected to study more eastern exposures of the fold belt. This area exposes rocks of the Cold Fish Volcanics, Spatsizi Formation, and Todagin assemblage (Evenchick and Thorkelson, 2004b). The Cold Fish Volcanics here include rusty-red weathering rhyolite, maroon amygdaloidal basalt, pink welded tuff thickly interbedded with green volcaniclastic sandstone, and interbedded rhyolitic tuff and ignimbrite ash flows. The Spatsizi Formation typically occurs as thinly interbedded siliceous blocky siltstones and recessive white tuff, with lesser amounts of fossiliferous sandstone. The Todagin assemblage comprises interbedded sandstone and siltstone, with occasional thick beds of chert-pebble conglomerate.

The most prominent structure in the Mount Will area is the Mount Will Thrust Fault (figure 2.3). This fault places lower Hazelton Group volcanics and sediments upon younger rocks of the Spatsizi Formation (figure 2.4). The fault in one location is estimated to be oriented 128°/66° SW at the base of a cliff of red rhyolite (figure 2.5). This fault cuts progressively younger units as the fault is traced northwest across the map area until it places Spatsizi Formation upon itself. The apparent difference in lower Hazelton Group stratigraphy from footwall to hangingwall is partially due to lateral variations of volcanic flows combined with difficulty accessing exposures in the northeast portion of the map area. A broad upright gentle anticline present in the footwall within the volcanics trends ESE. A rounded SSE trending anticline in the hanging wall is located near the trace of the thrust (figure 2.3). Both these structures are close in orientation to the overall NW-trend of the thrust, and conceivably are part of the same generation of structures. Equal-area lower hemisphere projection of poles to bedding show a moderately developed cluster in the northeast quadrant with scatter along a weak girdle with a gentle SE-trending π-axis (figure 2.6). Poles to cleavage are clustered and

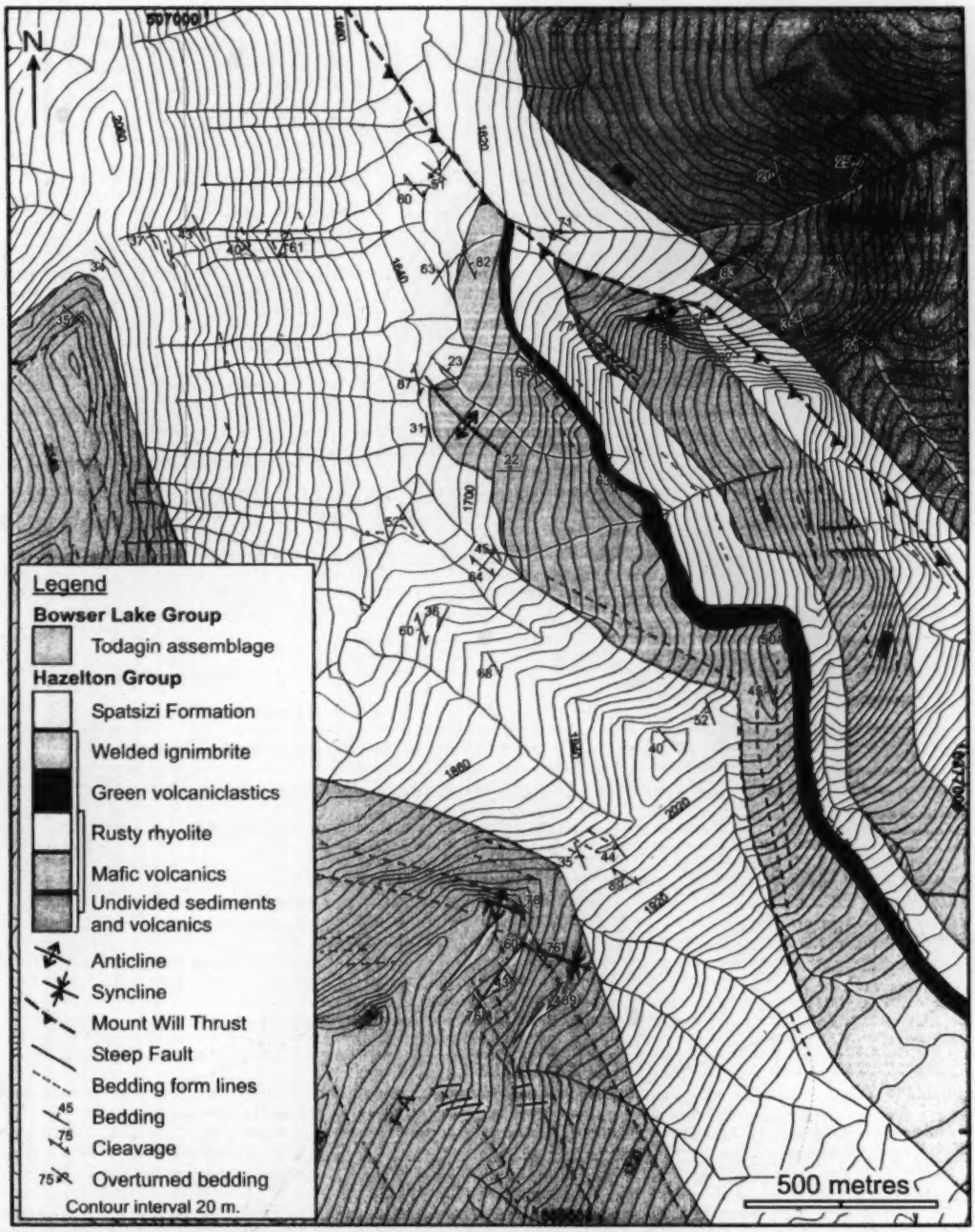

Figure 2.3: Structural map of the Mount Will area. Mount Will Thrust places older volcanics of the Lower Hazelton Group over younger strata of the Spatsizi Formation. A-A' indicates location of figure 2.4. Data collected shown in figure 2.6.

strike NW. These data do not signify multiple generations of folds.

Along the base of the Mount Will Thrust (figure 2.3), a layer of fault gouge ranges

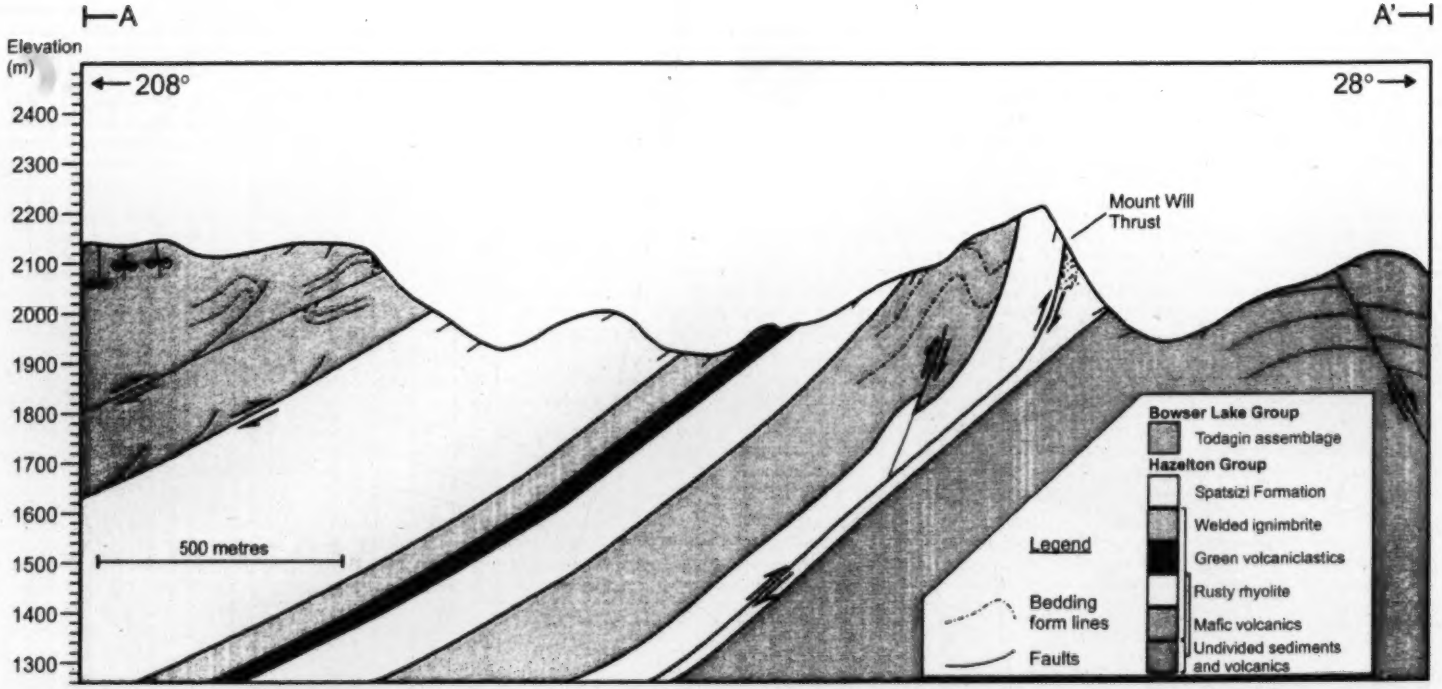

Figure 2.4: Natural scale cross-section of the Mount Will area. Mount Will Thrust places Lower Jurassic volcanics and overlying younger strata on the Upper Jurassic Spatsizi Formation. Detachment follows relatively ductile Spatsizi Formation. Blind thrusts causing folds in the Todagin assemblage are interpreted to eventually root in the Mount Will Thrust. Steep predominantly strike-slip faults in the Todagin assemblage and normal faults within interbedded sedimentary and volcanic rocks are discussed in Chapter 3.

in thickness from 20–100 cm (figure 2.5A). Gouge is friable, readily crumbles and is weakly lithified. Thin section petrography illustrates the ductile nature of the gouge, which appears to have flowed, and the more rigid clasts that are floating supported by the matrix (figure 2.5B-D).

In the northeast part of the Mount Will area (figure 2.3) several subvertical NE-striking faults, of normal and unknown sense with undetermined offset, were identified within undifferentiated sediments and volcanics of the lower Hazelton Group. These faults are aligned so as to crosscut the Mount Will Thrust. The lack of offset of the Mount Will Thrust suggests these faults predate thrusting. These steep faults are interpreted as normal faults that may have formed during initiation of the Bowser Basin.

Multiple small folds are exposed within sediments of the Todagin assemblage. Asymmetric NW-trending folds that have been faulted at their base further down slope from figure 2.7, as well as minor thrust faults, are found in the hanging wall of the thrust sheet (figure 2.3). A five metre exposure of a gently NW-plunging, NE-verging syncline has been cut multiple times by small SW-verging thrust faults that have stacked progressively smaller synclines into the core of the lowermost syncline (figure 2.8). All other folds and thrust faults in this area verge NE. The opposing vergence of this syncline and the small thrusts could be interpreted as resulting from separate phases of deformation. Alternatively, they could imply the lower bed detached at its base, and these small faults developed as roof thrusts above a duplexed wedge. The NW-trending orientation and NE-vergence of these small folds appears roughly compatible with the orientation of the N to NE-verging Mount Will thrust fault (figure 2.5A), suggesting their development was likely synchronous. These faults are likely linked via thrust faults cutting up-section into the Todagin assemblage rocks (figure 2.4). Steep faults are also found throughout these younger sediments, and do not appear deformed by folds. The

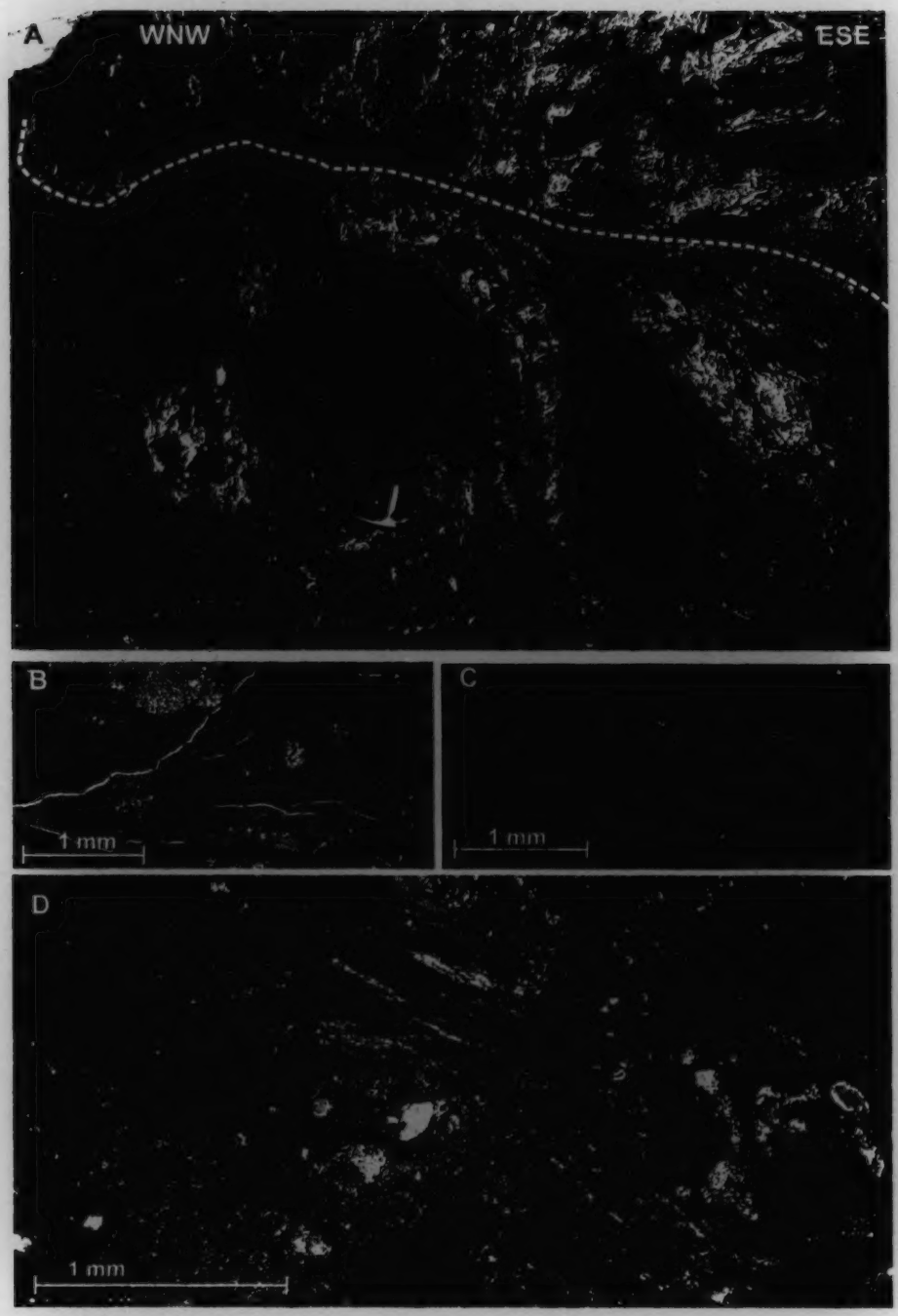

Figure 2.5: Views of the Mount Will Thrust. A: View to NNE of thrust placing older rhyolite over younger interbedded sediments of the Spatsizi Formation. Asymmetry of folds suggest north to northeast vergence; B-D: Thin section photomicrographs of fault gouge sampled from the thrust. B: View in plane-polarized light of gouge. Note fine-grained material appears to flow around light coloured chert clasts; C-D: View in cross-polarized light of fine-grained material that has flowed around chert.

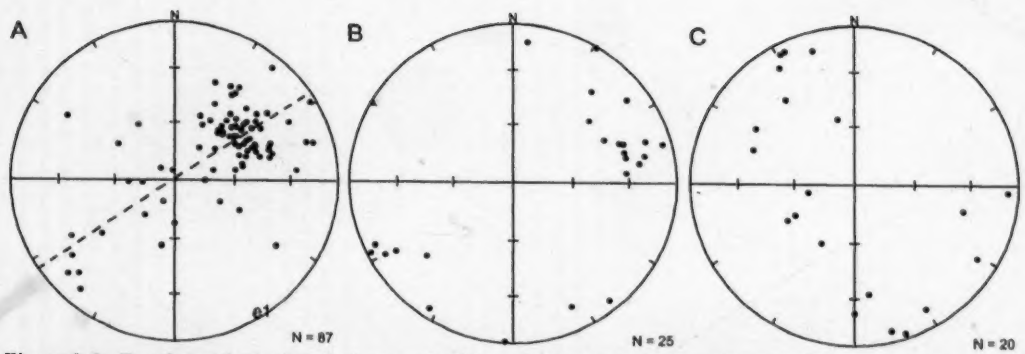

Figure 2.6: Equal-area lower hemisphere projections of structure data from Mount Will area. A: poles to bedding. e1= eigenvector 1. Dashed line represents girdle distribution; B: poles to cleavage; C: bedding-cleavage intersection lineations.

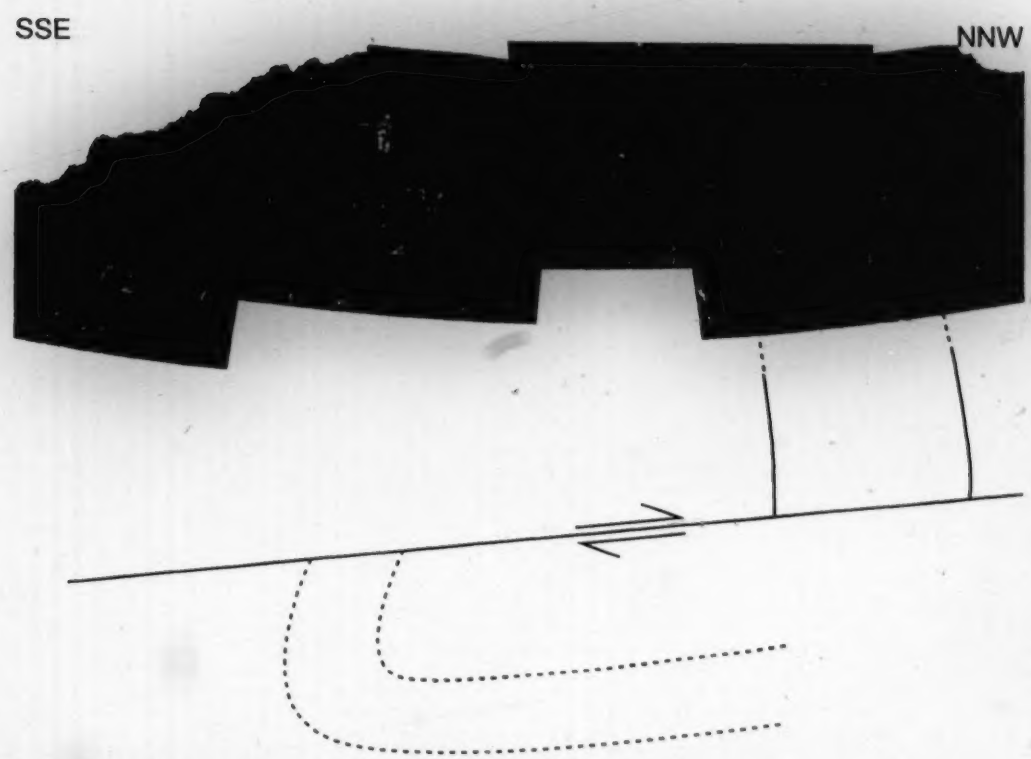

Figure 2.7: Panorama towards WSW of asymmetric anticline in the Mount Will area. Thick layers are pebble conglomerate, thin layers are sandstone and mudstone of the Todagin assemblage. Orientation of axial plane is approximately 085°/60° S. Appended line diagram is schematic representation of observed fault below anticline and inferred relationship with synclines in the area. Person for scale.

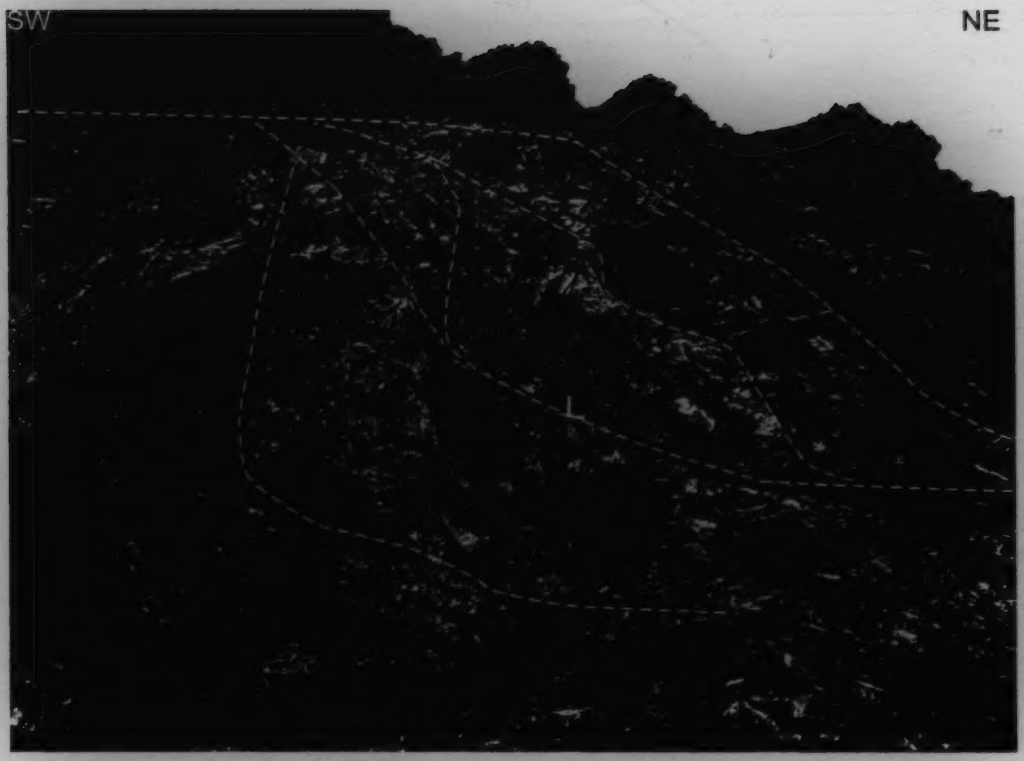

Figure 2.8: Syncline in the Mount Will area cut by multiple faults that form a duplex. View towards NW. Dashed lines represent interpreted thrust faults. Hinge orientation approximately 320°-21°

kinematics of these faults will be discussed further in Chapter 3.

2.2.3 Cartmel Lake

The Cartmel Lake area (figure 1.4) exposes rocks of the Eaglenest assemblage and was selected for study of previously documented overprinted folds (Evenchick and Green, 2004a). During mapping the Eaglenest assemblage here was informally subdivided into units of grey sandstone and siltstone, with rare coal and fossil plant leaves, and units comprising red-weathering chert-pebble conglomerate and sandstone (figure 2.9). Overall, cliff-forming conglomerate represents the majority of exposure, and in some localities represents up to 85% of exposed rocks.

Two groups of folds are exposed in the Cartmel Lake area, one trending NW and the other NE. A small outcrop in the southern valley demonstrates that these fold sets

interfere with each other. Bedding is gently folded about a moderately inclined axial plane oriented ~235°/45° NW (figure 2.10). The plunge of this fold changes to the NE and outlines the trace of an additional upright axial plane axial plane striking ~315°. These two folds give the outcrop a warped appearance and demonstrate outcrop-scale fold interference.

The most prominent folds in the Cartmel Lake area trend NW and transect the map area (figure 2.9). These upright to gently inclined symmetric folds have estimated minimum amplitude of 400 metres and wavelength of 400 to 600 metres (figure 2.11). They are open to close, subrounded class 1C and III folds. Equal-area lower hemisphere projections of poles to bedding show a moderately developed cluster with a girdle normal to a shallow ESE plunging π -axis (figure 2.12). This π-axis is consistent with NW-trending folds being the dominant structure in the area. In one locality a number of relatively consistently oriented small thrusts located on the NE-limb of a NW-trending anticline with centimetre-scale SW-vergent offsets are exposed (figure 2.13). They have an average orientation of 153/69 NW. These faults also cause a slight rotation of bedding. A map-scale SW-vergent thrust fault developed on the flank of a NW-trending anticline is shown in figure 2.11. This shows sporadic occurrence of faults on the limbs of NW-trending folds.

Many bedding-parallel minor faults are present in the Cartmel Lake area. Of 24 measured examples, most are found on SW and NE-dipping beds (19), and to a lesser extent SE-dipping beds (5). The likely interpretation of these faults is that they are a consequence of flexural-slip folding. Their relative abundance on beds striking NW-SE may indicate a more brittle deformation regime during development of NW-trending folds than NE-trending folds; however this could simply be a sampling effect.

The second group of folds observed at Cartmel Lake trends NE. These are gentle to open upright folds with wavelength varying from outcrop-scale to 300 metres. These folds are found in close proximity to a low angle surface that truncates bedding,

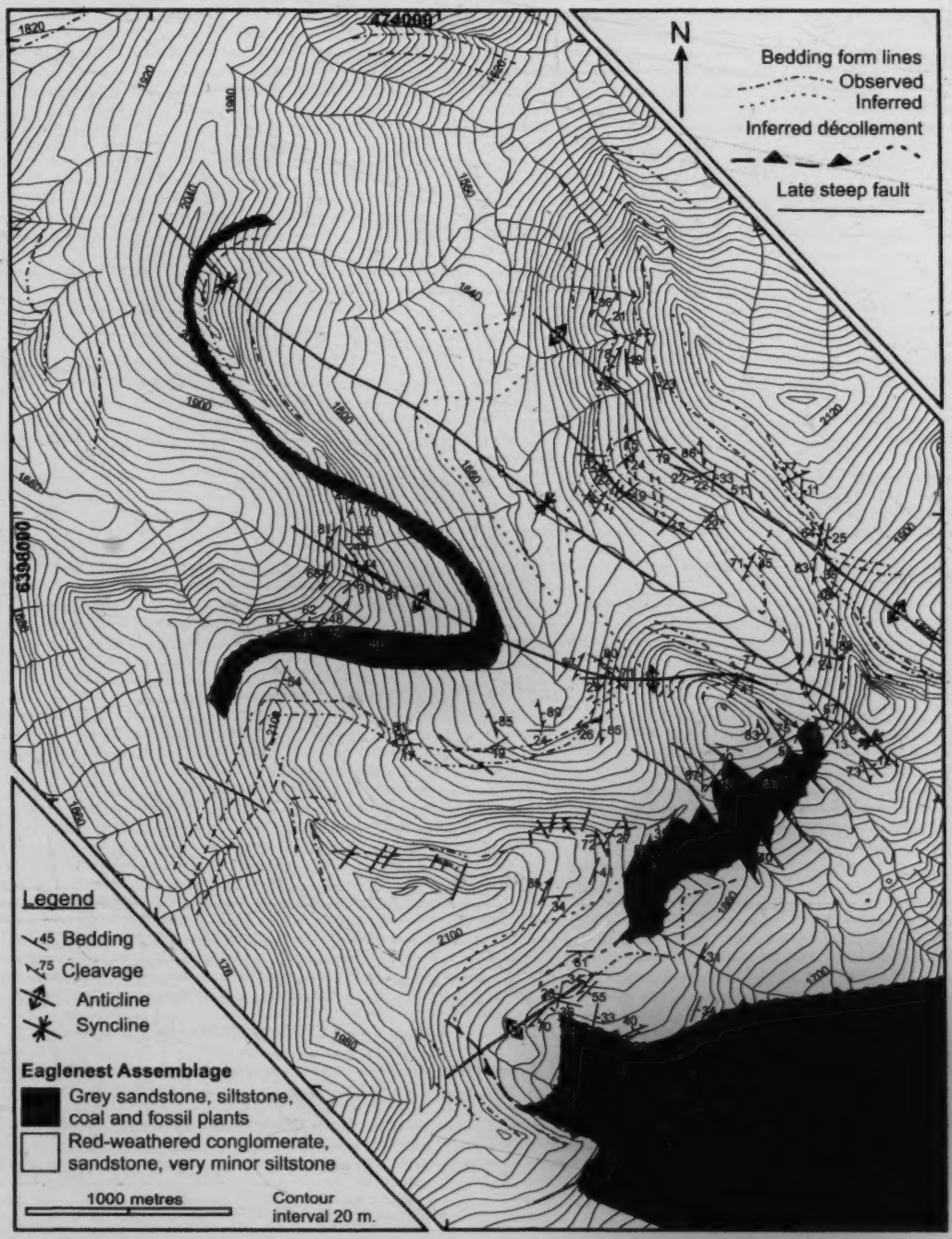

Figure 2.9: Structural map of the Cartmel Lake area. Note trajectories of large F2 NW-trending folds are unaffected by décollement associated with F1 NE-trending folds.

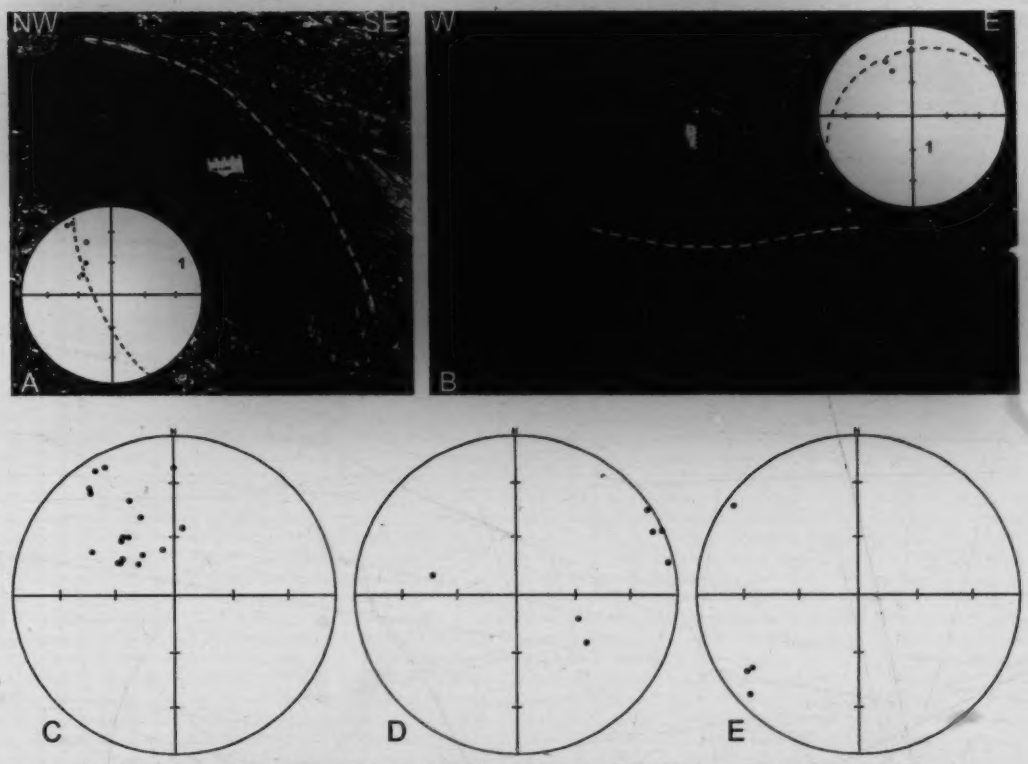

Figure 2.10: Metre-scale outcrop displaying fold interference. A-B: Photos of outcrop, dashed lines indicate source of bedding data in inset equal-area projections. On nets '1' indicates location of eigenvector 1, dashed line represents best-fit girdle for data. A: Profile of fold to NE with axial plane oriented 235°/45° NW. B: View north of outcrop, displaying warping that occurs about a moderately SE-plunging axis, causing a change in plunge of the NE-trending fold axis in A; C-E: Lower hemisphere equal-area projections of all data collected at outcrop. C: Poles to bedding forming a cluster distribution; D: Poles to cleavage; E: Bedding-cleavage intersection lineations.

interpreted as a fault that cuts up section to the N (figure 2.14). This fault is not cleanly exposed, and is also interpreted on the basis of bedding truncations and map unit boundaries. Lower angle (25° to 35°) bedding truncations in the north of the study area have been interpreted as erosional surfaces by Ricketts and Evenchick (2007). This fault has a strike that from structure contour construction varies between 000° and 060° and from view in profile varies in dip from 00° to 30°. The adjacent folds trend 235°-055°. These orientations suggest the fault may have developed synchronously with NE-trending folds as a result of the same deformation process. The variable strike and dip imply the fault is curviplanar. The large NW-trending folds can be traced through the map trace of the detachment without offset, implying that the fault must have been folded (figure 2.9).

Figure 2.11: Panorama towards the southeast of a km-scale NW-trending anticline. Dashed lines indicate trace of bedding, dotted line shows trace of a thrust fault on NE flank of fold. Width of view approximately 3 km.

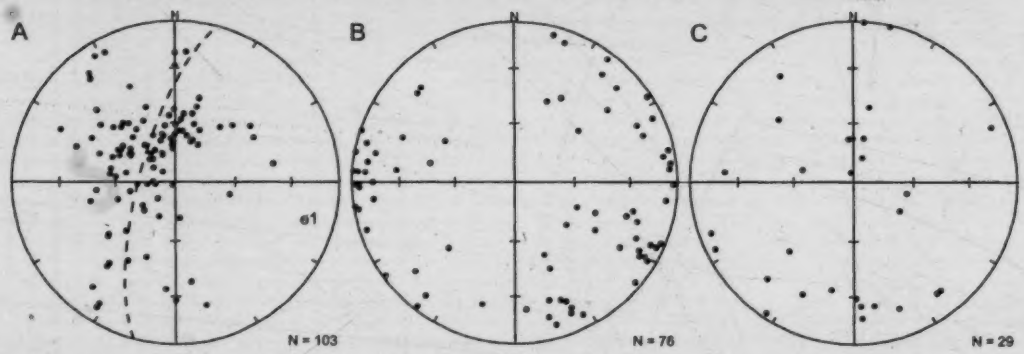

Figure 2.12: Equal-area lower hemisphere projections of structure data from Cartmel Lake area. A: poles to bedding. e1= eigenvector 1. Dashed line represents girdle distribution; B: poles to cleavage; C: bedding-cleavage intersection lineations.

The curviplanar shape of the fault, its association with NE-trending folds, and the lack of offset of NW-trending faults are interpreted to result from two deformations; F1 NE-trending folds and faults, followed by F2 NW-trending folds and faults.

Cleavage is particularly well-developed within conglomerates of the Eaglenest assemblage in the Cartmel Lake area. In some localities two, or more rarely three orientations of cleavage sets are visible within an outcrop. This cleavage is visible at a distance and gives a columnar appearance to outcrops. Cross-cutting relationships between cleavage sets are unclear, as no crenulations or clear offsets of one set by another are developed. Equal-area projections of poles to cleavage show a widely scattered distribution (figure 2.12B), indicating cleavage is not consistently oriented in the area. This is due to the presence of multiple cleavage sets with variable orientations; this variability may have been increased by folding of cleavage, thereby further scattering the

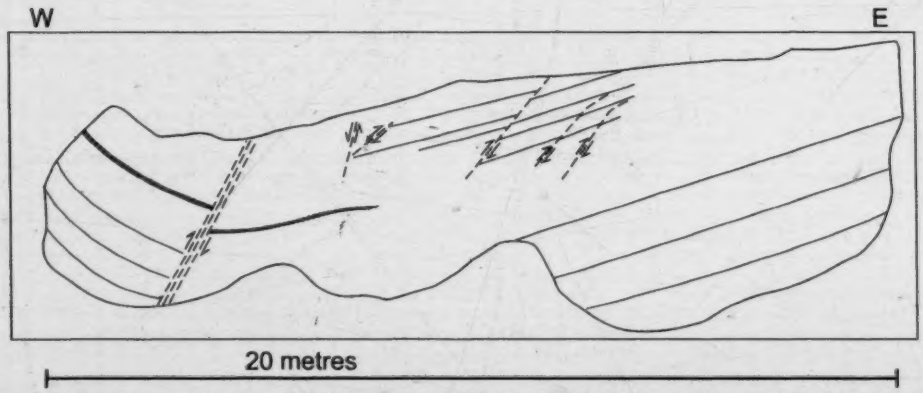

Figure 2.13: Schematic diagram of faulted outcrop in the Cartmel Lake area. Short dashed lines represent traces of bedding, long dashed lines are faults. Grey shading is a correlatable mud horizon. View to the north.

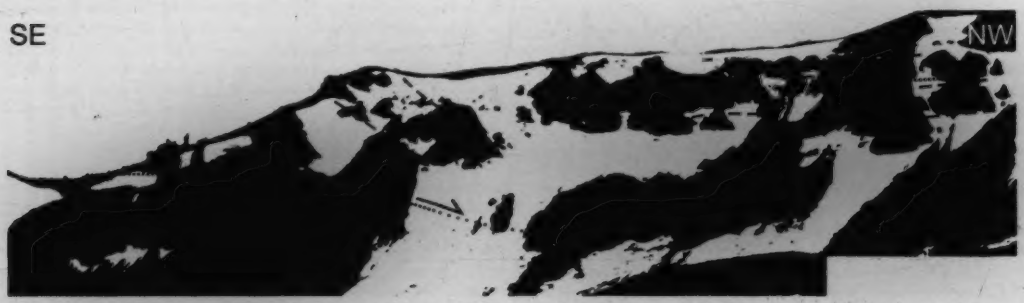

Figure 2.14: Panorama towards the southwest of NE-trending anticline and detachment fault. Dashed lines indicate trace of bedding, dotted line shows trace of detachment fault. Width of view approximately 750 m.

data.

In addition to folds and thrust faults, a large number of strike-slip and oblique-slip faults with offsets of metres were identified. These structures are not folded, and are interpreted to occur latest in the deformation history. The kinematics of their development will be discussed in Chapter 3.

2.2.4 Sweeny Creek

The Sweeny Creek area (figure 1.4) exposes rocks of the Skelhorne assemblage and is located southwest of a large domain of continuous NW-trending of folds, in an area with mapped cross-cutting, and elsewhere converging NE- and NW-trending folds (Evenchick, 2004a; Evenchick and Green, 2004d). The Skelhorne assemblage in this area comprises siltstone, sandstone, and chert-pebble conglomerate. These rock types are

stacked in prominent coarsening-upwards sequences. Rare fosssil beds contain bivalves or fossilized wood. The large glaciers in the southwest corner of the map divide the area into northwest and southeast portions (figure 2.15).

Bedding in the Sweeny Creek area predominantly dips NE or SW, except near folds. The majority of folds trend between NNW and NNE (figure 2.15). These folds have wavelengths varying from 700 to 200 metres. These NNE to NNW-trending folds are moderately plunging to subhorizontal. Axial surfaces are upright to steeply inclined, with two folds being overturned to the west (figure 2.16). The axial traces of these folds are somewhat irregular in strike from NNW to NNE. In some locations in the southeast portion of the map area fold trends converge but do not cut across one another. This implies they may be of the same generation. Bedding measurements were subdivided into domains along axial traces and plotted on equal-area projections to compare change in plunge of folds along their trace. Comparison of the π-axis of each projection reveals an increase in the plunge of each fold towards the N (figure 2.17), indicating likely fold interference. This is in the direction of a large NW-trending syncline observed from the air near the northern edge of the area approximately located on the map (figure 2.15). This fold is larger and more continuous than those that trend NNW to NNE and is interpreted as the southernmost of a separate domain of NW-trending folds (Evenchick, 2004a). It is likely that this syncline interfered with the N-trending folds. Construction of structure contours along well constrained N-trending folds reveals that axial planes slightly change in orientation to the north. This further indicates that N-trending folds have been deformed, and that N-trending folds represent F1 folds and NW-trending folds represent F2 folds.

An anticline-syncline pair in the northwest of the map area has a wavelength of ~200 metres. The syncline is open and the anticline is a gentle fold. Bedding form lines are closed around the syncline, in a pattern resembling a basin in a type I interference pattern. The bedding in this area dips in a circular manner towards the centre of the

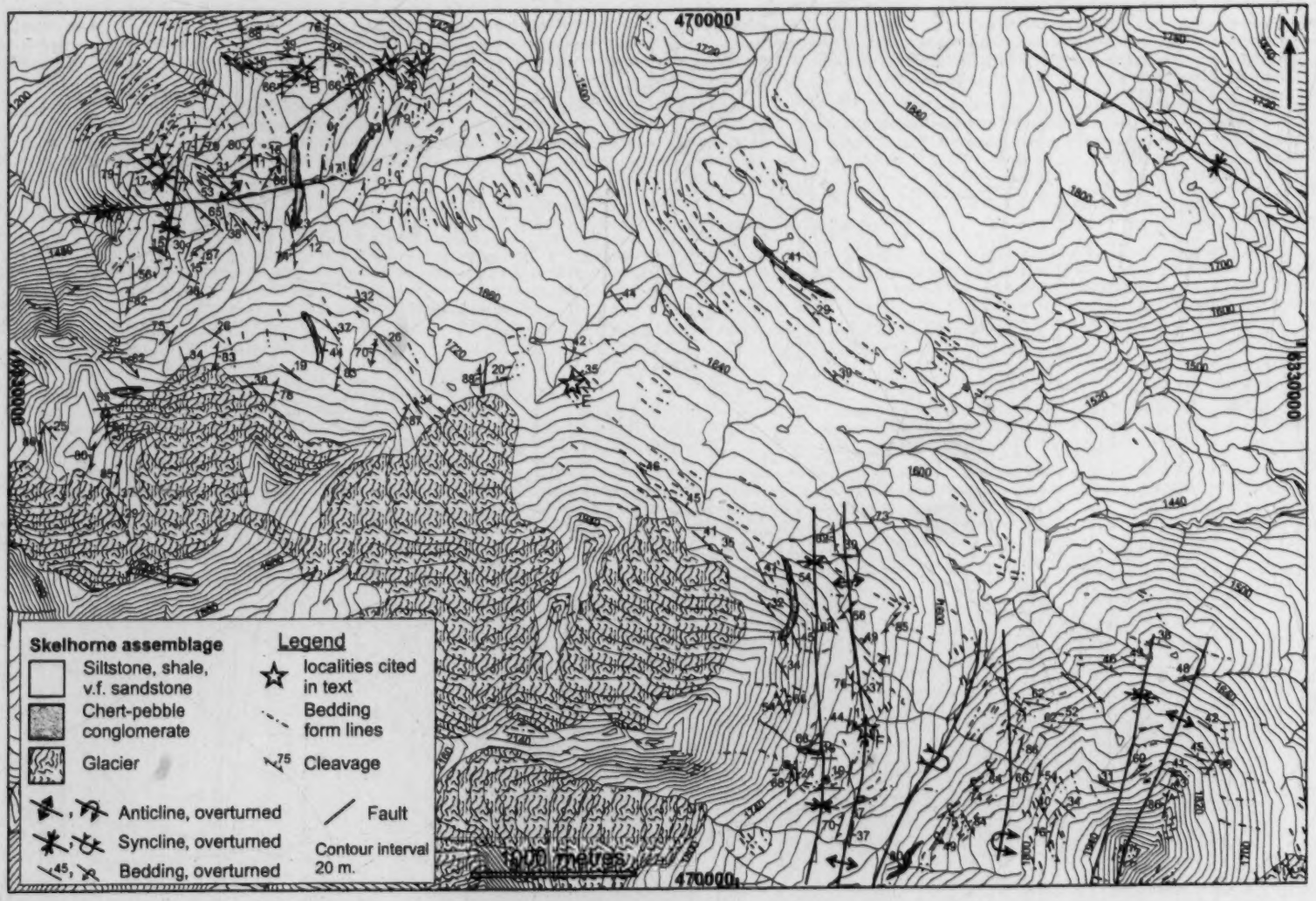
470000
N
6330000
Skelhorne assemblage
Siltstone, shale, v.f. sandstone
Chert-pebble conglomerate
Glacier
Anticline, overturned
Syncline, overturned
Bedding, overturned
Legend
localities cited in text
Bedding form lines
Cleavage
Fault
Contour interval 20 m.
1000 metres

Figure 2.15: (previous page) Structural map of the Sweeny Creek area. Area of sparse bedding data north of easternmost glacier marks division between 'northwest' and 'southeast' Sweeny Creek areas referred to in text. Stars indicate localities cited in text.

syncline indicating it is doubly-plunging and allows the inference of a cross-cutting NNE-trending syncline (locality F, figure 2.15). The presence of cross-cutting synclines further indicates two phases of folding in the northwest map area.

Equal-area lower hemisphere projection of poles to bedding throughout the Sweeny Creek area reveals a scattered cluster in the southwest quadrant, with some spread about a girdle defining a NE-plunging π-axis (figure 2.18A). Projection of poles to cleavage shows a cluster with average cleavage planes dipping steeply WNW (figure 2.18B). Projections of bedding-cleavage intersection lineations form a scattered cluster plunging gently to moderately to the N or NE, with some scatter. Poles to cleavage in the southeast of the map area show a moderately developed cluster with little scatter (figure 2.19E). This cleavage orientation is roughly consistent with the strike of the axial surfaces mapped in the southeast section of the map area. Bedding-cleavage intersection

Figure 2.16: View towards ESE of folded strata of the Skelhorne assemblage in the Sweeny Creek area. Dashed lines indicate traces of bedding. Dotted line indicates trace of an anticline overturned to the east.

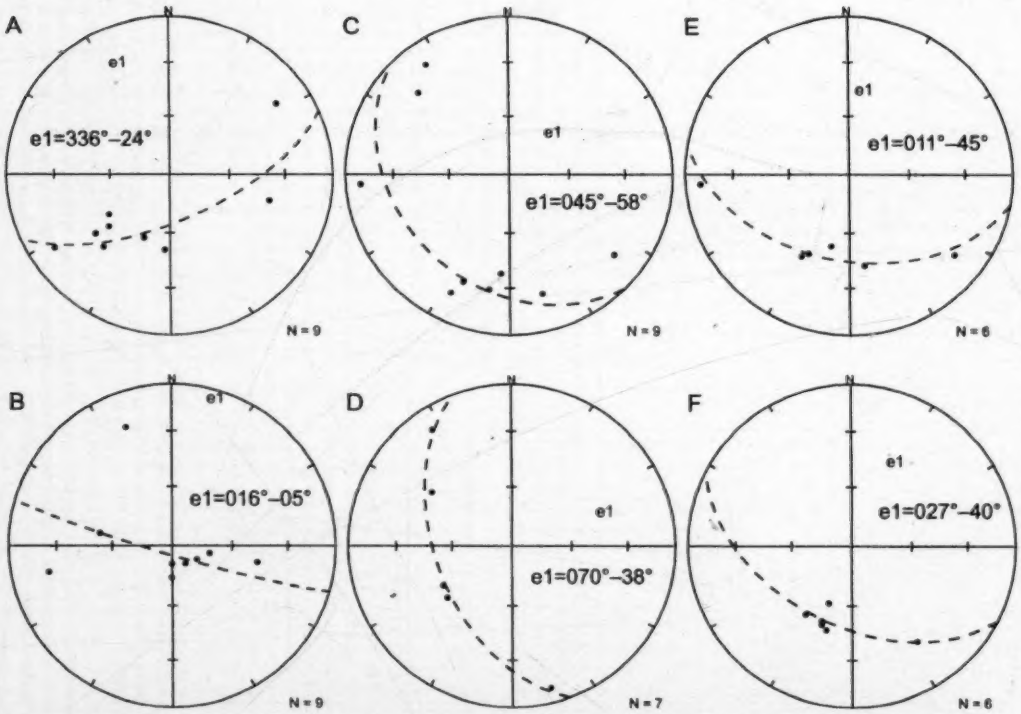

Figure 2.17: Equal-area lower hemisphere projections of poles to bedding collected along fold traces in the southwest Sweeny Creek area. Bedding data from the northern portion of mapped folds is separated from data collected along the southern portion of folds to illustrate downplunge steepening of folds. e1= eigenvector 1 location. Exact orientation is indicated by text. Dashed line represents girdle distribution. A: northern portion of westernmost syncline; B: southern portion of syncline in (A); C: northern portion of central anticline; D: southern portion of anticline in (C); E: northern portion eastern anticline; F: southern portion of western anticline in (E).

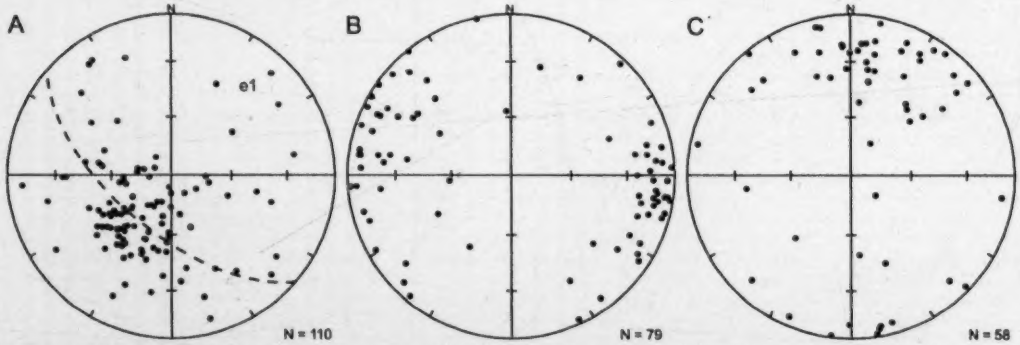

Figure 2.18: Equal-area lower hemisphere projections of structure data from Sweeny Creek area. A: poles to bedding. e1= eigenvector 1. Dashed line represents girdle distribution; B: poles to cleavage; C: bedding-cleavage intersection lineations.

lineations are constrained to a NNE-SSW axis. In the northwest of the map area two cleavage sets are frequently observed at individual outcrops; however clear cross-cutting

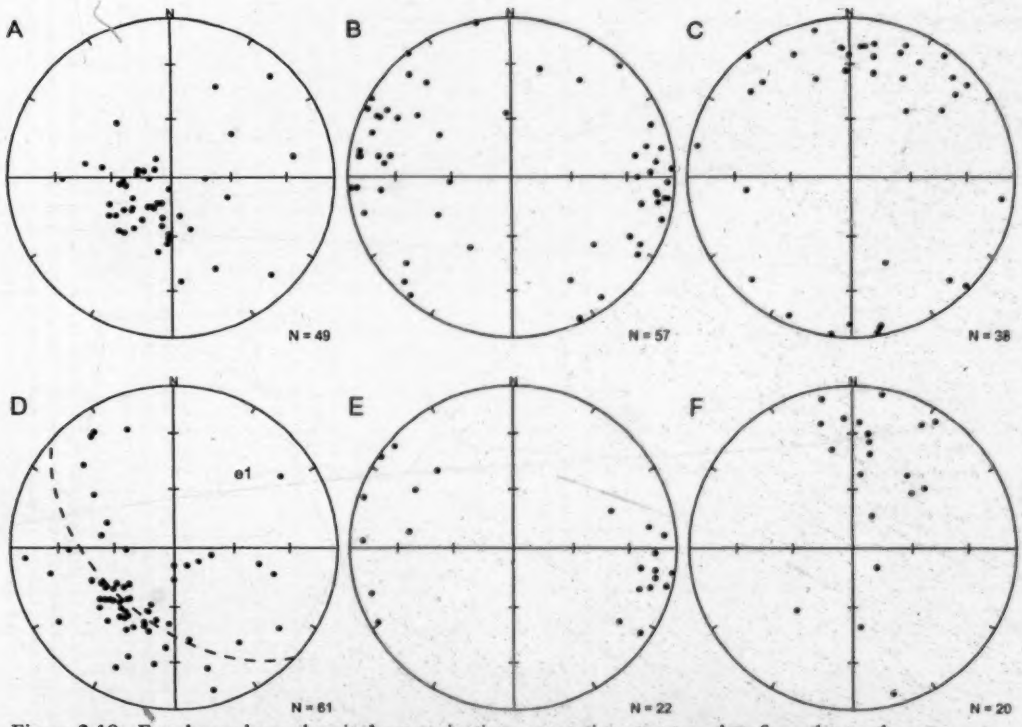

Figure 2.19: Equal-area lower hemisphere projections separating structure data from the northwest of Sweeny Creek and data from the southeast of Sweeny Creek. A-C: Data from northwest Sweeny Creek. A: poles to bedding; B: poles to cleavage; C: bedding-cleavage intersection lineations; D-F: Data from southeast Sweeny Creek. D: poles to bedding. e1= eigenvector 1. Dashed line represents girdle distribution; E: poles to cleavage; F: bedding-cleavage intersection lineations.

relationships could not be established. Overall, cleavage planes in the northwest map area also dip steeply WNW, but with much more scatter than in the southeast area (figure 2.19B). There is also a higher proportion of north-striking cleavage. Bedding-cleavage intersection lineations form a gentle N-plunging cluster. The more diffuse clustering of cleavage data is consistent with the presence of two cleavages and the inferred presence of cross-cutting folds described earlier that may fold cleavage. The N-S striking cleavage cannot be objectively associated with either fold set (figure 2.15). There are some possible explanations for this. One is that there is a third cleavage set that strikes N-S, and is unrelated to either NW or NE-striking cleavage. Another explanation is that N-S cleavage is an S1 cleavage that has been folded by F2 folds. This would also explain the wide scatter present in the cluster of cleavage data. A third explanation is

that the difference in orientation between folds and cleavage is due to transection of folds by cleavage indicating non-coaxial deformation. Transection of folds by cleavage is commonly observed in regions of transpressional deformation (Borradaile, 1978).

2.2.5 Oweegee Dome

Oweegee Dome is an inlier within the Bowser Basin (figure 1.4) exposing the Devonian through Permian Stikine assemblage, the Upper Triassic Stuhini Group, the Lower to Middle Jurassic Hazelton Group, including the Middle Jurassic Salmon River Formation, and the Middle Jurassic to Early Cretaceous Ritchie-Alger and Muskaboo Creek assemblages of the Bowser Lake Group (Greig and Evenchick, 1993). Due to the large size of the dome, mapping focused on 3 sub-areas, located on the north, east, and south sides of the dome (figure 2.20). Only the lower Hazelton Group, Salmon River Formation, and Ritchie-Alger assemblages were observed in the selected areas. Lower Hazelton Group rocks include rhyolite and intermediate volcanic rocks, maroon and green volcaniclastics, stratified tuffs, and volcanic breccia. Many of the units in the lower Hazelton are locally rusty weathering. On the north and east side of the dome green andesitic volcanic rocks of the lower Hazelton Group and overlying polymictic conglomerate of the basal Salmon River Formation are separated by an irregular contact that cuts down into the volcanic rocks and is interpreted as an unconformity. The Salmon River Formation here includes conglomerate with diorite, chert, feldspar, and fossiliferous limestone clasts derived from the Stikine assemblage (Greig, 1991), sandstone, thinly interbedded siltstone and tuff, and rare limestone. The Ritchie-Alger assemblage occurs mostly as metre(s) thick cyclic successions of sandstone and shale with rare conglomerate. The following discussion of deformation around the Oweegee dome is organized primarily on the basis of stratigraphy.

Rocks of the lower Hazelton Group were investigated mainly on the north side of Oweegee Dome. Equal-area projection of poles to bedding show a moderately developed NE-striking girdle (figure 2.21A). Poles to cleavage show a widely scattered distribution

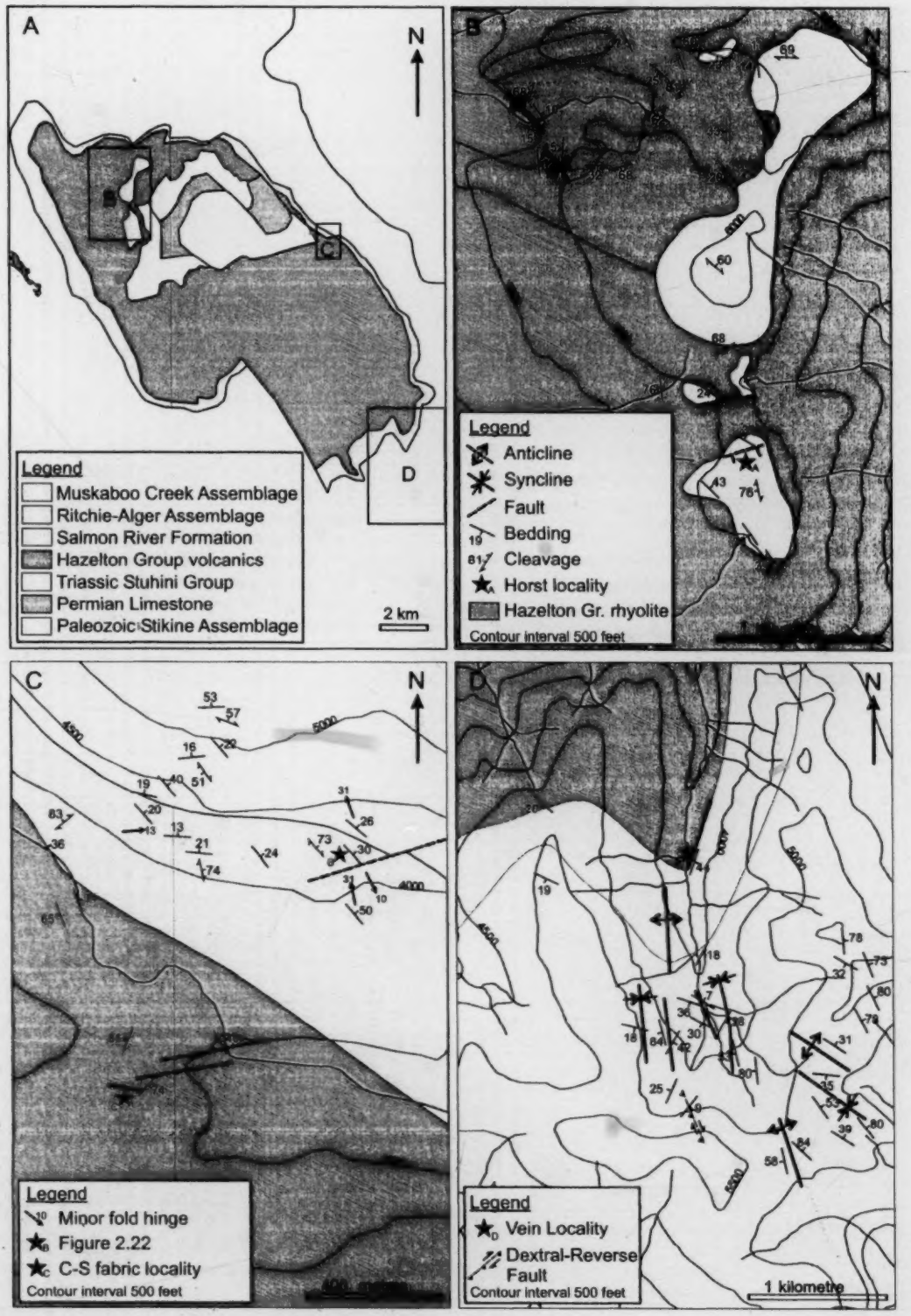
A
N
B
C
D
Legend
Muskaboo Creek Assemblage
Ritchie-Alger Assemblage
Salmon River Formation
Hazelton Group volcanics
Triassic Stuhini Group
Permian Limestone
Paleozoic Stikine Assemblage
2 km
B
N
Legend
Anticline
Syncline
Fault
Bedding
Cleavage
Horst locality
Hazelton Gr. rhyolite
Contour interval 500 feet
C
N
Legend
Minor fold hinge
Figure 2.22
C-S fabric locality
Contour interval 500 feet
D
N
Legend
Vein Locality
Dextral-Reverse Fault
Contour interval 500 feet
1 kilometre

Figure 2.20: (previous page) Geological maps of the Oweegee Dome area. A: Index map of Oweegee Dome. Rectangles indicate location of maps B-D. Legend also applies to B-D. Geology from Greig and Evenchick (1993); B: Geological map of area B (north side of dome). In this area thick rhyolite flows are subdivided from the rest of the Hazelton Group. Symbols in legend also apply to C-D. Stars indicate locations referred to in text; C: Geological map of area C (east side of dome). D: Geological maps of area D (south side of dome).

suggesting multiple deformations affecting the Hazelton Group. Folds affecting the lower Hazelton Group include a broad anticline shown by the distribution of map units on the south side of the dome, and an anticline-syncline pair identified on the north side of the dome.

The Salmon River Formation commonly has centimetre to rare metre-scale folds and faults. Folds include small gentle kink folds associated with small thrusts with flat-ramp-flat geometry, and open folds formed around small terminated thrust faults. Thrusts are often parallel to dipping strata with bedding-parallel transport directions, indicating that faults have likely been tilted after thrusting. Most fold hinges plunge NW or SE; rarely folds plunge to the NE.

On the east side of the dome at locality B (figure 2.20), at the contact between the Salmon River Formation and the first thick sandstone of the Ritchie-Alger assemblage, there is a zone of intense veining including folded veins, with fold hinges plunging NW. Adjacent to these veins, nearby shale has 3 wavy fabrics that are each penetrative in a different part of the exposure (figure 2.22). The lower fabric zone (A) is separated from the above zone by a moderately NE-dipping fault (321/62NE). The fabrics dip steeply NE (A), SW (B), and moderately NW (C). This exposure has been interpreted as a shear zone that initially developed as a thrust fault that produced fabric A in figure 2.22. This shear zone was then reactivated as a normal fault that rotated fabric A to orientation B and eventually produced fabric C. The presence of this zone of veining and shearing at the contact between the Salmon River Formation and Ritchie-Alger assemblage suggests the uppermost Salmon River Formation may have served as a local detachment below the more competent sandstone beds of the Ritchie-Alger assemblage. The extension interpreted from fabric C is consistent with local exposures of boudinaged sandstone in

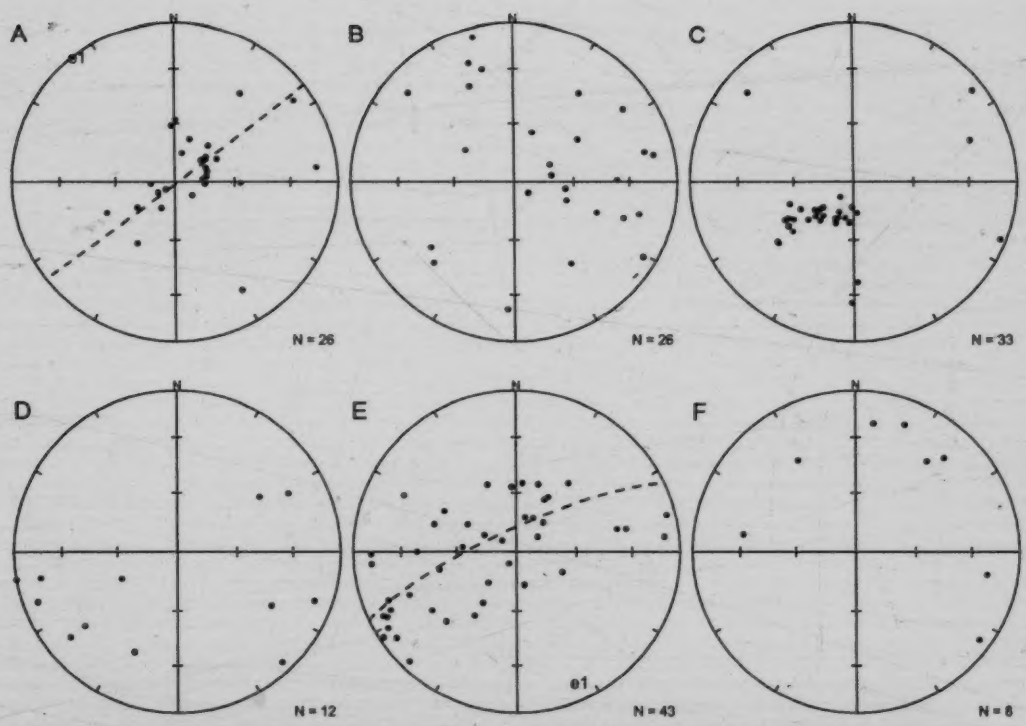

Figure 2.21: Equal-area lower hemisphere projections of structure data from three mapping areas at Oweegee Dome shown in figure 2.20. e1= eigenvector 1. Dashed lines represent girdle distributions. A: poles to bedding from north side of dome; B: poles to cleavage from north side of dome; C: poles to bedding from east side of dome; D: poles to cleavage from east side of dome; E: poles to bedding from south side of dome; F: poles to cleavage from south side of dome.

the overlying Ritchie-Alger assemblage.

The majority of folds observed in the Ritchie-Alger assemblage trend and plunge NW, with rare folds trending NNE. Most folds in the Oweegee Dome area as a whole have wavelengths on the order of hundreds metres (Greig and Evenchick, 1993) that are beyond the scale of the small mapping areas. However, locally smaller folds are developed, especially on the south side of the dome. Upright rounded folds are most abundant, while gently inclined kink and rounded folds are also sporadically developed (figure 2.23). These folds have wavelengths of tens of metres. Cleavage is sparsely developed in the Ritchie-Alger assemblage around the dome. Cleavage typically strikes NW-SE, consistent with NW-trending folds, but limited data hinder the interpretation of clusters. Equal-area projection of poles to bedding collected on the east side of the

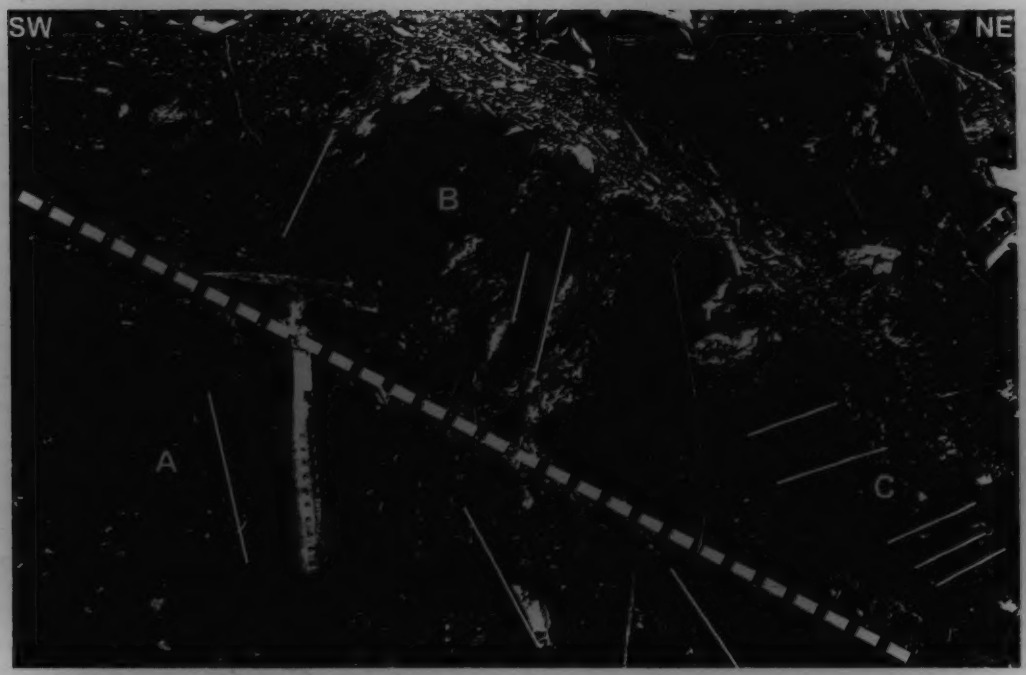

Figure 2.22: View to NW of shale with three strong fabrics developed. Solid lines represent traces of fabrics labelled A, B, and C in shale. Fabric domain A separated by B and C by a NE-dipping fault. Fabric orientations: A-321°/73° NE; B-152°/66° SW; C- 210°/56° W.

dome shows a well-developed cluster with little scatter (figure 2.21C), consistent with the lack of larger folds observed within the confines of the mapping area. Projections of bedding from the south side of the dome have a moderately developed girdle with a π-axis plunging gently SSE (figure 2.21E). All of these projections are consistent with NW-trending folds as the dominant structure in the Oweegee Dome area.

2.2.6 Iskut ridge

The Iskut ridge area is adjacent to the western margin of the basin (figure 1.4) and comprises thin to thickly bedded shale, siltstone, sandstone, and rare conglomerate of the Ritchie-Alger assemblage. Read et al. (1989) and Logan et al. (1997) identified multiple phases of foliation without mapping folds. This study shows the ridge is dominated by two major sets of structures. The most prominent of these are N and NNE-trending, gently plunging folds. These folds are open to close, upright rounded folds that are traceable along the length of the ridge. Exposed N-trending folds are class 1B and class 3

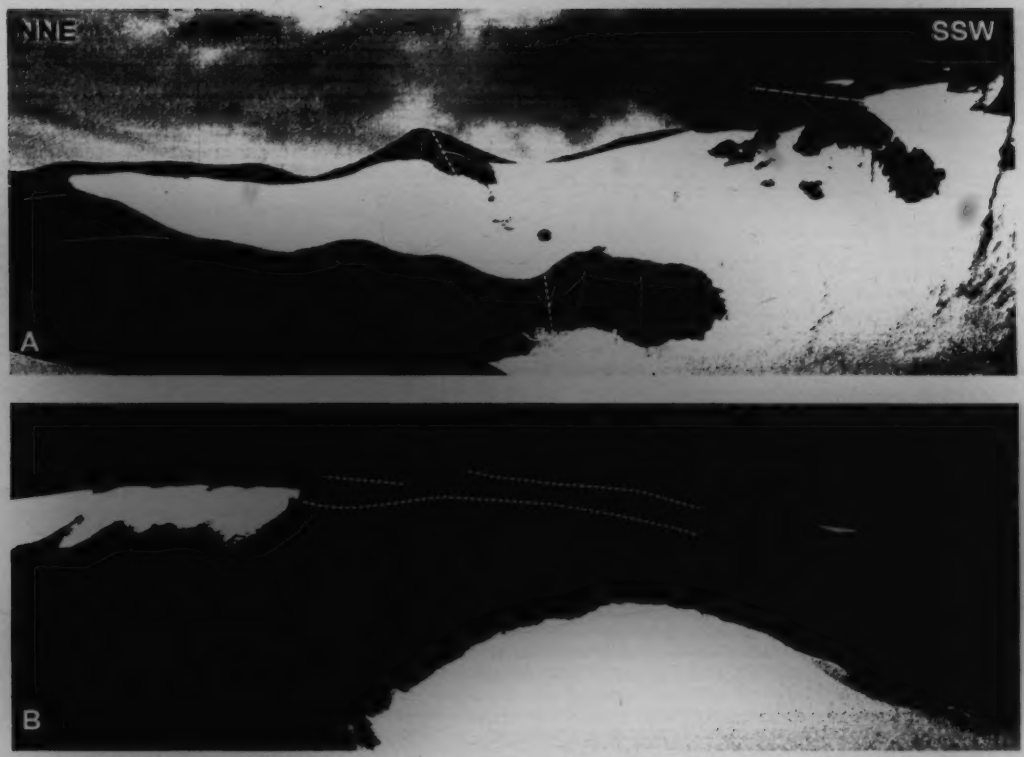

Figure 2.23: Exposures of folds in the southern Oweegee Dome area. Solid lines indicate bedding traces, dashed lines faults, and dotted lines folds. A: View towards ESE of anticline-syncline pair obscured by snow. Field of view ~500 m; B: View towards NE of gently inclined folds. Field of view ~300 m.

folds. In several localities fold hinges outcrop, displaying a well-developed axial planar cleavage (figure 2.24), and rarely a secondary cleavage is developed oblique to the axial plane of the fold (figure 2.25). Two cleavage sets can often be observed at outcrops not associated with the hinge of fold, and produce a steeply-plunging pencil lineation. The trace of N-trending folds can be estimated throughout the map area. Locally, the surface trace of these folds is deflected by folds that plunge steeply SE (figure 2.26).

Steep (~60°) SE-plunging folds are the second major set of structures at Iskut ridge and generally occur as upright anticline-syncline pairs spaced along the ridge. On either side of a pair of folds bedding gently bends to parallel the general grain of the ridge (figure 2.27). SE-plunging folds are rounded, open to close, and have a well-developed axial planar cleavage developed within finer units (figure 2.27). Exposed folds are class 1B, class II and class III folds. The wavelengths of these folds are generally short,

Figure 2.24: View to SSW of F1 anticline at Iskut Ridge. Vertical planes are an axial planar cleavage oriented 012°/88° E.

Figure 2.25: View to north of F1 syncline in Iskut Ridge area. Shaded planes illustrate orientations of two cleavage sets labelled 'A' and 'B'. Cleavage 'A' oriented 025°/85° E, cleavage 'B' oriented 319°/87° NE. Estimated axial plane orientation is 005°/70° E. Height of view is approximately 4 metres.

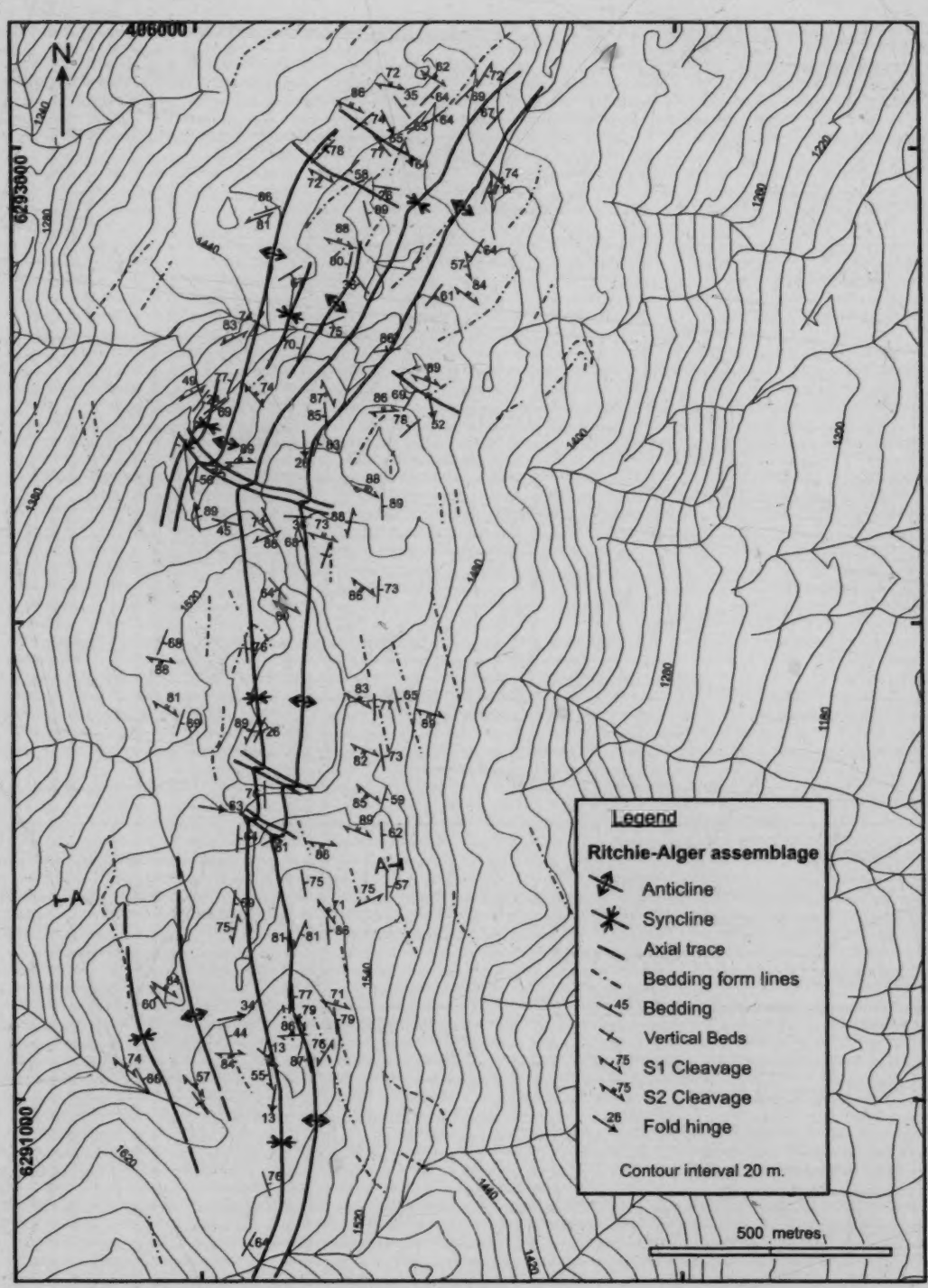

Figure 2.26: Structural map of the Iskut ridge area. Note deflection of N-trending F1 folds by SE-plunging F2 folds. A-A' marks location of cross-section in figure 2.30.

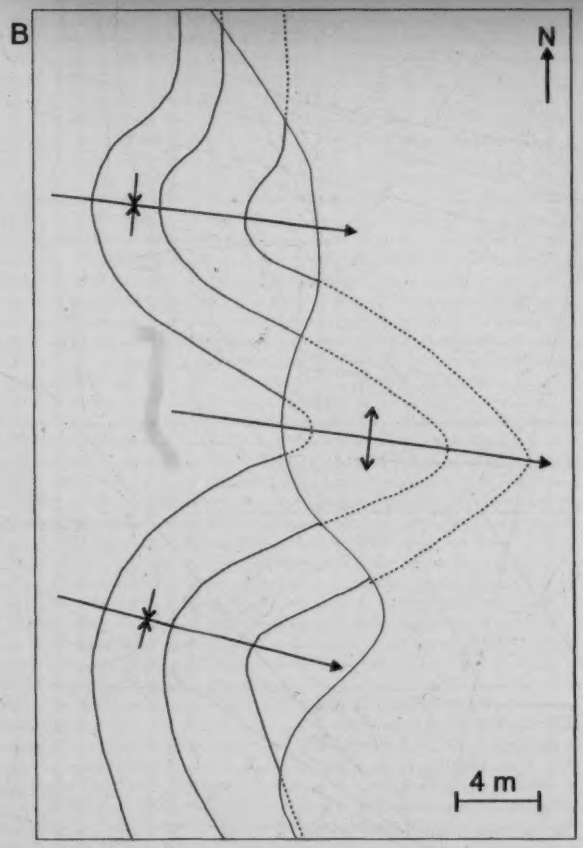

Figure 2.27: F2 folds in the Iskut ridge area. A: Profile view of SE-plunging F2 syncline. View is tilted ~50° down towards ESE. Fractures cutting siltstone are an axial planar cleavage oriented 098°/86° S; B: Schematic map of F2 folds. Fold displayed in 'A' is the northernmost syncline. Grey area is cover. Note how beyond folds bedding lineaments become north trending, as is found in most of the ridge.

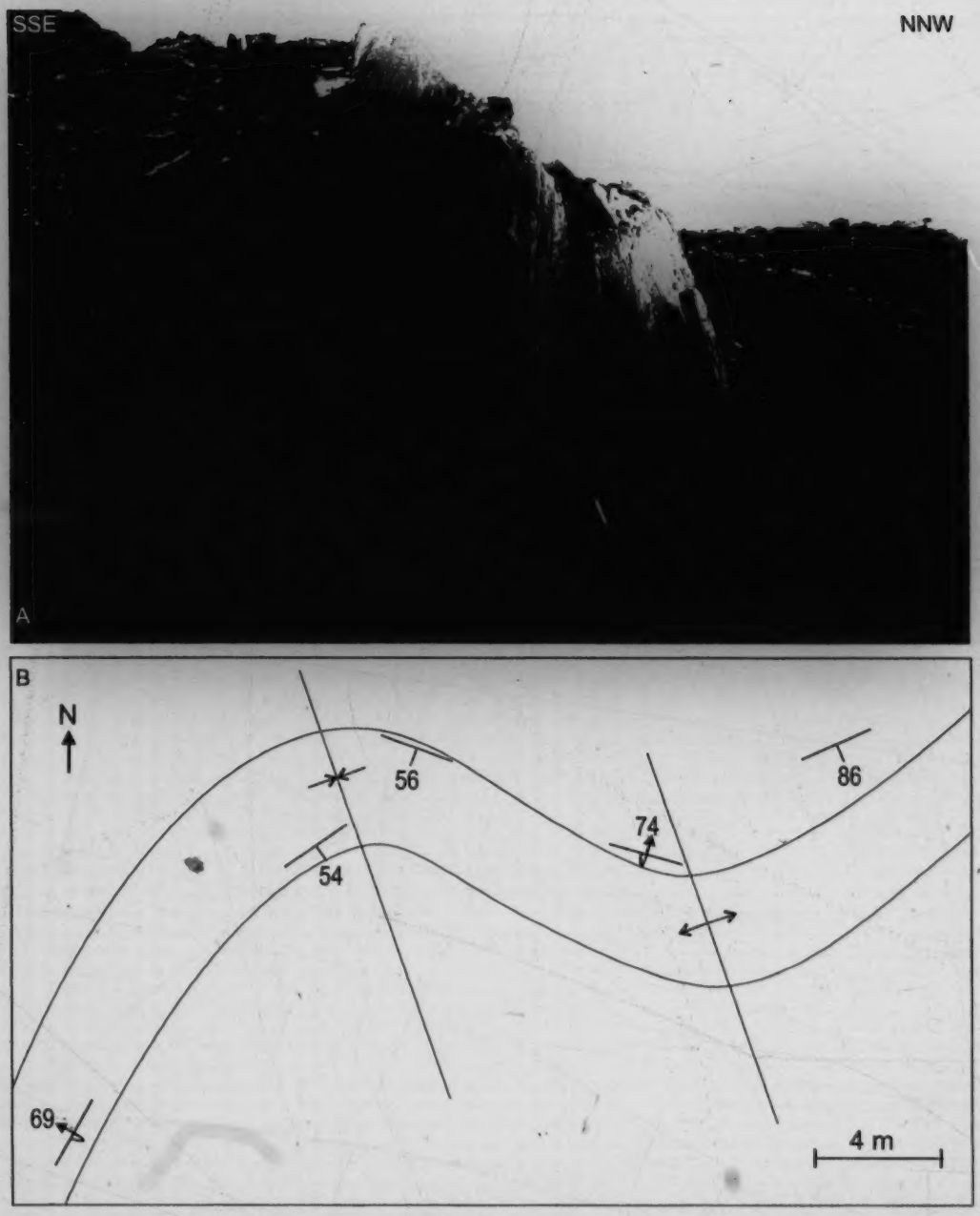

Figure 2.28: Outcrop-scale fold interference in the Iskut ridge area. A: Photo towards WSW of outcrop that is gently folded, in this view, about a gently inclined axial plane. Likely part of a larger, more upright fold, with only curvature on limbs seen here; B: Large-scale map of area around outcrop photographed in (A). At this scale in map view bedding is folded about SE-trending axes. Changes in dip direction (i.e. where bedding is overturned) are a result of folds seen in (A).

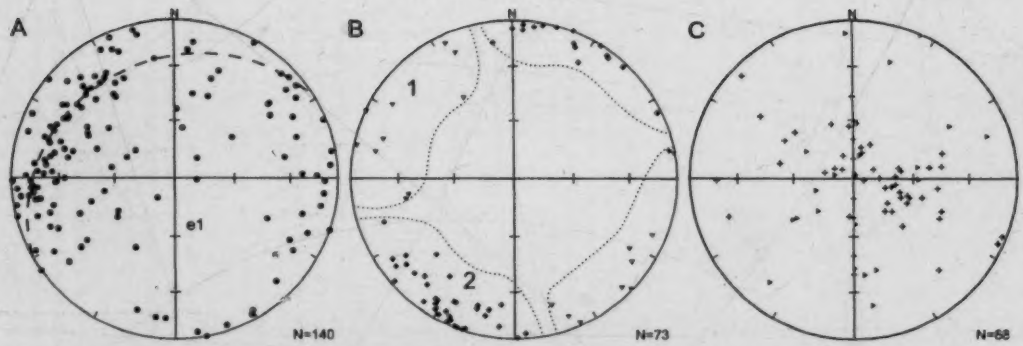

Figure 2.29: Equal-area lower hemisphere projections of structure data from Iskut ridge. A: poles to bedding. e1= eigenvector 1. Dashed line represents girdle distribution; B: poles to cleavage. Dashed lines outline clusters of S1 and S2 cleavage. ▼=S1, ♦ =S2; C: bedding-cleavage intersection lineations. ►=L1 lineations, +=L2 lineations.

on the order of metres. Rare outcrops demonstrate outcrop-scale fold interference as gently inclined NE-trending gentle folds are folded by SE-trending close folds (figure 2.28). The deflection of the map trace of N-trending folds by SE-plunging folds (figure 2.26) demonstrates a clear timing relationship, with late, F2 SE-plunging folds having overprinted early N to NE-trending F1 folds. This may also lend explanation to the overall change in orientation of the ridge, and the F1 folds within it, from a N-trending orientation in the south to the NNE-trending orientation towards the north of the ridge (figure 2.26). Abundant bedding-parallel slip planes suggest that flexural-slip deformation was an active process in the Iskut ridge area

Equal-area projection of poles to bedding shows a scattered girdle distribution with a steep SE-plunging π-axis (figure 2.29). The abundance of E-dipping strata throughout the area suggests the ridge may be on the east limb of a kilometre-scale anticlinorium (figure 2.30). Projection of poles to cleavage reveals two clusters of data that are interpreted as S1 and S2 cleavage, based on the map and outcrop relationships of F1 and F2 folds (figure 2.30B). The larger number of recorded values for S2 poles is in part a sampling bias, as more folds exposing clear S2 cleavage were found and measured at a tighter spacing. Detailed petrographic description of cleavage will follow in Chapter 4. Bedding-cleavage intersection lineations have a scattered distribution. L1 lineations

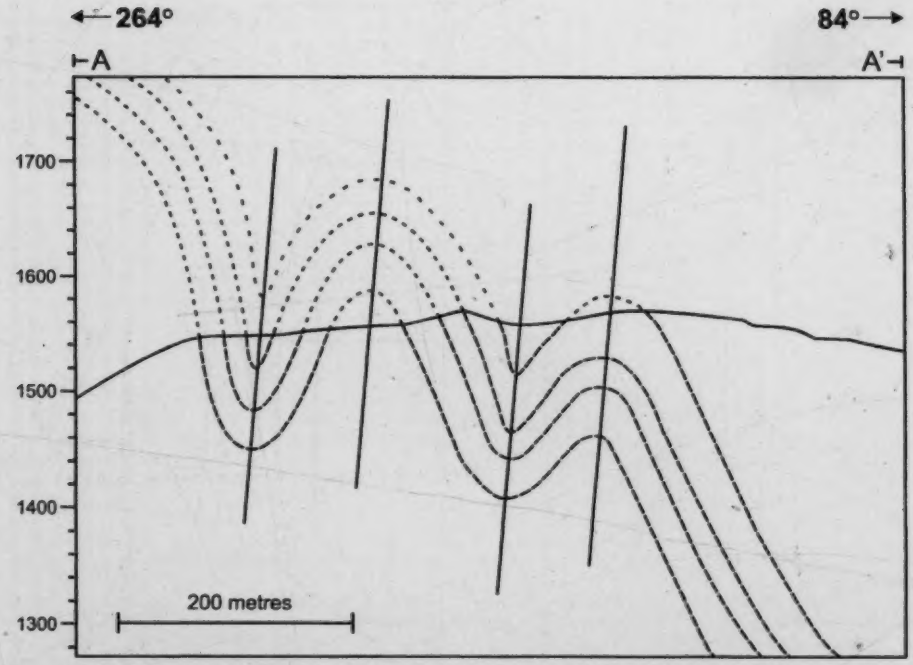

Figure 2.30: Schematic W-E natural scale cross-section of the Iskut ridge area from A-A.' Section located on figure 2.26. Structures illustrated result from ~N-trending F1 folds. Overall east-dipping bedding suggests ridge may be part of a large anticlinorium.

are thinly scattered along a near-vertical plane striking NE-SW (figure 2.29C). L2 lineations are greater in number and are more tightly spread NW-SE, with the majority plunging steeply to the SE. The steep L1 lineations are unexpected, since most observed F1 folds were gently plunging. The implications of this are that F1 folds have been steepened, presumably by F2 folds. This is generally consistent with field observations of F2 folds. The tighter distribution of L2 lineations suggests they have not been scattered by folding.

2.2.7 Eskay Creek

The Eskay Creek area is located near the Eskay Creek gold mine which operates within a normal-fault bounded, NE-plunging anticline (Roth et al., 1999). The Eskay Creek area comprises rocks of the Ritchie-Alger assemblage, within kilometres of the edge of the basin (figure 1.4). The mapped rocks can be subdivided into two facies, one

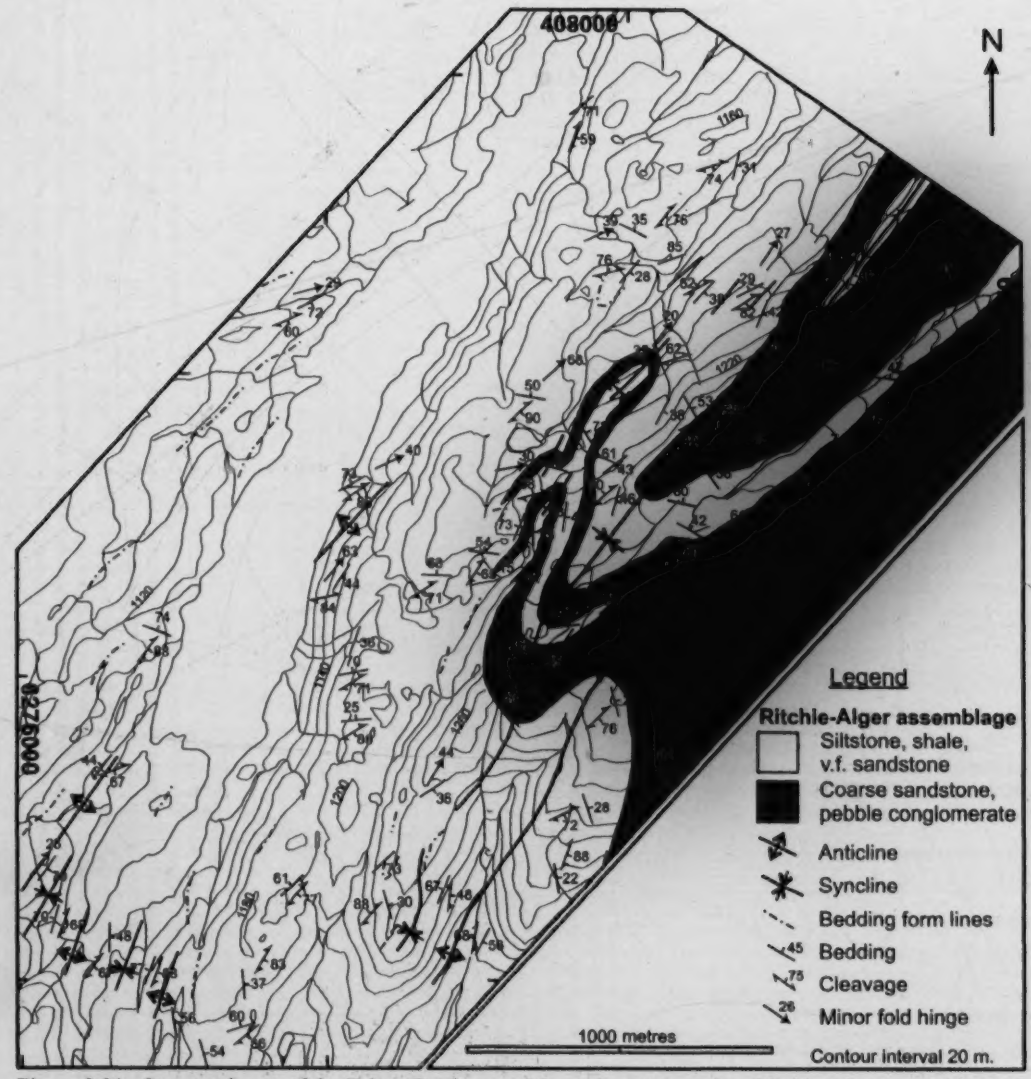

Figure 2.31: Structural map of the Eskay Creek area. Mapped area comprises Ritchie-Alger assemblage of the Bowser Lake Group. Coarse clastics gradually pinch out towards the west in favour of thinly bedded, cleaved siltstones and shale.

comprising thinly bedded siliceous siltstone and slaty shale and the other thin to thickly bedded sandstone and thickly bedded chert-pebble conglomerate (figure 2.31). The latter facies is often extensively veined with quartz.

The structure in the Eskay Creek area is dominated by map-scale open, gently NE-plunging folds (Lewis, 1992; Roth et al., 1999; Waldron et al., 2006), and by outcrop-scale folds inferred to be parasitic to the map-scale folds (figure 2.31). Two generations

Figure 2.32: Succession of tight folds in the Eskay Creek area within laminated siltstone and sandstone. View is down towards ENE. Folds plunge 40° towards 065°.

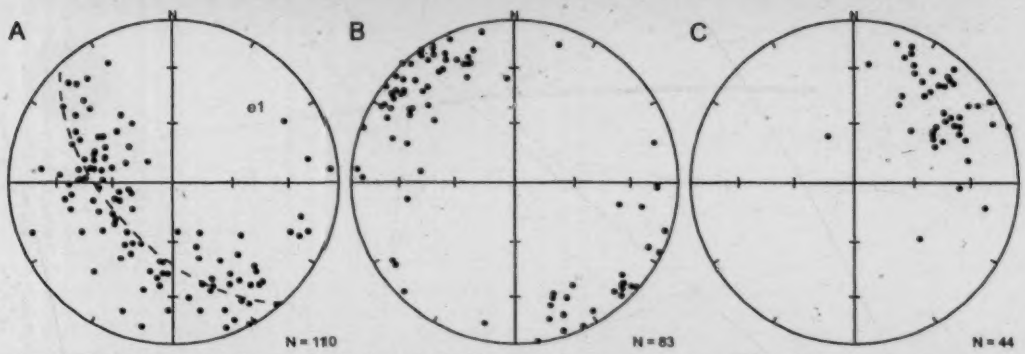

Figure 2.33: Equal-area lower hemisphere projections of structure data from Eskay Creek area. A: poles to bedding. e1= eigenvector 1. Dashed line represents girdle distribution; B: poles to cleavage; C: bedding-cleavage intersection lineations.

of folds are observed in the Eskay Creek area (F1 and F2). The presence of map-scale NE-plunging folds in the map area is confirmed by the distribution of the two map units. Outcrop-scale F1 folds are open to tight (figure 2.32), with the majority being close folds. Form is variable; most are subrounded with rare subangular and kink folds. Class II and class III folds were observed from well-exposed hinge areas. F1 folds trend between NE and ENE, and most verge SE. Equal-area projection of poles to bedding shows a well-developed girdle with a NE-plunging π-axis (figure 2.33). Commonly an axial planar S1

Figure 2.34: Strained ammonite in the Eskay Creek area. View towards SE, orthogonal to exposure plane (wooden board) oriented 234°/90°. Cleavage here is oriented 056°/71° SE.

cleavage is associated with these folds. S1 cleavage is steep and projected poles form a moderately developed cluster with a slight girdle, likely due to cleavage refraction. Rare ammonites appear strained subparallel to S1 cleavage (figure 2.34). Projections of bedding-cleavage intersection lineations show a clear cluster plunging NE, with minor scatter. F1 folds are crosscut by postkinematic mafic dikes. One of these dikes was dated using Ar-Ar geochronology and is discussed in Chapter 4.

F2 folds are consistently gentle subrounded folds. They trend between ESE and SSE. F2 folds plunge SE and verge NE, locally in association with small thrust faults with centimetre offset. F2 folds are observed on the limbs of larger F1 folds and locally fold both bedding and S1 cleavage (figure 2.35); at the localities observed, S1 cleavage is at a low angle to bedding. Gentle F2 folding is also seen at map-scale. Some of the limbs of large F1 folds have deflections that can be attributed to F2 gentle folds. This is consistent with the timing relationships interpreted from the nearby Iskut ridge area, although F2 folds are much less prominent in the Eskay Creek area.

2.2.8 Teigen Lake

The Teigen Lake area is located east of the Eskay Creek area (figure 1.4) and comprises rocks of the lower and upper Hazelton Groups and the Ritchie-Alger assemblage. The lower Hazelton Group here exposes green angular conglomerate

Figure 2.35: Distorted S1 cleavage in the Eskay Creek area. View towards SW. Distortion displays gentle F2 folding of S1 cleavage about a NW-SE axis.

and sandstone, tuff, rusty-weathering rhyolite and gossan. The upper Hazelton group exposes feldspathic fine to coarse-grained sandstone with abundant mud clasts interbedded with thinly bedded siltstone, thin tuff and rare thick tuff beds, and thin fossil beds rich in belemnites and pelecypods.

Folds are relatively rare in the Teigen Lake area. Bedding primarily dips moderately to steeply to the NE, with little variation in strike in the Hazelton Group (figure 2.36). Rare tight folds in the upper Hazelton Group plunge to the SE. Tight folds are not observed in the underlying volcanics. One outcrop in the overlying Bowser Lake Group of a tight anticline-syncline pair, with faults in the core, is the only outcrop scale example of folds identified in the youngest strata (figure 2.37). In the Bowser Lake Group bedding orientation is more variable, suggesting the presence of additional folds not viewed in outcrop. Folds interpreted from bedding measurements trend NW or NE, occurring as anticline-syncline pairs. Projection of poles to bedding shows a moderately developed girdle distribution with a moderately N-plunging π-axis (figure

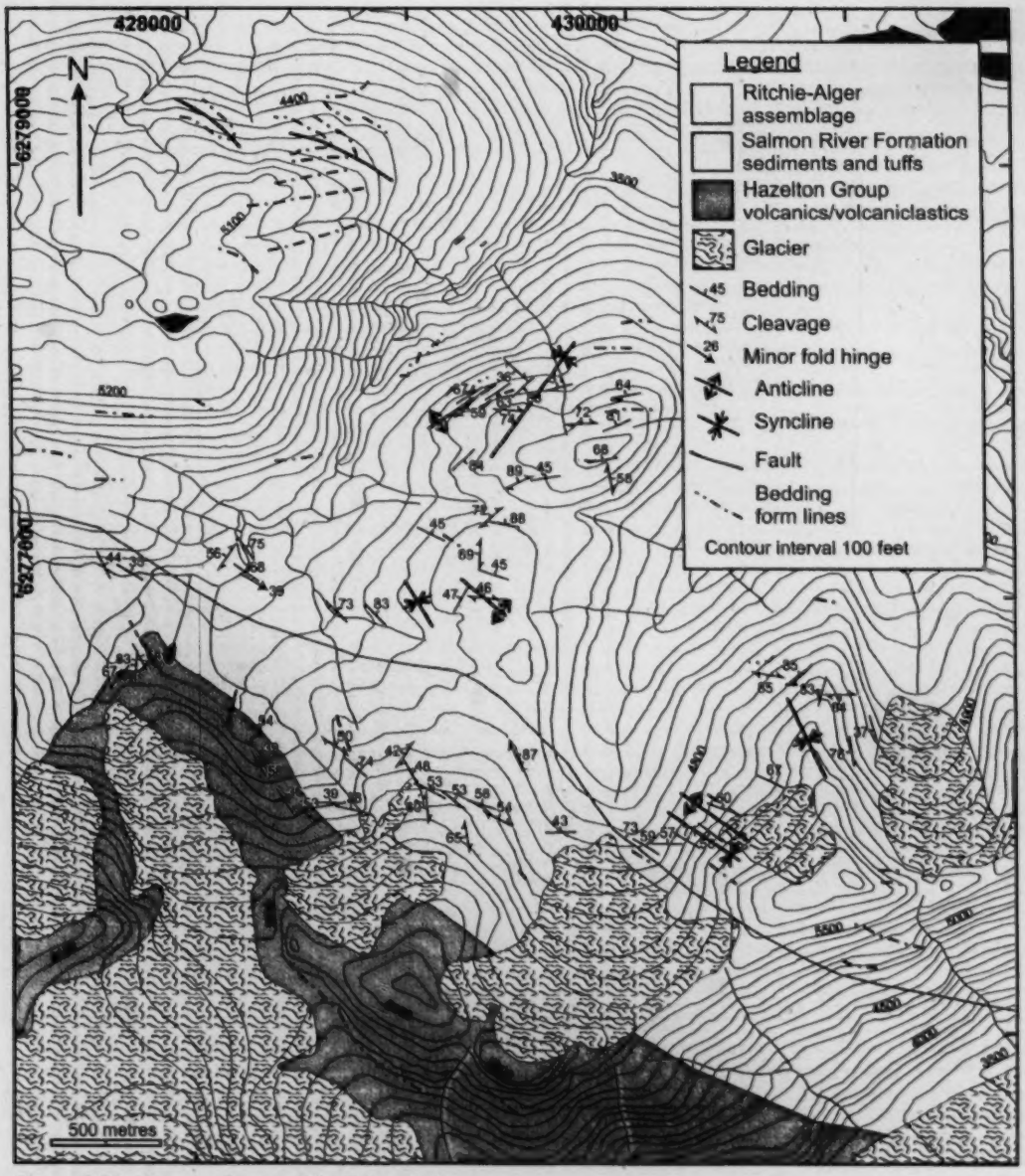

Figure 2.36: Structural map of the Teigen Lake area.

2.38), essentially averaging NW- and NE-trending folds. Despite the rarity of outcrop-scale folding, shale is locally penetratively cleaved, sometimes with two distinct cleavage sets striking E and SSW, indicating multiple episodes of deformation. Bedding-cleavage intersection lineations are consistent with NW-SE trending folds (figure 2.38C). The map relationships at Teigen Lake indicate the fold sets identified to the west at Iskut ridge

Figure 2.37: View to east of anticline-syncline pair in the Teigen Lake area.

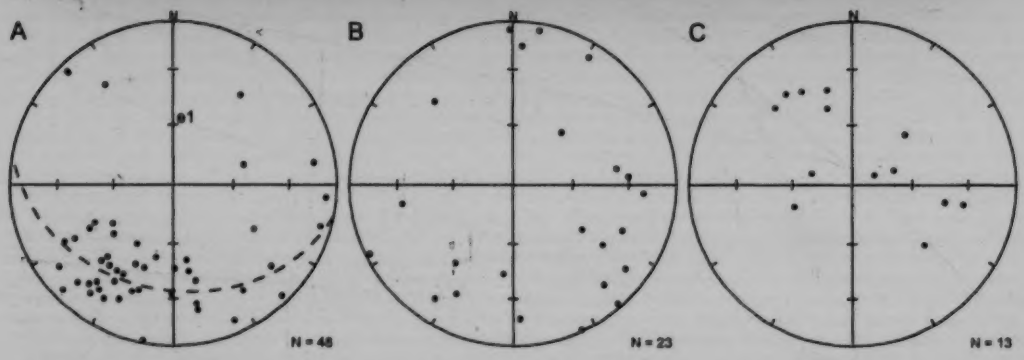

Figure 2.38: Equal-area lower hemisphere projections of structure data from Teigen Lake area. A: poles to bedding. e1= eigenvector 1. Dashed line represents girdle distribution; B: poles to cleavage; C: bedding-cleavage intersection lineations.

and Eskay Creek (figure 1.4) can be extended towards the east. The timing relationships identified in those areas suggested NE-trending folds formed first followed by NW-trending folds.

2.2.9 Nelson Creek

The Nelson Creek area is located along the western margin of the Bowser Basin

(figure 1.4) where subparallel NE-trending ridges exposes a domain of NW-trending folds (Evenchick et al., 2000). This area exposes rocks of the lower Hazelton Group, Salmon River Formation, and Ritchie-Alger assemblage. The lower Hazelton Group includes thick felsic and mafic flows, pyroclastic flows and rare mudstones. Extensive iron-staining indicates a high degree of alteration. The Salmon River Formation occurs as thinly interbedded mudstones and siltstones, with less common sandstone. The Ritchie-Alger assemblage here is largely siltstone and sandstone with abundant chert clasts of highly variable thickness, with only rare conglomerate exposure. Arrays of mafic dikes crosscut all structures. Locally steeply S-dipping dikes are associated with apparent 'drag folding' indicating a component of dextral movement during emplacement. These dikes are post-kinematic with respect to regional folds and have been dated to have been emplaced during the Eocene (51-48Ma) as part of a larger magmatic arc (Greig et al. 1995). This constrains deformation in this area to pre-date Eocene intrusion.

The lower Hazelton Group volcanics in the Nelson Creek area have experienced a degree of shearing and alteration similar to that seen in the Oweegee Dome area. Highly-stretched lapilli tuffs (figure 2.39) are dextrally sheared along steep N-S striking shear zones. Shear fabrics adjacent to quartz veins, and *en echelon* asymmetric vein arrays, with moderate to steeply SW-dipping shear zones further discussed in Chapter 3, indicate the presence of relatively ductile dextral-reverse strain. Sedimentary rocks of the Salmon River Formation are in contact with the lower Hazelton Group volcanics along a steeply NE-dipping (325/65 NE) fault (figure 2.40). This fault is a normal fault as it places younger Salmon River sedimentary rocks over older Hazelton Group volcanics. The contact between upper and lower Hazelton strata is also defined by a fault in the immediate vicinity of the map area (pers. comm. 2006, T. Baressi). In one location a mafic dike similar to those discussed above has intruded parallel to the contact between volcanics and sediments. This suggests extension associated with normal faults and dike emplacement may be coeval, occurring in the Eocene. This activity may have occurred

during post-orogenic extension.

Complexly deformed sediments of the Salmon River Formation are similar to those in the Mount Will area. These strata have been deformed through a series of small folds and faults (figure 2.41). Small thrust faults propagated sub-parallel to the strike of moderately ENE-dipping bedding, cutting up-section towards the SSE. If it is assumed faults initially formed with transport directions opposite to fault dip-direction it would indicate that faults have been tilted as part of regional folding. This indicates a period of faulting prior to fold development. These structures represent the only clear evidence in the Nelson Creek area for structures that may have formed in conjunction with regional

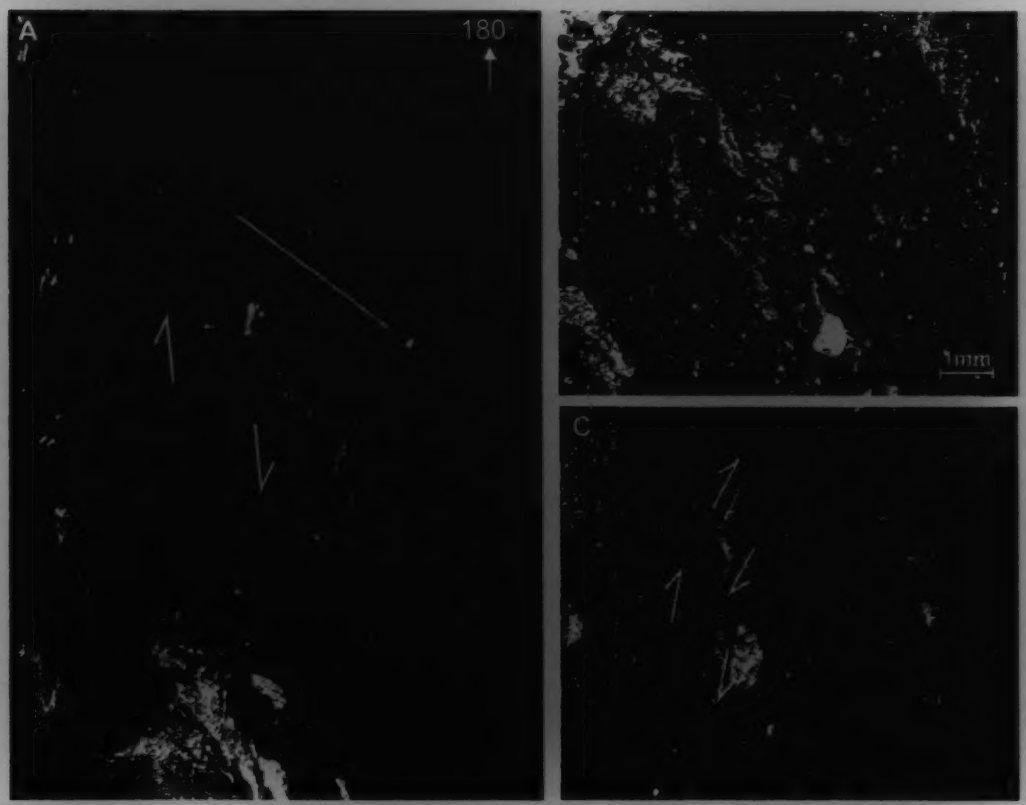

Figure 2.39: Elongate lapilli tuffs of the Hazelton Group in the Nelson Creek area. Clasts outlined have asymmetric shapes that taper towards tips, resulting in a stretched appearance. Half arrows indicate interpreted dextral sense of shear. A: View down to south of outcrop of lapilli tuff; B: Thin section photomicrographs of lapilli tuff in thin section, displaying same stretched appearance as outcrop in (A). B: Photomicrograph viewed in plane polarized light; C: Photomicrograph viewed in cross-polarized light.

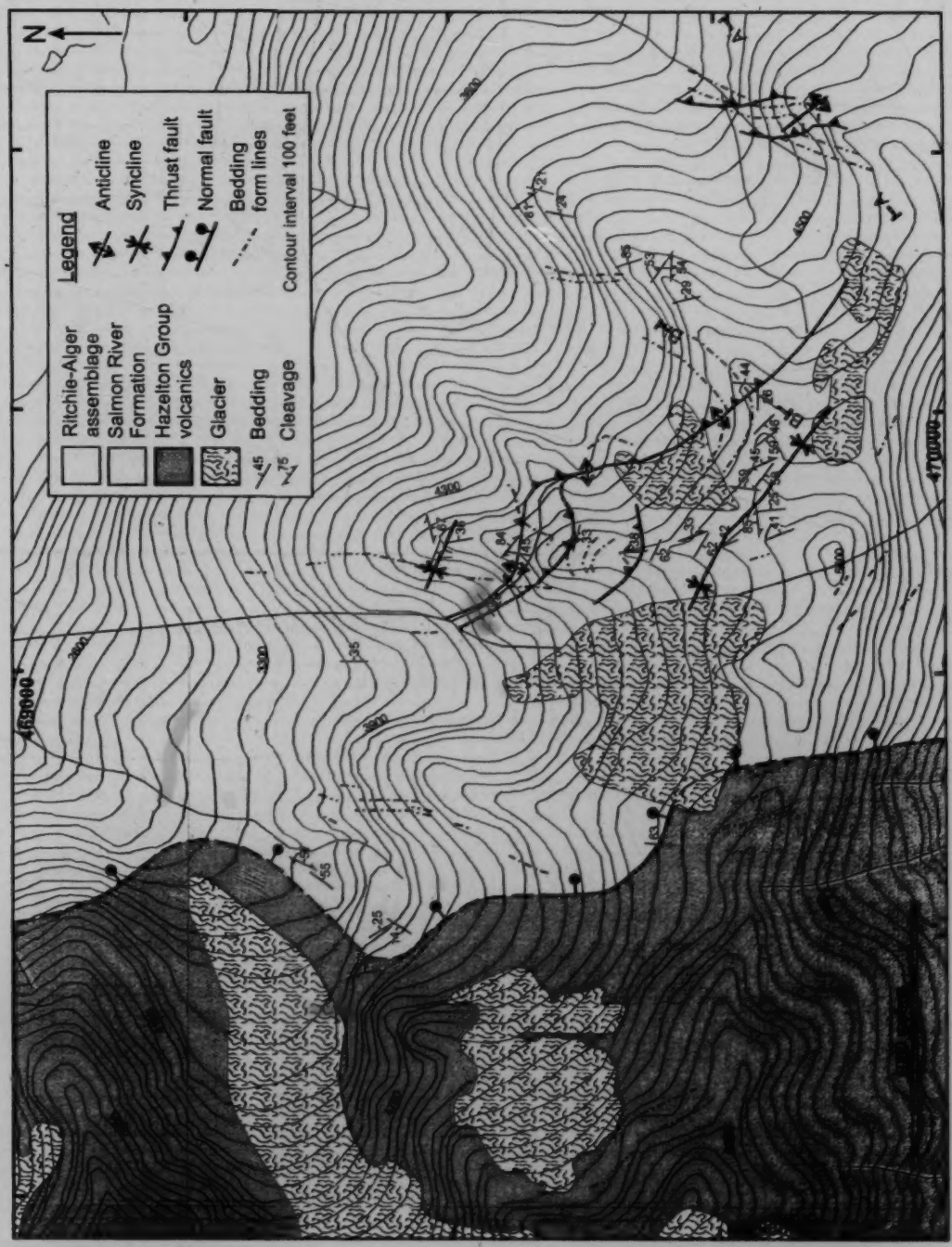

Figure 2.40: Structural map of Nelson Creek area. Folds superimposed by thrust faults have faulted hinges. Large normal fault forms contact between Lower Hazelton Group volcanics and thinly bedded sediments of the Salmon River Formation. A-A' and B-B' mark locations of cross-sections in figure 2.43.

Figure 2.41: View to east of complexly deformed sediments of the Salmon River Formation in the Nelson Creek area. Dashed lines represent small faults of unknown offset. Overlying strata are subhorizontal and in comparison relatively undeformed.

NE-trending folds.

The Nelson Creek area contains a number of hundred-metre scale folds trending NW, perpendicular to ridges trending NNE, thereby providing excellent cross-sectional exposure. Folds exposed on ridges are subrounded to rounded, in the form of class II folds. These folds are upright to steeply inclined, with a clear vergence to the SW. Equal-area projection of poles to bedding shows a moderately developed girdle with a π–axis plunging gently towards SE (figure 2.42). Cleavage has a scattered distribution, while bedding-cleavage intersection lineations predominantly plunge gently SE. Thrust faults associated with folds are gently inclined and verge SW, periodically cutting-up section (figure 2.43A). Folds form around the tips of faults that terminate in the form of fault propagation folds (figure 2.43B), and as fault-bend folds. Major structures

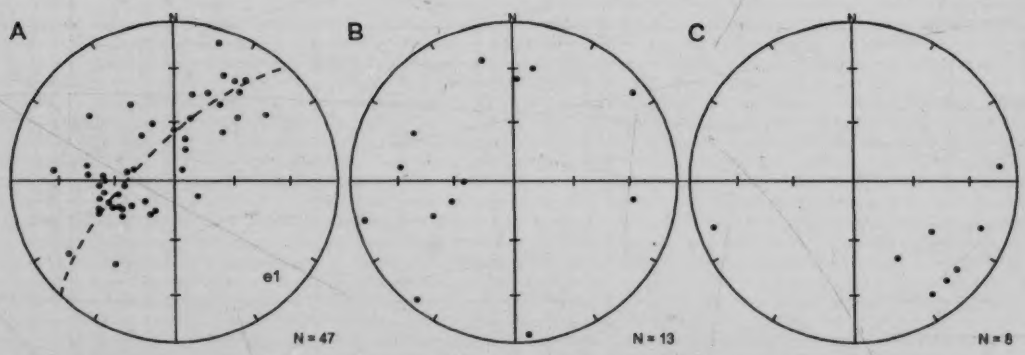

Figure 2.42: Equal-area lower hemisphere projections of structure data from Nelson Creek area. A: poles to bedding. e1= eigenvector 1. Dashed line represents girdle distribution; B: poles to cleavage; C: bedding-cleavage intersection lineations.

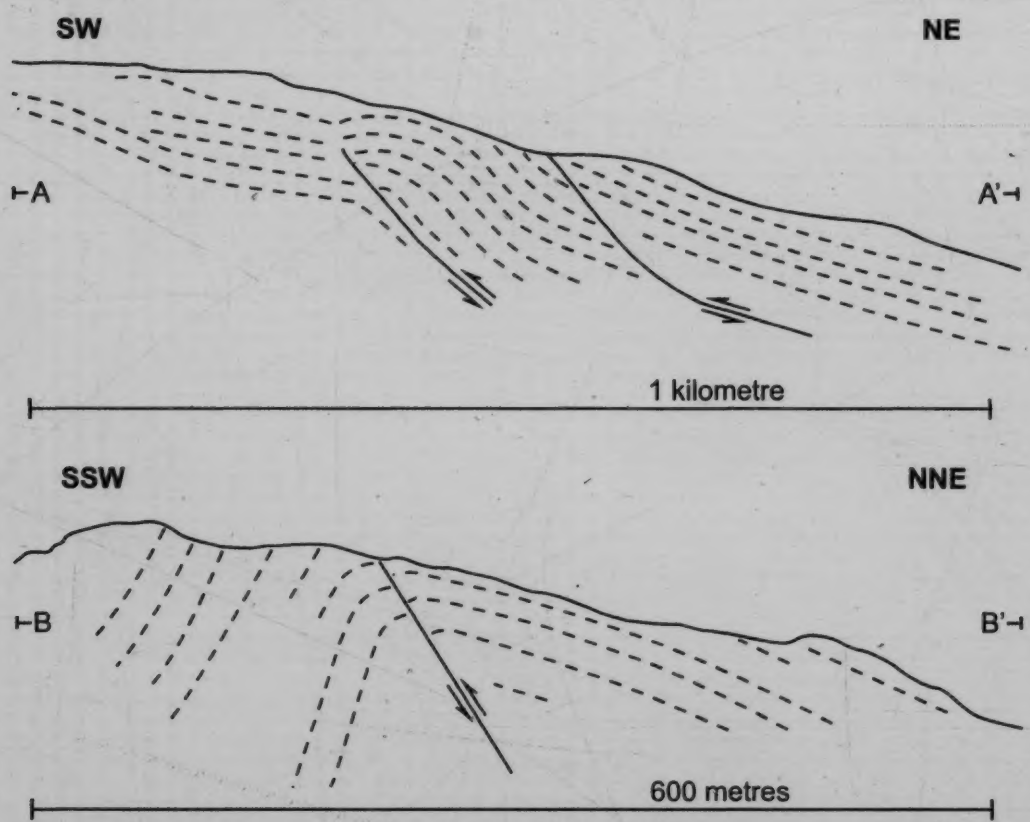

Figure 2.43: Schematic cross-sections of NE-trending ridges in the Nelson Creek area, located on figure 2.40. Both cross-sections are of sediments of the Ritchie-Alger assemblage. A-A': SW-NE cross-section demonstrating active role of thrust faults in the Nelson Creek area. Fault-bend folds develop as faults cut up-section and form hangingwall and footwall ramps and flats; B-B': SSW-NNE cross-section of anticline with fault at core of the fold. In this case the anticline is interpreted to develop from fault-propagation folding as the fault terminates up-section.

correlate from ridge to ridge; however there is a clear lateral variation in structure style towards younger strata to the east. The SW vergence of structures in the Nelson Creek area is contradictory to the NE vergence that has been reported elsewhere in the fold belt (Evenchick, 1991a). This suggests that SW-verging faults are backthrusts.

Structures in the Nelson Creek area are variable in form and timing. Ductile structures such as sheared lapilli tuffs found only in the lower Hazelton Group may pre-date formation of the fold belt. Limited evidence for NE-trending folds is consistent with a lack of documented NE-trending folds along the western margin of the basin below the latitude of the Nelson Creek area (figure 1.4). Observed folds, faults, and stereographic projection of structural data are all consistent with the area being structurally dominated by NW-trending folds. The normal fault developed between lower and upper Hazelton Group rocks is hypothesized to have developed last, possibly during the Eocene emplacement (Greig et al., 1995) of mafic dikes.

2.3 Discussion of Folds and Related Structures

The Skeena Fold Belt is dominated by two major fold sets: folds that trend generally NE and those that trend NW (Evenchick, 1991a, 2001). Several of the areas examined in this study display both fold sets, whereas others contain only folds trending NW. In the areas where timing relationships are best constrained, Iskut ridge and Eskay Creek, F1 folds trend NE and F2 folds trend NW. These timing relationships are indicated by cross-cutting F1 and F2 folds. The fold axial traces of F1 folds are deflected by F2 folds (figure 2.26, 2.31) indicating a clear timing relationship. The Cartmel Lake and Sweeny Creek areas support this timing relationship. A décollement in the Cartmel Lake area associated with NE-trending F1 folds does not deflect large NW-trending F2 folds that traverse the area. In the Sweeny Creek area, the strike of N-trending folds changes strike towards F2 NW-trending folds, suggesting likely refolding by F2 folds. In the Maitland plateau and Teigen Lake areas timing relationships are ambiguous. In Maitland plateau WNW-trending folds are generally more dominant, and traceable over

greater distances, suggesting they have not been folded by NNE-trending folds. These areas illustrate the difficulty typically encountered when establishing timing relationships in areas with nearly orthogonal fold trends and shallow-plunging fold hinges.

F1 folds are relatively large, map-scale structures in the areas where they are exposed. They are commonly N- to NE-trending subhorizontal to gently-plunging structures. Their impact on the geology of the areas studied is most pronounced in the more western Iskut ridge and Eskay Creek areas. Here they form open and gentle folds that can sometimes be traced for over 2 kilometres. Towards the east they become somewhat smaller and subordinate to F2 folds. In the Mount Will area, F1 folds are absent. This is consistent with F1 folds having formed in association with an eastward-propagating deformation front which became progressively less active before reaching the eastern half of the Bowser Basin.

The absence of F1 folds in the Oweegee Dome area is somewhat unexpected, given that they are found to the north and west (figure 1.4). Oweegee Dome may represent a basement heterogeneity that prevented expression of F1 folds in the immediate vicinity. Alternatively, the domal structure may potentially result from interference of regional F1 and F2 folds not apparent from local observation. The lack of F1 folds in the Nelson Creek area is consistent with regional mapping indicating a lack of NE-trending folds in the southern half of the fold belt (Evenchick et al., 2004), with a major exception being the Hoan region in the south westernmost fold belt (Evenchick, 2001).

Clear association of F1 folds with thrust faults is limited to the Cartmel Lake area. The apparent lack of thrust faults elsewhere may be a function of poor exposure, or subsurface terminations in the form of blind thrusts. Another possibility is that F1 folds primarily formed by detachment folding.

F2 folds are relatively abundant throughout the Skeena Fold Belt, yet highly variable in form and size. In the western Iskut ridge and Eskay Creek areas they are of

relatively short wavelength and amplitude, and are lesser in size than F1 folds. The steep (up to 60°) SE plunge of F2 folds observed in the Iskut ridge area may be attributed to their exposure on steep east-dipping limbs of F1 folds (figure 2.30). East of these areas F2 folds become more dominant structures, with wavelengths and amplitudes of hundreds of metres as F1 folds become comparatively minor structures.

Cleavage is commonly developed in association with the axial planes of both F1 and F2 folds in the fold belt. On the limbs of folds cleavage is more sporadically developed, and more erratically oriented. In some outcrops two cleavage sets can be observed; however convincing cross-cutting relationships cannot generally be determined. The nature of cleavage will be elaborated in Chapter 4. Equal-area projections of cleavage poles from those areas strongly dominated by a single fold set typically have a reasonably well-developed cluster in agreement with axial planes. Projections of cleavage poles from areas with two folds sets have more scattered distributions. This is consistent with cleavage development during both episodes of folding, and scattering of early cleavage. In areas where cleavage is only weakly developed, distributions are more random. This suggests that temporally development of cleavage was long-lived but sporadic, and in response to a changing strain regime.

The Mount Will area illustrates the overall mechanism of deformation related to F2 folds. A SW-dipping, NE-verging thrust carried Hazelton Group volcanic and sedimentary rocks and the Bowser Lake Group and placed this package on the Salmon River Formation (figure 2.4). The underlying sediments deformed from the overriding thrust sheet, while the thrust sheet itself deformed internally. Higher-up detachments cut up-section through sediments of the Todagin assemblage and form asymmetric fault-propagation folds. The Mount Will area illustrates the close association of F2 folds and thrusts in this part of the fold belt.

The Nelson Creek area confirms the relationship observed at Mount Will between NW-striking folds and faults but with the difference that folds and faults verge SW

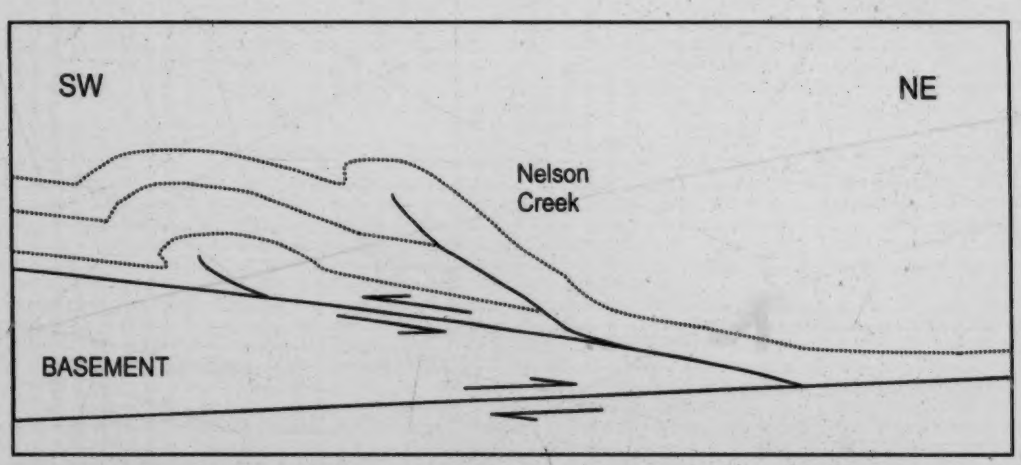

Figure 2.44: Schematic diagram illustrating possible relationship between SW-vergent structures in the Nelson Creek area and basement structure. Solid lines are faults, dashed lines schematically represent stratigraphy.

(figure 2.43). The faults at Nelson Creek area are backthrusts. Hinterland-vergent faults have been documented in the nearby Coast Belt (Rubin et al., 1990; Rusmore and Woodsworth, 1991; Journeay and Friedman, 1993). In the Coast Belt thrust faults form a 'fan' structure, which may also be the case at Nelson Creek. In 'fan' structures folds are commonly overturned, which is not the case at Nelson Creek. Another possibility is that deformation is being driven by a basement wedge, and that structures at Nelson Creek overly a west-vergent roof thrust (figure 2.44). Folds would be expected to switch to a NE-vergence east of the tip-line of the basement structure, which could explain NE-vergent folds in the majority of the fold belt.

Relationships between structures in this chapter and those in chapters 3 and 4 are synthesized in chapter 5.

Chapter 3: Veins and Brittle Structures

3.1 Background

Faults are less commonly observed in the Skeena Fold Belt than folds. The majority of faults identified in this study are steep strike-slip or oblique-slip normal faults. Some faults are low angle thrusts, associated with folds. These have been described in Chapter 2. In some areas enough data have been gathered during this study to isolate a solution for the kinematic regime that led to formation of these faults. Determining the kinematics of fault development allows comparison to fold development, and the relationship, if any, between the two types of structures. These quantitative kinematic methods have not been applied to brittle structures in the Skeena Fold Belt in previous studies.

Several of the areas mapped in the fold belt contain at least some exposure of *en echelon* vein arrays. *En echelon* veins were noted in a limited number of areas by Bone (2002) and Moffat (1985), but had not been systematically described or interpreted. Comparison of *en echelon* veins from a number of different areas in this study allows establishment of a possible common geometry, timing and genesis.

3.1.1 Fault terminology and methodology

In some locations numerous faults of a particular type were observed. When sufficient data have been acquired, the kinematics of fault development were analysed using the program FaultKinWin 1.2.2 by Allmendinger (2001). The operations reported here are the representation of faults via a slip-linear plot, and the calculation of P- and T-axes, P Dihedra grids, linked Bingham axes and fault plane solutions. The operations of FaultKinWin are described by Allmendinger (1989).

The data required to perform these calculations within FaultKinWin are the orientation of a given fault, orientation of slickenlines, and the sense of displacement of the fault. Sense-of-displacement indicators used include offset of stratigraphy, deflection

of fabrics by 'drag folding', and movement indicated by mineral 'steps' on quartz slickenfibres.

The P and T axes as used within FaultKinWin are analogous to the P and T axes determined from earthquake focal mechanism studies. Both are located on the 'movement plane' of a fault, which is the plane that includes the pole to a fault and the slickenlines corresponding to the sense of fault displacement (figure 3.1). The P and T axes (sometimes referred to as 'pressure' and 'tension' stress axes) both lie at an angle of 45° to both the fault pole and slickenlines. These axes do not necessarily represent principal stress directions, but rather are principal axes of incremental strain. The locations of these axes are objective; they represent an alternative display of fault data to conventional stereographic projection as a plane with striae (Marrett and Allmendinger, 1990). If the P and T axes coincide with principal stress directions, the fault plane and its conjugate must represent planes of maximum shear stress (Allmendinger, 1989). A slip-linear plot on an equal-area projection is another method or representation, which simply places a short segment of the movement plane through the pole to a fault with an arrow tip indicating the direction of footwall movement.

The method of P and T dihedra is used in FaultKinWin to help constrain the orientation of principal stresses for a given fault population. In this method the fault plane and the conjugate plane bisect a sphere into 4 quadrants (or two opposing pairs) (figure 3.2). The orientation of maximum principal stress for a given fault must lie within one pair (the P-quadrant), and the least principal stress must lie within the T-quadrant (Angelier, 1984). When applied to a population of related faults, those areas of a quadrant which are repeated with the most faults are most likely to contain the maximum and minimum principal stress axes (Angelier, 1984). FaultKinWin shows a series of grid nodes on an equal-area projection, each with a number corresponding to the number of faults with a P or T dihedron overlapping that node. These values can be contoured. From this an average estimation of the principal stresses orientations can be determined

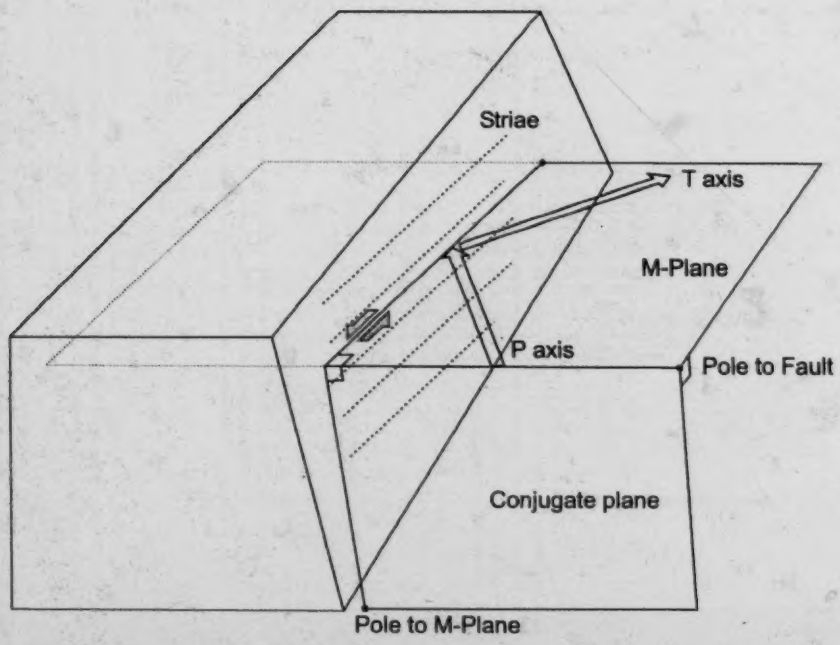

Figure 3.1: Schematic block diagram of near-vertical fault with subhorizontal striations indicating sinistral movement. Shaded area represents movement plane (M-plane) which is defined by the plane that contains the pole to the fault and striations. The movement plane also contains P and T axes, which lie at 45 degrees to both the fault pole and striations. The conjugate (or nodal) plane is defined by the plane that contains the pole to the fault and the pole to the movement plane.

from the node(s) with the greatest number of overlapping dihedra (Angelier, 1984; Allmendinger, 1989). A refinement of this method is discussed by Lisle (1987) who further constrains the location of principal stresses by dividing a sphere into two more quadrants, A & B, separated by the movement plane and conjugate plane. If a possible maximum principal stress occurs in the A quadrant and the P quadrant, then the minimum must lie in the B and the T quadrant, on the same side of the movement plane (Lisle, 1987).

The method of linked Bingham axes is a moment tensor summation that can be used to infer principal axes of strain (figure 3.3). In this method used in FaultKinWin faults are weighted equally and the moment tensors for all faults are added together to produce a tensor representation of bulk strain. Three eigenvectors 1, 2 and 3 (e1, e2, e3) are then calculated and represent principal axes of strain. The fault plane solution can

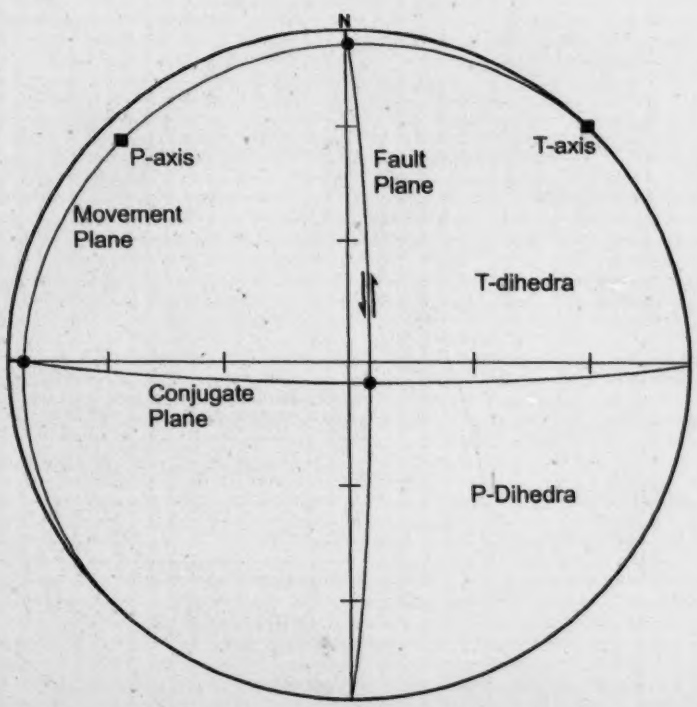

Figure 3.2: Lower hemisphere equal-area projection of P-T Dihedra in the case of a steep N-striking sinistral fault with subhorizontal slickenlines, based on the fault depicted in figure 3.1. Circular points are poles to labelled planes. Shaded area is region of T-Dihedra, white area represents P-Dihedra.

then be constructed by placing the intersection of two perpendicular planes through e2, and at 45 degrees from e1 and e3.

Application of the statistical methods used in FaultKinWin requires a number of assumptions. All stress calculation procedures require that slip on fault planes is not impeded by heterogeneity, and thus slip occurs towards the resolved shear stress (Angelier; 1979; Marrett and Allmendinger, 1990). The validity of this assumption is supported by numerous studies using these methods that produce sensible results (e.g. Marrett et al., 1994). Stress determinations also require that the fault population has not experienced subsequent deformation (Angelier, 1979). If deformation has occurred, orientations may be restored by rotating the faults by the value of bedding dip (Marrett and Allmendinger, 1990); however this obviously introduces uncertainty into the results.

Determination of strain from fault data requires the general assumption that the

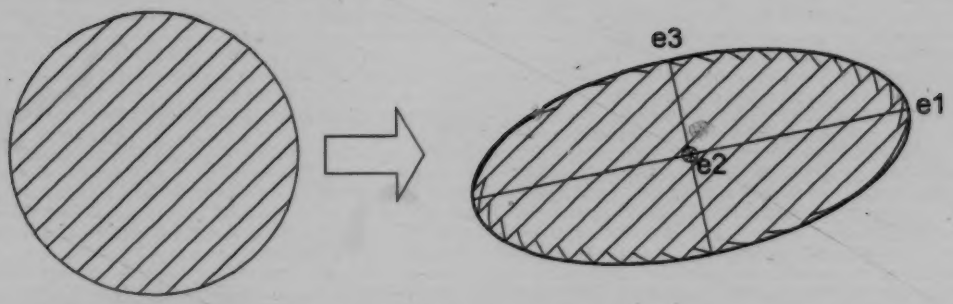

Figure 3.3: Schematic diagram of circular region cut by multiple parallel faults shown before and after faulting to illustrate summation used in FaultKinWin (Allmendinger, 2001) to develop linked Bingham Analysis. Dark ellipse represents strain ellipse after deformation. e1, e2 and e3 represent eigenvectors of maximum, intermediate, and minimum shortening respectively.

region being studied is significantly larger than the magnitude of slip (and therefore strain) on faults (Cladouhos and Allmendinger, 1993). As well, faults must be assumed to cut the boundaries of the region. This allows the assumption that the region rotates, rather than the fault itself (Cladouhos and Allmendinger, 1993). Calculation of linked Bingham axes requires that all faults are weighted equally. This assumption is also made when P and T axes are contoured (Allmendinger, 1989).

3.1.2 En echelon vein terminology

En echelon veins are brittle veins formed in subparallel arrangement in which a plane that contains the veins' tips is not oriented perpendicular to the veins themselves (figure 3.4). *En echelon* veins have received little attention in the Skeena Fold Belt. Moffat (1985) noted the presence of sigmoidal *en echelon* veins in the Groundhog Coalfield and suggested that they relate to shear zones. Bone (2002) briefly described *en echelon* veins in a few localities and interpreted sense of shear and general direction but did not offer a description of morphology or attempt to relate them to other structures in the area. Two morphologies are discussed here, those which are planar and those which are kinked or sigmoidal. The shear sense of planar arrays can be determined by assuming that the plane of the vein formed perpendicular to the minimum principal stress. The component of maximum principal stress, resolved parallel to the plane of

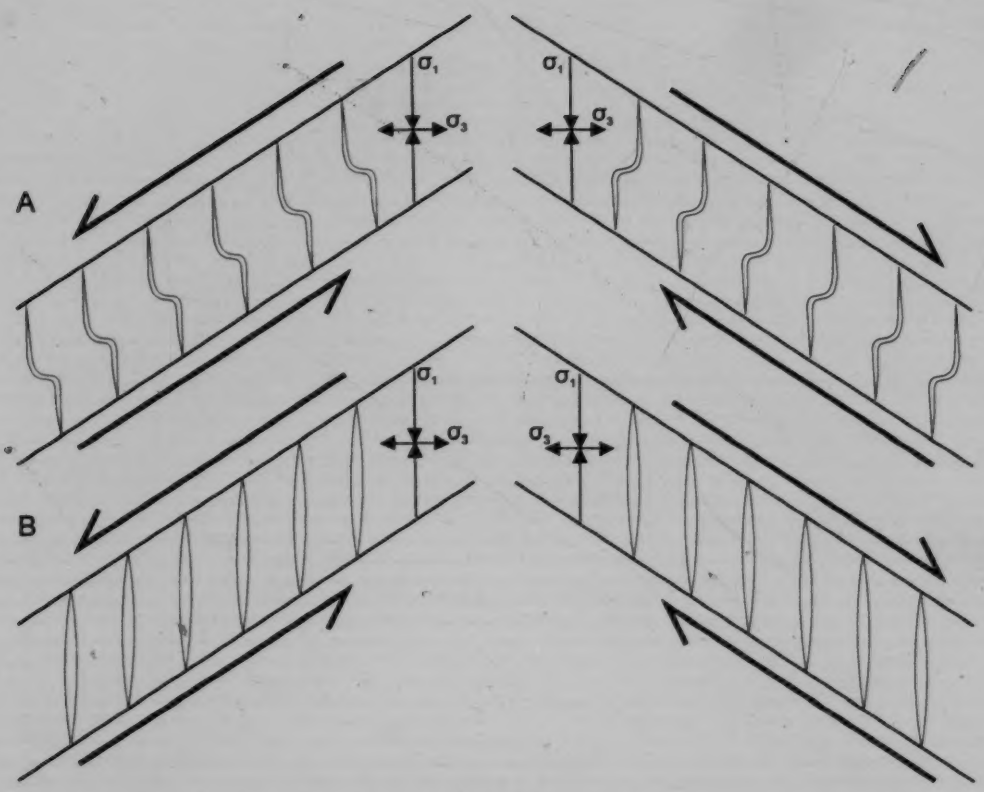

Figure 3.4: Idealized *en echelon* veins illustrating sinistral and dextral components of shear stress. σ1 indicates direction of maximum shortening and σ3 indicates direction of maximum extension. Half arrows indicate sense of component of shear. Rock beyond shaded area is not deformed. A: Asymmetric sigmoidal veins; B: Symmetric planar veins.

the array, corresponds to the direction of movement of that side of the array (figure 3.4). Shear sense of non-planar veins can also be determined in this fashion, or simply by classifying veins as either 'Z' shaped or 'S' shaped, in a manner similar to classifying fold asymmetry. 'Z' asymmetry then corresponds to a dextral component of shear relative to the direction of view, whereas 'S' asymmetry corresponds to a sinistral component of shear (figure 3.4).

Several mechanisms of vein filing have been proposed. Some e*n echelon* vein fills have been interpreted to precipitate via a crack-seal mechanism where fractures open in stages and fluid precipitates along bridges of wall rock, thereby sealing the fracture (Ramsay, 1980). Other veins may have formed as open fractures that are infilled by

precipating fluid. Pressure solution of host rock has been advocated as a mechanism to generate the saturated fluid that is precipitated (Beach, 1975; Ramsay and Huber, 1983).

En echelon vein arrays have been interpreted to form in a number of strain regimes and tectonic configurations. Some authors have advocated an origin from simple shear (Hancock, 1972; Beach, 1975; Ramsay and Huber, 1983; Becker and Gross, 1999) whereas others emphasize the dilational component of deformation (Pollard et al., 1982; Nicholson, 1991). Ultimately, it is necessary to have a component of extension to facilitate generation of cavities within which fluids can precipitate minerals and a component of shear to generate the asymmetry of the array. It is clear that *en echelon* veins can form in a variety of tectonic situations, including strike-slip settings (e.g. Swanson, 2006) and as part of fold belts (Johnston, 1993; Smith, 1996). Individual arrays must be examined in the context of other adjacent structures, in order to establish their kinematic significance.

Several aspects of vein geometry have been measured. For planar veins the vein itself, mineral fibres, and the orientation of the plane of shear were measured if exposure permitted. The orientation of mineral fibres within a vein corresponds to the direction of opening of the vein, and may be oblique to the vein wall. On non-planar veins the 'short limb' (i.e. the central of the three segments of a non-planar asymmetric vein), and the axis of rotation (the intersection of the central and an outer segment) can often also be estimated. Study of the three-dimensional geometry of *en echelon* veins has shown that they may not be symmetrical in three dimensions, but rather are twisted (Nicholson and Ejiofor, 1987). Unfortunately, those *en echelon* veins exposed in the areas studied are generally only exposed in two dimensions, or at the most in partial 3D with very little depth into the outcrop. Application of quantitative study of *en echelon* veins exposed

only in two dimensions is limited by this factor.

3.2 Field Observations

3.2.1 Maitland plateau

Faults are rarely exposed in the Maitland plateau area. Less than ten occurrences of bed-parallel veins and small slip planes with no sense-of-movement indicators were measured. Steep joints are common in fine to medium grained sandstone. Several outcrops contain multiple subvertical joints sets (figure 3.5). Two populations of joints are apparent when plotted in a rose diagram. One set strikes NW-SE and the other set NNE-SSW (figure 3.5). These joints are possibly conjugates, and may have resulted from brittle N-S directed shortening coupled with subhorizontal E-W extension.

3.2.2 Mount Will

An abundance of brittle structures was noted in the Mount Will area. These include thrust faults, strike-slip faults, normal faults, and sigmoidal *en echelon* veins. Steep brittle faults are relatively common in exposures of the Todagin assemblage. These faults appear undeformed and were initially interpreted to postdate local folding. Those faults with available sense-of-movement indicators were analysed using FaultKinWin (several additional faults have similar orientations but did not yield sense indicators). Slip-linear plots of 13 faults are consistent with mostly strike-slip motion on steep to moderately-dipping faults (figure 3.6). Analysis shows a concentration of P-dihedra plunging gently ENE. The maximum number of overlapping P-dihedra is 11 (84%) at grid nodes that plunge moderately E. Bingham analysis places e3 at 065°-32° and e1 at 187°-40°, indicating the principal finite strain directions are consistent with the predicted principal stresses. These data indicate overall ENE/WSW shortening with inclined extension. The e2 (intermediate axis of strain) is similar to fold axes in the area. This suggests the possibility that these faults are not part of a late brittle deformation but rather formed syntectonically during transport of the Mount Will Thrust Sheet described in

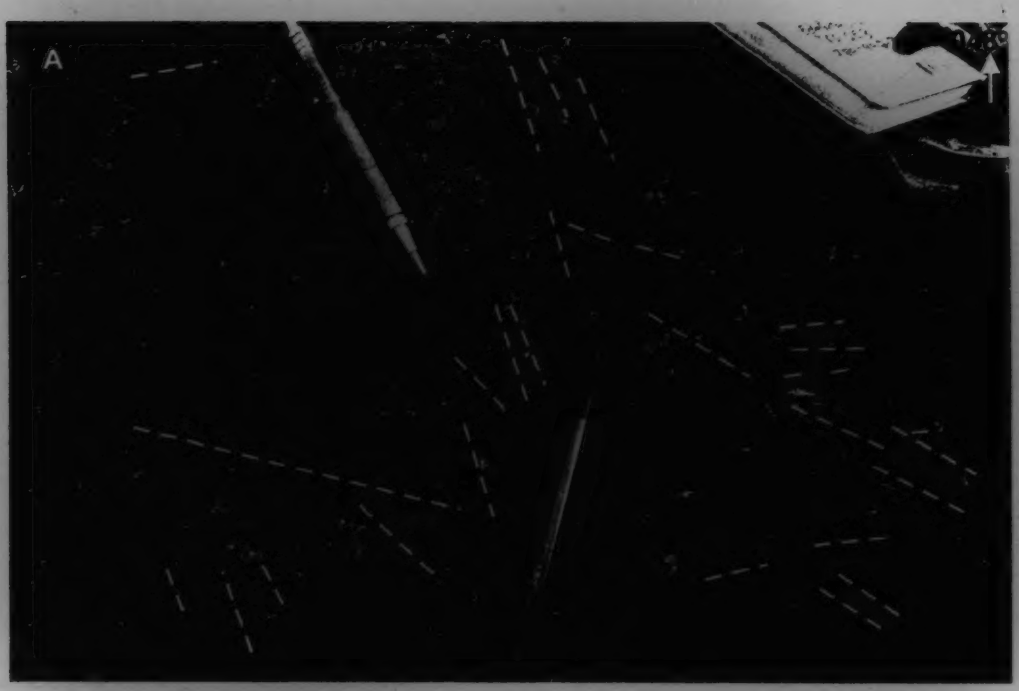

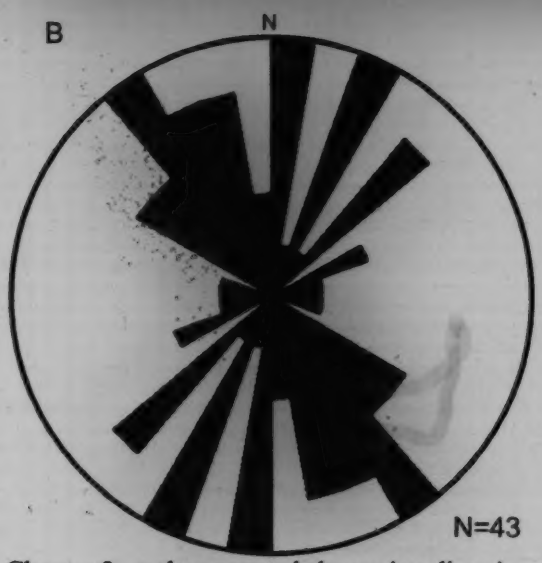

Figure 3.5: Joints in the Maitland Plateau area. A: View down to the NE of multiple joint sets exposed in vine-grained sandstone. Lines indicate traces of joints; B: 10 degree bin rose diagram of joint data collected. Two populations are revealed: one well constrained set strikes NW-SE and another more loosely defined set strikes N-S to NNE-SSW. Outer circle represents 5 measurements per bin.

Chapter 2, as the expected shortening directions are also similar. In this scenario folds in the thrust would have rotated the faults about a subhorizontal axis at a high angle to the faults, but would not have greatly affected the planar appearance of the faults. The inclined extension direction corroborates this as folds grow during vertical extension, whereas a separate strike-slip deformation would be expected to have a horizontal

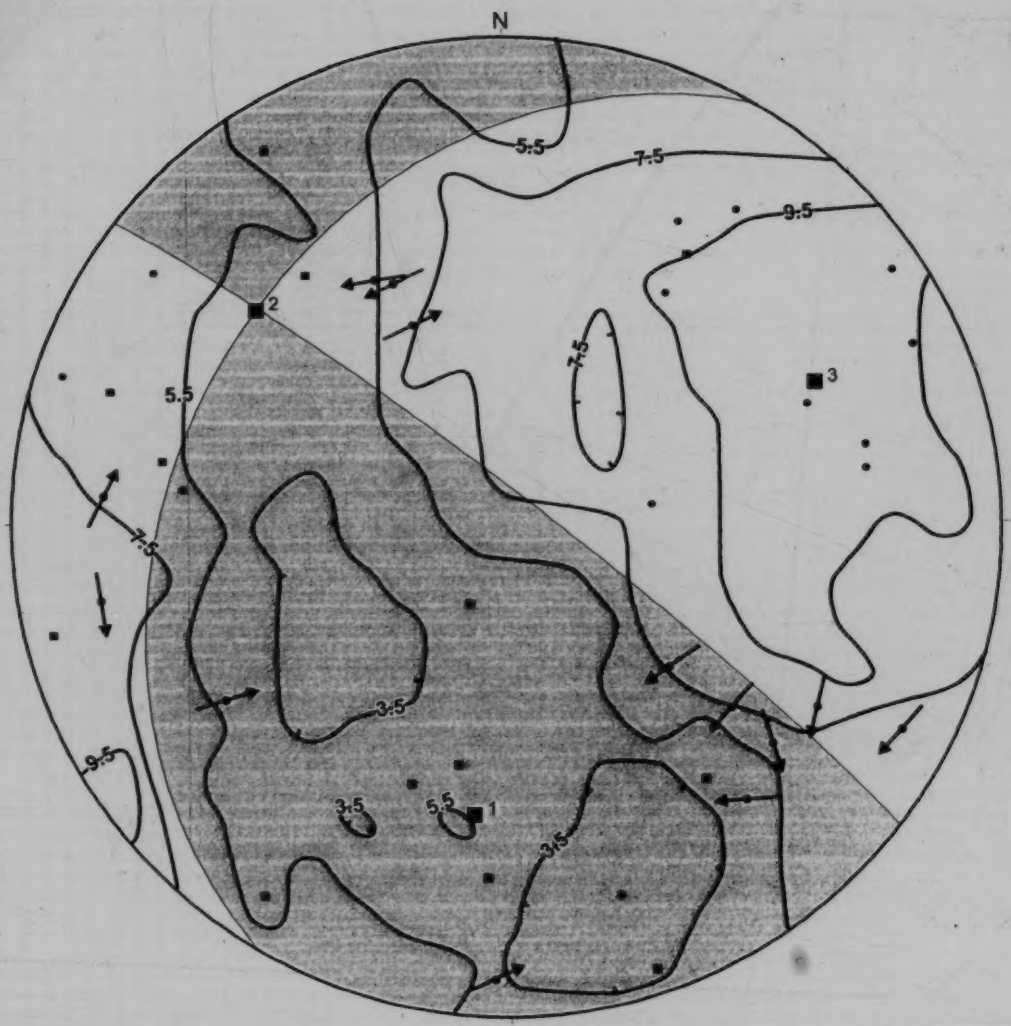

Figure 3.6: Plot of steep faults from the Mount Will area using FaultKinWin. Slip linear, P-Dihedra, and linked Bingham Analysis are all consistent with NNE-directed shortening producing these structures. Maximum number of faults at one grid node is 84%. P-Dihedra nodes contoured at a 2-point interval.

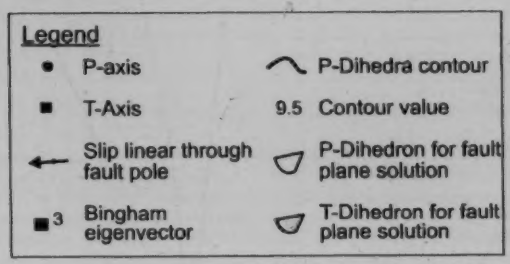

extension direction.

En echelon veins were noted in the Mount Will area at one location. This exposure is on a near-vertical face, in the long limb of an asymmetric NE-vergent

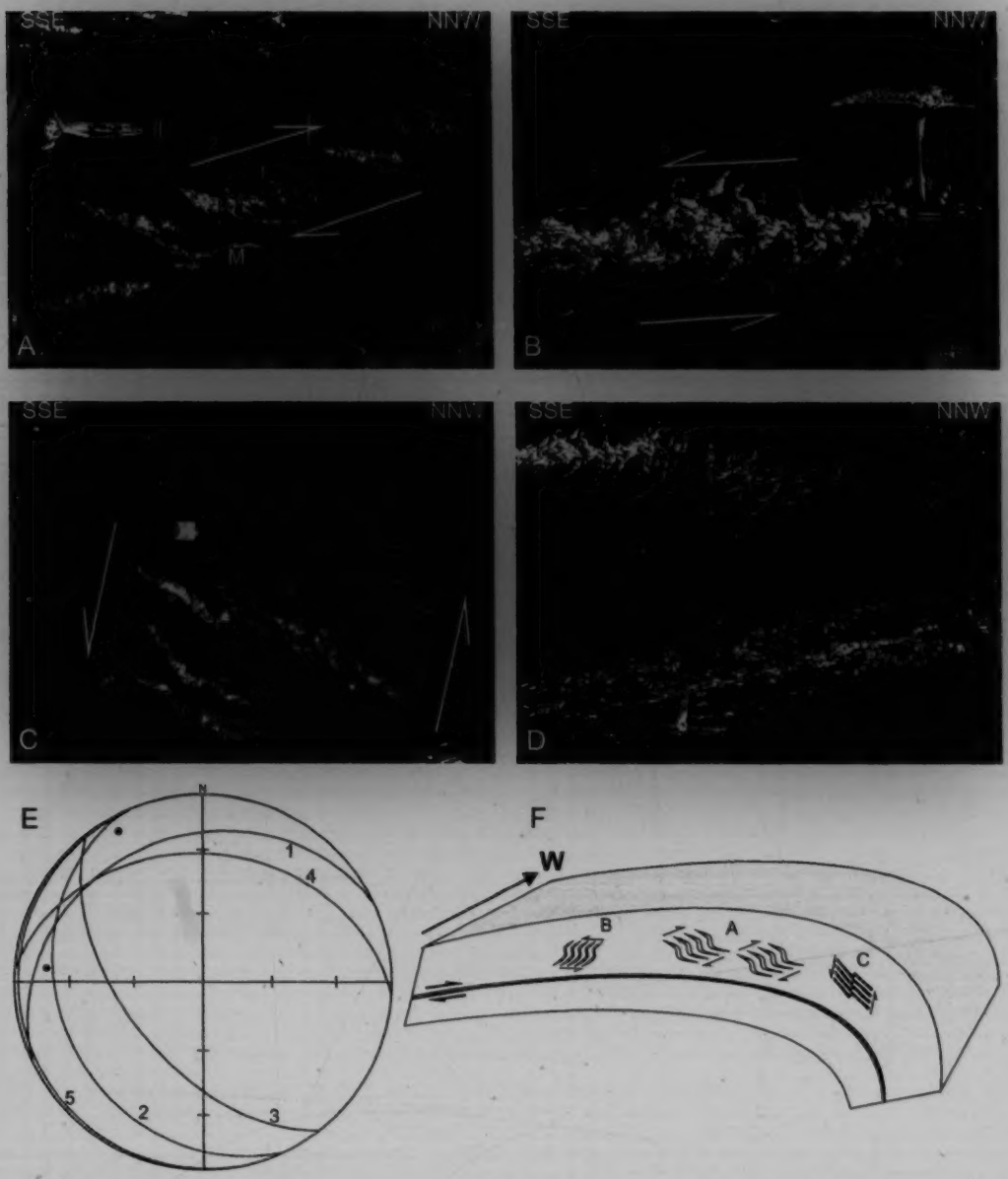

Figure 3.7: (A-D) View towards WSW of *en echelon* veins in the Mount Will area exposed near the hinge of an asymmetric NE-vergent anticline (shown in figure 2.7). A: Array 'A' showing 'Z' asymmetry and large central vein cavities. M=minor array that merges with above array to create appearance of a 'tail.'; B: Oblique view of array 'B' showing sigmoidal 'S' asymmetry veins and a subhorizontal shear plane; C: Array 'C' showing straight 'S' asymmetry veins with relatively straight vein limbs and a steeper shear zone boundary than other arrays; D: Location of array 'B' relative to shear zone at base of conglomerate bed; E: Lower hemisphere projection of vein orientation data. Numbers on projection correspond to veins in 'A' and 'B'; F: Schematic profile of fold and vein arrays towards west. Thin grey layer represents minor shear zone in 'D'. Size of veins greatly exaggerated relative to fold.

anticline (figure 2.7). These veins are located within a chert-pebble conglomerate, approximately half a metre above a thin bed of argillaceous shale with abundant curviplanar veins (figure 3.7). Fabric within this shale is also curviplanar. This shale bed is interpreted as a minor shear zone between conglomerate beds and in the vicinity of the veins dips gently SSW. All vein arrays shown in figure 3.7 are non-planar. Veins in array A have 'Z' asymmetry in the form of rhombohedral vein filled cavities. Small strings of vein that trail the bottom of the array are deflected counter-clockwise, subparallel to the dextral shearing direction. Array B veins are strongly sigmoidal and have 'S' asymmetry indicating sinistral shear. Array B appears to merge with the bed-parallel shear zone towards the hinge of the fold (figure 3.7). Arrays A and B have similarly oriented shear planes that dip gently to the SW, but with opposite sense of shear indicated by vein asymmetry. Array C has kinked veins of variable length but similar shape. The shear plane dips steeply SW. Several other arrays in the vicinity have steep shear orientations at high angles to bedding.

Arrays A-C may have formed contemporaneously with the minor bed-parallel shear zone as indicated by their relative proximity and similar dip directions. The most likely explanation for formation of the shear zone is that it accompanied dextral-reverse flexural-slip folding of the anticline that hosts these veins (figure 3.7). The growth of array A is also dextral-reverse and the moderate SW dip of the shear plane is similar to the axial plane of the fold. Array A is consistent with accommodating the direction of maximum extensional strain, which is assumed to be upward-facing and contained within the axial plane, during growth of the fold. Consequently *en echelon* vein array A likely also grew during folding. Array B may be a conjugate to A, therefore also developing during folding. The steeper array C noted may also have accommodated vertical growth of the fold during deformation. The W to NW trend of the axis of rotation for all arrays is similar to that of the fold axis; the simplest explanation for these arrays is that they

formed to accommodate rotation and vertical growth of the fold.

3.2.3 Cartmel Lake

Many brittle structures were observed affecting the Eaglenest assemblage in the Cartmel Lake area, including thrust faults, normal faults, strike-slip faults, veins and faults subparallel to bedding surfaces. Steep faults with clear sense-of-movement indicators were analysed using the program FaultKinWin. Faults with no sense-of-movement indicators were excluded, as were bedding-parallel faults and shallow thrust faults, in an effort to constrain the kinematics related to development of steep faults. These faults are relatively planar and appear to be undeformed, therefore occurring after fold development in the area. Two groups of faults are present; NW-striking steep faults are generally dextral whereas NE-striking faults are sinistral. An analysis of 23 steep faults places the highest concentration of P-axis dihedra in a gently N-plunging orientation (figure 3.8). The maximum number of overlapping P-dihedra is 21 (91%), at grid nodes that plunge gently N to NNE. Bingham analysis places e3 at 007°-09° and e1 at 276°-06° indicating that the principal finite strain directions are consistent with the predicted principal stresses. This indicates a N-S shortening direction coupled with E-W extension for this population of faults that occurred late in the deformation history. The subhorizontal extension and shortening directions indicates these faults formed during transcurrent deformation.

3.2.4 Sweeny Creek

Several mappable faults were identified in the Sweeny Creek area (figure 2.15). Exposed faults are planar in outcrop, and the surface traces of all faults are relatively linear, indicating that faults have not been affected by folding. Most of the faults with clear exposure have shallow-plunging slickenlines, indicating strike-slip movement. The northwest section of the Sweeny Creek area at locality A contains an E-striking fault with metre-scale apparent sinistral offset that traces through cross-cutting folds discussed in

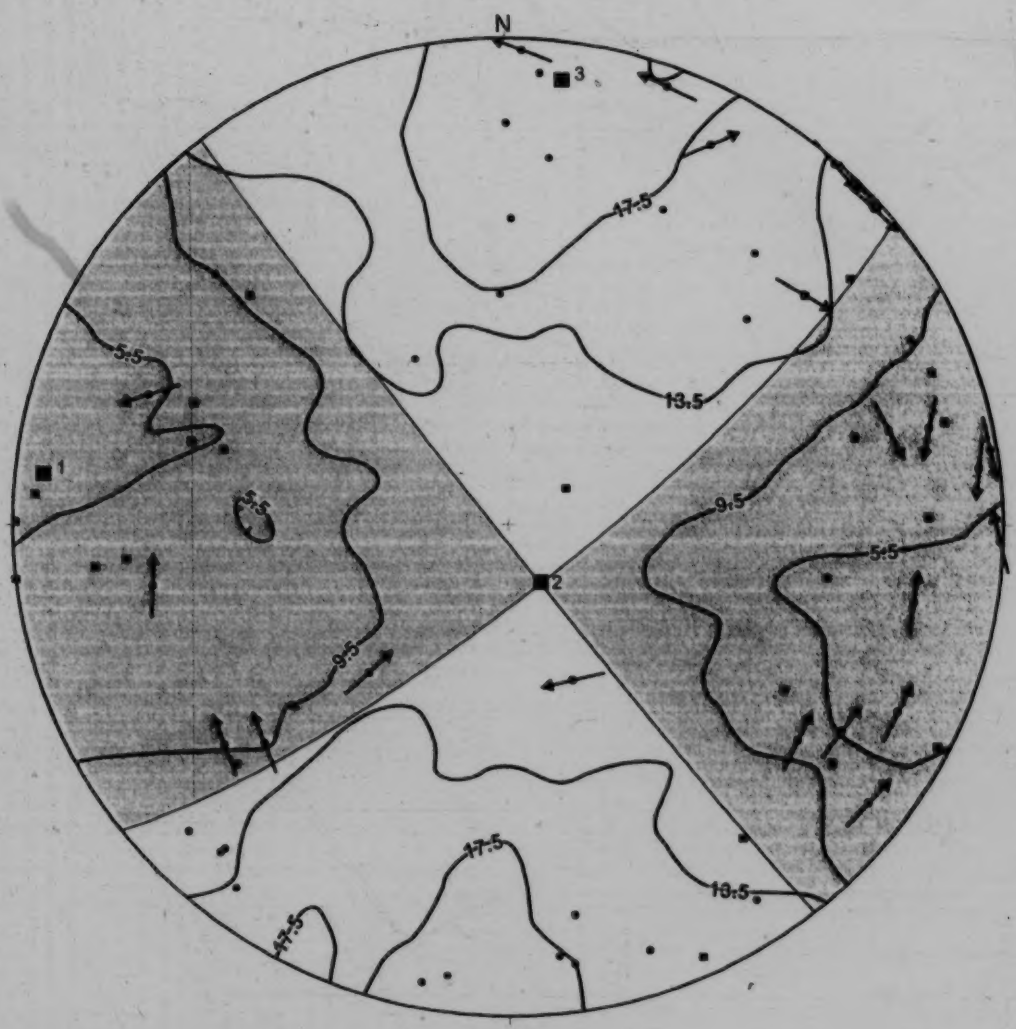

Figure 3.8: Plot of steep faults from the Cartmel Lake area using FaultKinWin. Slip linear, P-Dihedra, and linked Bingham Analysis are all consistent with N-S directed shortening producing these structures. Maximum number of faults at one grid node is 91%. P-Dihedra nodes contoured at a 4-point interval.

Legend

- P-axis
- T-Axis
- Slip linear through fault pole
- 3 Bingham eigenvector
- P-Dihedra contour
- 9.5 Contour value
- P-Dihedron for fault plane solution
- T-Dihedron for fault plane solution

Chapter 2 (figure 2.15). A number of steep NE-SW striking faults are located farther NE. One of these has an apparent dextral offset of 50 m shown by offset of distinctive beds observed in air photos (locality B). One exposure (locality C) includes two-subparallel

fault planes dipping steeply SE and spaced two metres apart. One of these planes has steeply plunging slickenfibres indicating normal movement and the other has gently-plunging slickenfibres indicating dextral-reverse oblique-slip movement. The adjacent parallel faults with significantly different slickenfibre orientations are clear evidence of two directions and phases of fault motion.

Locality D (figure 2.15) is along a steep-walled creek that has a two-metre wide section of complexly disturbed bedding, bounded laterally by shallow-dipping, relatively undisturbed strata that are truncated by steep NE-striking faults at the margins of the structure (figure 3.9). This structure is parallel to the fault at locality C which has apparent dextral offset. A prominent orange-weathering horizon can confidently be correlated on either side of disturbed bedding (figure 3.9) and is offset vertically by ~0.5 m. The complex internal deformation of this structure bounded by two subvertical faults and small vertical offset suggest this structure is a horse (Woodcock and Fischer, 1986),

Figure 3.9: View towards 025° of horse with chaotically folded internal structure bounded by lateral faults. Note small amount of dip-slip movement shown by correlation of thin light-coloured bed. Height of horse is approximately 5 metres.

resulting from sub-parallel adjacent strike-slip faults.

Exposure of veins is sporadic but veining is locally intense in the Sweeny Creek area. In the northwest Sweeny Creek area, veins filled with euhedral dolomite are common in a ~1 km^2 area. Some of these veins are associated with breccia and may be coeval with local reddening alteration of sandstones in the area. In other areas, steep quartz veins with shallow growth fibres are within metres of steep E-W striking normal faults and would appear to accommodate extension related to normal faulting.

One large exposure of abundant veins on the eastern flank of a N-trending syncline displays relatively consistently oriented steeply N-dipping veins spaced 1-5 cm apart (figure 3.10). These veins intersect a moderately W-dipping face exposing a large slip plane and quartz fibres plunging gently to the SW (222°-22°), indicating dextral-reverse oblique movement. The vein set, fault with slickenfibres, and bedding form three nearly mutually perpendicular planes. The fault may have developed during opening of the vein set, which in turn served as conduits for fluid flow during motion on the fault.

Two localities expose *en echelon* veins in the Sweeny Creek area. One of these is a set of *en echelon* quartz-filled tension gashes at locality E (figure 2.15). This set indicates a sinistral component of shear on a steeply SE-dipping shear plane (054°/72°

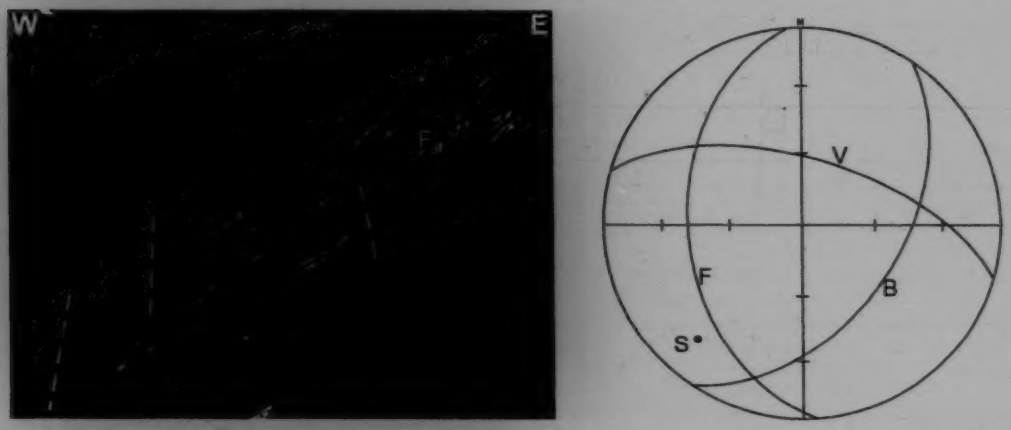

Figure 3.10: Left: View to north of fault surface (F) intersecting relatively planar quartz veins and bedding (dashed lines) at a high angle. Right: Lower hemisphere equal-area projection showing orientations of structures shown in photo. V=Vein, F=Fault, S=Striae, B=Bedding.

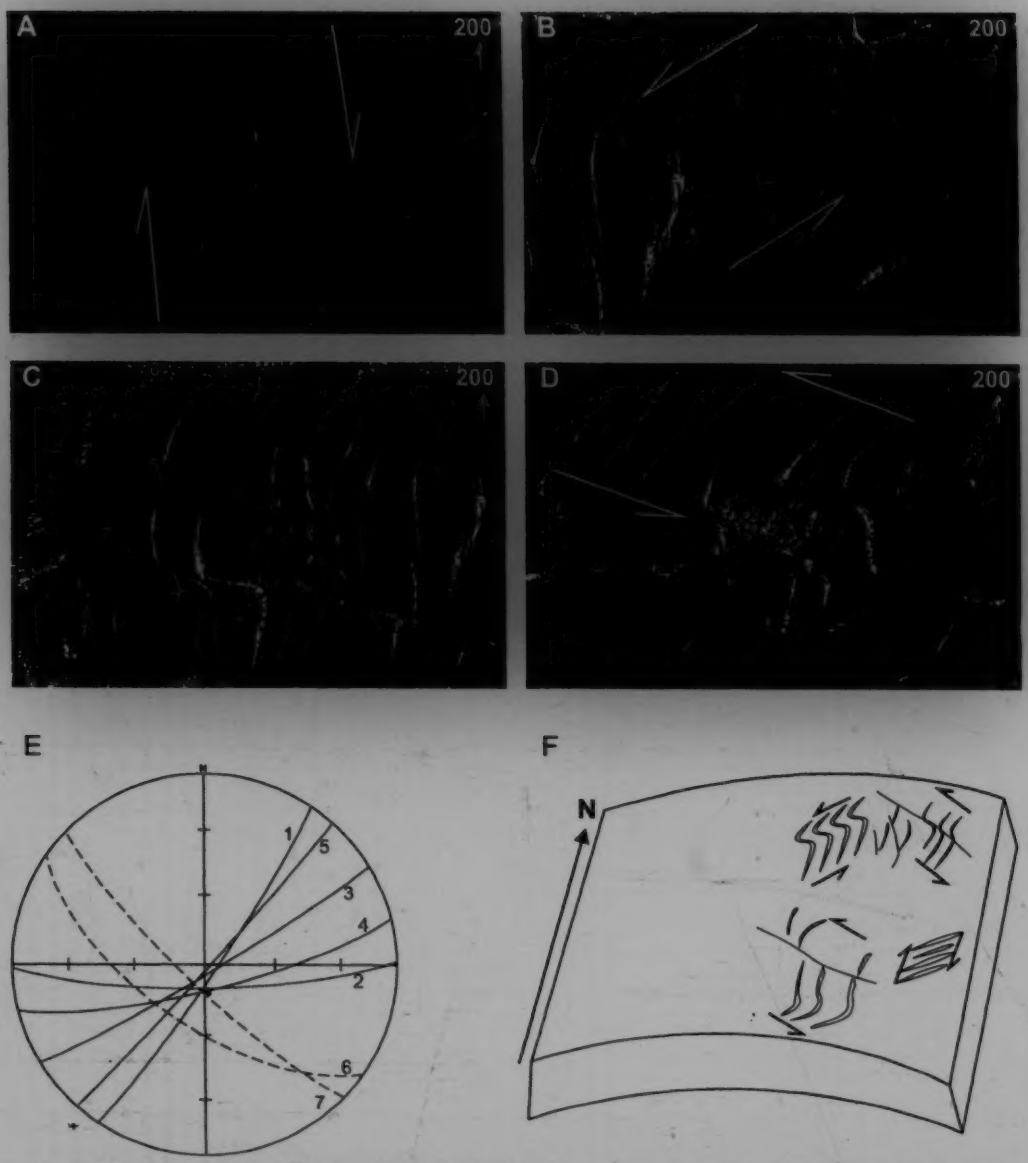

Figure 3.11: Veins from a glacially polished shallow dipping outcrop in Sweeny Creek area. All photos are viewed down towards 200°. Half-arrows indicate interpreted array boundaries and sense of shear. A: Tension gashes indicating dextral shear; B: Sigmoidal 'S' vein array; C: Sigmoidal 'S' array with some veins offset by minor faults and others appearing stretched; D: Additional example of sigmoidal veins cut at centre by faults; E: Lower hemisphere projection of vein orientation data. Numbers on projection correspond to veins in 'B' and 'C'. Point is axis of rotation for arrays in 'B'; F: Block diagram illustrating hypothesized development of *en echelon* veins within anticline. Vein size greatly exaggerated relative to fold.

SE). The other locality is an irregular outcrop of shallow-dipping medium-grained sandstone at locality F (figure 2.15) exposing multiple sigmoidal and planar *en echelon*

vein arrays and minor faults (figure 3.11). This large exposure is at a shallow angle to bedding and is located near the axial trace of an F1 N-trending anticline (figure 2.15). Most veins are at a high angle to the outcrop surface. A slip plane subparallel to bedding indicates this surface accommodated some motion as well. Those portions of this outcrop that are less densely veined are marked by slightly asymmetrical tension gashes spaced several centimetres apart (figure 3.11A). Their arrangement suggests a component of N-S dextral shear. Faults are not noted in these portions of the outcrop. Where veining is most intense, vein arrays are commonly strongly sigmoidal with 'S' asymmetry indicating a component of sinistral shear. Two shear orientations are found; most dip steeply SW while some dip SSE (figure 3.11B-D). Many of these are crosscut by small steep NW-SE striking faults with centimetre-scale sinistral offset (figure 3.11C-D) that often cut through the centre of the array, suggesting this portion of vein arrays represents a plane of weakness in the rock. Some veins appear stretched along these faults and appear to have continued growth during offset (figure 3.11C).

The axis of rotation for vein sets in figure 3.11 is contained within both the shear plane connecting tips of veins and sinistral faults that cross-cut the veins. Other steep minor faults strike NNW-SSE and cause centimetre-scale sinistral offset (figure 3.11). The similar kinematics likely to generate the sinistral faults and the vein arrays and the continued growth of some veins during faulting suggests their formation is linked; faults were generated as deformation progressed and the shear strength of the rock was exceeded, leading to brittle failure. This may also correspond to overall uplift and a change to a more brittle deformation regime.

The *en echelon* vein arrays described at locality F are oriented at a high angle to and appear to crosscut a nearby N-trending F1 anticline (figure 2.15). The axial traces of F1 folds have been deflected by F2 folds (figure 3.12A-B), as previously discussed in Chapter 2. This D2 NE-SW shortening imparted a counter-clockwise strain on F1 folds. A model for development of these veins is shown in figure 3.12C. This model assumes

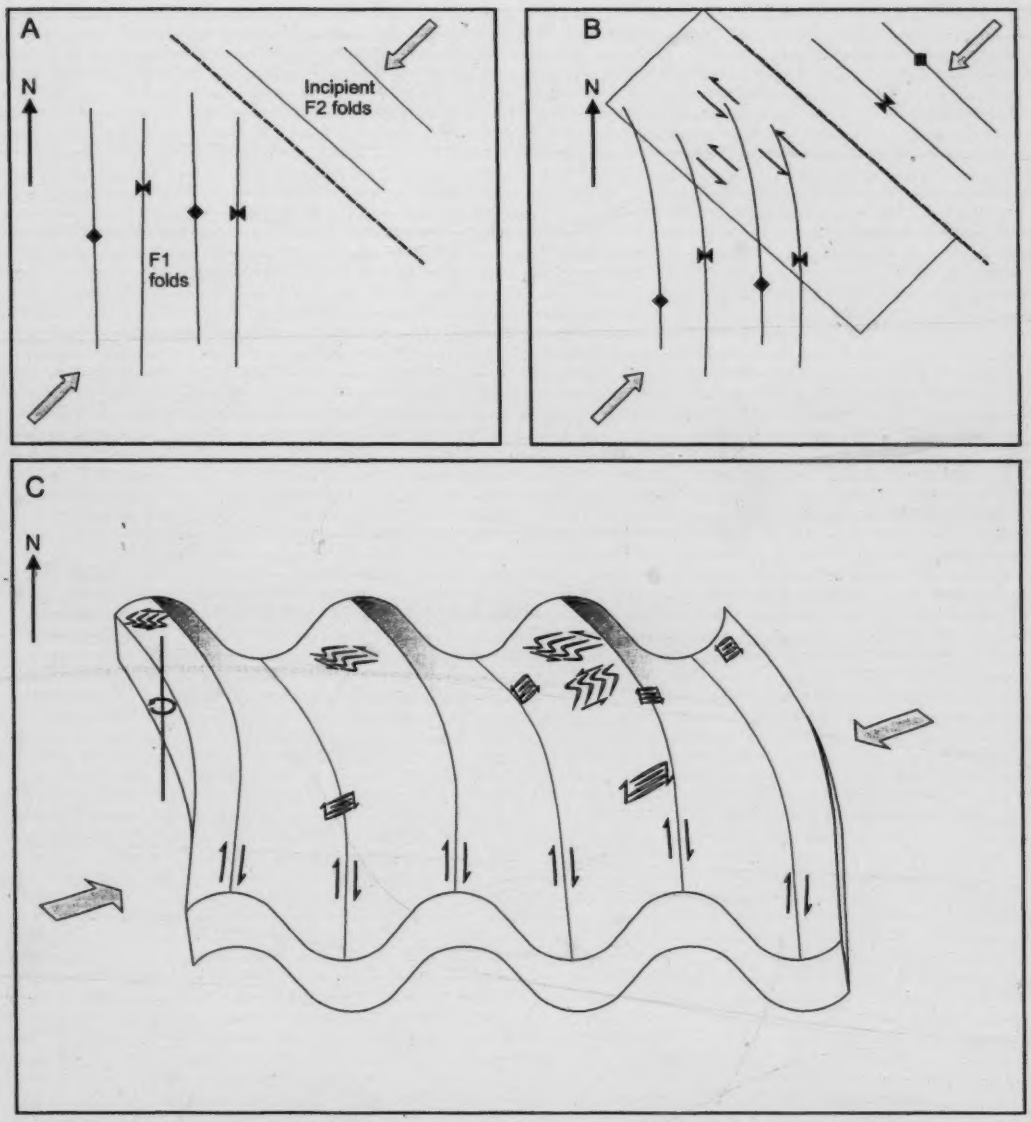

Figure 3.12: Model of development for *en echelon* veins in the Sweeny Creek area, as shown in figure 3.11. A: Schematic plan view of southeast Sweeny Creek area, just prior to development of domain of F2 folds discussed in Chapter 2. F1 folds interpreted to have initially N-trending orientations. Heavy dashed line represents inferred domain boundary, shaded arrows represent inferred D2 shortening direction; B: Schematic plan view of area in 'A' at present time. Trace of F1 folds has been deflected by F2 folds. Shaded region indicates zone of sinistral shear that produced deflection; C: Block diagram of F1 folds following deflection by F2 folds. Model requires that hinges of folds behave more rigidly than limbs of folds. Dextral ductile shear along fold hinges generates planar tension gashes. Sinistral shear in 'B' accommodated by sinistral sigmoidal *en echelon* vein arrays. Veins depicted are greatly exaggerated in size relative to size of folds.

that folds introduce mechanical anisotropy into previously horizontal strata, where folds limbs are somewhat more ductile than fold hinges. Deflection of F1 folds as depicted in figure 3.12 includes a component of counter-clockwise rotation about a vertical axis. This rotation can be accommodated by sinistral shear in the form of sigmoidal *en echelon* veins (figure 3.12). Some partitioning of D2 strain into dextral shear along the axes of F1 folds is also possible if folds behave mechanically as relatively rigid bodies during later deformation. This partitioning could be accommodated by the N-S dextral shear of planar vein arrays (figure 3.12), whose shear directions are subparallel to F1 fold hinges. Development of *en echelon* vein arrays during development of F2 folds indicates those folds developed in relatively brittle conditions.

3.2.5 Oweegee Dome

On the north side of Oweegee Dome, within clastic sediments of the Hazelton Group, faults include small thrusts and normal faults with offsets of centimetres (figure 2.20B). Thrusts faults are steep and strike N-S. Normal faults also strike N-S and generally dip moderately to steeply E or W. In one location a series of normal faults dipping steeply WSW are present in *en echelon* arrangement (figure 3.13). Conjugate to one of these faults is a normal fault dipping ESE that forms a small metre-scale horst structure. This horst is developed near a unit of highly sheared white conglomerate that hosts multiple cross-cutting quartz veins. The rock within the horst appears to have suffered a degree of shear not seen beyond. The level of deformation seen at these outcrops is localised and suggests a fault zone in the area (locality A, figure 2.20B).

Rocks in the lower Hazelton Group on the east side of the dome contain a number of WSW-striking steep faults, with and without associated gouge, that do not appear to continue into the overlying Salmon River Formation (figure 2.20C). Rock units adjacent to the faults are commonly gossanous (figure 3.14). At locality C near a fault through volcaniclastic rocks, C-S fabric interpreted to result from dextral ductile shearing and brecciated megacrysts are interpreted locally as weakly developed proto-mylonite. That

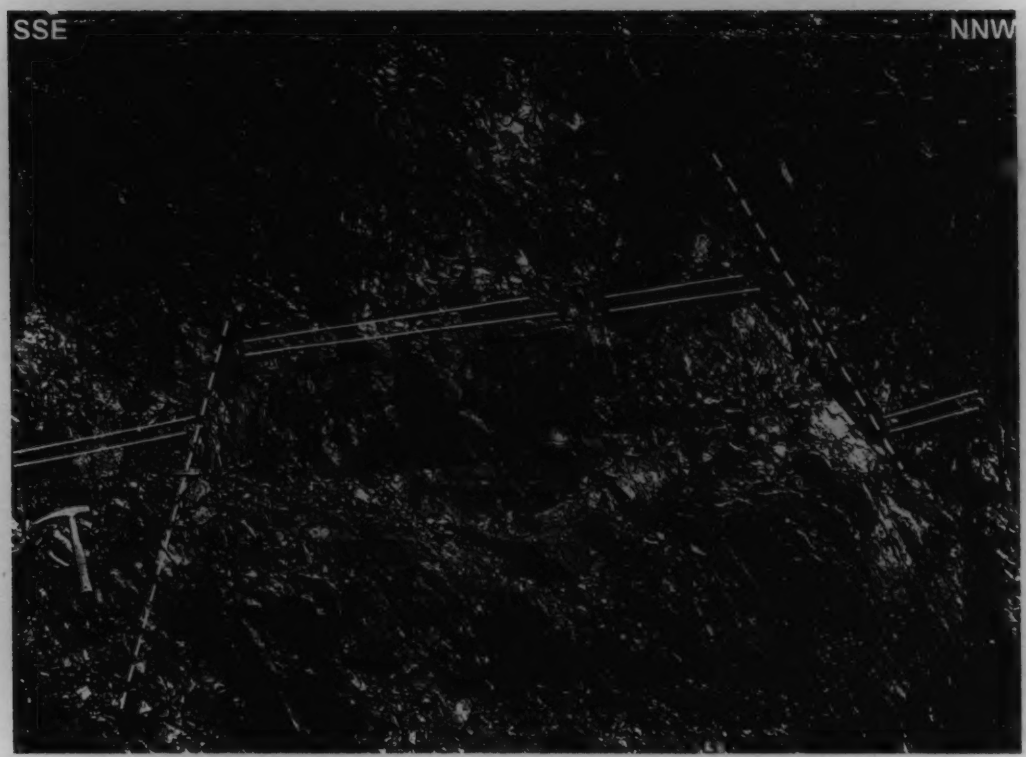

Figure 3.13: View towards SSE of horst in the Oweegee Dome area. Dashed lines outline location of faults, solid lines follow boundaries of a prominent orange weathering marker unit.

faults do not continue into the Salmon River Formation, and the presence of features such as fault gouge and C-S fabric were not observed elsewhere in strata above the lower Hazelton Group, suggest these structures predate deposition of the Salmon River Formation.

On the south side of the dome several faults within the Ritchie-Alger assemblage dip moderately to steeply WSW with moderately plunging slickenlines. Some of these are associated with bedding-parallel quartz veins and gouge up to 25 cm thick. Offset and sense of movement on these structures could not be determined. At locality D near the base of the Ritchie-Alger assemblage an outcrop of fine sandstone hosts abundant veins. These veins have an outer layer of quartz and an inner layer of calcite, indicating two stages of mineral precipitation. Elsewhere on the south side of the dome green volcaniclastic sandstone and polymictic conglomerate of the lower Hazelton Group

Figure 3.14: View to east of gossanous weathering near faults in the Oweegee Dome area. Host rocks are moderately NE-dipping volcaniclastic rocks of the lower Hazelton Group. Closed dotted lines indicate distinctive gossanous batches, dashed line indicates fault. Person at bottom for scale.

are separated from thinly interbedded very fine sandstone and tuff of the Salmon River Formation by a moderately NW-dipping fault whose sense could not be determined (figure 2.20D) and a very thin layer of green gouge. This fault may be a thrust fault that placed lower Hazelton strata on the younger Salmon River Formation.

3.2.6 Iskut ridge

Faults are rare in the Iskut ridge area. The most significant fault identified was a poorly exposed, steep W-striking fault that causes approximately ten metres of apparent sinistral offset and is also associated with clockwise rotation of beds to the N of the fault. Other faults in the area are limited to small slip planes of indiscernible offset that commonly strike NW-SE with variable dips.

Three localities in the Iskut ridge area were noted with well exposed *en echelon* veins. The first locality is exposed in medium-grained sandstone on the east-limb of a N-trending syncline (figure 2.26) and consists of a single set of S-shaped sigmoidal veins

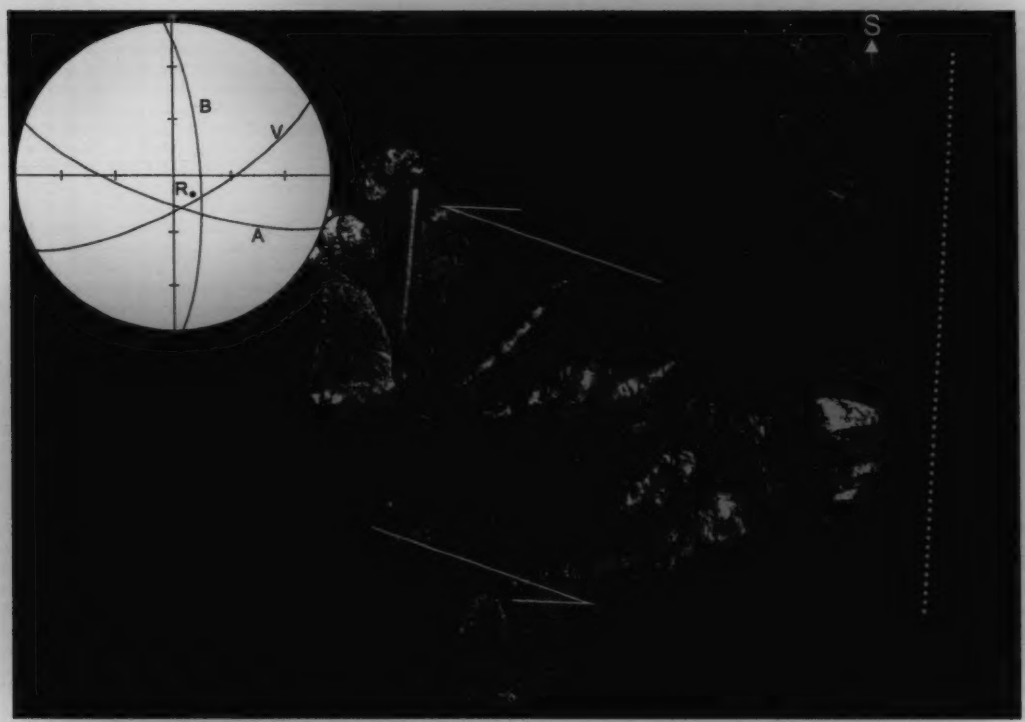

Figure 3.15: Sigmoidal 'S' asymmetry *en echelon* veins in the Iskut River area exposed in medium-grained sandstone of the Ritchie-Alger assemblage. View of veins is down to the south of veins, which increase in size towards the NW. Dashed line indicates trace of bedding, half-arrows indicate interpreted trace of shear plane bounding the array; Inset: Lower hemisphere projection of vein orientation data. B=Bedding, V=Straight upper portion of vein, A=Array boundary, R=Rotation axis of array.

that progressively increase in size to the NW (figure 3.15). Erosion has partially exposed these veins in three dimensions and their shape does not change with depth into the outcrop. These veins indicate a sinistral component of shear on a steeply SSW-dipping shear plane. The SW-NE shear direction is nearly perpendicular to steeply E-dipping bedding, and the vein array propagates across bedding planes. These veins are difficult to envisage as a product of N-trending folds as they appear to cut across the folds. Alternatively, relative proximity to SE-trending folds and an axis of rotation similar to the hinge direction observed for SE-trending folds suggests they may have a common origin. If this were the case these veins would indicate a component of sinistral shear during F2 folding. This is similar to the relationships observed at Sweeny Creek, where N-trending F1 folds are interpreted to have undergone a sinistral strain at a high angle to their axis

during development of F2 folds.

Another array of *en echelon* veins consists of tension gashes with distinctive growth fibres perpendicular to wall rock. The array has a moderately N-dipping shear plane with sinistral-reverse movement. These veins are close to a N-trending anticline and the W-striking fault mentioned above. These veins may represent the product of sinistral strain during F2 deformation, in the same manner as suggested for those in figure 3.15.

A third locality exposing *en echelon* veins is found in the southernmost portion of the Iskut map area and exposes multiple sets of sigmoidal *en echelon* vein arrays (figure 3.16). N-trending folds can be extrapolated to extend south towards this area, but exact relationships are unclear due to poor exposure. Vein arrays are exposed in massive coarse-grained sandstone. Vein size and spacing increase upwards. Two arrays of 'Z' and 'S' asymmetry are described further. The 'Z' asymmetry array has clearly developed quartz crystal growth at a high angle to wall-rock edges (figure 3.16A-B). Crystal growth appears to follow the curvature of vein walls. Seams can be observed within the vein parallel to wall-rock, indicating a phased crack-seal history of growth. Numerous other planar veins crosscut this array without discernible offset. Shear sense is dextral-reverse along a steep SSW-dipping shear plane.

The 'S' asymmetry sigmoidal veins are approximately a metre in length (figure 3.16C-D). The upper vein tips of this array are clipped by a minor thrust fault with apparent centimetre-scale offset. The shearing direction indicated by asymmetry is sinistral-reverse on a plane dipping moderately to the NW. The central segments of these veins are highly contorted and appear to have buckled and folded. The hinge of rotation plunges moderately to the SW. This suggests these veins grew with a strong component of rotation.

The orientation of the longer segments of veins in both arrays is similar (figure 3.16F). The average inferred extension direction for each array (shown by mineral

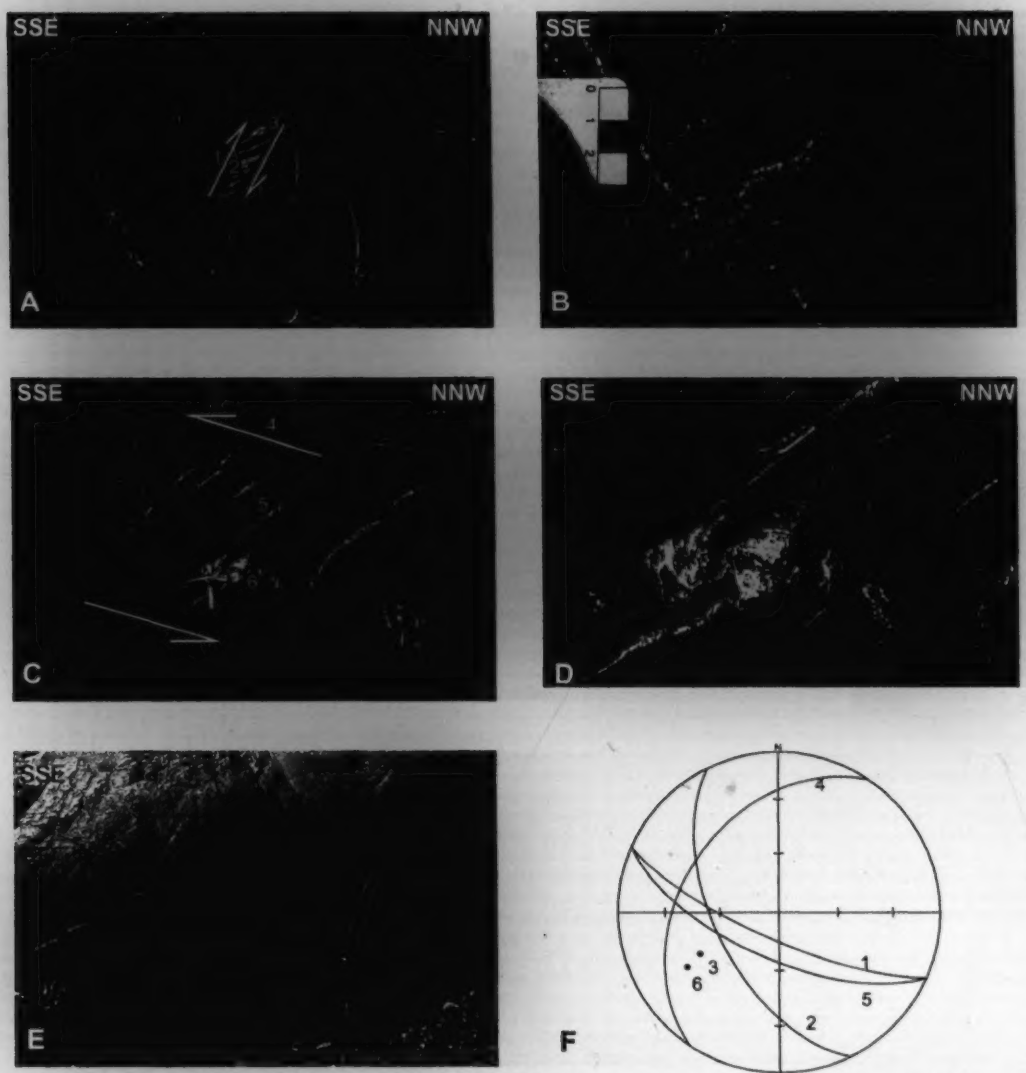

Figure 3.16: View of arrays of *en echelon* veins towards WSW from the Iskut River area hosted within a steep outcrop of medium-grained sandstone of the Ritchie-Alger assemblage. A: Sigmoidal 'Z' asymmetry veins; B: Close-up of veins shown in (A). Note thin seams of wall-rock within veins indicating crack-seal mechanism of growth; C: Sigmoidal 'S' asymmetry veins with minor thrust fault clipping upper tips of veins and some fracturing at centre of array; D: Close-up of (C). Note contorted nature of veins and minor fractures at centre; E: Exposure of additional vein arrays, both as sigmoidal arrays and tension gashes, and several dark brittle fractures resulting in minor offset of veins; F: Lower hemisphere projection of vein orientation data. Numbers refer to structures labelled in (A) and (C).

fibres, figure 3.16B, D) is also similar. The axes of rotation (points in figure 3.16E) are similar and represent the direction of intermediate strain. The similar kinematics of these arrays suggests they developed contemporaneously but resulted in two shear planes. These arrays are not typical conjugate *en echelon* vein arrays (Smith, 1996) as

the angle between them is 95°. The 'S' array described may have initially formed with a morphology akin to the 'Z' array but as deformation progressed, a greater component of shear was imparted onto the 'S' array which began to buckle and behave as a minor shear zone. This is also supported by the slippage seen on minor faults above the array. This interpretation suggests overall reverse shear towards the SE.

3.2.7 Eskay Creek

A variety of brittle structures were observed in the Eskay Creek area. Thrust faults can sometimes be seen at the core of folds causing minor offset and local rotation of bedding. Faults are also observed offsetting S1 cleavage indicating a clear post-F1 deformation. Larger faults commonly strike SE, parallel to S2 cleavage, and appear to contribute to map-scale deflection of F1 fold limbs described in Chapter 2. Synthetic Riedel shears were also observed in one locality associated with a small sinistral fault (figure 3.17). Another locality exposes three successive parallel steep fault planes each with steep but unique sets of slickenlines developed (figure 3.18). This indicates at least three pulses of steep brittle movement in the area, in addition to folds already described.

Three localities with exposure of *en echelon* veins were noted in the Eskay

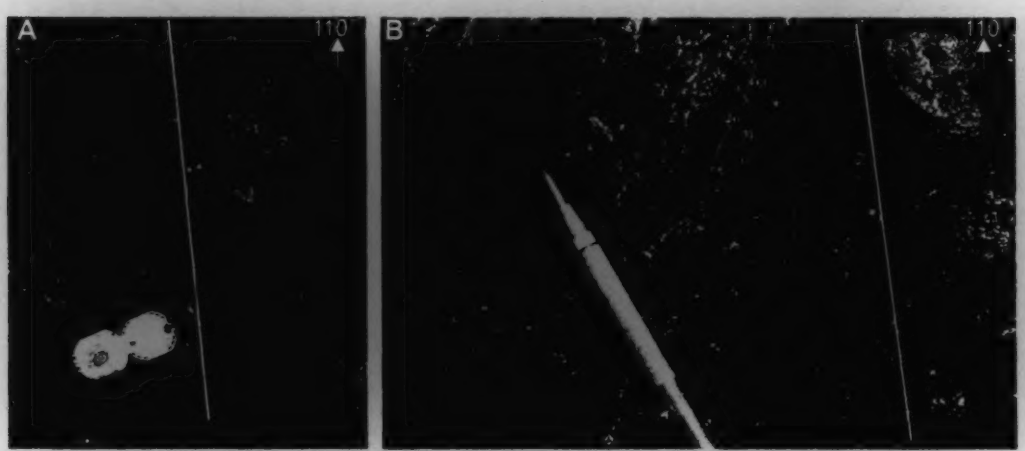

Figure 3.17: View down to the E of minor fault with synthetic Riedel shears in the Eskay Creek area. A: View of steep WNW-striking fault (solid line) with Riedel shears; B: Close-up view of Riedel shears. Solid line=fault, dashed line=Riedel shears, dotted line=bedding traces.

Figure 3.18: View to southeast of successive parallel northwest-dipping fault planes with unique sets of slickenline lineations. Lines emphasize orientation of slickenlines.

Creek area. One of these is exposed on a bedding face and suggests sinistral shear on a SE-striking vertical plane. The second array is an 'S'-shaped sigmoidal array with a moderately ENE-dipping sinistral shear plane formed perpendicular to bedding. These arrays are consistent with the maximum principal strain axis occurring at a high angle to and postdating axial planes of F1 folds, as observed in other areas (figure 3.12). The third array is an array of 'S' shaped sigmoidal veins developed on the SE limb of a NE-trending F1 fold (figure 3.19). The array has a gently SW-plunging rotation axis, similar to that of the fold hinge. The shear plane dips gently WSW. The shear plane geometry is consistent with development during NNW-SSE sinistral shear during D2 shortening.

3.2.8 Teigen Lake

Quartz veins are abundant in the Teigen Lake area. These have variable orientations but the majority are steeply to moderately dipping and strike NW-SE. A number of small faults were also identified with variable orientations. A thick (>30m)

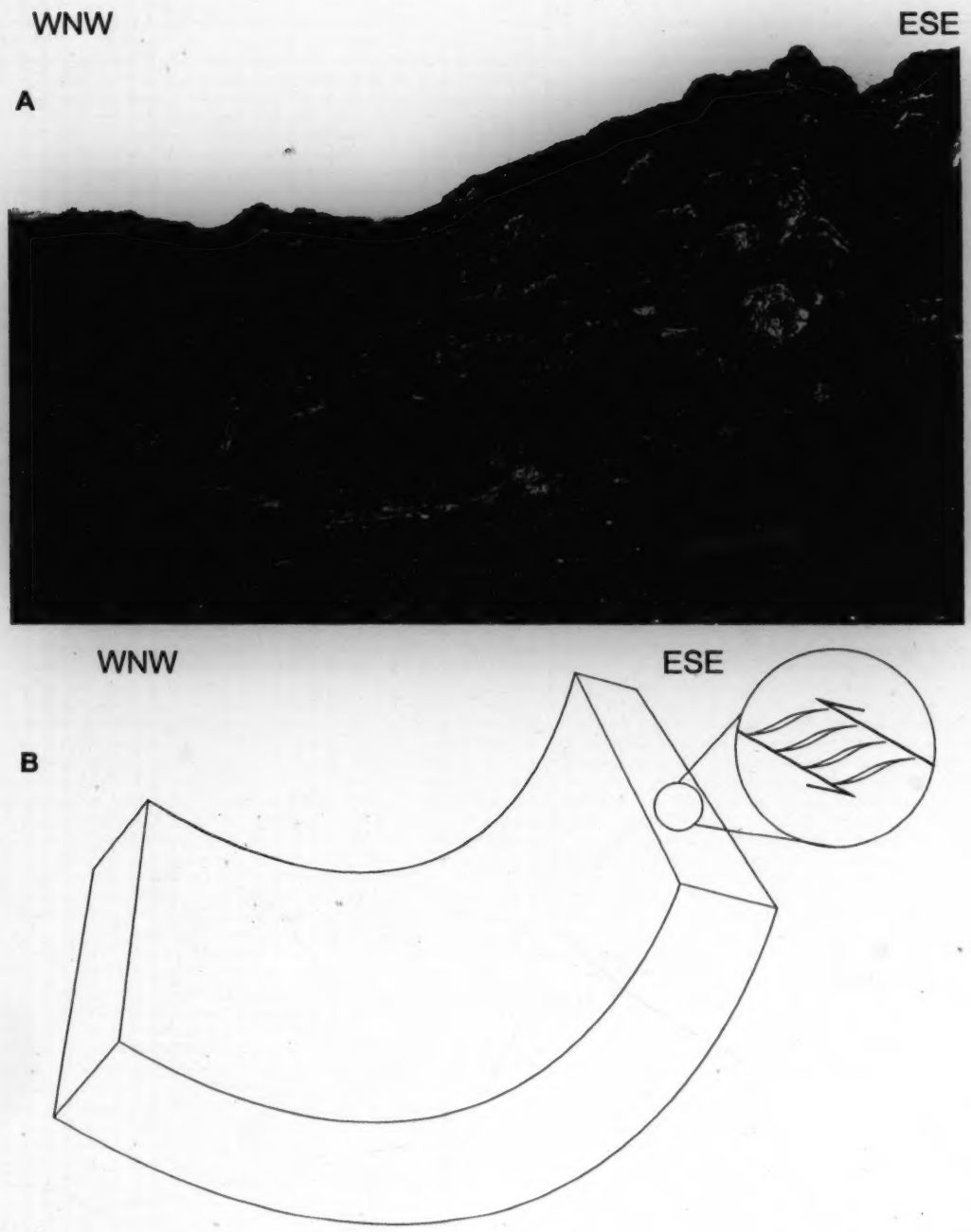

Figure 3.19: NE-trending fold from the Eskay Creek area. A: View of fold towards 030°; B: Block diagram of fold with inset showing orientation of sigmoidal *en echelon* vein array relative to fold.

orange-weathering outcrop that appears highly altered marks the contact between lower and upper Hazelton Group rocks in the area (figure 2.36). This contact is offset by a NNE-striking fault that juxtaposes a distinct fossil bed with green pebbly sandstone and has an apparent dextral offset of at least 30 m. The degree of alteration in the area and depth of alteration away from the fault may indicate a larger, vertical component of movement on this fault than expected by the 30 m apparent offset of the fault alone.

3.2.9 Nelson Creek

Numerous small faults and veins were noted in the Nelson Creek area. These are dominantly moderately to steeply dipping and strike NW. Bed-parallel slip surfaces are common. A number of steep NW-striking dikes also cross the area.

Two localities with *en echelon* vein arrays were noted in the Nelson Creek area. One of these displayed highly irregular 'S'-shaped sigmoidal veins hosted within volcanic strata of the lower Hazelton Group. This array has a moderately W-dipping shear plane and appears to have had fractures developed both on the edges and through the centre of the array (figure 3.20A). Portions of the center of the array appear to have undergone rotation. This array is consistent with sinistral-normal movement with down-to-the-W slip. Another array 40 m W has large vein cavities relative to the length of the vein and has 'Z' asymmetry (figure 3.20B). This array indicates dextral-reverse movement along a SSW-dipping shear plane. These two arrays are compatible as conjugate sets, and would indicate NW-SE directed shortening.

The other locality with an *en echelon* vein array described in the Nelson Creek area is a single array of slightly asymmetric 'Z'-shaped veins hosted in the lower Hazelton Group. The veins of this array have relatively consistent length, shape, and thickness and are developed along a shear plane dipping moderately SW (figure 3.20C). This array suggests dextral-reverse movement along the shear plane. This array is found a few metres N of a shear fabric developed adjacent to a SW-dipping vein also indicating dextral-reverse slip along the vein (figure 3.20D). The similar orientations of shear and

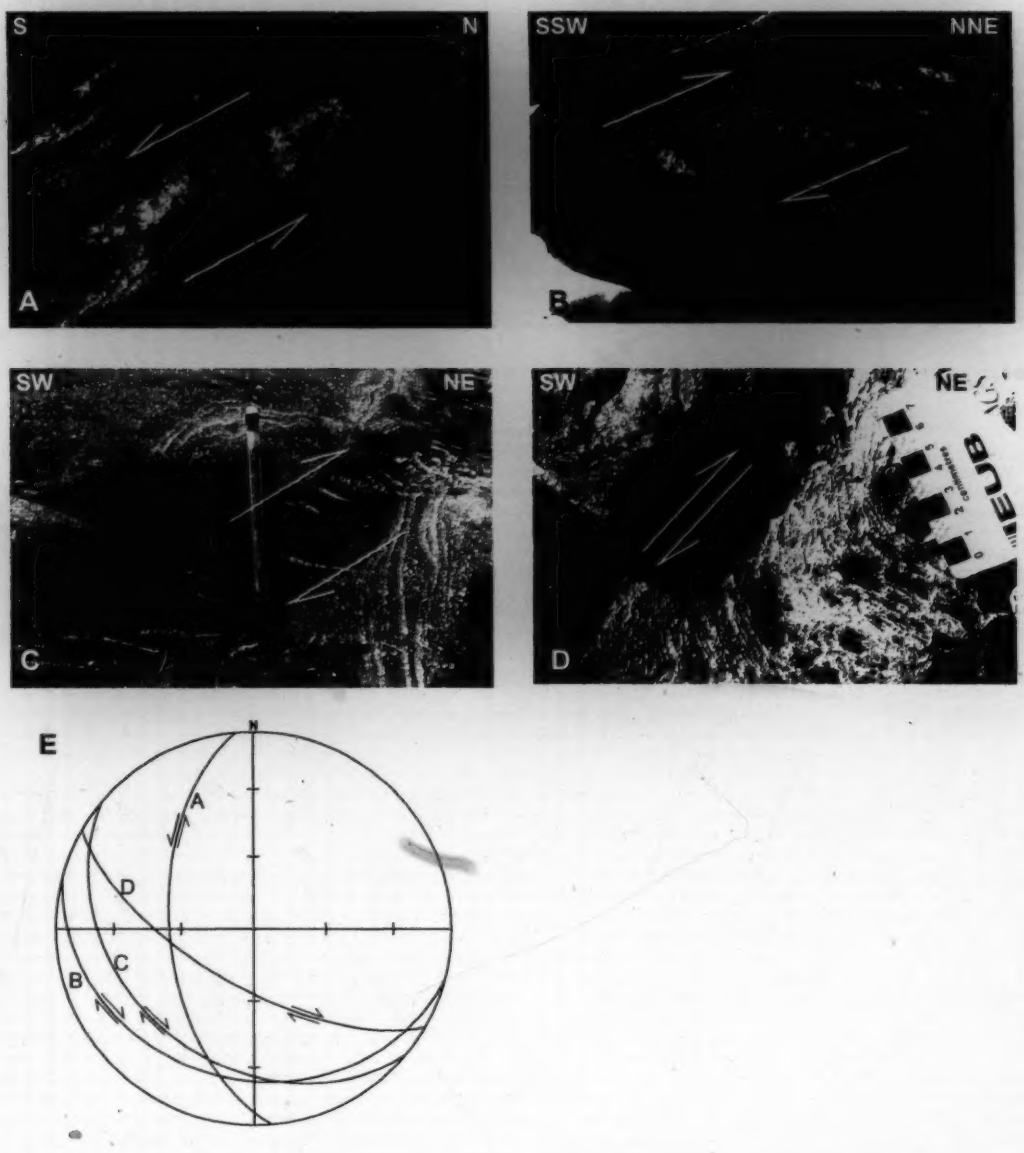

Figure 3.20: Veins in the lower Hazelton Group of the Nelson Creek area. A: View to W of highly irregular 'S'-asymmetry veins indicating sinistral-normal shear. Note minor fractures developed parallel to vein boundary; B: View to WNW of *en echelon* veins with large central cavities indicating dextral-reverse shear. Length of veins is approximately half a metre; C: View to NE of slightly asymmetric 'Z'-shaped *en echelon veins* with dextral-reverse shear; D: View to NE of vein (between half-arrows) nearby (C) with an adjacent shear fabric interpreted to result from reverse shear along the vein/fault surface; E: Equal-area lower hemisphere projection of shear planes with letters corresponding to above figures. If these structures are interpreted to form synchronously, they would indicate overall NW-SE shortening direction with an extension direction moderately inclined to the NE.

common sense of motion between the two structures suggest they may have developed during the same phase of deformation. These arrays also have a similar orientation and shear sense as the array in figure 3.20B. NW-SE directed shortening, as suggested by conjugate relationships between the three dextral-reverse structures and the sinistral-normal *en echelon* veins, is not generally compatible with development of NW-trending folds in the Bowser Lake Group discussed in Chapter 2. These structures may represent a deformation prior to those folds. As these structures are all found in the lower Hazelton Group, they may pre-date deposition of the upper Hazelton and Bowser Lake Groups.

3.3 Discussion of Veins and Brittle Structures

Outcrop-scale brittle structures are common in the northwestern Skeena Fold Belt. In many areas faults were observed with more than one set of slickenlines, indicating multiple episodes of slip, and possibly re-activation of brittle structures during different deformations. *En echelon* vein arrays were also identified in a number of areas.

Differences in the nature of structures within the Hazelton Group versus the Bowser Lake Group indicate the likelihood of an early Jurassic deformation prior to formation of the Skeena Fold Belt. In the Oweegee Dome area some faults within the Hazelton Group appear truncated by the Bowser Lake Group, indicating they may have developed during an early deformation. Faults were commonly associated with gossanous alteration. This was not observed in structures within the Bowser Lake Group and suggests altering fluids were limited to the Hazelton Group. Structures in the Nelson Creek area indicating NW-SE shortening may represent pre-Bowser structures. C-S fabric in the Oweegee Dome area and sheared tuffs in the Nelson Creek area indicate relatively ductile deformation of the Hazelton Group.

There is a general lack of brittle structures associated with development of F1 folds. Folds are related to thrust faults and bedding-parallel slip planes; however *en echelon* veins and steep faults associated with F1 structures were not identified. This

suggests conditions were relatively ductile. This is further elaborated in Chapter 4.

En echelon vein arrays were identified in a number of areas and can be plausibly associated with development of F2 folds. These arrays occur in a range of morphologies and orientations. *En echelon* arrays found within F1 folds are typically oriented at a high angle to the fold axis, so as to appear to crosscut these folds. In most cases where this relationship was observed, F1 folds were relatively N-trending, and at acute angles to NW-trending F2 folds (e.g. figure 3.12). Assuming F1 folds cause anisotropy in the form of corrugations with semi-rigid hinges, shortening during development of F2 folds would be expected to impose a sinistral shear on existing F1 folds. This strain is interpreted to result in those *en echelon* arrays that are oriented at a high angle to F1 folds, in order to accommodate extension subparallel to F2 fold hinges (figure 3.12). Most *en echelon* arrays can then be interpreted to result from sinistral shear of F1 folds during F2 fold growth.

The abundance of brittle structures associated with F2 fold development indicates that conditions were relatively brittle during D2 in comparison to D1 structures. In the Mount Will area abundant brittle structures are clearly associated with F2 fold development. Well-exposed *en echelon* arrays are interpreted to develop during formation of an F2 fold. Abundant steep strike-slip faults located on the Mount Will Thrust Sheet are interpreted to have developed synchronously with transport of the thrust. Faults form conjugate pairs and result from NE-SW shortening and have moderately inclined extension directions, consistent with development during growth of NW-trending F2 folds. The formation of these faults during F2 folding and the common occurrence of *en echelon* vein arrays developed during F2 fold formation suggest conditions were relatively brittle. The change from relatively ductile F1 conditions to more brittle F2 conditions likely corresponds to significant denudation of the Bowser Basin following F1 folding.

Evidence for a brittle D3 deformation that occurred late in the history of the

Skeena Fold Belt has been identified. In the Cartmel Lake area an array of steep brittle conjugate faults were observed that resulted from N-S shortening. These faults have horizontal extension directions, indicating development during transcurrent deformation. These postdate F2-folds in the area based on cross cutting relationships and contrasting kinematic arrangement. The joint array described on the Maitland plateau is also a brittle deformation resulting from N-S shortening. Correlation of the two areas suggests a brittle D3 deformation dominated by transcurrent faults, with N-S shortening and sub-horizontal E-W extension may be prevalent across much of the northwest fold belt. One possibility is that these structures are a result of strain partitioning during development of Late Cretaceous regional dip-slip faults located in the northeast Bowser Basin (figure 1.3) described by Evenchick and Thorkelson (2005). These faults are NE- and NW-striking dip-slip faults, with normal or uncertain sense. Some can be traced for several kilometres and intersect in block patterns. Displacement along individual faults reaches hundreds of metres. Given the significant difference in scale and displacement of these two sets of structures, nearly perpendicular slip directions, and a likely long-lived history of regional dip-slip faults, this correlation is considered unlikely.

The D3 structures identified in this study may correlate with Eocene dextral strike-slip faults elsewhere in the Cordillera (Gabrielse, 1985; Gabrielse et al., 2006) during the late Early Cretaceous and again in the Eocene. The nearest large dextral faults to the Cartmel Lake area are the Finlay-Ingenika-Takla Faults to the east, Teslin-Thibert-Kutcho Faults to the north, and the Denali/Coast Shear Zone to the west (figure 1.3). The strain regime between D3 structures and dextral orogen-parallel faults is more compatible than with dip-slip faults (Evenchick and Thorkelson, 2005). Eocene timing of dextral faults is also reasonable given that D3 structures post-date folding, which likely continued into the early Tertiary. At a regional scale D3 structures would amount to very minor fractures with little accumulated slip that occurred due to internal deformation. Structures within this chapter are combined with those of chapters 2 and 4 in chapter 5.

Chapter 4: Microstructural Analysis and Geochronology

4.1 Introduction

The range of areas encountered in this study allows examination of petrographic properties of cleavage and other microstructures and subsequent development of regional comparisons between identified deformations. Due to its relative ubiquity, the nature of cleavage in the field and in thin section is examined in greatest detail. Associated structures such as strain shadows are also discussed. Selected samples have also been analysed using standard microprobe procedures to image and track chemical variation in microstructures.

Owing to the regional potential of hosting active petroleum systems, and questions surrounding sedimentary sources in the Cordillera, previous petrographic studies on rocks hosted by the fold belt have focused primarily on porosity, permeability and organic material evaluations and clast provenance (Eisbacher, 1974a; Osadetz et al., 2003; Ritcey et al., 2005). The most detailed petrographic study of microstructures in rocks of the Bowser Lake Group was prepared by Moffat (1985) who conducted work in the Groundhog Coalfield (figure 1.4), located in the north-central Bowser Basin within the Bierne Synclinorium. Moffat (1985) documented strain shadows and pressure solution cleavage whose spacing decreased with depth while the general degree of deformation increased with depth. Clast angularity was also found to increase with depth as a result of solution of previously rounded clast surfaces. These observations were made within the stratigraphic subdivisions of the Groundhog Coalfield, which span a range of deltaic lithofacies, including the Groundhog-Gunanoot Assemblage.

Several of the most penetratively deformed samples collected have been analysed using a JEOL 8900 microprobe. Microscopic structures identified in thin section have been imaged using back-scatter electron imaging. Some samples were further analysed in order to identify the distribution of potassium content using element mapping and

qualitative energy dispersive spectroscopy (EDS) element analysis.

In order to better constrain absolute timing constraints on deformation, Ar-Ar geochronology was completed on selected samples to constrain the age of cleavage formation. A post-kinematic mafic dike that crosscuts a fold was also dated. These results allow refinement of previously postulated timings of deformation.

4.2 Cleavage – Field relationships

Cleavage is developed to varying degrees in each area of the Skeena Fold Belt described in Chapter 1. All cleavage appears to be spaced when viewed in outcrop and hand specimen. Spacing varies from less than a millimetre to centimetres and is partially controlled by host-rock lithology. In outcrop, cleavage is variably planar, wavy, and anastomosing, following the classification of Engelder and Marshak (1985). The wavy nature of cleavage is used in the field to help discriminate between joints and cleavage. In many of the study areas cleavage is most strongly developed in the hinges of folds, and is roughly axial-planar to those folds. Cleavage is therefore interpreted to have formed from the strain that resulted in fold development. Cleavage is most commonly classified in the field as a spaced disjunctive cleavage, and is presumed to form from pressure solution. Some outcrops in the fold belt contain pencil structures formed by the intersection of two cleavage sets. When two cleavage sets are present in a single outcrop and crosscut there is no sign of deflection of either cleavage in the form of crenulation.

The most penetratively (millimetre-spaced) cleaved rocks of the Bowser Lake Group collected in this study were found in the Iskut ridge and Eskay Creek areas (figure 1.4) along the western margin of the basin in the Ritchie-Alger assemblage. Although the rocks which appear the most deformed are located in the hinges of folds, strong cleavage can be observed in fine-grained rocks throughout much of these study areas. More moderately deformed samples, with millimetre to centimetre spaced cleavage, were collected in the Skelhorne and Eaglenest assemblages in Sweeny Creek and Cartmel Lake, respectively. In the Sweeny Creek area tightly spaced cleavage is

sporadically developed and is absent elsewhere. In the Cartmel Lake area cleavage is moderately spaced and is found throughout most of the area in pebble conglomerate. In the Oweegee Dome, Maitland plateau, Nelson Creek, Teigen Lake and Mount Will areas highly cleaved rocks were rare to absent. More widely spaced cleavage is sporadically developed in these areas.

In most areas studied outcrops containing relatively penetrative cleavage were sampled with an effort to keep the sample intact. Sampling density reflects perceived likelihood of seeing penetrative structures in thin section while in the field, as well as availability of such samples. Samples are considered to represent a first approximation of the most strongly deformed rocks of an area. Thin sections were cut at or nearly perpendicular to cleavage. Table 4.1 summarizes stratigraphic, lithologic, and mesoscopic and microscopic cleavage properties of samples collected for the purpose of examining cleavage in thin section.

4.3 Microscopic observations

Much of the coarse sandstone and conglomerate found within the Skeena Fold Belt, though incorporated in folds, appears relatively undeformed in thin section. This is particularly common along the limbs of folds, and within coarse units adjacent to fine-grained rocks that deform more readily. The structures described below are not generally observed in thin section in samples which appear undeformed in hand specimen.

4.3.1 Spaced Cleavage

The most penetratively deformed samples collected in the fold belt commonly display two scales of cleavage. The most commonly observed cleavage, visible in hand specimen, is a spaced cleavage with separations usually ranging from 1 to 50 millimetres (table 4.1). This cleavage is commonly planar or sutured. Often cleavage slabs viewed in thin section are separated by a millimetre or less (figure 4.1). At times these separations close and the cleavage is defined by sutured cracks. These slabs are sporadically lined

Sample #	Cleavage	Area	Stratigraphic	Lithology	Grain Size	Mean Spacing (mm)		Strain Shadow
	(rhr)		Unit	(Dott, 1964)	(mean)	Spaced	Slaty	(y/n/r=rare)
A*	192/55	Eskay	Ritchie-Alger	sublitharenitic	c. silt	5	0.05	y
B*	036/82	Eskay	Ritchie-Alger	quartz-wacke	m. silt	3	0.02	y
C*	056/71	Eskay	Ritchie-Alger	quartz-wacke	m. silt	2	0.02	y
D*	359/69	Iskut	Ritchie-Alger	quartz-wacke	m. silt	10	n/a	r
E*	064/81	Iskut	Ritchie-Alger	subarkosic	c. silt	6	0.025	y
F*	098/86	Iskut	Ritchie-Alger	lithic graywacke	m. silt	4	0.03	y
G*	004/87	Iskut	Ritchie-Alger	subarkosic	m. silt	2	0.02	r
H*	341/73	Iskut	Ritchie-Alger	sublitharenitic	m. silt	5	0.025	y
I*	295/84	Iskut	Ritchie-Alger	subarkosic	c. silt	5	0.1	r
J*	182/76	Sweeny	Skelhorne	sublitharenitic	m. silt	3	0.015	y
K*	318/84	Sweeny	Skelhorne	subarkosic	c. silt	4	0.05	y
L	031/42	Sweeny	Skelhorne	sublitharenitic	v.f. sand	10	0.025	n
M	018/83	Sweeny	Skelhorne	sublitharenitic	v.f. sand	15	n/a	n
N	180/66	Sweeny	Skelhorne	sublitharenitic	f. sand	20	n/a	n
O	029/75	Sweeny	Skelhorne	sublitharenitic	v.f. sand	10	n/a	n
P	092/54	Nelson	Ritchie-Alger	arkosic arenite	f. sand	25	discrete	r
Q	216/72	Cartmel	Eaglenest	quartz arenite	pebble	30	20	n
R	348/84	Cartmel	Eaglenest	quartz arenite	v.f. sand	20	discrete	n
S	249/67	Cartmel	Eaglenest	quartz arenite	m. sand	40	discrete	n
T	248/65	Cartmel	Eaglenest	quartz arenite	pebble	2	discrete	n
U	008/84	Cartmel	Eaglenest	quartz arenite	m. sand	50	discrete	n
V	324/81	Maitland	Skelhorne	sublitharenitic	v.f. sand	10	discrete	n
W	021/89	Maitland	Skelhorne	sublitharenitic	v.f. sand	20	n/a	n

Table 4.1: Summary of lithologic and cleavage properties of samples collected for purpose of cleavage description. * indicates samples processed for Ar-Ar geochronology. Clast lithology follows classification of Dott (1964), in this case applied to both sandstones and siltstones with aid of thin section petrography.

with insoluble clay materials, suggesting a possible origin related to pressure solution. Slabs are also often lined with an orange amorphous material (figure 4.1) that was found, using EDS microprobe analysis, to have high iron and phosphorous content. The material does not appear altered by diagenesis or deformation and is likely a precipitate. The presence of this precipitate indicates that separation of cleavage slabs occurred prior to sampling. Separation is interpreted to have occurred during a period of extension, likely occurring during exhumation. These cleavage planes represent planes of weakness in the rock which were then opened as fractures.

4.3.2 Slaty Cleavage

The spaced cleavage described above is easily discernible in hand specimen. A finer-scale cleavage is only observable in thin section, usually in dark siltstones. Spacing of this cleavage typically ranges from 15 to 50 micrometres (table 4.1) and morphology is commonly wavy or anastomosing (figure 4.2). This cleavage is a disjunctive slaty

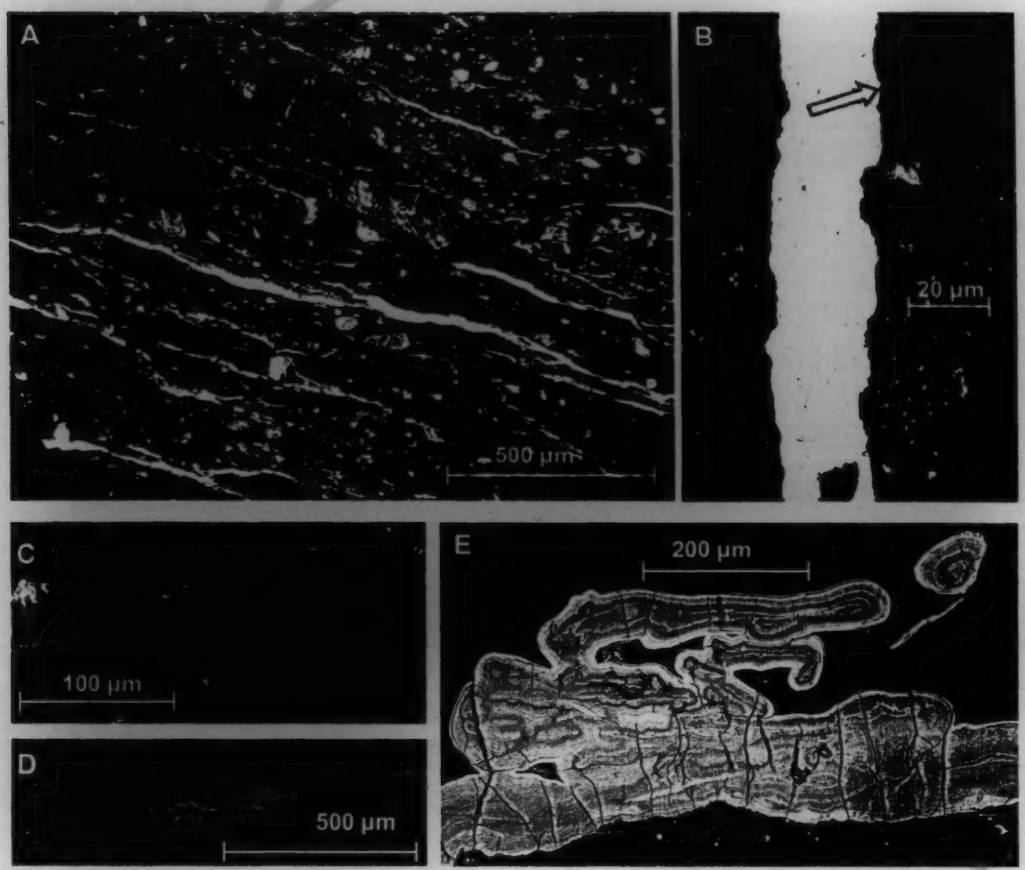

Figure 4.1: Images of spaced cleavage and amorphous residue lining cleavage. A-B: Thin section photomicrographs in cross-polarized light of fracture cleavage from Eskay Creek and Iskut ridge areas, respectively; C-E: CP electron microprobe backscatter images of fracture cleavage. Brightest portions reflect high iron content. C-D: Bright feature is orange residue seen in (A) and (B). Note fracturing of residue may have occurred during sampling process; E: Unusually large build-up of orange residue along a cleavage slab boundary.

cleavage, referring to its domain spacing and lack of rotation of sedimentary layering (Powell, 1979). Dark insoluble clay material is commonly concentrated along finer-scale cleavage seams. Dissolution of grain boundaries (figure 4.3A) and dissolution within clasts (figure 4.4) parallel to cleavage indicates this is a pressure solution cleavage. Other evidence of conditions suitable for pressure solution are rare stylolites present in pebble conglomerate, particularly in the Cartmel Lake area (figure 4.5), and dissolution of grain contacts not parallel to cleavage (figure 4.3B).

In most areas of the fold belt cleavage is primarily identified in siltstone and

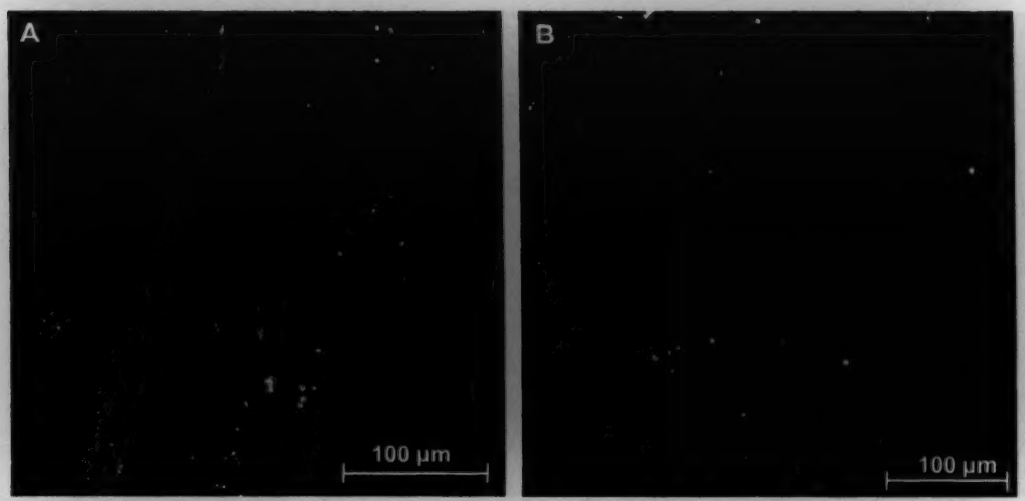

Figure 4.2: CP electron microprobe backscatter images of penetrative cleavage illustrating anatomising nature. Bright lines defining cleavage reflect elevated iron content. A: Deformed sample from the Iskut ridge area displaying penetrative cleavage and its subparallel alignment with spaced cleavage (far right); B: More evenly developed cleavage in the Eskay Creek area. Note cleavage appears to develop around coarse clasts.

very fine-grained sandstone. In thin section fine sandstone and pebble conglomerate also rarely displays a discrete wavy cleavage, parallel to fracture cleavage observed in outcrop. Conglomerate beds do not commonly develop strong cleavage with the exception of those in the Cartmel Lake area (figure 4.3), as noted in Chapter 2, where cleavage is found throughout the area. Cleavage development serves to accommodate strain during deformation, and fine-grained lithologies more readily take up that strain. This effectively partitions strain to finer-grained units. The limited amount of fine-grained lithologies in Cartmel Lake (as little as <20%) may limit this partitioning of strain. Instead strain can be expected to have evenly affected all conglomerates, resulting in spaced pressure-solution cleavage developed throughout the map area.

4.3.3 Metamorphic Minerals

Chlorite is only sporadically present in samples examined indicating some minor metamorphism. In some samples chlorite is an alteration product of previous minerals, whereas in other cases it is more euhedral and appears to have grown due to

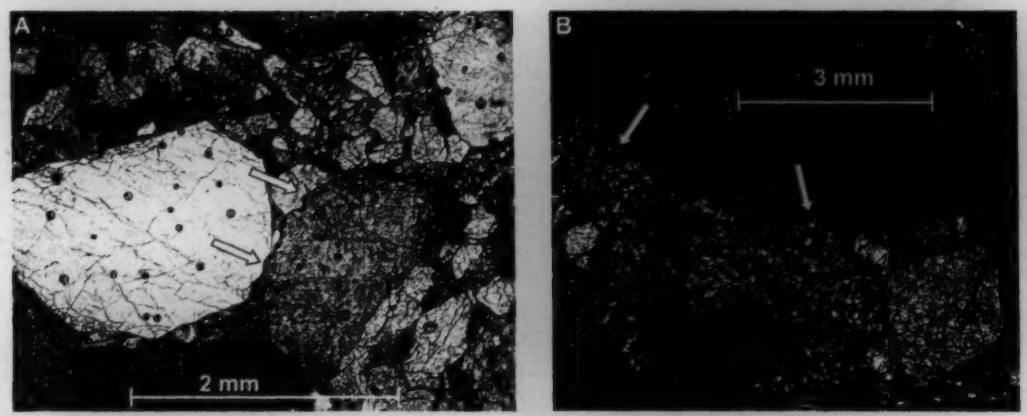

Figure 4.3: Thin section photomicrographs of grain boundary dissolution within conglomerates from the Cartmel Lake area. Arrows indicate sites of clear grain dissolution. A: Grain boundary dissolution subparallel to cleavage; B: Grain boundary dissolution not parallel to cleavage.

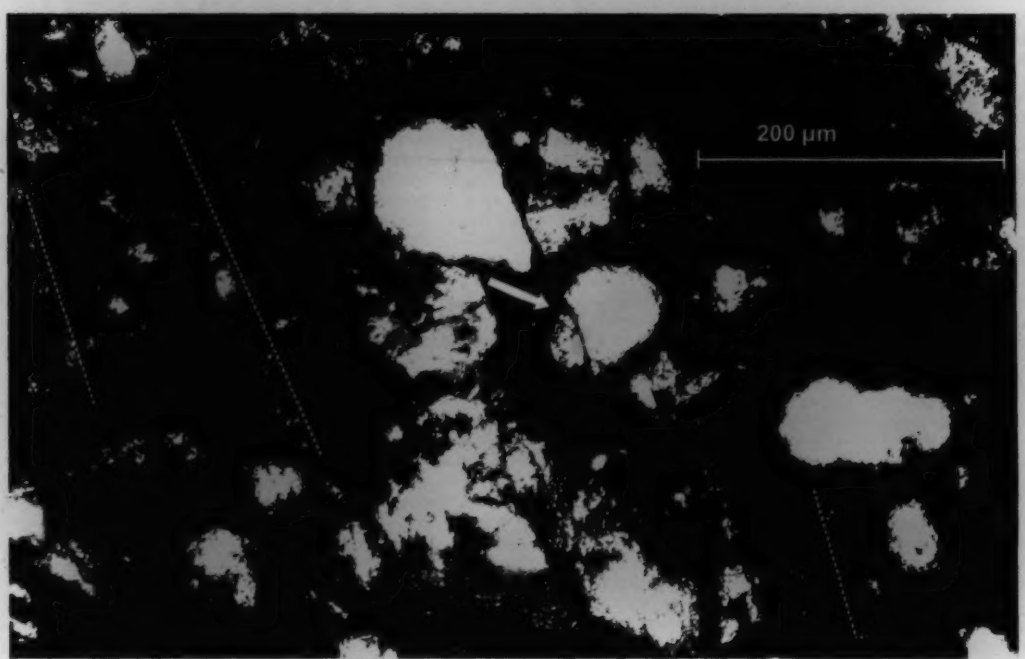

Figure 4.4: Thin section photomicrograph of pressure solution occurring parallel to cleavage and within a grain from the Iskut ridge area. White dashed lines indicate general trace of cleavage in thin section.

metamorphism. Using EDS analysis, potassium-rich layers interpreted as muscovite were found to be intergrown with magnesium-rich chlorite layers. Muscovite identifiable in thin section is rare (<1%) in samples studied. In most cases grains are not oriented parallel to bedding. Some mica grains appear to be kinked parallel to cleavage. This

Figure 4.5: Thin section photomicrograph of stylolitic dissolution within conglomerate of the Cartmel Lake area. Sky blue areas are regions of dye-staining indicating porosity in fractures.

suggests muscovite may be detrital and was altered during deformation. The rarity of detrital muscovite is well-documented in rocks of the Bowser Lake Group (Eisbacher, 1974b; Ritcey et al., 2003; Evenchick and Thorkelson, 2005). The paucity of secondary muscovite is attributed to insufficient temperature/pressure conditions and unsuitable host-rock chemistry for mica growth.

4.3.4 Strain Indicators

In the most penetratively deformed siltstones a clear elongation of clasts parallel to pressure solution cleavage is evident (figure 4.6). Length/width ratios are in some cases in excess of 4:1. In samples that have a less pervasive cleavage this elongation is not as apparent. More moderate strain ratios have been observed in outcrop exposures

of conglomerates. This elongation is commonly oriented at a high angle to bedding and therefore is not related to imbrication during sedimentation. Clast elongation is interpreted to result from a combination of grain dissolution and cleavage-parallel strain.

The majority of siltstones examined contain a small (<5%) percentage of opaque grains, commonly framboidal pyrite. The opaque grains vary in shape from circular to angular and elongate. Many pyrites have a growth of clay or chlorite formed around opposite sides of the grain in the form of strain ('pressure') shadows (figure 4.7). Though some strain shadows have been observed around feldspar grains, the vast majority of strain shadows are observed around opaque grains and their distribution appears to be strongly controlled by the abundance of pyrite in highly deformed siltstones. Strain shadows commonly have fibres oriented subparallel to pressure solution cleavage when viewed in thin section cut perpendicular to cleavage. Elongate grains are at times at a high angle to cleavage (figure 4.8). They do not appear to be affected by pressure solution (i.e. solution seams do not traverse grains). Growth fibres are still oriented

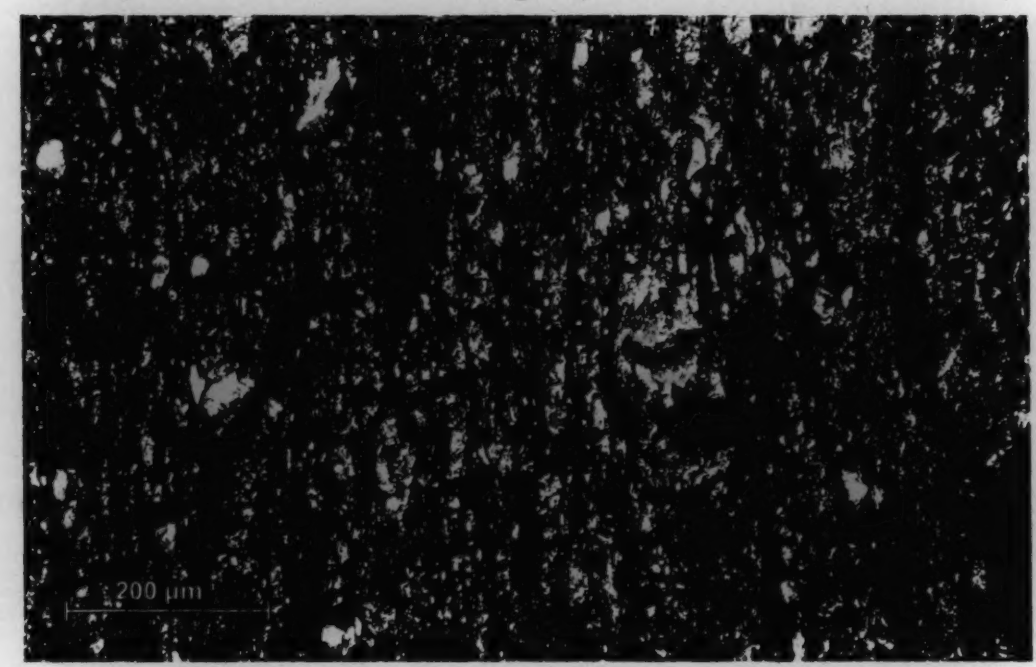

Figure 4.6: Thin section photomicrograph of penetrative cleavage in the Eskay Creek area and clasts that have been strained parallel to cleavage.

parallel to cleavage, suggesting syn-kinematic formation of growths and pre-kinematic deposition/diagenesis of opaque grains.

The application of strain shadows for use as kinematic indicators has been demonstrated by several studies (e.g. Durney and Ramsay, 1973; Ramsay and Huber, 1983; Tillman and Byrne, 1995). As a test of the suitability of strain shadows for generating coherent interpretations of strain history in the fold belt, an oriented sample of siltstone with S1 cleavage from the Eskay Creek area was cut into two thin sections: one parallel to cleavage (192/55 W), equivalent to the XY plane, and one a vertical section perpendicular to cleavage (282/90), roughly equivalent to the XZ plane. Shadows formed around framboidal or slightly elongate pyrite were analysed. Growth of fibres is assumed to be antitaxial (Durney and Ramsay, 1973). Fibre growth occurs in the direction of elongation in the form of displacement-controlled fibres, as opposed to perpendicular to the pyrite surface as is seen in face-controlled fibre growth (Ramsay and Huber, 1983). Fibres are consistently optically continuous, and exhibit sweeping extinction. The pyrite radius *(l)*, length of fibres *(δl)* (figure 4.9A) and rake of fibres within the thin section was measured. This allows calculation of the finite elongation (*e*), given by

$$e = \frac{\delta l}{l}$$ (Ramsay and Huber, 1983)

Where fibre orientation changes incrementally by a value θ, a correction is generally applied to account for differing extension directions

$$e = \frac{\delta l_1 + \delta l_2}{l + \delta l_1 \cos\theta}$$ (Ramsay and Huber, 1983)

In the case of strain shadows analysed here, fibres are either straight or the change in fibre orientation (θ) is small (<10°). Due to the negligible effect on calculated values of *e* (<2%) this correction was not applied. Those fibres that do exhibit changes in orientation have a counter-clockwise sense of curvature when looking north and east on respective sections.

Calculations of finite elongation for the selected sample range between 0.3 and

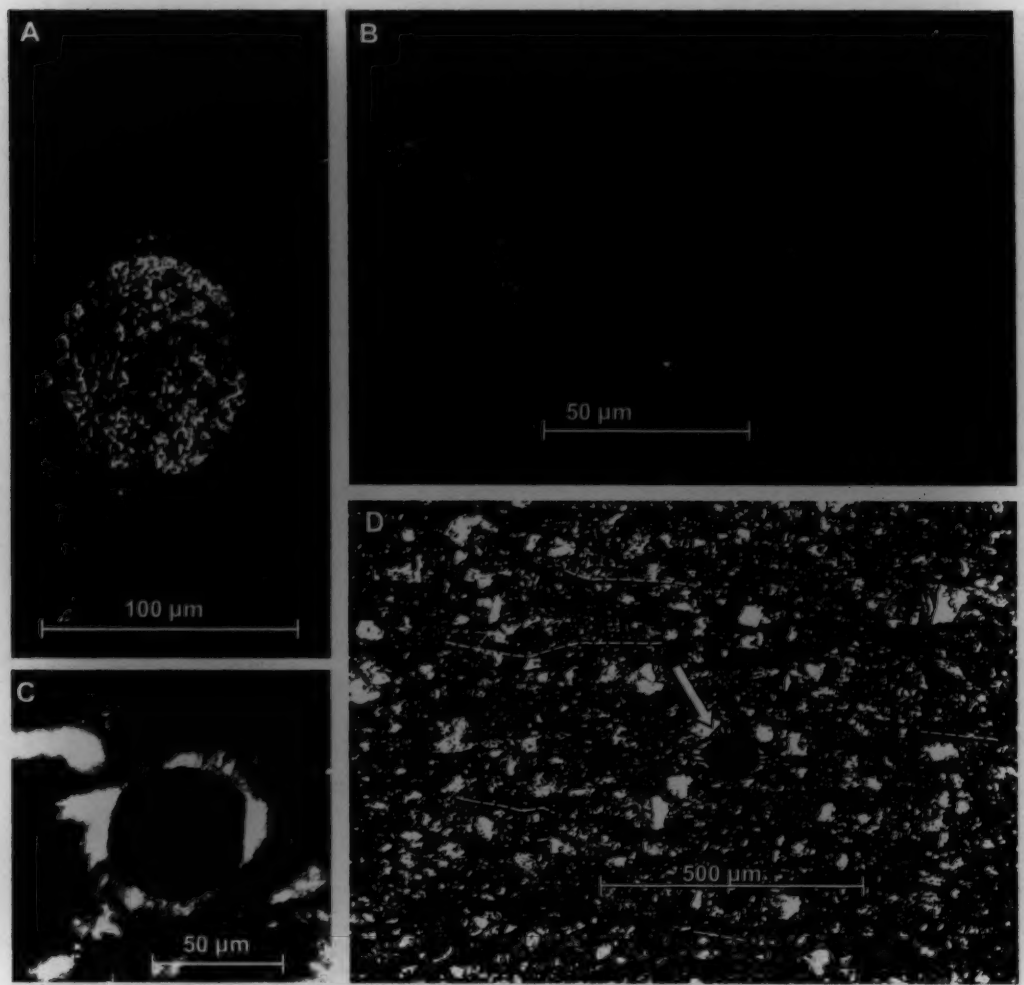

Figure 4.7: Images of strain shadows developed in rocks of the Eskay Creek area. A-B: CP electron microprobe backscatter images of strain shadows developed around framboidal pyrite; C-D: Thin section photomicrographs of strain shadows; D: Strain Shadow illustrating subparallel relationship between fibre growth (solid lines) and cleavage (dashed lines).

1.0, with one outlier at 1.67 (table 4.2). Both Slide A (~XZ section) and AA (XY section) (figure 4.9B), yield similar values of *e*, with a mean of 0.57 and 0.55, respectively. At first glance the two data sets appear to have contradictory trends of *e* with respect to lineation plunge (figure 4.9C-D). However, both trends suggest greater extension in more easterly-plunging orientations. If it is assumed that shadows from both sections are similarly oriented, it must be interpreted that sections cut fibres obliquely and neither

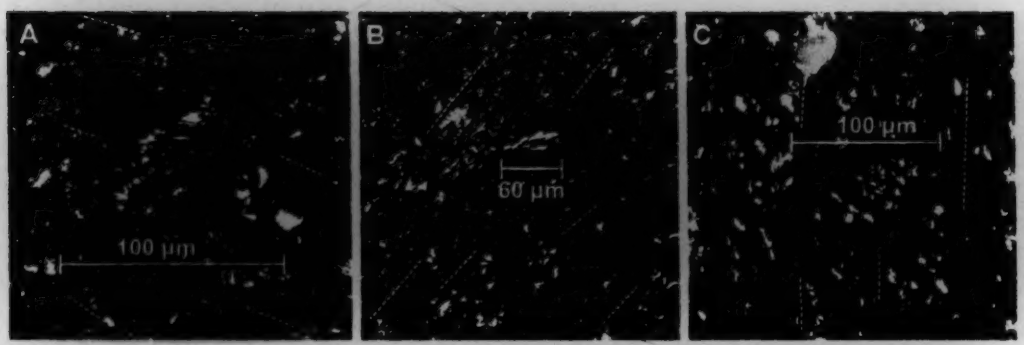

Figure 4.8: Thin section photomicrographs of strain shadows developed around elongate opaque grains from the Sweeny Creek area. All views in cross-polarized light. Dashed lines indicate trace of cleavage.

contain the direction of greatest extension. Combining the trends and orientations of figure 4.9B-D, it is likely the greatest extension occurred in a plane with a greater dip than Slide AA. An orientation likely to contain the direction of greatest extension is the mean cleavage orientation, shown in figure 4.9E. The sample selected has a cleavage orientation that falls well outside the mean S1 cleavage orientation, likely due to cleavage refraction. The implication of extension occurring in an orientation steeper than refracted cleavage is that strain shadow growth is not directly controlled by cleavage formation, but rather by overall strain related to folding. The counter-clockwise curvature of some strain shadows is consistent with a sinistral-reverse component of simple shear when looking northeast. These data indicate that strain shadows in this area are suitable indicators of extension direction and developed in conjunction with folding. Application of these methods to other rocks in the area such as at Iskut ridge, Eskay Creek, and Sweeny Creek, where strain shadows are most abundant, would allow the development of local and regional comparisons of strain history.

4.4 Ar-Ar geochronology

4.4.1 Cleaved samples

In the Iskut ridge and Eskay Creek areas, and to a lesser extent the Sweeny Creek area, cleavage is generally more penetrative than in other areas. Whole-rock $^{40}Ar/^{39}Ar$

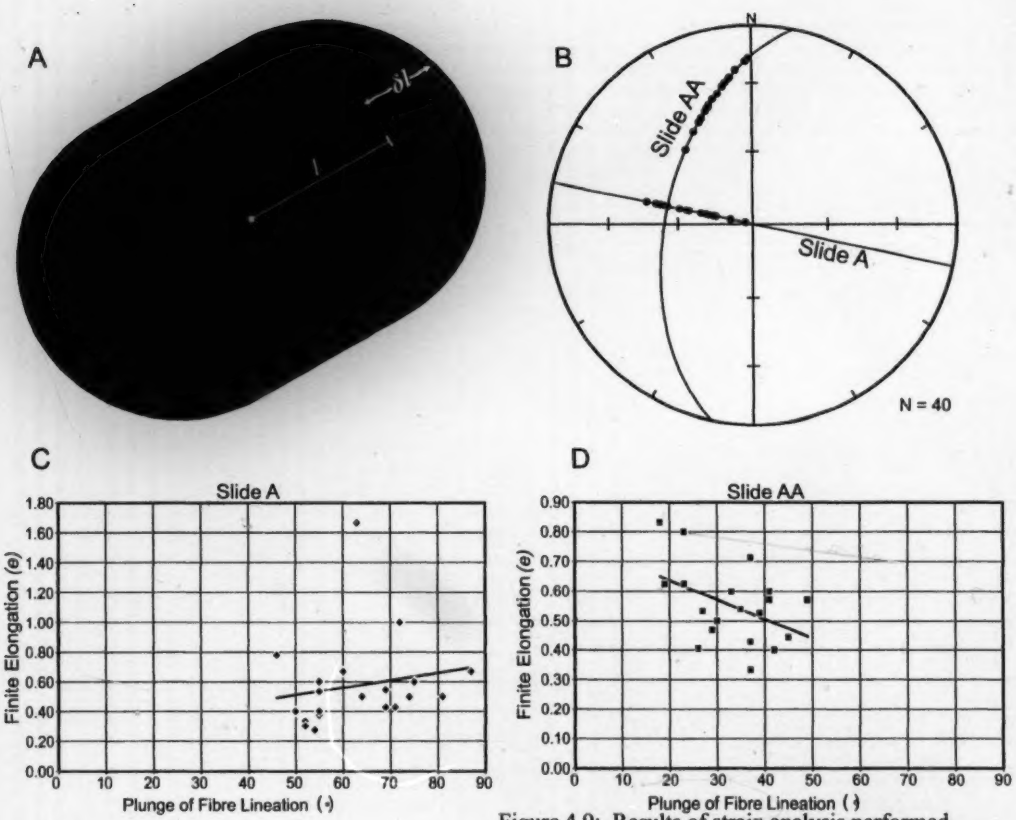

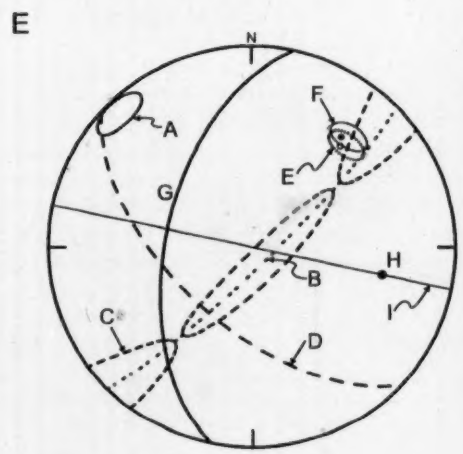

Figure 4.9: Results of strain analysis performed using strain shadows within cleaved siltstone from the Eskay Creek area. A: Idealized strain shadow, illustrating relationship of fibres to pyrite margin and measured properties; B: Equal-area lower hemisphere projection of Slides A and AA (great circles) and fibres plotted using rakes measured within thin section; C-D: XY Scatter plots of finite elongation vs. growth fibre plunge for Slides A and AA. Thick lines represent best-fit linear trendlines; E: Summary of structural data from Eskay Creek area shown in figure 2.33 and orientations of Slide A and AA. Cones of confidence are 95%. A=Cone of confidence around e3 which centres cluster of cleavage poles. B=Mean cleavage orientation. C=Cone of confidence around e1 and e2, which define mean S1 cleavage orientation. D=Best fit girdle through bedding poles. E=Cone of confidence around π-axis (open circle). F=Cone of confidence around e3 (solid circle) defining cluster of bedding-cleavage intersection lineations. G=Orientation of slide AA. H=Orientation of pole to slide AA (clvg pole). I=Orientation of slide A.

Slide A

#	Pyrite Radius (μm)	Fibre length (μm)	Finite Elongation (e)	Rake (°)
1	18.75	10	0.53	55
2	20	7.5	0.38	55
3	17.5	7.5	0.43	69
4	22.5	17.5	0.78	46
5	7.5	12.5	1.67	63
6	12.5	7.5	0.60	75
7	12.5	12.5	1.00	72
8	11.25	7.5	0.67	60
9	15	6	0.40	50
10	22.5	7.5	0.33	52
11	10	5	0.50	74
12	25	7.5	0.30	52
13	27.5	7.5	0.27	54
14	25	15	0.60	55
15	12.5	5	0.40	55
16	11.25	7.5	0.67	87
17	15	7.5	0.50	81
18	17.5	7.5	0.43	71
19	13.75	7.5	0.55	69
20	15	7.5	0.50	64

Slide AA

#	Pyrite Radius (μm)	Fibre length (μm)	Finite Elongation (e)	Rake (°)
1	45	15	0.33	133
2	7	5	0.71	132
3	25	15	0.60	127
4	16	7.5	0.47	144
5	22.5	10	0.44	121
6	25	15	0.60	139
7	25	12.5	0.50	142
8	20	10	0.50	142
9	35	20	0.57	127
10	12.5	10	0.80	151
11	37.5	20	0.53	146
12	17.5	10	0.57	113
13	18.5	10	0.54	136
14	15	12.5	0.83	158
15	18.5	7.5	0.41	147
16	19	10	0.53	130
17	20	12.5	0.63	151
18	25	10	0.40	125
19	17.5	7.5	0.43	132
20	20	12.5	0.63	156

Table 4.2: Table of properties of strain shadows measured and calculated finite elongations (e). Rakes are clockwise.

geochronology was attempted on samples from these areas with the goal of constraining the age of new mica growth within these samples. New mica growth visible in thin section is generally restricted to strain shadows developed around pyrite grains and other sulfides, and chlorite-muscovite intergrowths, as discussed in the above sections. When muscovite grows it incorporates potassium (^{40}K) into its structure. Radioactive ^{40}K then progressively decays into ^{40}Ar and ^{40}Ca. If grains are not altered by fluids, and the mineral is not heated beyond closure temperature which would allow argon to escape the mineral, then the amount of ^{40}Ar within the crystal will increase with time according to its decay constant. Comparison of daughter ^{40}Ar with the parent isotope allows calculation of the number of half-lives to have occurred, and thusly the amount of time elapsed since crystallization. If it is interpreted that mica growth occurred during deformation, then the time elapsed corresponds to the time since deformation, in this case cleavage formation. $^{40}Ar/^{39}Ar$ geochronology methods are further discussed in Appendix A.

Eleven samples were chosen for Ar-Ar dating of cleavage formation. General

characteristics of these samples are summarized in table 4.1. These samples were chosen using the criteria of being the most fine-grained rocks samples, having well-developed cleavage, and containing strain shadows with chlorite-mica intergrowths. Some samples used possess S1 cleavage, others S2 cleavage. Analyses were carried out at the University of British Columbia Ar Geochronology Laboratory. Samples were crushed, treated with nitric acid and analysed using a laser-equipped noble gas mass spectrometer (NGMS) VG5400. Incremental heating of the sample for Ar recovery used a MR-10 infrared CO_2 laser. Results are plotted as Age vs. Cumulative ^{39}Ar graphs.

Of the eleven samples on which dating was attempted, seven did not yield plateaus (figure 4.10). The ages at individual steps generally range from 165 to 186 Ma. Sample K yielded a plateau age of 174.7±1.3 Ma (figure 4.10K), corresponding to the early Aalenian using the timescale of Gradstein et al. (2004). Rocks in this area (Sweeny Creek) are likely Late Jurassic (Oxfordian) in age (Evenchick et al., 2001); therefore the Aalenian age yielded corresponds to the age of a detrital component. This is the only sample from the interior of the basin to yield a coherent result, but on its own suggests that this part of the basin did not reach conditions necessary for resetting the Ar-Ar system.

Three samples, all from the Iskut ridge area, yielded plateaus that are interpreted to relate to ages of deformation. The rocks in this area are likely of Middle Jurassic age (Evenchick et al., 2001). Sample E hosts S1 cleavage and yielded an age of 146.0±1.7 Ma (figure 4.10E). Samples G and H host S2 cleavage and have similar plateau ages of 128.86±0.82 and 129.16±0.87 Ma, respectively (figure 4.10G-H). These ages do not satisfy the "accepted" criteria for plateaus (>50% ^{39}Ar); however inverse isochron plots of $^{36}Ar/^{40}Ar$ versus $^{39}Ar/^{40}Ar$ (figure 4.11) produce linear trends suggesting the plateau ages are geologically meaningful. Further data on samples E, G and H and K is provided in Appendix A. The difference in age between sample E and samples G and H is consistent with relative timing constraints of cleavage formation. This is an

encouraging sign that the ages have significance for deformation ages. Since all three samples are from the same area this eliminates the possibility that the differences in ages are due to regional variations in timing of deformation across the fold belt. The 146 Ma age corresponds to the latest Jurassic (Gradstein et al., 2004) whereas the ages of 128 and 129 Ma correspond to the Early Cretaceous (Barremian). These ages indicate that deformation was active in the Iskut ridge area by the Jurassic-Cretaceous boundary. Previous constraints on age of deformation, based on strata in the Sustut Basin as discussed in Chapter 1, indicated the earliest evidence for deformation occurred in the Albian (Evenchick and Thorkelson, 2005). These data also indicate a protracted history of deformation, with a possible separation of F1 and F2 folding events of ~17 my. This study represents the first attempt at directly dating structures produced by deformation in rocks of the Bowser Lake Group in the western Skeena Fold Belt. The ages here are slightly older than 110±10 Ma ages of peak metamorphism determined from K-Ar dating of Hazelton Group rocks west of the Bowser Basin near Stewart, BC (Alldrick, 1993). This suggests that either metamorphism was diachronous and that deformation may have begun earlier than previously interpreted, or that mineral growth, and therefore the start of the K-Ar system 'clock', began earlier than peak metamorphism.

4.4.2 Mafic Post-Kinematic Dike

In the Eskay Creek area several mafic dikes were observed. These dikes range in thickness from ~30 to 100 centimetres. Two such dikes were found near the hinge of an upright F1 anticline-syncline pair with axial planes oriented 225°/82° NW and fold hinges oriented 044°–07° (figure 4.12). These dikes are parallel to each other and oriented 236°/58° NW. These dikes are not folded and cleavage, identified in the adjacent strata, is not present within the dikes in outcrop or thin section. Minor slip planes with moderately W plunging (281°–42°) slickenlines are developed on the edge of the larger dike and offset strata obliquely by ~10 cm. These dikes are postkinematic with respect to folding, and syn- or pre-kinematic with respect to oblique slip. One dike

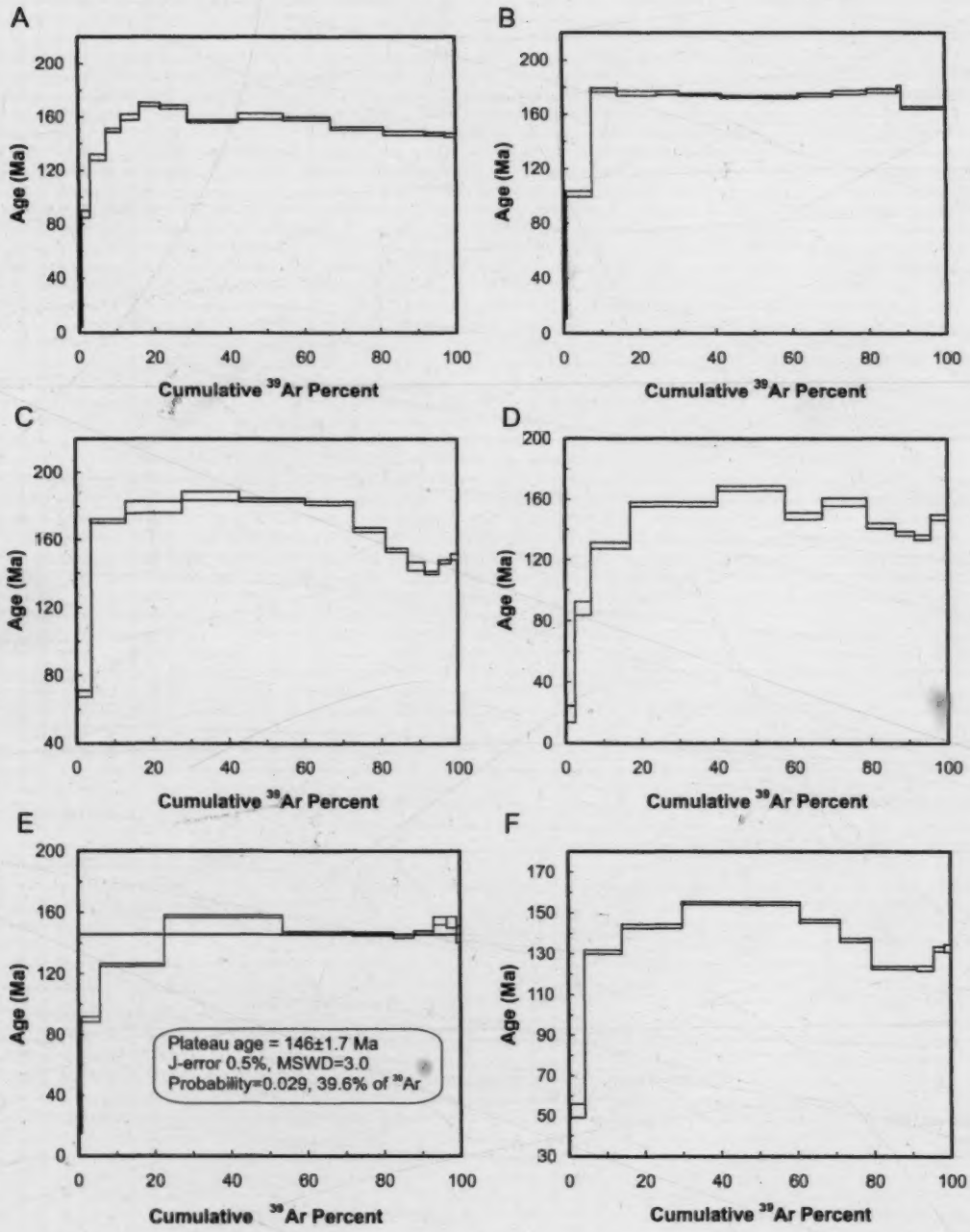
A
B
C
D
E
F
Age (Ma)
Cumulative ^{39}Ar Percent
Plateau age = 146±1.7 Ma
J-error 0.5%, MSWD=3.0
Probability=0.029, 39.6% of ^{39}Ar

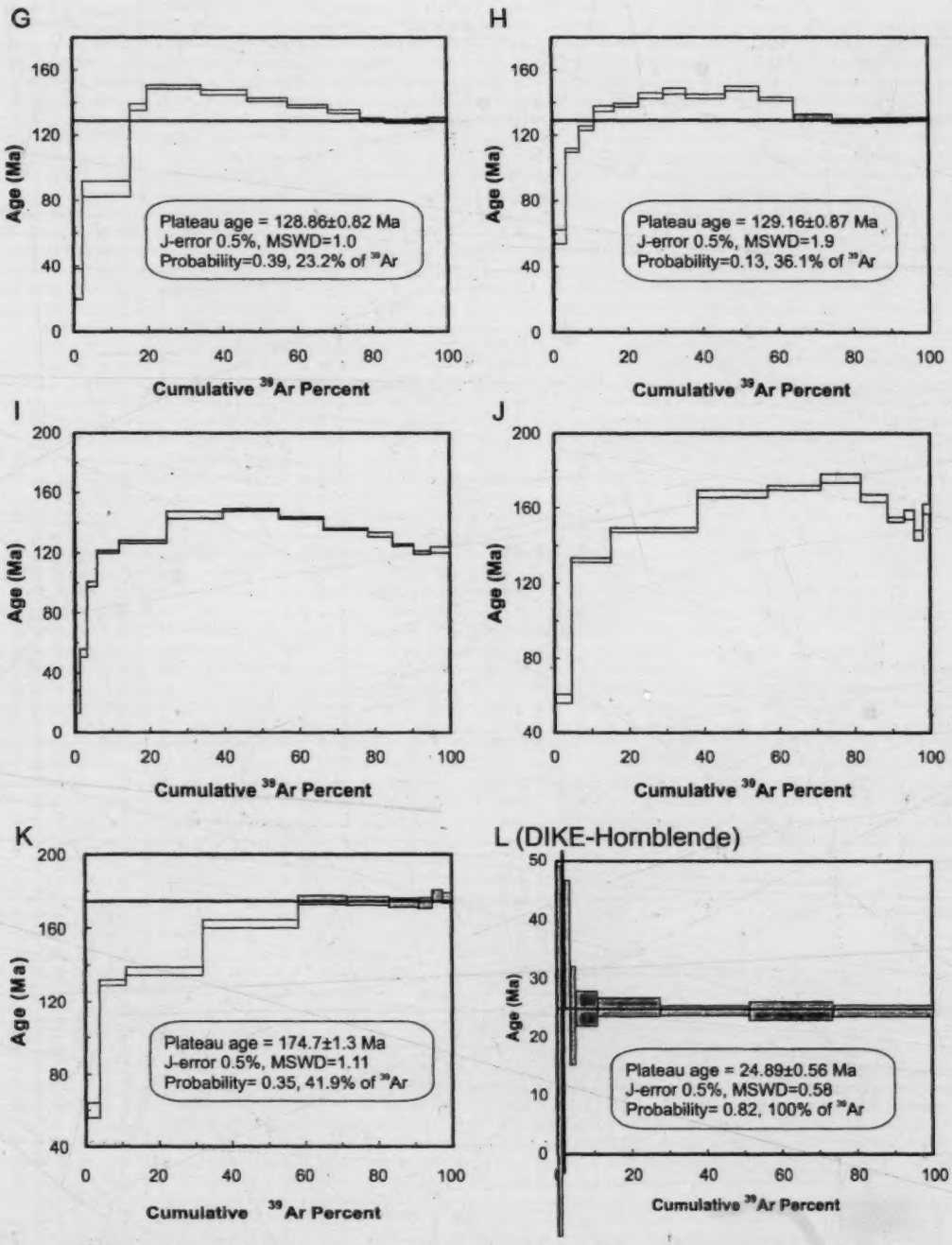

Figure 4.10: (includes previous page) First-run cumulative ^{39}Ar % versus age plots generated using step-heating Ar-Ar geochronology. Where plateaus are picked, statistics are included on graphs. Plateau steps are filled, rejected steps are open. Box height=2σ (variance, 95% confidence), MSWD=mean sum weighted deviations A-K: Cleaved samples dated. Figure labels correspond to sample labels in table 4.1; L: Dike from the Eskay Creek area, shown in figure 4.12.

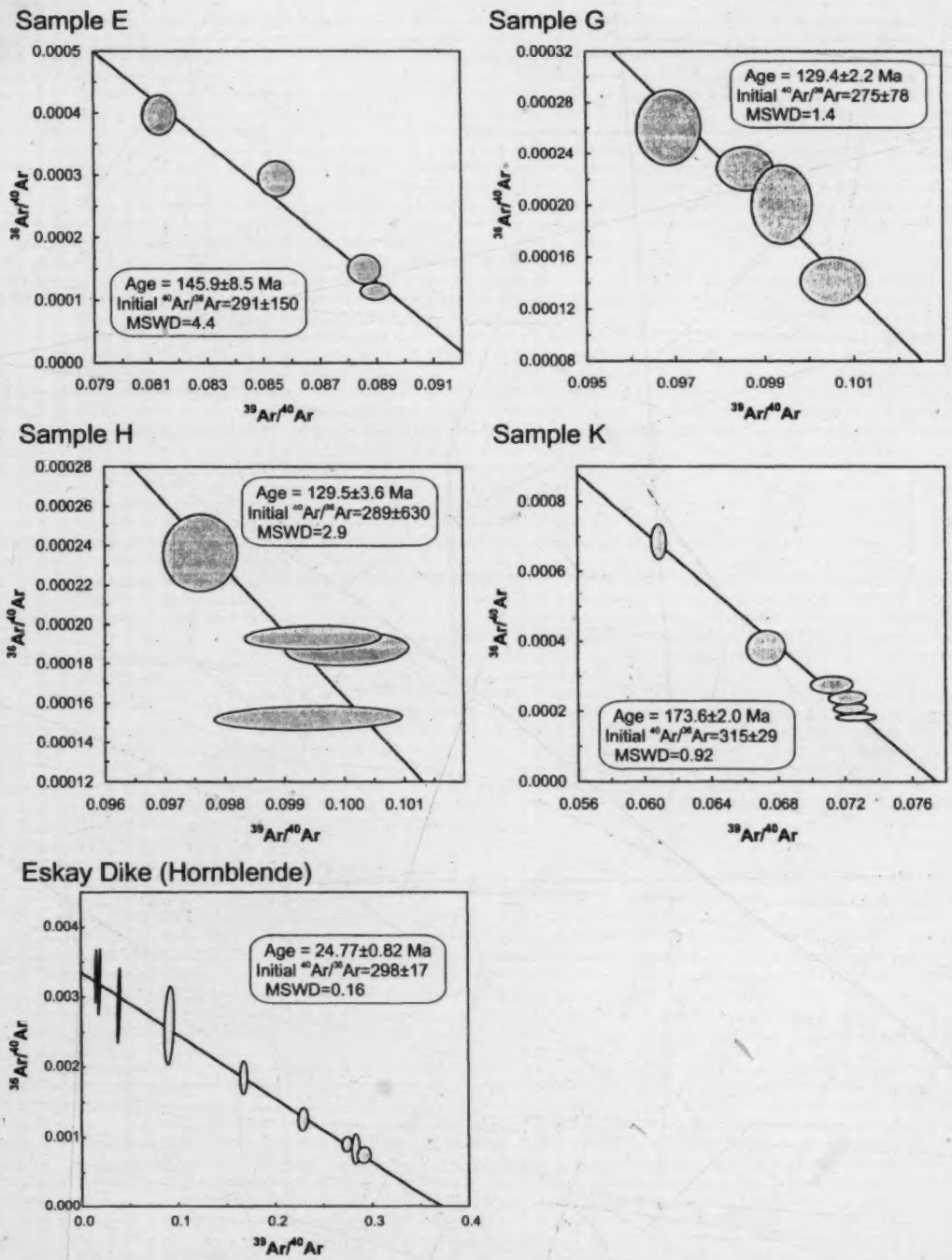

Figure 4.11: Inverse isochron $^{36}Ar/^{40}Ar$ vs. $^{39}Ar/^{40}Ar$ plots of samples E, G, H, K and steps 2-10 of 'Eskay Dike'. Statistics indicated on graph. Data point error ellipses are 2σ.

Figure 4.12: Mafic dike in the Eskay Creek area. View towards NE of syncline-anticline pair and cross-cutting dikes, indicated by white dashed lines. Person for scale.

was sampled and analysed using Ar-Ar geochronology. This dike contains abundant biotite and plagioclase feldspar, amphibole, altered olivine that appears serpentinized and is classified as a lamprophyre. The same geochronology procedures used for cleaved samples discussed above were used for dating this dike, with the exception that hornblende was separated and dated. A plateau age of 24.89±0.56 Ma (hornblende) was determined (figure 4.10 'Eskay Dike'). This age is consistent with Oligocene emplacement and minimum age of deformation in the Eskay Creek area. This and other dikes in the Eskay Creek area may be correlative with Oligocene lamprophyre dikes west of the Bowser Basin reported by Alldrick (1993). In an extensive study of the Eskay Creek deposit, dikes younger than Cretaceous were not documented (Roth, 2003). Though this age does not greatly constrain timing of deformation, this late intrusion may have influenced mineralization of the nearby deposit, following the main hydrothermal event.

4.5 Discussion of Microstructures and Geochronology

The most prominent structure type observable in thin section within deformed rocks of the Bowser Lake Group is cleavage. Cleavage is variably expressed in outcrop

and section as a disjunctive spaced cleavage with sutured or planar morphology, and as a disjunctive, slaty pressure solution cleavage. This is consistent with conditions of pressure solution documented by Moffat (1985). Based on several indicators of pressure solution, such as grain boundary solution, within-clast solution, clay-lined selvages, and greatly increased clast length/width ratios, volume loss due to cleavage formation is interpreted to be significant. The results of this study also indicate stronger cleavage development in western areas than eastern areas and demonstrate an eastward decrease in the degree of cleavage development. This has implications for petroleum exploration in the region, as porosity/permeability of potential reservoirs is more likely to have been reduced along the western margins. Extensive pressure solution, precipitation of new minerals, and strain of rocks are all likely to contribute to reduction of reservoir quality in the west of the fold belt.

Strain shadows with fibres composed of chlorite and lesser chlorite-muscovite intergrowths are commonly developed around framboidal pyrite grains in strongly cleaved siltstones. Fibre growth is steep and subparallel to cleavage, suggesting growth during cleavage formation. Analysis of one sample with abundant strain shadows indicates typical finite elongation values of ~0.6 associated with shadow growth. This sample suggests elongation occurred in a slightly steeper plane than cleavage. Strain shadows may represent a valuable quantitative kinematic indicator for future strain analysis studies in the region.

Growth of metamorphic minerals such as chlorite-mica intergrowths in strain shadows and within the rock matrix presents an opportunity to attempt Ar-Ar geochronology and constrain absolute timing of deformation in the fold belt. Three samples from the Iskut ridge area yielded reasonable plateaus corresponding to deformation. One sample was associated with S1 cleavage and produced an age of 146.0±1.7 Ma, and the other two associated with S2 cleavage produced ages of 128.86±0.82 and 129.16±0.87 Ma. These ages are consistent with relative timing

constraints in the Iskut ridge area and indicate D1 deformation near the Jurassic-Cretaceous boundary, and mid-Early Cretaceous D2 deformation. This significantly extends the known period of deformation in the fold belt, which was previously only confirmed to have been active by the Albian (Evenchick and Thorkelson, 2005). Another implication of these ages is that early deformation in western areas was coeval with deposition of fluvial and possibly shallow marine units of the Bowser Lake Group in central and eastern areas (figure 1.1, 1.2). The shallowing of sedimentary facies through time and ultimate demise of the basin may therefore be controlled by uplift due to deformation, rather than a decrease in effectiveness of subsidence mechanisms that initially formed the basin.

Ar-Ar dating of a dike that is post-kinematic with respect to F1 folding from the Eskay Creek area produced a plateau age of 24.9 Ma. This indicates D1 deformation in the Eskay Creek area was completed by the Oligocene. Dikes in the Eskay Creek area may be correlative with those reported by Alldrick (1993).

Chapter 5: Discussion

5.1 Introduction

The Skeena Fold Belt is an extensive mountain range recording deformation of the clastic Jurassic-Cretaceous Bowser Lake and Sustut Groups and associated deformation of the sedimentary and volcanic Stikine assemblage, Stuhini and Hazelton Groups. Structures in the fold belt fall into four broad episodes:

- Pre-D1 structures only affecting Hazleton Group and older strata.
- D1 structures predominantly exposed in the western third of the fold belt.
- D2 structures present throughout the fold belt.
- D3 structures identified in northern portions of the fold belt.

This chapter will synthesize characteristics of these structural groupings presented in the previous chapters and evaluate relationships bearing significance on current models of fold belt evolution.

5.2 Pre-D1 Structures (Early Jurassic or older)

Structures that pre-date development of the Skeena Fold Belt have been well documented by Logan et al. (2000). In this thesis structures are considered to pre-date the fold belt if they formed prior to initial deposition of the Bowser Lake Group in the Middle Jurassic. There is a general difference in character between structures affecting the lower Hazelton Group and the upper Hazelton and Bowser Lake Groups. Structures such as C-S fabric (Berthe et al., 1979), identified in volcanic rocks of the Hazelton Group are relatively high-strain structures in comparison with overlying sedimentary strata that have well-preserved sedimentary structures. Steep faults in the Hazelton Group are commonly associated with gossanous alteration and are not identified in the Bowser Lake Group. The kinematics of identified structures appears widely variable but identification of structures limited to the lower Hazelton Group suggests the existence of

a deformation occurring in the Early Jurassic.

One documented 'collision' of the Stikine terrane with a neighbouring geologic unit has been interpreted to result from the closure of the Cache Creek Basin followed by exhumation and overthrusting of the Cache Creek Complex (Gabrielse, 1991). It is possible that this sequence of events may have resulted in deformation of the Stikine assemblage and overlying units due to either subduction-related shortening or later overthrusting (Logan et al., 2000). Exhumation is interpreted to have occurred rapidly during the Aalenian (early Middle Jurassic), with deformation in the form of SW-verging folds and thrusts also initiating at this time (Mihalynuk et al., 2004). Although this timing of events does not permit comparison with structures of the Skeena Fold Belt, they may have influenced interpreted pre-D1 structures in the lower Hazelton Group. These structures may correlate with the late Early Jurassic deformation of the Hazelton and Stuhini Groups described by Logan et al. (2000). Another possibility is that these structures correspond to extension that accommodated rifting postulated to occur prior to deposition of the Bowser Lake Group (Alldrick et al., 2005; Gagnon et al., 2007).

5.3 D1 Structures (Late Jurassic to Early Cretaceous)

In this study F1 folds generally trending N to NE were found to be overprinted by F2 folds and associated structures with NW trends. D1 structures consist primarily of outcrop to map-scale folds, rare detachment faults, and a disjunctive S1 pressure-solution cleavage. Structures identified in this study that correspond to D1 deformation are found in six of the nine areas mapped. Spatially F1 folds become less dominant relative to F2 folds eastward. Folds are most commonly subrounded open to tight folds with wavelengths ranging from 50 to 200 metres. Associated disjunctive cleavage formed from pressure solution as indicated by clast dissolution. Cleavage spacing is highly variable, ranging from ~20 microns to centimetre spacing. The high degree of cleavage development during D1 deformation is likely to have had a negative effect on reservoir quality in terms of hydrocarbon potential. Areas without D1 structure development may

have higher reservoir quality. Strain shadows developed around framboidal pyrite have steeply plunging growth fibres, with orientations subparallel to cleavage. The rarity of identified D1 thrust faults may be a recognition problem, or may indicate that F1 folds formed via detachment folding.

The distribution of D1 structures shown by this study, and by previous workers (Evenchick, 2001; Bone, 2002; Evenchick et al., 2004), allows delineation of an approximate limit of extent, or domain boundary, of D1 structures (figure 5.1). The absence of D1 structures at Mount Will (figure 1.4), and in other more eastern regions of the fold belt (Evenchick et al., 2004), is most easily attributed to the progressive formation of D1 structures from west to east. This deformation then faded out before reaching the Mount Will area. The absence of D1 structures at the Nelson Creek and Oweegee Dome areas (figure 1.4) is more unusual given their relative proximity to the western margin of the fold belt, and the abundance of D1 structures in the southwest corner of the fold belt (Evenchick, 2001). It is possible, given the relatively wide separation of D1 structures in this study and those in the southwest area, that structures in the two areas are unrelated and simply coincidently oriented. Another possibility is that the basement structure hypothesized in the Nelson Creek area (figure 2.44, 5.1), and an already uplifted Oweegee Dome, hindered the development of D1 structures. It is likely that the structure at Oweegee Dome existed in some form prior to deformation given the relatively low thickness of deep water facies along the east side of the dome (Evenchick et al., 2004), compared to elsewhere in the Bowser Basin. Such a structure controlling absence of D1 structures between the southwestern fold belt and the Eskay Creek-Teigen Lake areas (figure 1.4, 5.1) would have a length of up to 100 km.

Preliminary whole-rock Ar-Ar geochronology of siltstone collected in the Iskut ridge area (figure 1.4) with strong S1 cleavage produced an age of 146.0±1.7 Ma (Tithonian Late Jurassic, Gradstein et al., 2004). Samples associated with S2 cleavage produced ages of 128.86±0.82 and 129.16±0.87 Ma (Early Cretaceous Barremian,

Gradstein et al., 2004). Interpretations derived from Ar-Ar geochronology are based on a small data set that ultimately needs to be expanded. These ages indicate that D1 deformation was occurring in the latest Jurassic and that if a time lapse occurred between D1 and D2 deformation, it was no longer than ~15 my. Given that strata of the fluvial Jenkins Creek, Devil's Claw and possibly other assemblages of the Bowser Lake Group were deposited in the late Early Cretaceous (figure 1.2), early deformation in the west must then have been coeval with late sedimentation of the Bowser Lake Group towards the east. This is consistent with interpretation of the Devil's claw assemblage as having formed in 'piggy-back' basins (Evenchick and Thorkelson, 2005), and suggests the progressive shallowing of facies in the Bowser Lake Group was at least in part controlled by uplift related to formation of the fold belt. Some of the basin was then cannibalized during D2 deformation (figure 5.2) following coeval deposition during D1 (figure 5.3). The interpretation above requires that deposition was completed in areas with F1 folds prior to the earliest Cretaceous, which can be verified through fossil identification. Generally fossils with Jurassic lower age limits are present in these areas (Evenchick et al., 2001). Where this is not the case the fossil age appears questionable, such as near Eskay Creek where in two locations a Valanginian (Early Cretaceous) fossil is surrounded by Middle Jurassic fossils. This site is also within the Salmon River Formation, which is considered to have an upper age limit in the Bajocian (Middle Jurassic) (Evenchick et al., 2001). The data set supporting the ages derived from Ar-Ar geochronology is admittedly small and not statistically robust, but does provide a basis for hypotheses described above.

5.4 D2 Structures (Early to Late Cretaceous)

In all areas examined in this study, F2 folds with generally northwest trends were identified. These structures overprint D1 structures where present. Folds have variable forms, typically with tightness ranging from gentle to tight, and chevron to subrounded shapes. Folds are associated with thrust faults and sporadically developed spaced

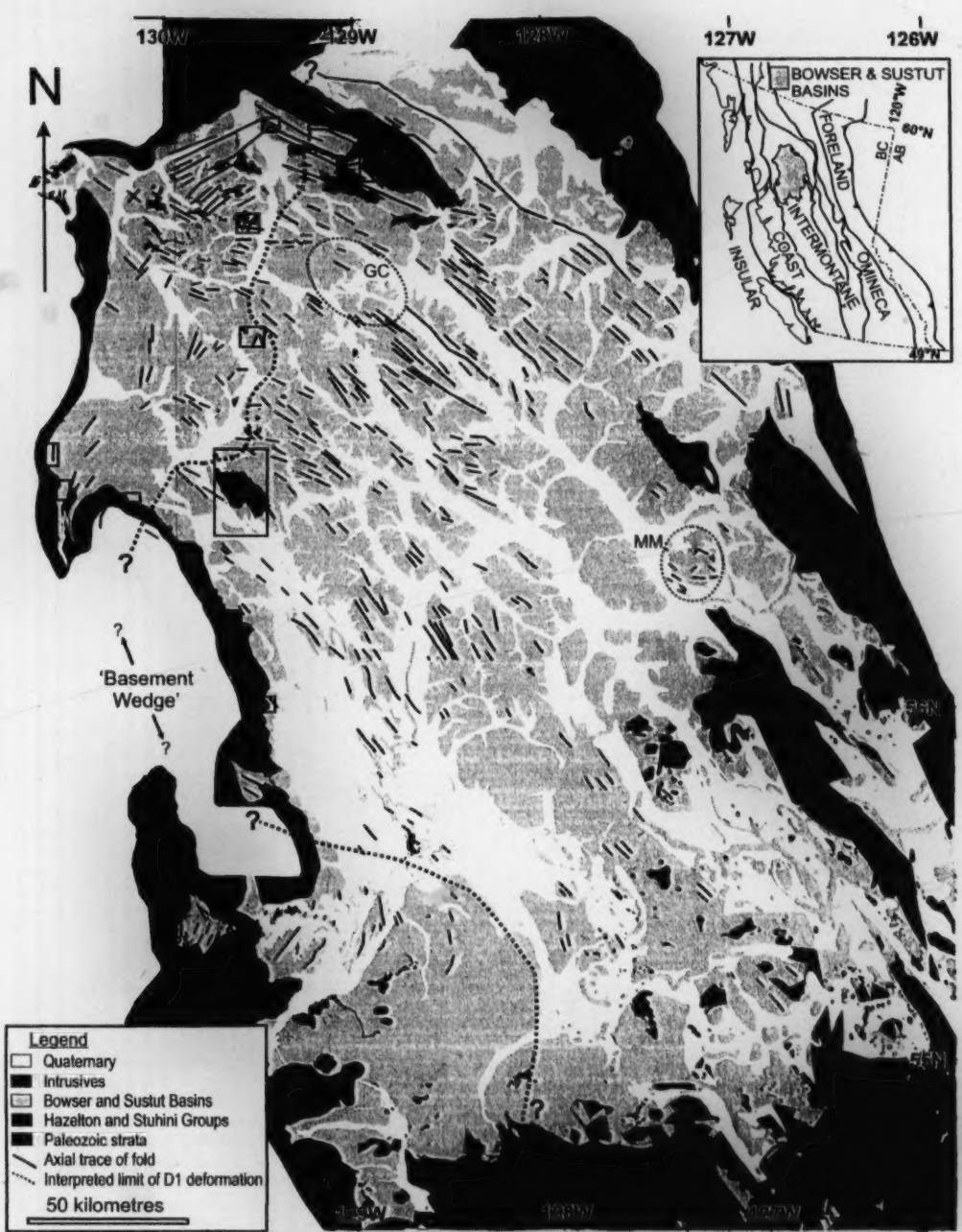

Figure 5.1: Simplifed geological map of the Bowser Basin modified after Evenchick et al. (2006) indicating interpreted limits of D1 deformation (west of dashed line), associated primarily with NE-trending folds. As discussed in text, similarly oriented folds beyond these limits (dashed circles), such as those noted by Moffat (1985) and McMechan (2007) are speculated to have formed primarily due to basement heterogeneity and reactivation. GC=Groundhog Coalfield, MM=Mosque Mountain. 'Basement wedge' refers to hypothesized structure that may have inhibited formation of D1 structures. Boxes outline study areas which are named in figure 1.4. Inset: Location within the Canadian Cordillera after Wheeler et al., (1991); Evenchick et al. (2002).

pressure-solution cleavage. In several areas, *en echelon* arrays were identified that are interpreted to have formed during D2 deformation. In one area (Mount Will) steep brittle faults have shortening directions consistent with development during F2 folding. These brittle structures, as well as lesser development of S2 cleavage relative to S1, suggest that conditions of D2 deformation were more brittle than D1.

D2 structures also vary spatially. Cleavage is most strongly developed in the western areas while fold wavelength and amplitude generally increase eastward. Part of this variability may be attributed to varied rock competence. Turbidites preferentially exposed in the west show more cleavage development then deltaic assemblages higher-up section, which are predominantly exposed in the centre of the basin.

In one area (Nelson Creek) D2 structures with clear SW vergence were identified. This contrasts with NE vergence of D2 structures elsewhere in the fold belt identified in this study and by Evenchick (1991a). Figure 5.2 is a schematic cross-section through the fold belt from north of Bowser Lake to the Mount Will area, constructed by extrapolating the relationships at Nelson Creek along strike to the northwest. SW-vergent structures are inferred to result from tectonic wedging (figure 2.44). This interpretation invokes a 'switch-over' to NE vergence at a location west of Oweegee Dome which corresponds to the tip-line of the hypothetical basement wedge (figure 5.2). Multiple stacked thrust sheets at Oweegee Dome serve to bring older strata near to the surface. The rise of basement near the Mount Will area is inferred in part to account for surface exposure of Hazelton Group strata and in part to mimic the eastern depositional edge of the Bowser Basin.

5.5 D3 Structures (Paleogene?)

In the Cartmel Lake area in the north of the fold belt a D3 generation of structures was identified. This consists of brittle NW and NE striking strike-slip or slightly oblique-slip faults, consistent with developing in a strain regime of N-S shortening and E-W extension as discussed in Chapter 3. These faults postdate local F2 folds. Joints in

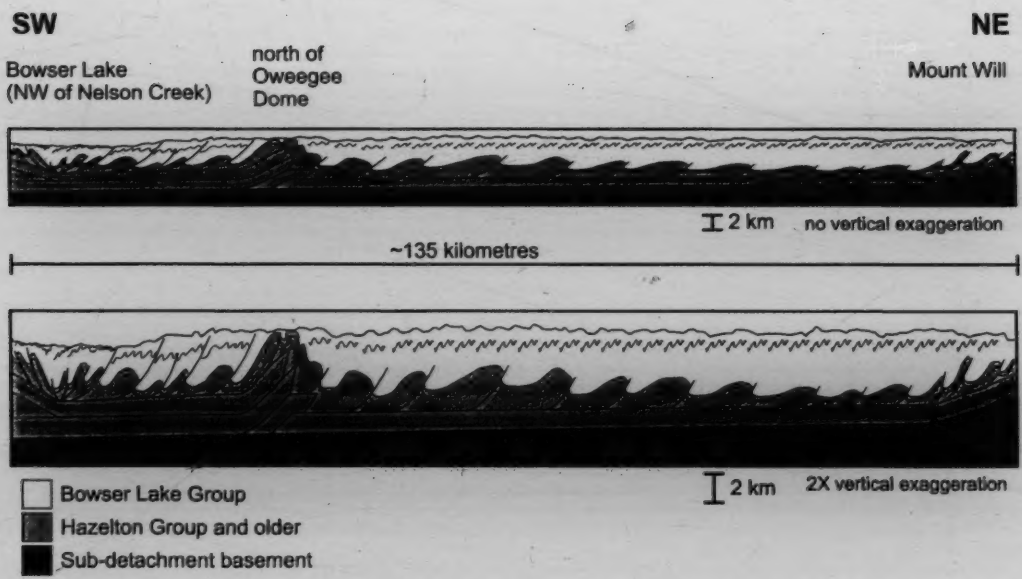

Figure 5.2: Schematic cross-section from northwest of Nelson Creek to the Mount Will area emphasizing D2 structures. Upper section has no vertical exaggeration, lower section is identical section with 2X vertical exaggeration applied. Thickness of Bowser Lake Group strata approximated from Lowe et al. (2006). Topography is schematic, dotted lines illustrate folds. Dark-shaded region is interpreted basement below a décollement below the Hazelton Group, light grey is overlying strata excluding the Bowser Lake Group shown in white).

the Maitland plateau area are also consistent with development during N-S shortening, and may be correlative. The relationship of D3 structures with dip-slip faults in the northeast of the fold belt, described in Chapter 3 and Evenchick and Thorkelson (2005), is unknown. It seems likely D3 faults are correlative with Eocene faults with dextral strike-slip components within the fold belt, (Forrest-Kerr Fault, Logan et al., 2000; figure 1.3) and elsewhere in the Cordillera (Gabrielse, 1985; Price and Carmichael, 1986; Price, 1994; Gabrielse et al., 2006).

5.6 Tectonic Synthesis

5.6.1 Models developed within the Skeena Fold Belt

Various models for development of structures in the Skeena Fold Belt have been proposed, as outlined in Chapter 1. Moffat (1985) proposed a model involving deformation of the Stikine terrane as it moved north relative to North America.

McMechan (2007) suggested basement reactivation developed transverse structure in the Mosque Mountain area. Evenchick (2001) proposed early folds formed during sinistral transpression while later folds formed due to convergence of an orogenic wedge in the Coast Belt. This synthesis seeks to test these models using the observations outlined in the previous chapters and explore alternative explanations for structures in the fold belt using relationships described elsewhere in the Cordillera.

The model of basement reactivation proposed for development of transverse structure in the Mosque Mountain area (McMechan, 2007) can be considered a local explanation given the area's complete separation from other structures in the fold belt with similar configuration. It also seems unlikely that basement reactivation occurred at a scale sufficient to account for the entire domain of NE-trending folds along the west of the fold belt.

The model proposed by Moffat (1985) and discussed in Chapter 1 suggests that northward displacement of the Stikine terrane speculated during the Early Cretaceous resulted in early NW-trending folds and that subsequent restriction of this displacement by bends in dextral strike-slip faults resulted in a switch of maximum paleostresses to produce NE-trending folds. Part of the justification for this inferred 'restriction' is assumed contemporaneous thrusting of the King Salmon Fault. However, later studies have shown that exhumation of the Cache Creek Group (which in part borders the King Salmon Fault) was completed during the early Middle Jurassic (Mihalynuk et al., 2004) and that detritus from Cache Creek was shed into the Bowser Basin following exhumation (Ricketts et al., 1992). These timings are strongly at odds with those suggested by Moffat (1985), refuting that aspect of the model. Also in question is the number of NE-trending folds presented by Moffat (1985). Subsequent maps of the Groundhog Coalfield (figure 1.4) area display a much reduced abundance of NE-trending folds (Evenchick, 2004a, b; Evenchick and Green, 2004b; Evenchick and Thorkelson, 2004a; Evenchick et al., 2006), leading to uncertainty regarding their importance in

this area in terms of amount of shortening. The relative timing of structures presented by Moffat (1985) is also at odds with that of this thesis. It is possible the D2 structures discussed by Moffat (1985) developed due to reactivation of early formed structures, leading to timing relationships that appear to conflict with this study. Another possibility is that a form of basement reactivation, possibly similar to that described for the Mosque Mountain area by McMechan (2007) is also applicable to the Groundhog Coalfield area. Large aeromagnetic anomalies described by Lowe et al. (2006) beneath the Groundhog Coalfield have been attributed to buried plutons (Evenchick et al., 2002; Lowe et al., 2004, 2006). Emplacement of these plutons may have been facilitated by activation of basement structures that potentially generated transverse structures in the overlying strata.

The general requirements of the model prepared by Evenchick (2001) are:

1. NE-trending structures formed prior to NW-trending structures. Evidence for this provided by Evenchick (2001) is tenuous; two out of three sub-domains of NE-trending folds examined proved inconclusive in terms of fold timing, while one area in the southwest contains early NE-trending folds that are transected by N-striking cleavage.
2. Validity of plate-motion reconstructions by Engebretson et al. (1985) which are described in Chapter 1, and occurrence of D1 and D2 deformation within the appropriate time intervals;
3. D1 deformation occurred in a sinistral transpressive setting (i.e. included a component of sinistral strike-slip strain);
4. D2 deformation was driven by an orogenic wedge developed in the Coast Belt.

As discussed above and in Chapter 2, the results of this thesis have shown that NE-trending folds consistently formed first while NW-trending folds formed second. This supports the basic premise of Evenchick's (2001) model. Regarding plate-motion reconstructions, Engebretson et al. (1985) interpret sinistral-oblique convergence of the Farallon Plate relative to the North American margin for the 135-145 Ma interval.

During the 100-115 Ma interval the sense of motion between the plates is dextral-oblique convergence, becoming progressively more convergent by 65 Ma following rifting and eventual disappearance of the Kula Plate. If D1 structures in the fold belt result from sinistral convergence, then most structures would be expected to have formed prior to 115 Ma. Ar-Ar dates collected in this study support this prediction, with an S1 date of ~146 Ma and S2 dates of ~129 Ma. It is likely that these exact dates do not hold for all areas of the fold belt, as deformation appears diachronous and prolonged; however they do provide a framework to interpret timing of deformation that can be extrapolated elsewhere. It is also possible that transverse structures also formed at later times through re-activation of early-formed structures, accounting for structural domains with apparently contradictory sequences of development (Bone, 2002). The third aspect of the model proposed by Evenchick (2001) predicts that major margin-parallel sinistral faults, comtemporaneous with F1 folds, developed along the west of the fold belt. This study did not find clear evidence of such structures, neither refuting nor supporting that aspect of the model.

Evenchick (1991a, b, 2001) speculated that the Skeena Fold Belt developed in response to eastward-propagating detachment faults rooted in the Coast Belt that were subsequently destroyed by intrusion of the Coast Plutonic Complex. However, west of the Coast Plutonic Complex there may be a record of deformation equivalent to the Skeena Fold Belt in the form of an extensive (>1200 km strike length) belt of W and SW-vergent structures known as the Coast Belt Thrust System (CBTS) (figure 5.3) (Rubin et al., 1990; Rusmore and Woodsworth, 1991; Journeay and Friedman, 1993). The CBTS stretches along the southwest British Columbia coast from near the American border to the latitude of the southern Bowser Basin. Structures within the CBTS include strong NE-dipping foliation, and overturned W and SW-vergent folds. Rare outcrops and doubly-plunging folds inferred from stereographic projections display Type I fold interference (Klepeis et al., 1998). Interpreted ages of structures forming the CBTS vary

by author, but can generally be bracketed between 100 and 85 Ma, and possibly older (Rubin et al., 1990; Journeay and Friedman, 1993; Klepeis et al., 1998). The eastern Coast Mountains include NE-vergent thrusts that developed in the Late Cretaceous (Rusmore et al., 2000). P-T paths of kyanite and staurolite schists identified on imbricate thrust sheets within the CBTS reach pressures as high as ~8 kbars, corresponding to ~30 km burial depth (Crawford et al., 1987, Cook et al., 1991). In contrast, burial depths in the Bowser Lake Group are less than 10 km, making lateral correlations between the two belts difficult. The Coast Shear Zone (CSZ) generally bounds the east side of the CBTS and is a major regional feature (figure 1.3). Complex and variable kinematic indicators have confused interpretation of the CSZ such that it and other similar structures in the eastern Coast Belt are variably interpreted as accommodating major components of contraction, transpression and/or strike-slip motion, and dip-slip motion (Klepeis et al., 1998; Andronicos et al., 1999; McClelland and Mattinson, 2000; Rusmore et al., 2000). It has also been postulated as a possible location for the "Baja BC Fault" which is discussed below. Klepeis et al. (1998) interpreted two phases of deformation along the CSZ, the first as east-side-up, top-to-the southwest displacement occurring between 65 and 57 Ma. Kinematic indicators interpreted to show overall dextral-transpression east of the CSZ (Andronicos et al., 1999) may be accounted for in this first phase of movement. The second phase of movement of the CSZ involves west-side-up displacement from ~57 to 55 Ma (Klepeis et al., 1998) that would have at least in part uplifted the CBTS to present structural levels. The interval of development of the CBTS is in part compatible with that of the Skeena Fold Belt postulated by this study and others (Eisbacher, 1974b; Evenchick, 1991a, 2001; Logan et al., 2000).

Figure 5.3 is a schematic diagram that examines the linkage of the Coast Belt with deformation in the Skeena Fold Belt suggested by Evenchick (1991a, b) by comparing temporal development and the general characteristics outlined above. 'Stage 3' illustrates the present configuration of the fold belt relative to the CBTS. Stages 1 and

2 illustrate how Skeena Fold Belt development through time can be linked with stages of development of the CBTS. In this model, NE-trending folds and early NW-trending folds, including SW-vergent structures at Nelson Creek (figure 5.2) are interpreted to develop during 'stage 1'. Type I fold interference in the CBTS (Klepeis et al., 1998) supports the occurrence of two fold events during this period. Dextral transpression in stage 2 is inferred to build upon NE-vergent structures developed in stage 1 and continue through the remainder of the Late Cretaceous. This accounts for deformation of Maastrichtian (Upper Cretaceous) strata of the Sustut Group. Later dip-slip movement along the CSZ and other structures served to exhume the Coast Belt to its present level (stage 3). These structures have variably been obscured by plutonic activity during and after stage 2.

5.6.2 Baja BC Hypothesis

The "Baja BC hypothesis" for development of the western Canadian Cordillera has several implications for this study. This theory (summarized by Cowan et al., 1997) suggests that >1500 km of dextral strike-slip displacement occurred between ~90 and 70 Ma along the western North American margin, bringing north large fault-bounded blocks exotic to Canadian latitudes. This theory is based primarily on paleomagnetic evidence (e.g. Beck, 1991; Irving et al.,1995; Wynne et al., 1995), and paleofaunal studies and plutonic 'piercing points.' (Keppie and Dostal, 2001). In attempting to test this model, Cowan et al. (1997) hypothesized that the "Baja BC fault" would generally have to strike N to NW, accommodate large magnitudes of dextral strike-slip motion from 90 to 70 Ma and lie in the Coast Mountains. Rusmore et al. (2000) examined a seemingly continuous thrust belt in the southern Coast Mountains (Mt. Waddington thrust belt) located between two paleomagnetic sites separated by ~200 km that suggest 1200 km of dextral translation. They concluded that, provided their own stratigraphic and structural correlations were correct, any significant fault would have to pass east of this belt and therefore through the Stikine terrane. The stratigraphic continuity and integrity of the

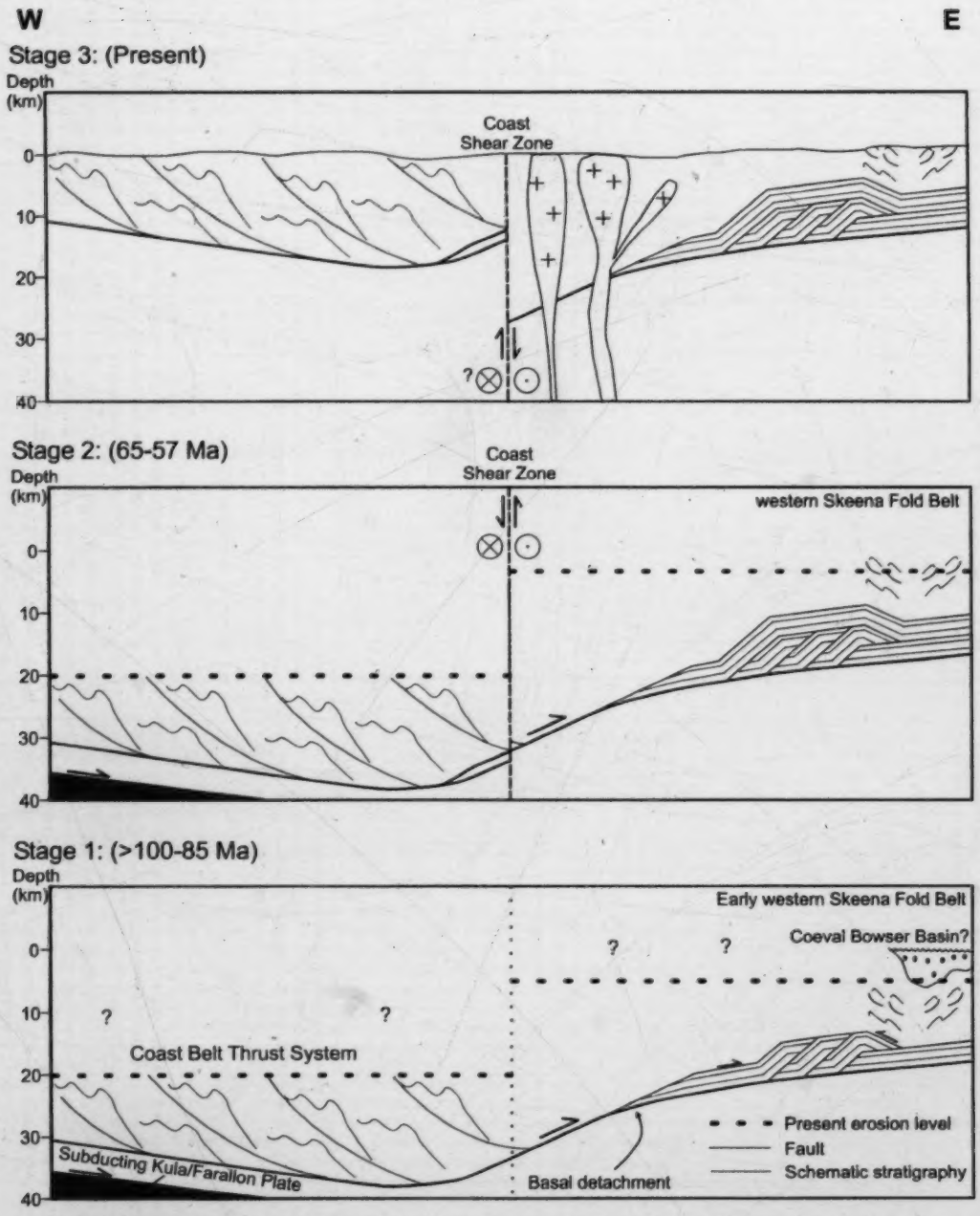

Figure 5.3: Cartoon depicting possible relationships between the Coast Belt and Skeena Fold Belt. Stage 1: Development of the Coast Belt Thrust System from >100 Ma to 85 Ma in response to subduction of the Kula-Farallon plate and early development of fold belt; Stage 2: Continued development of fold belt during east-side up dextral movement along the Coast Shear Zone (CSZ); Stage 3: present configuration of respective features, following west-side up displacement of CSZ and emplacement of Tertiary plutons. Duplex style of western fold belt modelled after Boyer and Elliott (1982) to account for west-vergent structures. Aspects of model compiled from Evenchick (1991a), Klepeis et al., (1998) and McClelland and Mattinson (2000). Stratigraphic lines illustrate folds, not specific stratigraphic units. Not to scale.

geology of the Stikine terrane from E-W, including the stratigraphy of the Bowser Lake Group (Evenchick et al., 2006), structural style and timing of structures shown by this study and Evenchick (1991a, 2001, Evenchick et al., 2006), and positions of older strata including those forming the Stikine and Skeena arches (figure 1.3), make the likelihood of a Baja BC fault cutting through this region doubtful.

The CSZ has also been postulated as a possible location for this fault but intervals of dip-slip movement discussed earlier limit possible time frames for motion. Significant magnitudes (40-50 km, possibly 180 km, Israel et al., 2006) of sinistral deformation also occurred on shear zones in the southern Coast Belt prior to 89 Ma; this requires that 'Baja BC' type dextral deformation was immediately preceeded by sinistral deformation. The model for Skeena Fold Belt development examined in figure 5.3 suggests west-vergent thrusts in the Coast Belt were linked with the fold belt. Acceptance of this model requires 'Baja BC' type displacements to be relatively small so as to allow the CBTS, or a geometrically and temporally similar deformation belt, to remain west of the fold belt.

5.6.3 Terrane Rotation

One of the few paleomagnetic studies that does not generally support the 'Baja BC' hypothesis for units of the Intermontane belt suggested that inclinations of paleopoles are likely to have been shallowed by a number of factors including remagnetization, sedimentary compaction and failure to account for rotation when calculating paleo-inclination values (Symons et al., 2005). This study also found that large (~51°) clockwise rotation of the Intermontane belt has occurred since 102 Ma with less northward translation (8.3°±7.0°) (figure 5.4) than suggested by other paleomagnetic studies described previously. It was also suggested that rotation of this type has occurred since ~215 Ma, although the data is poorly constrained for this older interval. Given the time frame allotted, it is possible that F1 folds in the Skeena Fold Belt may have been generated during clockwise vertical axis rotation and resulting collision of Stikine terrane with a landmass outboard at that time (or possibly the North American margin). There

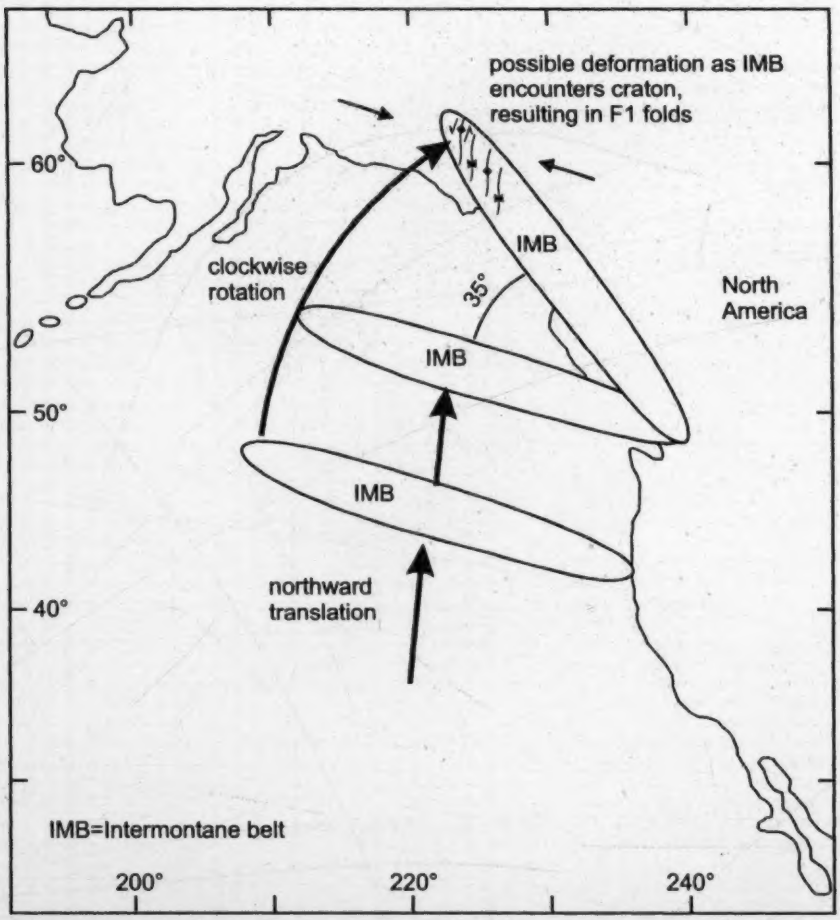

Figure 5.4: Schematic diagram illustrating northward translation and clockwise rotation of the Intermontane belt, modified after Symons et al. (2005). Diagram shows interpreted movement of belt between ~98 and ~83 Ma. Folds drawn schematically represent F1 (NE-trending) folds from this study that may have formed due to rotation and abutment against the North American margin as discussed in text. This process may be expected to be coupled with sinistral shear along the edges of the Intermontane belt assuming some frictional resistance to rotation. Continued rotation may have rotated folds into their present position.

is strong evidence in the form of consistent southwest-directed paleocurrents (Eisbacher, 1974a; Green, 1992; Evenchick and Thorkelson, 2005) demonstrating that block rotation was not a strong factor affecting deformation *within* the fold belt, a scenario evaluated by Evenchick (2001) and discussed in Chapter 1. However, that evidence does not preclude rotation of the Bowser Basin (and therefore fold belt) as a whole. In this scenario one would conclude that early 'rotation-generated' F1 folds were overprinted by F2 folds that

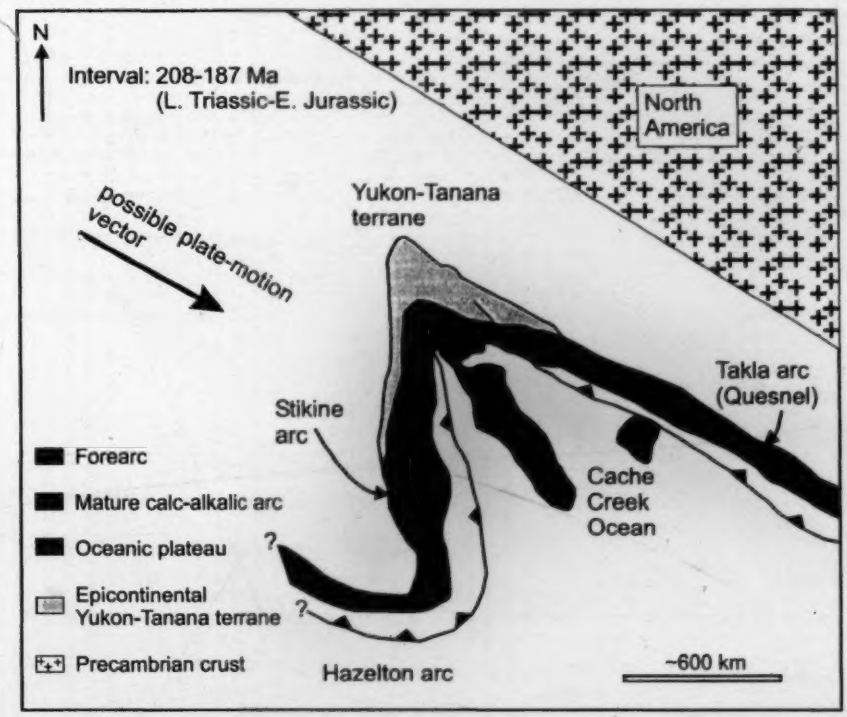

Figure 5.5: Schematic diagram of hypothesized orocline development after Nelson and Mihalynuk (1993). Interval (208-187 Ma) is during closure and tightening of orocline resulting in isolation of Cache Creek Ocean. In this model the Stikine and Quesnel arcs are inferred to have been originally contiguous. The possible plate-motion indicated is interpreted to be necessary to tighten the arc. Extrapolation of that vector to the Early Cretaceous suggests this process may have been related to early NE-trending folds as discussed in text.

developed either as rotation continued or due to convergence of the Coast Mountains orogen. It is also likely that folds would have developed non-coaxially in this scenario, possibly with strong components of sinistral shear; evidence for this is lacking. Also, faults that would have accommodated this rotation are not known. The correlation of F1 folds in the NW fold belt with those in the SW fold belt also does not support this mechanism as it would be expected that folds generated from rotation of the underlying rocks would develop at the 'corners' of the rotating block rather than down the length of the fold belt. Although a block-rotation mechanism for fold generation does not seem likely, it cannot be explicitly ruled out.

The Stikine terrane lies outboard of the Cache Creek Complex (figure 1.3), which

in turn is west of the Quesnel arc (Wheeler et al., 1991). The Stikine terrane has been speculated to have previously situated in a position 120° clockwise from its current position (Nelson and Mihalynuk, 1993). This theory suggests it developed as a volcanic arc continuous and coeval with the Quesnel arc, and was rotated into its present position through oroclinal enclosure following indentation of the Cache Creek terrane (figure 5.5) (Nelson and Mihalynuk, 1993; Mihalynuk et al., 1994; Colpron et al., 2007). The appeal of this model is that it explains exotic fauna within Cache Creek, coeval and similar volcanism in the Stikine and Quesnel arcs, and the difficulty distinguishing the base of these arcs from Yukon-Tanana terrane at their northern limits. Ultimately this model requires additional plate interactions besides the indentation of Cache Creek to facilitate closure of the orocline (Nelson and Mihalynuk, 1993). At its late stages this would likely include a southeast-directed plate-motion vector (figure 5.5). If this vector continued during sedimentation and later deformation of the Bowser Lake Group, the deformation associated with this plate interaction could potentially explain NE-trending folds in the Skeena Fold Belt. This would also suggest that the Yukon-Tanana terrane, not a Coast Belt orogenic wedge as discussed earlier, was the main driver of deformation. This model predicts 120° counterclockwise rotation of the Stikine terrane throughout its evolution. This sense of rotation is supported by some paleomagnetic studies (e.g., Irving and Wynne, 1990; Vandall and Palmer, 1990), but not others that describe clockwise rotation of Stikine terrane throughout its Mesozoic history (e.g., Symons et al., 2005).

5.6.4 Summary

In summary, although other mechanisms described above may have resulted in development of some structures in the Skeena Fold Belt, the model proposed by Evenchick (2001) appears to be the most adept at explaining its evolution. The lack of evidence for early sinistral structures and clear linkage with the Coast Belt represent the most fundamental unanswered questions of Evenchick's model. Based on appropriate timing, both relative and absolute, and a reasonable mechanism, at this time

the fundamental aspects of Evenchick's model appear to best represent the kinematic evolution of the fold belt. The improved understanding of the structure of the fold belt and the spatial variation of respective deformations provided by this study may potentially benefit hydrocarbon exploration within the region.

5.7 Conclusions

1. Folds and associated D1 structures that trend to the NE formed early, likely over a relatively short time interval, while NW-trending D2 structures formed later over an extended time period.
2. Structures formed during D2 deformation generally have a more brittle character than D1 structures. This may indicate early denudation of the Bowser Basin resulting in more brittle conditions during D2 deformation.
3. A minor brittle deformation is recognized in the form of NW- and NE-striking predominantly strike-slip faults. This may correlate with Eocene dextral motion along strike-slip faults elsewhere in the Cordillera.
4. Cleavage can be clearly shown to have formed through pressure solution processes.
5. Application of ^{40}Ar-^{39}Ar geochronology methods to the most strongly deformed rocks along the western Bowser Basin yields limited but promising results; mineral separations may provide more statistically robust dates. An age of 146 Ma was obtained from a rock with strong S1 cleavage while ages of ~129 Ma were obtained from rocks with S2 cleavage.
6. Development of the Skeena Fold Belt may have begun as early as the latest Jurassic, and was more convincingly active by the Early Cretaceous Barremian. Given that deformation continued into the latest Cretaceous, this indicates a long, protracted and possibly intermittent history for the Skeena Fold Belt spanning roughly 60-80 my.

References

Alldrick, D.J., 1993. Geology and Metallogeny of the Stewart Mining Camp, Northwestern British Columbia, Bulletin 85. BC Ministry of Energy, Mines, and Petroleum Resources, 105 pp.

Alldrick, D.J., Nelson, J.L. and Barresi, T., 2005. Geology and Mineral Occurrences of the Upper Iskut River area: Tracking the Eskay Rift through Northern British Columbia. British Columbia Ministry of Energy and Mines, Geological Fieldwork 2004, Paper 2005-1: 1-30.

Allmendinger, R.W., 1989. Notes on Fault Slip Analysis, Prepared for the Geological Society of America Short Course on "Quantitative Interpretation of Joints and Faults". Cornell University, pp. 56.

Allmendinger, R.W., 2001. FaultKinWin 1.2.2. http://www.geo.cornell.edu./geology/faculty/RWA/programs.html.

Anderson, R.G., 1989. A stratigraphic, plutonic, and structural framework for the Iskut River map area, northwestern British Columbia. Current Research Part E, Geological Survey of Canada, Paper 89-1E: 145-154.

Anderson, R.G., 1993. A mesozoic stratigraphic and pluton framework for northwestern Stikinia (Iskut River area), northwestern British Columbia, Canada. In: G. Dunn and K. McDougall (Editors), Mesozoic Paleogeography of the Western United States-II. Pacific Section SEPM, Book 71, pp. 477-494.

Anderson, R.G. and Thorkelson, D.J., 1990. Mesozoic stratigraphy and setting for some mineral deposits in Iskut River map area, northwestern British Columbia. Current Research, Geological Survey of Canada, Paper 90-1F: 131-139.

Andronicos, C., Hollister, L.S., Davidson, C. and Chardon, D., 1999. Kinematics and tectonic significance of transpressive structures within the Coast Plutonic Complex, British Columbia. Journal of Structural Geology, 21: 229-243.

Angelier, J., 1979. Determination of the mean principal directions of stresses for a given fault population. Tectonophysics, 56: T17-T26.

Angelier, J., 1984. Tectonic analysis of fault slip data sets. Journal of Geophysical Research, 89: 5835-5848.

Beach, A., 1975. The geometry of *en-echelon* vein arrays. Tectonophysics, 28: 245-263.

Beck, M.E., 1991. Case for northward transport of Baja and coastal southern California: Paleomagnetic data, analysis, and alternatives. Geology, 19: 506-509.

Becker, A. and Gross, M.R., 1999. Sigmoidal wall-rock fragments: application to the origin, geometry and kinematics of *en echelon* vein arrays. Journal of Structural Geology, 21: 703-710.

Berthe, D., Choukroune, P., and Jegouzo, P., 1979, Orthogneiss, mylonite and non coaxial deformation of granites; the example of South Armorican shear zone: Journal of Structural Geology, v. 1, p. 31-42.

Bone, K.E., 2002. Relative Timing and Significance of Folding in the Western Skeena Fold Belt, Northwestern Bowser Basin, British Columbia: Interpretation of Structural and Seismic Reflection Data, M. Sc. Thesis, University of British Columbia, Vancouver, 171 pp.

Borradaile, G.J., 1978. Transected folds: A study illustrated with examples from Canada and Scotland. Geological Society of America Bulletin, 89: 481-493.

Boyer, S.E. and Elliott, D., 1982. Thrust Systems. AAPG Bulletin, 66: 1196-1230.

Brown, D.A. and Greig, C.J., 1990. Geology of the Stikine River - Yehiniko Lake area, northwestern British Columbia (104G/11W, 12E). Geological Fieldwork 1989, British Columbia Ministry of Energy, Mines and Petroleum Resources Paper 1990-1: 141-151.

Brown, D.A., Harvey-Kelly, F.E.L., Neill, I. and Timmerman, J., 1992. Geology of the Chutine River

- Talhtan Lake area, northwestern British Columbia (104G/12W, 13). Geological Fieldwork 1991, British Columbia Ministry of Energy, Mines and Petroleum Resources Paper 1992-1: 179-195.

Bustin, R.M. and Moffat, I.W., 1989. Semianthracite, anthracite and meta-anthracite in the central Canadian Cordillera: their geology, characteristics and coalification history. In: P.C. Lyons and B. Alpern (Editors), Coal: Classification, Coalification, Mineralogy, Trace-element Chemistry, and Oil and Gas Potential. International Journal of Coal Geology. Elsevier Science, pp. 303-326.

Cladouhos, T.T. and Allmendinger, R.W., 1993. Finite strain and rotation from fault-slip data. Journal of Structural Geology, 15: 771-784.

Colpron, M., Nelson, J.L. and Murphy, D.C., 2006. A tectonostratigraphic framework for the pericratonic terranes of the northern Cordillera. In: M. Colpron and J.L. Nelson (Editors), Paleozoic Evolution and Metallogeny of Pericratonic Terranes at the Ancient Pacific Margin of North America, Canadian and Alaskan Cordillera. Geological Association of Canada, Special Paper 45, pp. 1-23.

Colpron, M., Nelson, J.L. and Murphy, D.C., 2007. Northern Cordilleran terranes and their interactions through time. GSA Today, 17: 4-10.

Cook, R.D., Crawford, M.L., Omar, G.I. and Crawford, W.A., 1991. Magmatism and deformation, southern Revillagigedo Island, southeastern Alaska. Geological Society of America Bulletin, 103: 829-841.

Cowan, D.S., Brandon, M.T. and Garver, J.I., 1997. Geologic tests of hypotheses for large coastwise displacements - A critique illustrated by the Baja British Columbia controversy. American Journal of Science, 297: 117-173.

Crawford, M.L., Hollister, L.S. and Woodsworth, G.J., 1987. Crustal deformation and regional metamorphism across a terrane boundary, Coast Plutonic Complex, British Columbia. Tectonics, 6: 343-361.

Currie, L.D. and Parrish, R.R., 1993. Jurassic accretion of Nisling terrane along the western margin of Stikinia, Coast Mountains, northwestern British Columbia. Geology, 21: 235-238.

Davis, D., Suppe, J. and Dahlen, F.A., 1983. Mechanics of Fold-and-Thrust Belts and Accretionary Wedges. Journal of Geophysical Research, 88: 1153-1172.

Dott, R.H., 1964. Wacke, Graywacke and Matrix - What Approach to Immature Sandstone Classification? Journal of Sedimentary Petrology, 34: 625-632.

Durney, D.W. and Ramsay, J.G., 1973. Incremental Strains Measured by Syntectonic Crystal Growths. In: K.A. De Jong and R. Scholten (Editors), Gravity and Tectonics. Wiley & Sons, New York, pp. 67-96.

Eisbacher, G.H., 1974a. Deltaic sedimentation in the northeastern Bowser Basin, British Columbia, Paper 73-33. Geological Survey of Canada, 13 pp.

Eisbacher, G.H., 1974b. Sedimentary history and tectonic evolution of the Sustut and Sifton Basins, north-central British Columbia, Paper 73-31. Geological Survey of Canada, 57 pp.

Engebretson, D.C., Cox, A. and Gordon, R.G., 1985. Relative motions between oceanic and continental plates in the Pacific Basin, Special Paper 206. Geological Society of America, Boulder, Colorado, 59 pp.

Engelder, T. and Marshak, S., 1985. Disjunctive cleavage formed at shallow depths in sedimentary rocks. Journal of Structural Geology, 7: 327-343.

Evenchick, C.A., 1987. Stratigraphy and structure of the northeast margin of the Bowser Basin, Spatsizi map area, north-central British Columbia. Current Research Part A, Paper 87-1A: 719-726.

Evenchick, C.A., 1991a. Geometry, evolution, and tectonic framework of the Skeena Fold Belt, north central British Columbia: Tectonics, v. 10, p. 527-546.

Evenchick, C.A., 1991b. Structural relationships of the Skeena Fold Belt west of the Bowser Basin, northwest British Columbia. Canadian Journal of Earth Sciences, 28: 973-983.

Evenchick, C.A., 1991c. The Skeena Fold Belt: a link between the Coast Plutonic Complex, the Omineca belt and the Rocky Mountain fold and thrust belt. In: K.R. McClay (Editor), Thrust tectonics. Chapman & Hall, London, pp. 365-376.

Evenchick, C.A., 2001. Northeast-trending folds in the western Skeena Fold Belt, northern Canadian Cordillera: a record of Early Cretaceous sinistral plate convergence. Journal of Structural Geology, 23: 1123-1140.

Evenchick, C.A., 2004a. Geology, Sweeny Creek, British Columbia, Map 2037A, Geological Survey of Canada, scale 1:50,000.

Evenchick, C.A., 2004b. Geology, Tahtsedle Creek, Map 2038A. Geological Survey of Canada, scale 1:50,000.

Evenchick, C.A., and Green, G.M., 2004a. Geology, Eaglenest Creek, British Columbia, Map 2029A, Geological Survey of Canada, scale 1:50,000.

Evenchick, C.A. and Green, G.M., 2004b. Geology, Little Klappan River, Map 2034A. Geological Survey of Canada, scale 1:50,000.

Evenchick, C.A., and Green, G.M., 2004c. Geology, Maitland Creek, British Columbia, Map 2035A, Geological Survey of Canada, scale 1:50,000.

Evenchick, C.A. and Green, G.M., 2004d. Geology, Tumeka Creek, British Columbia, Map 2036A. Geological Survey of Canada, scale 1:50,000.

Evenchick, C.A., Hayes, M.C., Buddell, K.A. and Osadetz, K.G., 2002. Vitrinite and bitumen reflectance data and preliminary organic maturity model for the northern two-thirds of the Bowser and Sustut basins, north-central British Columbia, Geological Survey of Canada Open File 4343, BC Ministry of Mines Open File 2002-1. Geological Survey of Canada, 26 pp.

Evenchick, C.A., Mustard, P.S., Greig, C.J., Porter, J.S., and McNeill, P.D., 2000. Geology, Bowser Lake (104A), British Columbia, Open File Map 3918, Geological Survey of Canada, scale 1:250,000.

Evenchick, C.A., Mustard, P.S., Woodsworth, G.J. and Ferri, F., 2004. Compilation of geology of Bowser and Sustut basins draped on shaded relief map, north-central British Columbia, Open File 4638. Geological Survey of Canada, scale 1:500,000.

Evenchick, C.A., Mustard, P.S., McMechan, M., Ferri, F., Ritcey, D.H., Smith, G.T., 2006. Compilation of Geology of Bowser and Sustut Basins draped on shaded relief map, north-central British Columbia, Geological Survey of Canada, Open File 5313; BC Ministry of Energy, Mines and Petroleum Resources, Petroleum Geology Open File 2006-1. Geological Survey of Canada.

Evenchick, C.A., Poulton, T.P., Tipper, H.W. and Braidek, I.G., 2001. Fossils and facies of the northern two-thirds of the Bowser Basin; British Columbia, Geological Survey of Canada, Open File 3956. Geological Survey of Canada, scale 1:250,000.

Evenchick, C.A. and Thorkelson, D.J., 2004a. Geology, Buckinghorse Creek, Map 2033A. Geological Survey of Canada, scale 1:50,000.

Evenchick, C.A., and Thorkelson, D.J., 2004b. Geology, Cold Fish Lake, British Columbia, Map 2030A, Geological Survey of Canada, scale 1:50,000.

Evenchick, C.A. and Thorkelson, D.J., 2005. Geology of the Spatsizi River Map Area, North-central British Columbia. Geological Survey of Canada Bulletin, 577. Geological Survey of Canada, 276 pp.

Faure, G. and Mensing, T.M., 2005. Isotopes: Principles and Applications. 3rd edition. John Wiley & Sons, Hoboken, New Jersey, 897 pp.

Fleuty, M.J., 1964. The Description of Folds. Proceedings of the Geologists' Association, 75: 461-492.

Gabrielse, H., 1985. Major dextral transcurrent displacements along the Northern Rocky Mountain Trench and related lineaments in north-central British Columbia. Geological Society of America Bulletin, 96:

1-14.

Gabrielse, H., 1991. Late Paleozoic and Mesozoic terrane interactions in north-central British Columbia. Canadian Journal of Earth Sciences, 28: 947-957.

Gabrielse, H., 1998. Geology of Cry Lake and Dease Lake map areas, North-Central British Columbia, Bulletin 504. Geological Survey of Canada, 147 pp.

Gabrielse, H., Murphy, D.C. and Mortensen, J.K., 2006. Cretaceous and Cenozoic dextral orogen-parallel displacements, magmatism, and paleogeography, north-central Canadian Cordillera. In: J.W. Haggart, R.J. Enkin and J.W.H. Monger (Editors), Paleogeography of the North American Cordillera: Evidence For and Against Large-Scale Displacements. Geological Association of Canada, Special Paper 46, pp. 255-276.

Gagnon, J.-F., Loogman, W., Waldron, J.W.F., Cordey, F. and Evenchick, C.A., 2007. Stratigraphic record of initiation of sedimentation of the Bowser Basin (104A, H), northwest British Columbia. Geological Fieldwork 2006, Paper 2007-1 and Geoscience BC Report 2007-1: 275-284.

Gareau, S.A. and Woodsworth, G.J., 2000. Yukon-Tanana terrane in the Scotia-Quaal belt, Coast Plutonic Complex, central-western British Columbia. In: H.H. Stowell and W.C. McClelland (Editors), Tectonics of the Coast Mountains, Southeastern Alaska and British Columbia. Special Paper 343. Geological Society of America, Boulder, Colorado, pp. 23-43.

Gradstein, F.M., Ogg, J.G., and Smith, A.G., Agterberg, F.P., Bleeker, W., Cooper, R.A., Davydov, V., Gibbard, P., Hinnov, L.A., House, M.R., Lourens, L., Luterbacher, H.P., McArthur, J., Melchin, M.J., Robb, L.J., Shergold, J., Villeneuve, M., Wardlaw, B.R., Ali, J., Brinkhuis, H., Hilgen, F.J., Hooker, J., Howarth, R.J., Knoll, A.H., Laskar, J., Monechi, S., Plumb, K.A., Powell, J., Raffi, I., Röhl, U., Sadler, P., Sanfilippo, A., Schmitz, B., Shackleton, N.J., Shields, G.A., Strauss, H., Van Dam, J., van Kolfschoten, T., Veizer, J., and Wilson, D., 2004. A Geologic Time Scale. Cambridge University Press, 589 pp.

Green, G.M., 1992. Detailed sedimentology of the Bowser Lake Group, northern Bowser Basin, north-central British Columbia, M. Sc. Thesis, Carleton University, Ottawa, Ontario, 197 pp.

Greig, C.J., 1991. Stratigraphic and structural relations along the west-central margin of the Bowser Basin, Oweegee and Kinskuch areas, northwestern British Columbia. Current Research, Paper 91-1A: 197-205.

Greig, C.J., and Evenchick, C.A., 1993. Geology of Oweegee Dome (geochemistry and paleontology), Delta Peak (104A/12) and Taft Creek (104A/11W) map areas, northwestern British Columbia, Open File 2688, Geological Survey of Canada, scale 1:50 000.

Greig, C.J. and Gehrels, G.E., 1995. U-Pb zircon geochronology of Lower Jurassic and Paleozoic Stikinian strata and Tertiary intrusions, northwestern British Columbia. Canadian Journal of Earth Sciences, 32: 1155-1171.

Greig, C.J., McNicoll, V.J., Anderson, R.G., Daubeny, P.H., and Harakal, J.E., 1995. New K-Ar and U-Pb dates for the Cambria Icefield area, northwestern British Columbia: Current Research, v. 1995-A, p. 97-103.

Gunning, M.H., 1990. Stratigraphy of the Stikine assemblage, Scud River area, northwest British Columbia (104G/5, 6). Geological Fieldwork 1989, British Columbia Ministry of Energy, Mines and Petroleum Resources Paper 1990-1: 153-161.

Haggart, J.W., Woodsworth, G.J. and McNicoll, V.J., 2006. Uranium-lead geochronology of two intrusions in the southern Bowser Basin, British Columbia. Geological Survey of Canada, Current Research, 2006-F2: 6.

Hancock, P.L., 1972. The analysis of *en echelon* veins. Geological Magazine, 109: 269-276.

Hanes, J.A., 1991. K-Ar and $^{40}Ar/^{39}Ar$ Geochronology: Methods and Applications. In: L. Heaman and J.N.

Ludden (Editors), Mineralogical Association of Canada Short Course Handbook on Applications of Radiogenic Isotope Systems to Problems in Geology, Toronto, ON.

Irving, E., Thorkelson, D.J., Wheadon, P.M. and Enkin, R.J., 1995. Paleomagnetism of the Spences Bridge Group and northward displacement of the Intermontant Belt, British Columbia: A second look. Journal of Geophysical Research, 100: 6057-6071.

Irving, E. and Wynne, P.J., 1990. Paleomagnetic evidence bearing on the evolution of the Canadian Cordillera. Royal Society of London Philosophical Transactions, 331: 487-509.

Israel, S., Schiarizza, P., Kennedy, L., Friedman, M. and Villeneuve, M., 2006. Evidence for Early to Late Cretaceous sinistral deformation in the Tchaikazan River area, southwestern British Columbia: Implications for the tectonic evolution of the southern Coast belt. In: J.W. Haggart, R.J. Enkin and J.W.H. Monger (Editors), Paleogeography of the North American Cordillera: Evidence For and Against Large-Scale Displacements. Geological Association of Canada, pp. 331-350.

Johnston, J.D., 1993. Three-dimensional geometries of veins and their relationship to folds: examples from the Carboniferous of eastern Ireland. Irish Journal of Earth Sciences, 12: 47-63.

Journeay, J.M., 1993. Tectonic assemblages of the Eastern Coast Belt, southwestern British Columbia: implications for the history and mechanisms of terrane accretion. Current Research, Paper 93-1A(Part A): 221 - 233.

Journeay, J.M. and Friedman, R.M., 1993. The Coast Belt Thrust System: Evidence of Late Cretaceous shortening in southwest British Columbia. Tectonics, 12: 756-775.

Keppie, J.D. and Dostal, J., 2001. Evaluation of the Baja controversy using paleomagnetic and faunal data, plume magmatism, and piercing points. Tectonophysics, 339: 427-442.

Klepeis, K.A., Crawford, M.L. and Gehrels, G.E., 1998. Structural history of the crustal-scake Coast Shear Zone north of Portland Canal, southeast Alaska and British Columboia. Journal of Structural Geology, 20: 883-904.

Lewis, P.D., 1992. Structural geology of the Prout Plateau Region, Iskut River map area, British Columbia (104B/9): Geological Fieldwork 1991, v. Paper 1992-1, p. 521-527.

Lisle, R.J., 1987. Principal stress orientations from faults: an additional constraint. Annales Tectonicae, 1: 155-158.

Logan, J.M., Drobe, J.R. and Elsby, D.C., 1992. Geology of the More Creek area, northwestern British Columbia (104G/2). Geological Fieldwork 1991, British Columbia Ministry of Energy, Mines and Petroleum Resources Paper 1992-1: 161-178.

Logan, J.M., Drobe, J.R., Koyanagi, V.M. and Elsby, D.C., 1997. Geology of the Forrest Kerr-Mess Creek Area, Northwestern British Columbia (104B/10, 15 & 104G/2 &7W), Geoscience Map 1997-3. Ministry of Employment and Investment.

Logan, J.M., Drobe, J.R. and McClelland, W.C., 2000. Geology of the Forrest Kerr-Mess Creek Area, Northwestern British Columbia, NTS 104B/10, 15, & 104G/2 & 7W. GSB Bulletin, 104. British Columbia Ministry of Energy and Mines, 164 pp.

Logan, J.M. and Koyanagi, V.M., 1989. Geology and Mineral Deposits of the Galore Creek area, northwestern BC (104G/3, 4). Geological Fieldwork 1998, British Columbia Ministry of Energy, Mines and Petroleum Resources Paper 1989-1: 269-284.

Lowe, C., Evenchick, C.A., Bellamy, C.S. and Smith, G.T., 2004. Density and magnetic susceptibility of rocks from the Bowser and Sustut basins and underlying Stikinia, north-central British Columbia, Open File 4629. Geological Survey of Canada, 23 pp.

Lowe, C., Baker, J. and Evenchick, C.A., 2006. Constraints on the nature and thickness of sedimentary fill and underlying basement rocks in Bowser and Sustut basins, north-central British Columbia from analysis of potential field data. Bulletin of Canadian Petroleum Geology, 54: 62-84.

Ludwig, K.R., 2003. Isoplot 3.09, A geochronological toolkit for Microsoft Excel, Special Publication No. 4. Berkeley Geochronology Center.

Marrett, R. and Allmendinger, R.W. 1990. Kinematic analysis of fault-slip data. Journal of Structural Geology, 12: 973-986.

Marrett, R., Allmendinger, R.W., Alonso, R.N., and Drake, R.E., 1994, Late Cenozoic tectonic evolution of the Puna Plateau and adjacent foreland, northwest Argentine Andes: Journal of South American Earth Sciences, v. 7, p. 179-207.

Marsden, H. and Thorkelson, D.J., 1992. Geology of the Hazelton volcanic belt in British Columbia: Implications for the Early to Middle Jurassic evolution of Stikinia. Tectonics, 11: 1266-1287.

McClelland, W.C. and Mattinson, J.M., 2000. Cretaceous-Tertiary evolution of the western Coast Mountains, central southeastern Alaska. In: H.H. Stowell and W.C. McClelland (Editors), Tectonics of the Coast Mountains, Southeastern Alaska and British Columbia. Special Paper 343. Geological Society of America, Boulder, Colorado, pp. 159-182.

McMechan, M., 2007. Nature, origin and tectonic significance of anomalous transverse structures, southeastern Skeena Fold Belt, British Columbia. Bulletin of Canadian Petroleum Geology, 55: 262-274.

Mihalynuk, M.G., Erdmer, P., Ghent, E.D., Cordey, F., Archibald, D.A., Friedman, R.M., Johannson, G.G., 2004. Coherent French Range blueschist: Subduction to exhumation in <2.5 m.y.? Geological Society of America Bulletin, 116: 910-922.

Mihalynuk, M.G., Nelson, J.L. and Diakow, L.J., 1994. Cache Creek terrane entrapment: Oroclinal paradox within the Canadian Cordillera. Tectonics, 13: 575-595.

Moffat, I.W., 1985. The nature and timing of deformational events and organic and inorganic metamorphism in the northern Groundhog Coalfield; implications for the tectonic history of the Bowser Basin, Ph. D Thesis, University of British Columbia, Vancouver, 205 pp.

Moffat, I.W. and Bustin, R.M., 1993. Deformational history of the Groundhog Coalfield, Northeastern Bowser Basin, British Columbia; styles, superposition and tectonic implications. Bulletin of Canadian Petroleum Geology, 41: 1-16.

Monger, J.W.H., 1977. Upper Paleozoic rocks of the western Canadian Cordillera and their bearing on Cordilleran evolution. Canadian Journal of Earth Sciences, 14: 1832-1859.

Monger, J.W.H., Price, R.A. and Tempelman-Kluit, D.J., 1982. Tectonic accretion and the origin of the two major metamorphic and plutonic welts in the Canadian Cordillera. Geology, 10: 70-75.

Monger, J.W.H., Souther, J.G. and Gabrielse, H., 1972. Evolution of the Canadian Cordillera: A plate-tectonic model. American Journal of Science, 272: 577-602.

Nelson, J.L. and Mihalynuk, M.G., 1993. Cache Creek ocean: Closure or enclosure? Geology, 21: 173-176.

Nicholson, R., 1991. Vein morphology, host rock deformation and the origin of the fabrics of echelon mineral veins. Journal of Structural Geology, 13: 635-641.

Nicholson, R. and Ejiofor, I.B., 1987. The three-dimensional morphology of arrays of echelon and sigmoidal mineral-filled fractures: data from north Cornwall. Journal of the Geological Society, London, 144: 79-83.

Osadetz, K.G., Evenchick, C.A., Ferri, F., Stasiuk, L.D. and Wilson, N.S.F., 2003. Indications for Effective Petroleum Systems in Bowser and Sustut Basins, North-Central British Columbia. Geological Fieldwork 2002, Paper 2003-1: 257-264.

Pollard, D.D., Segall, P. and Delaney, P.T., 1982. Formation and interpretation of dilatant echelon cracks. Geological Society of America Bulletin, 93: 1291-1303.

Powell, C.M., 1979. A Morphological Classification of Rock Cleavage. Tectonophysics, 58: 21-34.

Price, R.A., 1994. Cordilleran tectonics and the evolution of the Western Canada Sedimentary Basin. In: G.D. Mossop and I. Shetson (Editors), Geological Atlas of the Western Canada Sedimentary Basin. Canadian Society of Petroleum Geologists and Alberta Research Council, Calgary, Alberta, pp. 13-24.

Price, R.A. and Carmichael, D.M., 1986. Geometric test for Late Cretaceous-Paleogene intracontinental transform faulting in the Canadian Cordillera. Geology, 14: 468-471.

Ramsay, J.G., 1967. Folding and fracturing of rocks. McGraw-Hill, New York, 567 pp.

Ramsay, J.G., 1980. The crack-seal mechanism of rock deformation. Nature, 284: 135-139.

Ramsay, J.G. and Huber, M.I., 1983. The techniques of moden structural geology, Volume 1: Strain Analysis. Academic Press, London, 307 pp.

Read, P.B., Brown, R.L., Psutka, J.F., Moore, J.M., Journeay, M., Lane, L.S., and Orchard, J.J., 1989. Geology, More and Forrest Kerr Creeks (Parts of 104B/10, 15, 16, and 104G/1,2), Open File 2094, Geological Survey of Canada, scale 1:50,000.

Read, P.B. and Psutka, J.F., 1990. Geology of Ealue Lake east-half (104H/13E) and Cullivan Creek (104H/14) map areas, British Columbia, Open File 2241. Geological Survey of Canada, scale 1:50,000.

Read, P.B., Woodsworth, G.J., Greenwood, H.J., Ghent, E.D. and Evenchick, C.A., 1991. Metamorphic map of the Canadian Cordillera, Map 1714A. Geological Survey of Canada, scale 1:2,000,000.

Renne, P.R. Swisher, C.C. III, Deino, A.L., Karner, D.B., Owens, T., Depaolo, D.J., 1998. Intercalibration of standards, absolute ages and uncertainties in 40Ar/39Ar dating. Chemical Geology, 145: 117-152.

Ricketts, B.D. and Evenchick, C.A., 2007. Evidence of different contractional styles along foredeep margins provided by Gilbert deltas: examples from Bowser Basin, British Columbia, Canada. Bulletin of Canadian Petroleum Geology, 55: 243-261.

Ricketts, B.D., Evenchick, C.A., Anderson, R.G. and Murphy, D.C., 1992. Bowser basin, northern British Columbia: Constraints on the timing of initial subsidence and Stikinia-North America terrane interactions. Geology, 20: 1119-1122.

Ritcey, D.H., Evenchick, C.A. and Ratcliffe, K.T., 2005. Geochemical and heavy mineral analyses of the Bowser Lake and Sustut groups, north-central British Columbia, Canada. Geological survey of Canada, Open File, 5072: 1 CD-ROM.

Roth, T., 2003. Physical and chemical constraints on mineralization in the Eskay Creek deposit, northwestern British Columbia: Evidence from petrography, mineral chemistry, and sulfur isotopes, The University of British Columbia, Vancouver, 401 pp.

Roth, T., Thompson, J.F.H., and Barrett, T.J., 1999. The Precious Metal-Rich Eskay Creek Deposit, Northwestern British Columbia, Chapter 15, *in* Barrie, C.T., and Hannington, M.D., eds., Volcanic-associated massive sulfide deposits: processes and examples in modern and ancient settings, Volume 8, Reviews in Economic Geology, p. 357-373.

Rubin, C.M. and Saleeby, J.B., 1991. Tectonic framework of the upper Paleozoic and lower Mesozoic Alava sequence: a revised view of the polygenetic Taku terrane in southern southeast Alaska. Canadian Journal of Earth Sciences, 28: 881-893.

Rubin, C.M., Saleeby, J.B., Cowan, D.S., Brandon, M.T. and McGroder, M.F., 1990. Regionally extensive mid-Cretaceous west-vergent thrust system in the northwestern Cordillera: Implications for continent-margin tectonism. Geology, 18: 276-280.

Rusmore, M.E. and Woodsworth, G.J., 1991. Coast Plutonic Complex: A mid-Cretaceous contractional orogen. Geology, 19: 941-944.

Rusmore, M.E., Woodsworth, G.J. and Gehrels, G.E., 2000. Late Cretaceous evolution of the eastern Coast Mountains, Bella Coola, British Columbia. In: H.H. Stowell and W.C. McClelland (Editors), Tectonics of the Coast Mountains, Southeastern Alaska and British Columbia. Special Paper 343. Geological

Society of America, Boulder, Colorado, pp. 89-105.

Saleeby, J.B., 2000. Geochronologic investigations along the Alexander-Taku terrane boundary, southern Revillagigedo Island to Cape Fox areas, southeast Alaska. In: H.H. Stowell and W.C. McClelland (Editors), Tectonics of the Coast Mountains, Southeastern Alaska and British Columbia and British Columbia. Special Paper 343. Geological Society of America, Boulder, Colorado, pp. 107-143.

Smith, J.V., 1996. Geometry and kinematics of convergent conjugate vein array systems. Journal of Structural Geology, 18: 1291-1300.

Swanson, M.T., 2006. Late Paleozoic strike-slip faults and related vein arrays of Cape Elizabeth, Maine. Journal of Structural Geology, 28: 245-273.

Symons, D.T.A., Harris, M.J., McCausland, P.J.A., Blackburn, W.H. and Hart, C.J.R., 2005. Mesozoic-Cenozoic paleomagnetism of the Intermontane and Yukon-Tanana terranes, Canadian Cordillera. Canadian Journal of Earth Sciences, 42: 1163-1185.

Thomson, R.C., Smith, P.L. and Tipper, H.W., 1986. Lower to Middle Jurassic (Pliensbachian to Bajocian) stratigraphy of the northern Spatsizi area, north-central British Columbia. Canadian Journal of Earth Sciences, 23: 1963-1973.

Thorkelson, D.J., Mortensen, J.K., Marsden, H. and Taylor, R.P., 1995. Age and tectonic setting of Early Jurassic episodic volcanism along the northeastern margin of the Hazelton Trough, northern British Columbia. In: D.M. Miller and C. Busby (Editors), Jurassic Magmatism and Tectonics of the North American Cordillera. Special Paper 299, Geological Society of America Boulder, Colorado, pp. 83-94.

Tillman, K.S. and Byrne, T.B., 1995. Kinematic analysis of the Taiwan Slate Belt. Tectonics, 14: 322-341.

Tipper, H.W. and Richards, T.A., 1976. Jurassic stratigraphy and history of north-central British Columbia. Geological Survey of Canada Bulletin, 270, 73 pp.

Vandall, T.A. and Palmer, H.C., 1990. Canadian Cordilleran displacement: Paleomagnetic results from the Early Jurassic Hazelton Group, Terrane I, British Columbia, Canada. Geophysical Journal International, 103: 609-619.

Waldron, J.W.F., Gagnon, J.-F., Loogman, W., and Evenchick, C.A., 2006. Initiation and Deformation of the Jurassic Cretaceous Bowser Basin: Implications for Hydrocarbon Exploration in north-central BC: Geological Fieldwork 2005, v. Paper 2006-1 and Geoscience BC Report 2006-1, p. 347-360.

Wheeler, J.O., Brookfield, A.J., Gabrielse, H., Monger, J.W.H., Tipper, H.W., Woodsworth, G.J., 1991. Terrane Map of the Canadian Cordillera, Map 1713A. Geological Survey of Canada.

Wheeler, J.O. and McFeely, P., 1991. Tectonic assemblage map of the Canadian Cordillera and adjacent parts of the United States of America, Map 1712A. Geological Survey of Canada, scale 1:2 000 000.

Woodcock, N.H. and Fischer, M., 1986. Strike-slip duplexes. Journal of Structural Geology, 8: 725-735.

Wynne, P.J., Irving, E., Maxson, J.A. and Kleinspehn, K.L., 1995. Paleomagnetism of the Upper Cretaceous strata of Mount Tatlow: Evidence for 3000 km of northward displacement of the eastern Coast Belt, British Columbia. Journal of Geophysical Research, 100: 6073-6091.

Appendix A

This appendix accompanies Chapter 4 and more fully describes the $^{40}Ar/^{39}Ar$ method of geochronology and the specific analyses undertaken in this study. Included is the full data set of samples for which ages have been quoted in the text and graphs have been derived.

The $^{40}Ar/^{39}Ar$ Method

The $^{40}Ar/^{39}Ar$ method of geochronology utilizes the breakdown of ^{40}K to its stable daughter ^{40}Ar. ^{40}K undergoes branched decay to both ^{40}Ar and ^{40}Ca in proportions of roughly 11.2% and 88.8% (Faure and Mensing, 2005). Decay to ^{40}Ar occurs via electron capture and subsequent positron emission. The basis of the method is that ^{40}K in potassium bearing minerals will break down to ^{40}Ar at a rate proportional to its half-life. It is then assumed that ^{40}Ar will be trapped by the mineral's crystal lattice. Comparison of proportions of parent ^{40}K with daughter ^{40}Ar allows calculation of ages using standard decay formulae. For newly-crystallized minerals, the ^{40}Ar age is coeval with the age of the mineral, and hence the rock, assuming no ^{40}Ar has escaped. In general, minerals can 'hold' ^{40}Ar provided they remain below the mineral's closure temperature, which varies from mineral to mineral. This study attempts to utilize muscovite as an ^{40}Ar host, which has a closure temperature of ~350°C. As metamorphic muscovite crystallizes below closure temperature the ^{40}Ar age will represent the mica age, provided it has not subsequently been heated past closure or altered by fluids (Faure and Mensing, 2005).

Initial use of this decay system involved measuring ^{40}K and ^{40}Ar in separate aliquots, and relied on absolute measurement of isotopes. A refinement of this method is the $^{40}Ar/^{39}Ar$ method. In this case a rock chip or mineral separate of the sample is placed in a reactor and bombarded by neutrons. This results in conversion of ^{40}K to ^{39}Ar. In the step-heating method the sample is subsequently placed in a high-vacuum and heated incrementally using a furnace or, as in the case of this study, with a laser. At the first step of heating, the outer portion of the mineral will release the argon trapped in its lattice. This argon is 'spiked' with a known tracer amount of ^{38}Ar. Relative proportions of isotopes of argon can then be measured in a mass spectrometer. A correction must then be made for the naturally occurring argon isotopes (^{40}Ar, ^{38}Ar, and ^{36}Ar) as well as interfering Ar from atmospheric contamination and the irradiation of Ca, Cl and K (Isotope production ratios: $(^{40}Ar/^{39}Ar)_K=0.0302\pm0.00006$, $(^{37}Ar/^{39}Ar)_{Ca}=1416.4\pm0.5$, $(^{36}Ar/^{39}Ar)_{Ca}=0.3952\pm0.0004$, $Ca/K=1.83\pm0.01(^{37}Ar_{Ca}/^{39}Ar_K)$.

Continued step-heating of the sample at higher temperature releases argon from deeper into the mineral grains. The ages calculated at each steps are conventionally plotted against cumulative $^{39}Ar\%$. If the grain has not suffered argon loss, the ages calculated at each step will be the same, representing a 'plateau' and the age of the grain. Commonly steps are discordant, and are called 'disturbed' (Hanes, 1991). Where several consecutive steps produce similar ages, an inverse isochron plot of $^{36}Ar/^{40}Ar$ versus $^{39}Ar/^{40}Ar$ is made as a check for concordancy. If the above ratios for each step plot on a concordant line, the slope can be used to calculate an age for the sample, which in principle should agree with the plateau age.

Methodology Specific to this Study

Samples utilized in this study were crushed, washed in nitric acid, rinsed in deionized water, dried and sieved (1.5 to 0.25mm fraction). Samples were then washed in acetone, dried, wrapped in aluminum foil and stacked in an irradiation capsule with similar-aged samples and neutron flux monitors (Fish Canyon Tuff sanidine (FCs), 28.02 Ma (Renne et al., 1998). Hornblende in sample 'Eskay Dike' was hand-picked following a Frantz separation.

Irradiation occurred at the McMaster Nuclear Reactor in Hamilton, Ontario, with a neutron flux of approximately $6x10^{13}$ neutrons/cm^2/s. Samples A-K were irradiated July 11-12, 2007 for 30 MWH, while 'Eskay Dike' was irradiated on February 7 and 8 for 45 MWH. Samples A-K utilized analyses (n=57) of 19 neutron flux monitor positions, while 'Eskay Dike' utilized analyses (n=52) of 13 positions, all producing errors of <0.5% in the J value. The samples were analyzed at the Noble Gas Laboratory, Pacific Centre for Isotopic and Geochemical Research, University of British Columbia, Vancouver, BC, Canada. Samples were step-heated at incrementally higher powers in the defocused beam of a 10W CO_2 laser (New Wave Research MIR10) until fused. Gas was analysed by a VG5400 mass spectrometer equipped with an ion-counting electron multiplier. All measurements were corrected for total system blank, mass spectrometer sensitivity, mass discrimination, radioactive decay during and subsequent to irradiation, as well as interfering Ar from atmospheric contamination and the irradiation of Ca, Cl and K. Errors are at the 2-sigma (95% confidence) level and are propagated from all sources except mass spectrometer sensitivity and age of the flux monitor. Plateaus were picked based on the following criteria:

1. Having three or more adjacent steps*;
2. Probability of fit of the weighted mean age greater than 5%;
3. Slope of the error-weighted line through the plateau ages equals zero at 5% confidence;
4. For plateaus with six or more steps, the weighted-mean plateau age must be similar to the ages of the two outermost steps (at 1.8σ);
5. The slope of the outer two steps on each side must not have non zero slopes of the same sign (at 1.8σ, nine or more steps only).

*Ideally plateaus should also contain >50% of ^{39}Ar in adjacent steps. For plateaus on samples that satisfy the above criteria but do not have sufficient >50% ^{39}Ar, inverse isochron plots were generated to check reasonability of prospective plateaus. Interpretation of these plateaus is thereby conditional on accepting plateaus with smaller proportions of ^{39}Ar.

Supplementary Data

The data presented below are for samples E, G, H, K (table 4.1) and 'Eskay Dike'. Age versus ^{39}Ar% and inverse isochron plot of $^{36}Ar/^{40}Ar$ versus $^{39}Ar/^{40}Ar$ have been included in Chapter 4 (figures 4.10 and 4.11, respectively). Plots have been generated using the Excel add-on Isoplot 03.09 (Ludwig, 2003). These data represent first-run analyses obtained from whole-rock samples with the exception of the dike sample from Eskay Creek, for which a separate of hornblende was analysed. Re-run analyses and analyses produced from mineral separates may be published in future works.

Sample E WR

Laser Power(%)	Isotope Ratios 40Ar/39Ar	38Ar/39Ar	37Ar/39Ar	36Ar/39Ar	Ca/K	Cl/K	%40Ar atm	f 39Ar	40Ar*/39ArK	Age
2	26.8591±0.0109	0.0757±0.1226	0.0474±0.1294	0.0854±0.0352	0.144	0.011	92.34	0.62	1.838±0.857	25.65±11.87
2.3	12.2211±0.0091	0.0295±0.0964	0.0174±0.0684	0.0192±0.0212	0.066	0.003	44.71	4.91	6.550±0.137	89.77±1.84
2.6	10.0443±0.0045	0.0168±0.0443	0.0176±0.0526	0.0026±0.0575	0.072	0.001	6.7	16.72	9.248±0.062	125.49±0.82
2.9	12.1203±0.0043	0.0135±0.0301	0.0083±0.0545	0.0015±0.0364	0.034	0	3.13	31.1	11.652±0.054	156.73±0.69
3.1	11.3666±0.0048	0.0135±0.0391	0.0070±0.0585	0.0016±0.0606	0.028	0	3.33	18.33	10.868±0.066	146.59±0.85
3.3	11.4761±0.0053	0.0140±0.0571	0.0100±0.0854	0.0022±0.0963	0.039	0	4.35	10.62	10.800±0.086	145.72±1.12
3.5	12.0230±0.0061	0.0155±0.0728	0.0105±0.0464	0.0045±0.0599	0.038	0	8.63	5.41	10.689±0.105	144.28±1.36
3.7	12.6295±0.0059	0.0141±0.0836	0.0082±0.0989	0.0060±0.0541	0.028	0	11.67	5.24	10.860±0.118	146.50±1.52
3.9	13.1686±0.0062	0.0153±0.1282	0.0092±0.1339	0.0058±0.1054	0.028	0	9.51	3.31	11.462±0.207	154.27±2.67
4.1	13.7693±0.0083	0.0166±0.1577	0.0124±0.1910	0.0082±0.1117	0.039	0	13.27	2.54	11.383±0.288	153.26±3.71
4.5	17.7086±0.0083	0.0257±0.1121	0.0240±0.1693	0.0239±0.0557	0.073	0.002	34.35	1.21	10.764±0.404	145.25±5.24
Total/Average	11.6500±0.0010	0.0157±0.0094	0.0230±0.0059	0.0035±0.0094	0.042	0.001		100	10.918±0.016	

J = 0.007789±0.000006

Volume 39ArK = 298.57

Integrated Date = 142.96±0.42

Volumes are 1E-13 cm3 NPT

Neutron flux monitors: 28.02 Ma FCs (Renne et al., 1998)

Isotope production ratios : (40Ar/39Ar)K=0.0302±0.00006, (37Ar/39Ar)Ca=1416.4±0.5, (36Ar/39Ar)Ca=0.3952±0.0004, Ca/K=1.83 0.01(37ArCa/39ArK).

Run Date: 23-Aug-07

Sample G WR

Laser Power(%)	Isotope Ratios 40Ar/39Ar	38Ar/39Ar	37Ar/39Ar	36Ar/39Ar	Ca/K	Cl/K	%40Ar atm	f 39Ar	40Ar*/39ArK	Age
2	31.8791±0.0056	0.0650±0.0240	0.0075±0.1865	0.1006±0.0229	0.028	0.007	93.47	2.28	2.052±0.684	28.63±9.46
2.2	25.6318±0.0054	0.0381±0.0245	0.0043±0.0863	0.0651±0.0178	0.015	0.003	75.19	12.84	6.325±0.342	86.83±4.59
2.5	17.6345±0.0070	0.0206±0.0602	0.0032±0.0994	0.0254±0.0199	0.012	0	42.31	4.53	10.115±0.165	136.93±2.15
2.6	13.6283±0.0056	0.0138±0.0368	0.0019±0.0787	0.0085±0.0214	0.007	0	18.36	14.65	11.073±0.086	149.37±1.11
2.7	12.1849±0.0113	0.0131±0.0338	0.0019±0.1214	0.0045±0.0307	0.007	0	10.58	12.24	10.837±0.135	146.32±1.75
2.8	11.5347±0.0070	0.0139±0.0355	0.0069±0.0674	0.0035±0.0383	0.024	0	8.67	10.81	10.472±0.086	141.58±1.12
2.9	11.0341±0.0060	0.0128±0.0339	0.0018±0.1839	0.0028±0.0433	0.007	0	7.15	10.81	10.182±0.073	137.80±0.95
3	10.4464±0.0059	0.0126±0.0360	0.0021±0.1916	0.0017±0.1144	0.008	0	4.41	8.6	9.914±0.084	134.32±1.10
3.1	10.0331±0.0059	0.0132±0.0968	0.0029±0.1550	0.0017±0.0893	0.011	0	4.16	6.7	9.534±0.072	129.34±0.95
3.3	10.2288±0.0052	0.0135±0.0814	0.0024±0.1695	0.0025±0.0548	0.009	0	6.71	6.94	9.464±0.066	128.43±0.86
3.5	10.1681±0.0055	0.0137±0.0687	0.0022±0.2180	0.0024±0.1045	0.009	0	5.89	4.51	9.468±0.092	128.48±1.20
4	10.4231±0.0060	0.0136±0.0566	0.0039±0.1000	0.0030±0.0834	0.014	0	7.65	5.09	9.534±0.096	129.34±1.26
Total/Average	13.9757±0.0011	0.0178±0.0063	0.0063±0.0090	0.0148±0.0055	0.011	0.001		100	9.500±0.029	

J = 0.007796±0.000006

Volume 39ArK = 615.32

Integrated Date = 129.67±0.76

Volumes are 1E-13 cm3 NPT

Neutron flux monitors: 28.02 Ma FCs (Renne et al., 1998)

Isotope production ratios : (40Ar/39Ar)K=0.0302±0.00006, (37Ar/39Ar)Ca=1416.4±0.5, (36Ar/39Ar)Ca=0.3952±0.0004, Ca/K=1.83 0.01(37ArCa/39ArK).

Run Date: 12-Aug-07

Sample H WR

Laser Power(%)	Isotope Ratios 40Ar/39Ar	38Ar/39Ar	37Ar/39Ar	36Ar/39Ar	Ca/K	Cl/K	%40Ar atm	f 39Ar	40Ar*/39ArK	Age
2	21.2006±0.0152	0.0436±0.1541	0.1038±0.1379	0.0719±0.0426	0.359	0.004	100.5	0.18	-0.131±0.870	-1.85±12.26
2.2	15.7349±0.0153	0.0265±0.0551	0.1019±0.0355	0.0391±0.0256	0.352	0.001	73.37	2.99	4.143±0.315	57.44±4.29
2.4	11.3481±0.0062	0.0166±0.0450	0.0990±0.0187	0.0110±0.0215	0.342	0	28.3	3.7	8.068±0.091	110.21±1.21
2.5	10.1184±0.0112	0.0144±0.0503	0.0932±0.0268	0.0034±0.0311	0.322	0	9.33	4.13	9.100±0.111	123.83±1.46
2.6	10.6982±0.0131	0.0132±0.0444	0.0831±0.0251	0.0022±0.0467	0.287	0	5.59	5.28	10.032±0.136	136.06±1.81
2.7	10.7534±0.0076	0.0134±0.0361	0.0793±0.0242	0.0018±0.0392	0.274	0	4.66	6.63	10.189±0.083	138.11±1.08
2.8	11.1950±0.0119	0.0128±0.0419	0.0706±0.0282	0.0018±0.0828	0.244	0	4.36	6.52	10.644±0.137	144.03±1.78
2.9	11.4110±0.0129	0.0129±0.0457	0.0648±0.0219	0.0018±0.0391	0.224	0	4.35	6.06	10.849±0.145	146.69±1.88
3	11.1112±0.0091	0.0127±0.0411	0.0657±0.0187	0.0017±0.0402	0.227	0	4.27	10.31	10.582±0.101	143.22±1.31
3.1	11.4551±0.0091	0.0122±0.0317	0.0606±0.0240	0.0015±0.0363	0.209	0	3.65	9.04	10.980±0.104	148.40±1.34
3.3	10.9734±0.0065	0.0126±0.0213	0.0563±0.0216	0.0016±0.0266	0.195	0	4.01	9.07	10.477±0.071	141.85±0.92
3.6	10.1166±0.0129	0.0130±0.0414	0.0599±0.0234	0.0016±0.0335	0.207	0	4.48	10.32	9.610±0.128	130.53±1.68
3.9	10.0504±0.0084	0.0129±0.0262	0.0605±0.0216	0.0020±0.0337	0.209	0	5.51	10.62	9.443±0.085	128.34±1.11
4.1	10.1094±0.0093	0.0137±0.0383	0.0646±0.0203	0.0020±0.0261	0.223	0	5.67	9.41	9.481±0.092	128.84±1.21
4.7	10.3148±0.0052	0.0161±0.0347	0.0877±0.0231	0.0026±0.0633	0.303	0	6.96	5.73	9.532±0.071	129.51±0.93
Total/Average	10.8417±0.0014	0.0137±0.0052	0.1322±0.0019	0.0034±0.0054	0.242	0		100	10.147±0.016	

J = 0.007808±0.000006

Volume 39ArK = 1188.2

Integrated Date = 133.32±0.44

Volumes are 1E-13 cm3 NPT

Neutron flux monitors: 28.02 Ma FCs (Renne et al., 1998)

Isotope production ratios : (40Ar/39Ar)K=0.0302±0.00006, (37Ar/39Ar)Ca=1416.4±0.5, (36Ar/39Ar)Ca=0.3952±0.0004, Ca/K=1.83±0.01(37ArCa/39ArK).

Run Date: 13-Aug-07

Sample K WR

Laser Power(%)	Isotope Ratios 40Ar/39Ar	38Ar/39Ar	37Ar/39Ar	36Ar/39Ar	Ca/K	Cl/K	%40Ar atm	f 39Ar	40Ar*/39ArK	Age
2	17.3314±0.0074	0.0533±0.0473	0.0411±0.0557	0.0444±0.0231	0.146	0.007	74.88	3.72	4.281±0.300	59.39±4.09
2.2	12.8583±0.0071	0.0242±0.0253	0.0342±0.0368	0.0112±0.0275	0.122	0.002	24.92	7.26	9.557±0.120	129.99±1.57
2.4	11.2242±0.0158	0.0160±0.0525	0.0474±0.0259	0.0040±0.0241	0.17	0	10.21	20.96	10.015±0.169	136.00±2.21
2.6	12.8721±0.0132	0.0135±0.0260	0.0620±0.0219	0.0029±0.0425	0.223	0	6.27	26.13	12.004±0.168	161.83±2.16
2.8	13.8496±0.0134	0.0128±0.0475	0.1140±0.0236	0.0028±0.0379	0.41	0	5.33	13.06	13.029±0.181	175.00±2.32
3	13.9188±0.0114	0.0129±0.0200	0.1845±0.0250	0.0032±0.0493	0.676	0	6.07	11.58	12.989±0.159	174.48±2.04
3.2	13.9748±0.0127	0.0143±0.0557	0.2571±0.0230	0.0038±0.0531	0.943	0	6.95	8.16	12.901±0.180	173.36±2.31
3.4	14.2335±0.0144	0.0157±0.0617	0.2768±0.0238	0.0049±0.0582	1.014	0	8.09	3.81	12.906±0.211	173.42±2.70
3.6	15.1302±0.0140	0.0174±0.0976	0.1105±0.0435	0.0070±0.0862	0.402	0	11.16	2.59	13.204±0.265	177.24±3.38
4	16.6789±0.0060	0.0285±0.0904	0.1380±0.0361	0.0125±0.0545	0.503	0.003	20.15	2.74	13.112±0.219	176.05±2.80
Total/Average	13.1757±0.0027	0.0166±0.0081	0.2074±0.0030	0.0055±0.0065	0.38	0.001		100	12.984±0.035	

J = 0.007818±0.000006

Volume 39ArK = 515.69

Integrated Date = 155.82±0.91

Volumes are 1E-13 cm3 NPT

Neutron flux monitors: 28.02 Ma FCs (Renne et al., 1998)

Isotope production ratios : (40Ar/39Ar)K=0.0302±0.00006, (37Ar/39Ar)Ca=1416.4±0.5, (36Ar/39Ar)Ca=0.3952±0.0004, Ca/K=1.83 0.01(37ArCa/39ArK).

Run Date: 15-Aug-07

Eskay dike Hornblende

Laser Power(%)	Isotope Ratios 40Ar/39Ar	38Ar/39Ar	37Ar/39Ar	36Ar/39Ar	Ca/K	Cl/K	%40Ar atm	f 39Ar	40Ar*/39Ar/K	Age
2	105.4655±0.0406	0.1220±0.2205	1.6172±2.8206	0.3602±0.0930	5.018	0.004	96.31	0.19	3.218±9.550	29.61±87.15
2.3	70.0026±0.0257	0.0609±0.1558	15.9904±0.0376	0.2411±0.0493	50.032	0.004	97.23	0.77	1.815±3.574	16.76±32.85
2.5	55.0559±0.0338	0.0564±0.1670	35.1303±0.0359	0.1961±0.0564	112.41	0	94.76	0.89	2.758±3.079	25.40± 28.17
2.7	27.5492±0.0253	0.0730±0.0736	25.5042±0.0412	0.0937±0.0463	80.422	0.009	84.56	1.45	3.940±1.219	36.19±1.08
2.9	13.7094±0.0410	0.0671±0.0694	8.7543±0.0963	0.0436±0.0744	27.282	0.01	76.21	1.38	2.595±0.931	23.92±8.52
3.2	6.6307±0.0177	0.0870±0.0471	4.8193±0.0279	0.0159±0.0702	14.903	0.016	54.02	5.82	2.725±0.333	25.11±3.04
3.5	4.6011±0.0184	0.0793±0.0314	5.5283±0.0258	0.0089±0.0598	17.104	0.015	36.44	16.85	2.763±0.171	25.45±1.56
3.8	3.8187±0.0151	0.0728±0.0314	5.4702±0.0203	0.0064±0.0426	16.93	0.013	25.92	24.02	2.694±0.094	24.82±0.86
4.1	3.7145±0.0114	0.0726±0.0323	5.4551±0.0212	0.0061±0.0954	16.887	0.013	23.84	22.28	2.680±0.177	24.69±1.62
4.4	3.5852±0.0187	0.0678±0.0274	5.3487±0.0233	0.0056±0.0518	16.56	0.012	21.39	26.35	2.687±0.102	24.75±0.94
Total/Average	5.2685±0.0036	0.0727±0.0071	10.2163±0.0037	0.0115±0.0110	18.832	0.01		100	2.714±0.040	

J = 0.005142±0.000012

Volume 39ArK = 135.38

Integrated Date = 25.00±0.73

Volumes are 1E-13 cm3 NPT

Neutron flux monitors: 28.02 Ma FCs (Renne et al., 1998)

Isotope production ratios: (40Ar/39Ar)K=0.0302±0.00006, (37Ar/39Ar)Ca=1416.4±0.5, (36Ar/39Ar)Ca=0.3952±0.0004, Ca/K=1.83±0.01(37ArCa/39ArK).

Run Date: 05-Mar-08